Nested modelling of wave processes from deep to shallow water: Building an operational wave model system

Dissertation

submitted to and approved by the

Department of Architecture, Civil Engineering and Environmental Sciences
University of Braunschweig – Institute of Technology

and the

Department of Civil and Environmental Engineering
University of Florence

in candidacy for the degree of a
Doktor-Ingenieur (Dr.-Ing.) /
Dottore di Ricerca in Civil and Environmental Engineering*)

by
Dario Pelli
born 21/09/1979
from Livorno, (Italy)

Submitted on	25 August, 2017
Oral examination on	08 November, 2017
Professorial advisors	Prof. Lorenzo Cappietti Prof. Hocine Oumeraci

2018

*) Either the German or the Italian form of the title may be used.

Abstract

In this thesis, a model system for simulating the wave processes from the open ocean to the shoreline is proposed. In particular, the focus is put on modelling extreme wave conditions in the Mediterranean Sea and the aim is to develop a supporting tool for decision making in the early-warning process.

This aim is motivated by the high number of damages due to extreme high waves conditions which occur worldwide every year. Moreover, the increasing population density and climate change in coastal zones enhance the risk for human life and coastal activities in the next future.

The model system is built by linking three existing models, properly selected for their ability of simulating physical processes that affect waves at different spatial scales. In particular, the WAVEWATCH III model is selected for the wave processes in deep water, the SWAN model for wave processes in intermediate/shallow water, and the XBeach model for wave processing in the nearshore where changes of seabed will affect wave propagation.

The three models are nested by adopting a modular approach, in which each model works separately, and a new module is developed in order to transfer the initial and boundary conditions from the largest scale to the smallest scale of the model chain. The advantage of the modular approach is that no or only slight modifications of the source code of the existing models are needed. Moreover, the system can be easily updated by introducing improvements/extensions, or fully new versions of the single models without modification of the structure of the system.

The developed model system, called NEMO system, is calibrated and validated, and applied to a real test case in the coast of Versilia (North Tuscany, Italy).

Sommario

In questa tesi viene proposto lo sviluppo di una catena modellistica per la simulazione del moto ondoso, dal largo fino alla costa. In particolare viene posta l'attenzione sulla modellazione delle tempeste più rilevanti verificatesi nel Mar Mediterraneo, con lo scopo di ottenere uno strumento a supporto dei sistemi di allerta meteo-marino.

Lo scopo della tesi è motivato dal crescente numero di tempeste che ogni anno si abbattono sulle coste di tutto il mondo, causando ingenti danni in termini econimici e di vite umane. Inoltre, ad aumentare i rischi per la vita umana e le attività costiere, sta contribuendo la tendenza all'aumento della densità di popolazione sulla costa.

La catena modellistica proposta nella tesi è stata sviluppata concatenando tre modelli numerici esistenti, propriamente selezionati per la loro abilità nel simulare i processi che determinano il moto ondoso alle diverse scale di risoluzione spaziale, dalle acque profonde fino alla costa. In particolare, il modello spettrale WAVEWATCH III è stato scelto per simulare il moto ondoso in acque profonde, il modello spettrale SWAN per la simulazione delle onde in acque intermedie e basse, ed il modello costiero XBeach per simulare i fenomeni costieri legati al moto ondoso, quali correnti e trasporto sedimentario che determinano la morfologia del fondale. Questi ultimi processi risultano determinanti in quanto vanno ad interagire con l'evoluzione delle onde nella fascia costiera.

I tre modelli sono stati innestati adottando un approccio a moduli, dove ogni modulo è costituito da una singola griglia di calcolo che può lavorare separatamente dall'altro. Un nuovo modulo è stato sviluppato per gestire i diversi modelli con un'unica interfaccia, compreso il trasferimento delle condizioni iniziali ed al contorno dei modelli annidiati che rappresenta il contributo scientifico principale del lavoro. L'approccio a moduli ha il vantaggio di concatenare i tre modelli selezionati senza il bisogno di modifiche sostanziali del codice sorgente dei singoli modelli. Inoltre, la catena modellistica così sviluppata può facilmete essere aggiornata con una nuova versione di un modello, semplicemente sostituendo un modulo e lasciando invariata la struttura della catena modellistica.

La catena modellistica sviluppata, chiamata "NEMO system", è stata infine calibrata, validata ed applicata ad un caso di studio sulla costa della Versilia, nel nord della Toscana.

Zusammenfassung

In dieser Doktorarbeit ist ein Modellsystem zur Simulation der Wellenprozesse vom offenen Ozean bis zur Küstenlinie entwickelt worden. Insbesondere liegt der Schwerpunkt dieser Studie auf der Modellierung extremer Wellenereignisse, welche durch extreme Sturmereignisse im Mittelmeer erzeugt werden. Das Ziel ist es ein Frühwarnsystem zu entwickeln, welches bei der Entscheidungsfindung über Küstenschutzmaßnahmen, auch im Katastrophenfall, unterstützen kann.

Diese Arbeit ist durch die hohe Anzahl und die Größe der weltweiten Schäden in Küstengebieten, welche jedes Jahr als Folge von extremen Wellenereignisse auftreten, motiviert worden. Darüber hinaus erhöht sich in der nahen Zukunft das Risiko für die zunehmende Bevölkerung, welche in den Küstengebieten lebt und arbeitet, durch den Klimawandel, welcher zu einer Zunahme von Schlechtwetterereignissen führt.

Das Modellsystem besteht aus der Verknüpfung von drei vorhandenen Modellen. Jedes Modell ist entsprechend seiner Fähigkeiten ausgewählt worden, um die Gesamtheit der physikalische Prozesse zu simulieren, welche die räumliche und zeitliche Verteilung der Wellen beeinflusst. Insbesondere sind das WAVEWATCH III-Modell für die Wellenprozesse in tiefem Wasser, das SWAN-Modell für Wellenprozesse in intermediärem/seichtem Wasser und das XBeach-Modell für Wellenprozesse im Küstenbereich, wo Veränderungen des Meeresbodens die Wellenausbreitung beeinflussen, ausgewählt worden.

Die drei Modelle werden verschachtelt, indem ein modularer Ansatz gewählt wird, bei dem jedes Modell separat arbeitet und ein neues Modul entwickelt, um die Anfangs- und Randbedingungen vom größten M aßstab auf den kleinsten Maßstab der Modellkette zu übertragen. Der Vorteil des modularen Ansatzes besteht darin, dass keine oder nur geringfügige Modifikationen des Quellcodes der vorhandenen Modelle erforderlich sind. Darüber hinaus kann das System leicht aktualisiert werden, indem Verbesserungen/Erweiterungen oder vollständig neue Versionen der einzelnen Modelle einfach eingeführt werden, ohne die Struktur des Systems zu verändern.

Das entwickelte Modellsystem, welches NEMO-System genannt wird, ist auf einen realen Testfall an der Küste der Versilia (Nordtoskana, Italien) kalibriert und validiert und angewendet worden.

To Chiara and Guido

Acknowledgement

Firstly, I would like to thank the Italian Police that gave me the opportunity to conduct this PhD research. Secondly, I would like to thank the University of Florence and the University of Braunschweig those gave me the material and scientific resources to carry out the research.

A special gratitude goes to my supervisors Prof. Dr. Ing. Hocine Oumeraci and Prof. Dr. Ing. Lorenzo Cappietti, who guided me over the last four years with precious suggestions.

Thanks to my family and my future wife Chiara who supported and encouraged my research.

Thanks to my colleagues and friends of the international doctorate course and to the guys of the Department of Hydromecanics and Coastal Engineering of the TU Braunschweig.

The author would like to thank ISPRA - Servizio Mareografico "Rete Ondametrica Nazionale" (RON) for the provision of the network buoys data, "Servizio Idrografico Regionale" of Regione Toscana for the provision of the Gorgona buoy data, and "Autorità Portuale di Marina di Carrara" for the provision of the Carrara buoy data.

Contents

1

Introduction

1.1 Motivations and Problem Statement

Modelling of wind waves travelling from the open ocean to the coastline in an operational environment has been the focus of interest for several years (Tolman et al., 2013). The first method for forecasting heights and periods of wind waves was developed by Sverdrup and Munk (1946, 1947) during World War II, to predict waves for the D-day invasion in Normandy and the preceding landings in Africa and Italy. A big step towards operational modelling was achieved with the development of spectral models by Gelci et al. (1956, 1957), who described the complex wave field with its energy spectrum.

After the development of spectral models, different wave models were proposed (see SWAMP Group, 1985; Tolman et al., 2002, for a review), but they mainly focus on large-scale evolution of wind-waves. To capture wave features on smaller scales due to the presence of irregular bathymetry (e.g. refraction, depth-induced breaking) or obstacles, such as small islands or man-made structures (e.g. reflection, overtopping), several nearshore wave models are proposed, based for example on mild slope equation (Berkhoff, 1972), parabolic-equation (Kirby and Dalrymple, 1983), nonlinear shallow water equations (NLSWEs) (Brocchini and Dodd, 2008) or Boussinesq-type equations (Kirby, 2003).

Furthermore, severe storms may affect nearshore bathymetry, causing shoreline changes and eroding the dry beach and dunes. These bathymetry changes modify wave dynamics (e.g. moving onshore the point break) and consequently wave-induced currents and other coastal processes like wave run-up and run-down, or overtopping. Therefore, modelling waves in a dynamic environment like the coastal zone needs to take into account also morphological changes resulting from sediment transport.

A possible strategy for including in a model all the processes affecting different time-scale waves from their source to the breaking may be the nesting of different purpose models operating over grids with different resolutions. The use of multiple grids is necessary to capture the features of the different physical processes at its own appropriate spatial resolution (e.g. Chawla et al., 2007).

In this study, a new nesting approach is described for the building of a model system able to simulate the wave field from the open ocean until a detailed shoreline scale. Therefore, the obtained multi-scale model system can be used as a tool for supporting Coastal Early Warning Systems (CEWS) (e.g. Barnard et al., 2014; Vousdoukas et al., 2012).

The needs of a model system for supporting CEWS is justified by the increasing worldwide trend of damages due to extreme waves and storm surge conditions.

The major examples are the well-know hurricanes Katrina in 2005 (Knabb et al., 2005) and

Sandy in 2012 (Blake et al., 2013), which caused catastrophic flooding in USA, or the cyclone Xynthia in 2010 (Bertin et al., 2012) that caused severe flooding in the South-West of France. Moreover, several minor flooding events and damages due to waves occur worldwide every year, causing deaths and economical damages. The work of Kolen et al. (2010) concluded that in the specific case of the Xynthia storm, disaster management mainly failed because the storm surge warning issued by Meteo France was not understood by the disaster management authorities and the public.

Another factor of risk is the fact that population density in coastal zones is significantly higher than in inland areas, with an increasing tendency in the next future (Neumann et al., 2015). This trend transforms natural extreme events in hazards for human life and coastal activities.

Given the significant advances in parallel computing and the decreasing of CPU costs, a multi-scale operational model, able to simulate waves from their origin in deep water to their dissipation in coastal zone, becomes increasingly feasible.

Beside the main purpose (CEWS), the building of an operational wave model system is motivated also as a support for:

- Industries operating on the continental shelf and the coastal zone (e.g. fisheries, shipping and offshore industry).
- Coastal and ocean engineering companies (e.g. in the design and operation of offshore and coastal structures, and the development of coastal management strategies).
- Operators of offshore renewable energies farm, particularly for wind farms located in shallow coastal areas (e.g. Rugbjerg et al., 2006).
- Analysis of the wave energy potential in deep and shallow water, for projects of "Wave Energy Park" (WEP) (e.g. Pelli et al., 2016; Rusu and Guedes Soares, 2009).
- Coastal recreation for which reliable knowledge of waves height and currents is particularly important.

1.2 Objectives and Methodology

The main objectives of this study are summarised as follows:

- Identification of the physicals processes affecting the evolution of the waves from the open ocean to the shoreline.
- Selection of the existing models able to simulate all individuated physical processes.
- Building, calibrating and validating an Operational Wave Model System (OWMS) to simulate the wave evolution from the open ocean to the shoreline.
- Practical implementation of the OWMS for a selected test case.

The present thesis is organised in six chapters, including this introductory chapter.

Chapter 2 analyses the State of The Art of water waves mechanics in deep and shallow water, and nearshore processes, including hydrodynamic circulation, wave setup and morphodynamic processes that strongly affect waves in shallow water. A review of the available models is also carried out.

Chapter 3 describes the main features (i.e. governing equation and numerical schemes), calibration and validation of the models selected to simulate deep water processes (WAVEWATCH III), intermediate and shallow water processes (SWAN), and nearshore processes (XBeach).

Chapter 4 describes the methodology followed for the nesting of the three models and the obtained model system.

Chapter 5 presents the results of the application of the model system to a selected test case.

Chapter 6 summarises key results and concluding remarks. Suggestion for further research are also provided.

The research is organised in four work packages as depicted in Fig. 1.1. The objectives and methodologies tentatively formulated above and in Fig. 1.1 will be specified more precisely in the concluding section on Chapter 2.

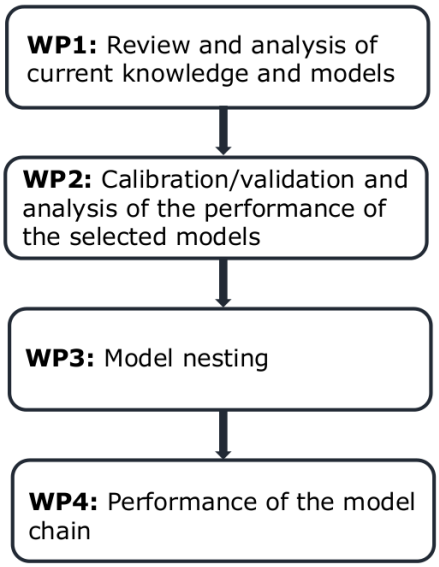

Figure 1.1: Flow chart illustrating the organization of the Work Packages (WP).

2

Wind Wave Generation, Propagation and Nearshore Processes: State of The Art

This chapter describes the review and analysis of the current knowledge of water waves mechanics in deep and shallow water and nearshore processes, including hydrodynamic circulation, wave setup and morphodynamic processes that strongly affect waves in shallow water. Moreover, a State of The Art review of the available numerical wave models is carried out.

Waves can be classified in deep, intermediate and shallow water by means of the relationship between water depth d and wavelength L (or wave number k and water depth d) as shown in Figure 2.1. This relationship represents the interaction between waves and seabed: (a) when there is no interaction between waves and seabed, $d/L > 1/2$ (or $k/d > \pi$), waves are in deep water, (b) when there is mild to fair interaction between waves and seabed, $1/2 > d/L > 1/20$ (or $\pi > k/d > 10/\pi$), waves are in intermediate water, (c) when there is strong interaction between waves and seabed, $1/20 > d/L$ (or $10/\pi > k/d$), waves are in shallow water.

The generation of waves usually start in deep water by means of the wind force. Then, waves are free to propagate through seas and oceans until they encounter an obstacle, e.g. island, coastline, man-made structure. The interaction between waves and bottom activates a series of processes which modify the waves themselves. In shallow water, waves become too steep and collapse, generating nearshore currents and sediment transport.

It is worth to mention that the variability of the water levels associated the waves to be forecasted/hindcasted is excluded from the study, since tides in the Mediterranean Sea (that is the area of interest) are negligible. However, during the storms, in some areas of the Mediterranean Sea (e.g. North Adriatic, Gulf of Genoa). It is possible to observe a considerable high water level (up to 1 metre). This is due to the storm surge associated to wind and barometric pressure changes. The implication of the non-consideration of water level variability on the final results at the shoreline are discussed in Section 5.3.

In this chapter, wave processes are separated in deep water, analysed and discussed in Section 2.1, and intermediate and shallow water, analysed and discussed in Section 2.2. Section 2.3 is dedicated to wave breaking induced by the bottom and the other physical processes induced by wave breaking (i.e. hydro- and morphodynamic processes). The review and analysis of the available numerical models able to simulate the aforementioned wave processes is discussed in Section 2.4. Finally, the objectives and methodology of the present PhD study are specified in Section 2.6.

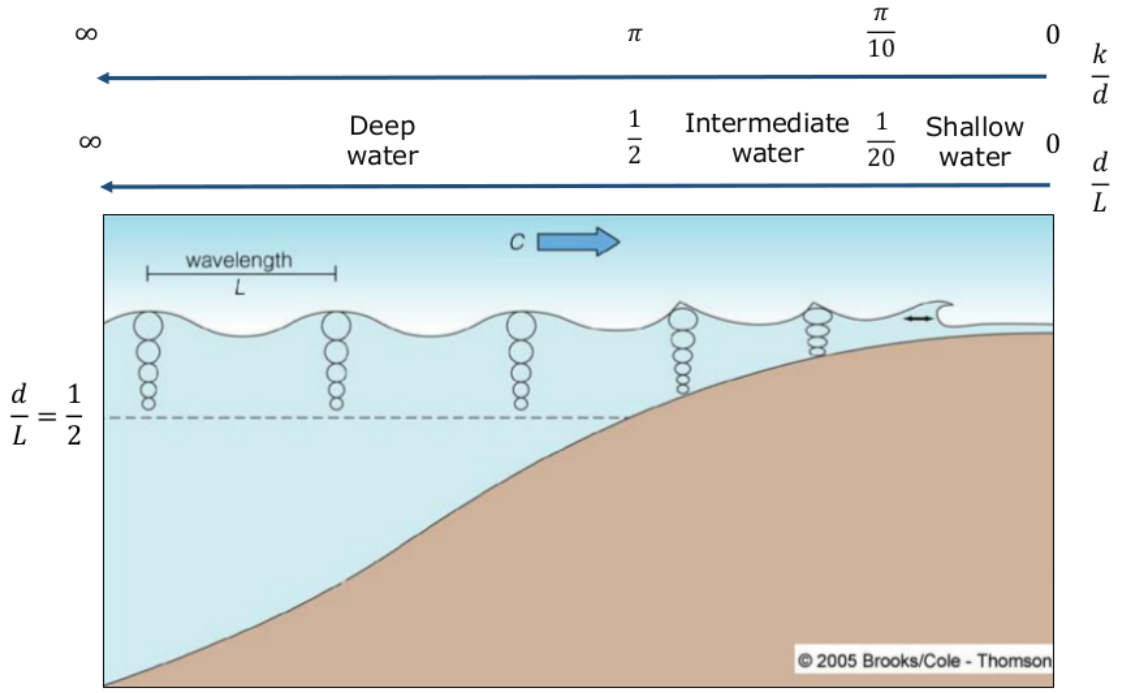

Figure 2.1: Definition of deep, intermediate and shallow water waves (modified from `http://ksuweb.kennesaw.edu/~jdirnber/oceanography/LecturesOceanogr/LecWaves/LecWaves.html`).

2.1 Deep Water Waves

The main physical processes affecting waves in deep water are (Fig. 2.2):

- Generation by wind
- Energy dissipation due to "whitecapping"
- Nonlinear quadruplet wave-wave interactions

Dissipation processes include also interaction of wave with turbulence, damping of swell propagating against the wind and interaction of waves with the vertical structure of upper layer of the ocean (i.e. wave-current interaction). However, these processes are still not well understood and tentative formulations for swell damping and turbulence are usually included in the whitecapping sink term, that is also used to balance uncertainties in the parameterization of wind generation and nonlinear interactions at higher frequencies. Therefore, the parameterization of the aforementioned processes are strictly connected among them.

Deep water processes are relevant on a spatial scale from tens to thousands of kilometres. Modelling waves at this scale is computationally feasible by means of spectral models only, which describe the evolution of the wave field through the variation of the two dimensional energy density spectrum $E(f, \theta)$ in time and space. Therefore, deep water processes are described as source (or sink) terms $S(f, \theta)$ representing the effect of each physical process on the wave energy.

2.1.1 Generation by wind ($S_{\mathbf{in}}$)

When the wind start to blow above the still water surface, the formation of ripples can be observed. If the wind continues to blow, these ripples develop in irregular and short-crested waves, this sea state is usually called *wind-sea*. The total length of sea over which the wind blows is called *fetch*. Waves stop to grow when the wave speed approaches the wind speed,

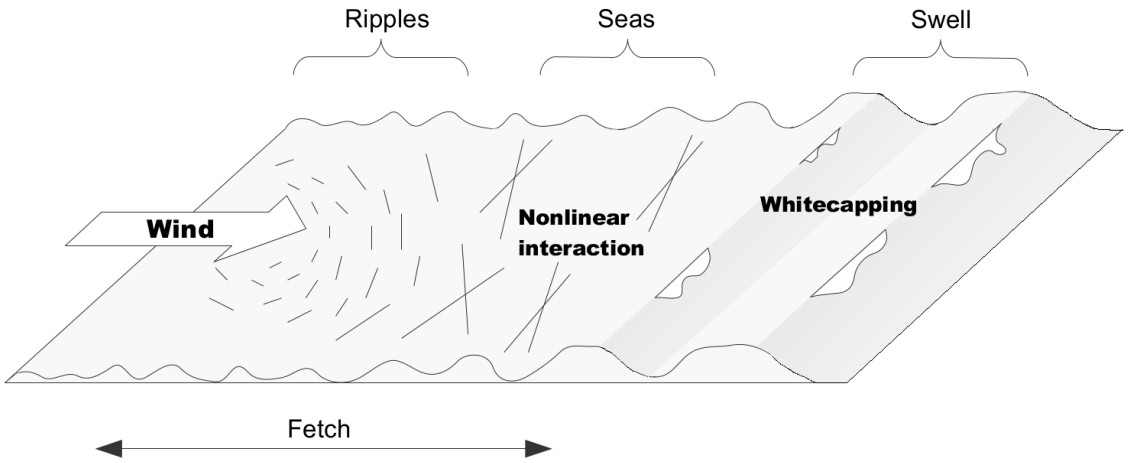

Figure 2.2: Main physical processes affecting waves in deep water (principle sketch).

this condition is called *fully-developed sea*. Waves leaving the area of wave generation by wind become regular and long-crested, this sea state is called *swell* (Fig. 2.2).

The initial generation of waves on the water surface is certainly caused by the wind flow, but the real interaction mechanism between water and airflow is still not well understood. However, this shortcoming is not very important to predict accurately the development of waves over the seas, since the energy implicated in this process is significant lower than the other wave processes. The initial (or linear) wave growth is usually implemented in numerical wave models by means of the empirical expression of Cavaleri and Rizzoli (1981).

When ripples are generated, waves continue to develop due to the air pressure induced by the wind on the water surface. Miles (1957) proposed a model in which the air pressure reaches its maximum on the windward side of the crest (where the water surface is moving down), and its minimum on the leeward side of the crest (when water surface is moving up). The resonance between air pressure and water surface motion transfers energy to waves. This mechanism becomes more efficient when waves are higher and thus, the wave growth for a constant wind is exponential until the condition of fully-developed sea is reached. The formula proposed by Miles (1957) for the exponential wind input source term (S_{in}) is:

$$S_{\text{in}}(f,\,\theta) = \beta E(f,\,\theta) \tag{2.1}$$

in which the Miles parameter $\beta \sim [U_w \cos(\theta - \theta_w)/c]^2$, where U_w is a reference wind speed, θ is the angle of wave propagation, θ_w is the wind direction and c is the wave phase speed. However, the Miles' theory neglect the back-effect of waves on the sea-air boundary layer that modifies again the wind-induced pressure on the water surface.

Based on the Miles' resonance mechanism, the *quasi-linear* theory of Janssen (1991) includes the back-effect of waves on the sea-air boundary layer (coupled system). It is valid for high-frequency waves only, the effects of viscosity and air turbulence on the air-water interface being neglected. Janssen (1991) founds also that the aerodynamic drag over sea waves depends on the sea state, i.e. the aerodynamic drag for a young sea state was higher than for an old sea state. This confirms the exponential nature of the wave generation induced by wind. However, the physical mechanisms underlying the wave age dependence of the spectrum are not yet well-understood (Cavaleri et al., 2007).

To avoid the shortcomings of the theories based on Miles (1957), several studies on numerical modelling of the turbulent boundary layer flowing on the water surface have been carried out and models were proposed (e.g. Chalikov and Belevich, 1993; Chalikov and Makin, 1991). However, due to the lack of information about the vertical structure of this layer, the proposed models tend either to underestimate or overestimate the wave field.

The uncertainties highlighted for the wind generation theories are generally avoided by tuning the sink term due to whitecapping. This is the reason why the the wind input source term is usually coupled with the sink term due to whitecapping. Therefore, the most used parameterizations for coupled wind input and whitecapping source term are summarized in Table 2.1.

2.1.2 Energy dissipation due to "whitecapping" ($S_{\mathbf{ds}}$)

Wave breaking occurs when the orbital velocity at the wave crest approaches to the phase speed. In deep water, this process is usually called *whitecapping* (Fig. 2.3). Following Donelan and Yuan (1994), and Young and Babanin (2006), theoretical models of spectral dissipation due to whitecapping can be classified into four types:

- Whitecap models (e.g. Feng and Yeli, 1992; Yuan et al., 1986)
- Quasi-saturated models (e.g. Phillips, 1985)
- Probability models (e.g. Hasselmann, 1974)
- Turbulent models (e.g. Polnikov, 1993)

The first two classes of models attempt to relate the unstable wave state before incipient breaking to the energy dissipation due to wave breaking. The other classes relate the dissipation to the residual wave and turbulent features after wave breaking. None of the aforementioned classes of models deal with the dynamics of wave breaking, and all the theories lack experimental support or validation. However, the parameterizations summarised in Tab. 2.1 were developed starting from the aforementioned theories.

It is important to specify that the parameterizations in Tab. 2.1 have been validated by means of spectral models in combination with the Discrete Interaction Approximation (DIA) source term for nonlinear quadruplet interactions (see Subsec. 2.1.3). For example, the high-frequency dissipation term in TC parameterization is a tuning term to balance wind input and nonlinear interaction (DIA) source terms. Therefore, the use of a quadruplet source term different from DIA implies a new calibration and validation of the model.

Considering the remarks of Tab. 2.1, the most appropriate parameterizations for an operational model result TC and AR.

The TC source term consists of one input source term by wind (Chalikov and Belevich, 1993) based on the theory of Janssen (1991), and two dissipation terms. The first TC dissipation term represents the dominant low-frequency dissipation due to the *turbulence* induced by whitecapping:

$$S_{\mathrm{ds,l}}(f,\theta) = -2u_* h k^2 \phi\, E(f,\theta) \tag{2.2}$$

in which u_* is the wind friction velocity, h is the high-frequency energy waves and ϕ is an empirical function accounting for the development stage of the wave field (i.e. wave age). The function ϕ is composed by a linear part describing the dissipation for growing waves and a nonlinear part controlling the fully development conditions (Tolman and Chalikov, 1996). This dissipation term is strongly related with the wind input source term S_{in}, since the wind friction velocity u_* appears in Eq. (2.2).

Table 2.1: Main parameterizations for coupled wind input and whitecapping source term.

Methods	References	Description	Remarks
TC	Tolman and Chalikov (1996)	Wind input of Chalikov and Belevich (1993), low-frequency dissipation due to turbulence, and high-frequency dissipation.	Widely used. Negative biases of wave height are observed for short fetch.
ECWAM	Bidlot et al. (2005)	Wind input derived from Janssen (1991) and BJA dissipation term (Bidlot et al., 2005).	Implemented in the operational wave model WAM at the ECMWF. Positive biases for wave height are observed for long fetch.
AR	Ardhuin et al. (2010)	Wind input derived from Janssen (1991) and whitecapping of Ardhuin et al. (2010)	Improvement of ECWAM parameterization. Few comparisons with TC, especially for short fecth.
BYDZR	Rogers et al. (2012)	Recent developed formulation for wind input and whitecapping based on field observation.	Not extensively validated in operational wave modelling.

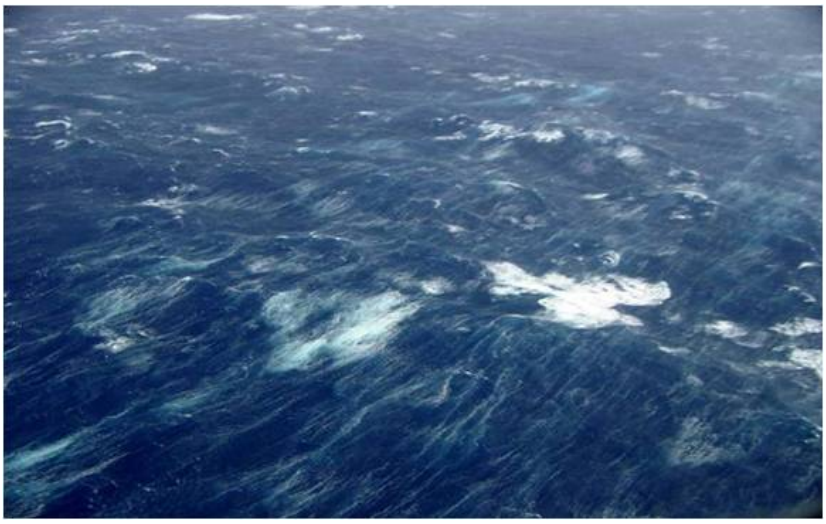

Figure 2.3: Wave breaking in deep water (*whitecapping*) (`http://homepages.see.leeds.ac.uk/~eardjs/work.html`).

The second TC dissipation term represents the empirical high-frequency dissipation defined as

$$S_{\mathrm{ds,h}}(f,\theta) = -a_0 \left(\frac{u_*}{g}\right)^2 f^3 \alpha_n^B E(f,\theta) \tag{2.3}$$

$$B = a_1 \left(\frac{f u_*}{g}\right)^{-a_2} \tag{2.4}$$

$$\alpha_n = \frac{\sigma^6}{c_g\, g^2 \alpha_r} \sum_0^{2\pi} E(f,\theta) d\theta \tag{2.5}$$

where α_n is Phillips' non-dimensional high-frequency energy level normalised with α_r, and where a_0, a_1, a_2, and α_r are empirical constants. This is a tuning term for the high-frequency energy designed to result in a consistent source term balance when combined with the wind input source term of Chalikov and Belevich (1993) and the nonlinear source term DIA (Hasselmann et al., 1985). The tuning term for the higher frequency of the energy spectrum is justified by the uncertainties of the other source terms (i.e. wind input and nonlinear interactions) for the development of this part of the energy spectrum. Thus, the TC total dissipation term is given by the sum of low- and high-frequency dissipation:

$$S_{\mathrm{ds}}(f,\theta) = S_{\mathrm{ds,h}}(f,\theta) + S_{\mathrm{bk,l}}(f,\theta) \tag{2.6}$$

The TC parameterization has the advantage that has been implemented in the spectral model WWIII (Tolman, 2015) during the last 20 years and it has been widely calibrated and validated. The shortcoming is represented by a general underestimation of significant wave height for short fetch conditions.

The AR parameterization is composed by a wind input source term derived from Janssen (1991) and two dissipation terms due to spontaneous and induced breaking, respectively.

The AR dissipation term due to spontaneous breaking is based on the saturation spectrum (see Banner et al., 2002):

$$S_{\mathrm{ds,sat}}(k,\theta) = \sigma \frac{C_{\mathrm{ds}}^{\mathrm{sat}}}{B_r^2} \{\delta_d \max\left[B(k) - B_r, 0\right]^2 + (1-\delta_d) \max\left[B'(k,\theta) - B_r, 0\right]^2\} E(k,\theta) \tag{2.7}$$

where $C_{\mathrm{ds}}^{\mathrm{sat}}$ is a dissipation constant, $B(k)$ is the saturation spectrum integrated over the all the direction proposed by van der Westhuysen (2007), B_r is a constant saturation threshold, and $B'(k,\theta)$ is the directional saturation spectrum proposed by Ardhuin et al. (2010). Therefore, the saturation-based term is composed by an isotropic part (i.e. the term that multiplies δ_d) and a part dependent from the wave direction (i.e. the term that multiplies $1-\delta_d$).

The AR dissipation term due to induced breaking (i.e. the cumulative breaking term $S_{\mathrm{bk,cu}}$) represents the smoothing of the surface by large scale breakers that wipe out smaller waves. Ardhuin et al. (2010) defined this term with a probability model. Thus, the total AR dissipation term is defined as the sum of the saturation-based term and the cumulative breaking term:

$$S_{\mathrm{ds}}(k,\theta) = S_{\mathrm{ds,sat}}(k,\theta) + S_{\mathrm{bk,cu}}(k,\theta) \tag{2.8}$$

The AR parameterization is an improvement of the ECWAM parameterization, but only a recent study of Mentaschi et al. (2015) have compared TC and AR. Mentaschi et al. (2015) have shown that both TC and AR result in negative biases for significant wave heights and periods. Moreover, results might be considerably dependent on the wind data used as input. Therefore, further research is needed.

2.1.3 Nonlinear quadruplet wave-wave interactions ($S_{\mathbf{nl4}}$)

The mechanism of nonlinear wave-wave interactions transfers energy among waves by resonance. As illustrated in Fig. 2.4, this mechanism, called *quadruplet*, occurs in deep water if the wave numbers and frequencies of the two corresponding diamond pattern A & B, which respectively result from the interaction between one pair of waves (waves 1 & 2) and another pair of waves (waves 3 & 4) match. The resonance conditions proposed by Hasselmann (1962) are:

$$\begin{aligned} \vec{k}_1 + \vec{k}_2 &= \vec{k}_3 + \vec{k}_4 \\ \sigma_1 + \sigma_2 &= \sigma_3 + \sigma_4 \end{aligned} \tag{2.9}$$

in which the intrinsic radian frequency σ_i and the wave number vectors $\vec{k}_i(k_x, k_y)$ (e.g. of waves 1, 2, 3 and 4 in Fig. 2.4) are related by the *linear dispersion relationship*:

$$\sigma^2 = gk \tanh(kd) \tag{2.10}$$

The effect of the quadruplet nonlinear interactions is to redistribute energy over the spectrum. As it shown in Figure 2.5, quadruplet interactions transfer a significant part of the energy due to the wind from mid-range to lower frequency of the spectrum, and a small part from mid-range to higher frequency. At high frequency, this energy is dissipated by "whitecapping" (a process included in S_{ds}; see Subsection 2.1.2), whereas at low frequency it is absorbed without any significant dissipation. Therefore, the growth of energy at low frequency causes a shifting of the peak of the spectrum to lower frequency. This process tends to stabilize any wave spectrum in a JONSWAP spectrum shape (Hasselmann et al., 1973).

Quadruplet nonlinear interactions are described in Hasselmann (1962, 1963a,b) in terms of wave action density $N(\vec{k}) = E(\vec{k})/\sigma$, where $E(\vec{k})$ is the wave energy density. The rate of change of $N(\vec{k})$ at a wave number $\vec{k}_1$ due to all nonlinear interactions involving $\vec{k}_1$ is given by the so-called *collision integral* (or Boltzmann integral). Due to its complexity, the computation for the full solution of the collision integral is very time consuming. For this reason, it cannot be incorporated in any operational wave models. Therefore, a number of approximations have been developed. In Table 2.2 are summarized the most known and used parameterization for quadruplet.

Nowadays, any comprehensive study to determine the best method for computing the nonlinear quadruplet wave-wave interactions has been performed. Gaps of knowledge appear in presence of multi-peaked spectra, i.e. slanting fetch, turning wind and mixed sea state (where a wind sea develops on top of a background swell). Moreover, the role of the nonlinear interactions in the propagation of swell over very long distance is still not well understood.

However, in conditions of relative short fetch, the DIA method assures good results and acceptable computational time. Furthermore, validations for the main wind input and whitecapping source terms have been conducted in combination with DIA.

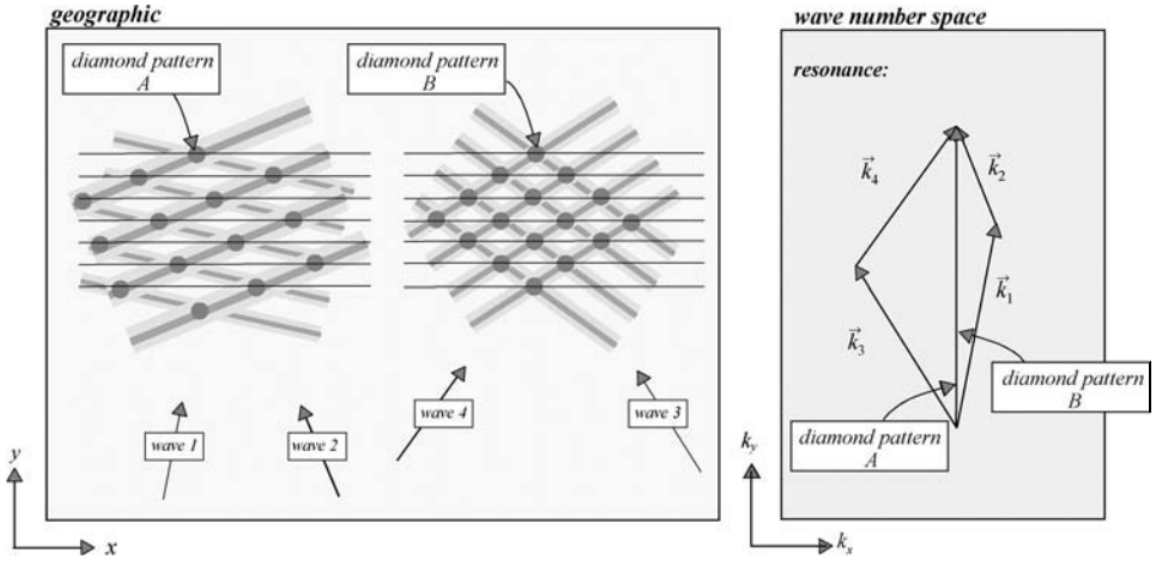

Figure 2.4: Quadruplet wave-wave interaction in deep water (Holthuijsen, 2007).

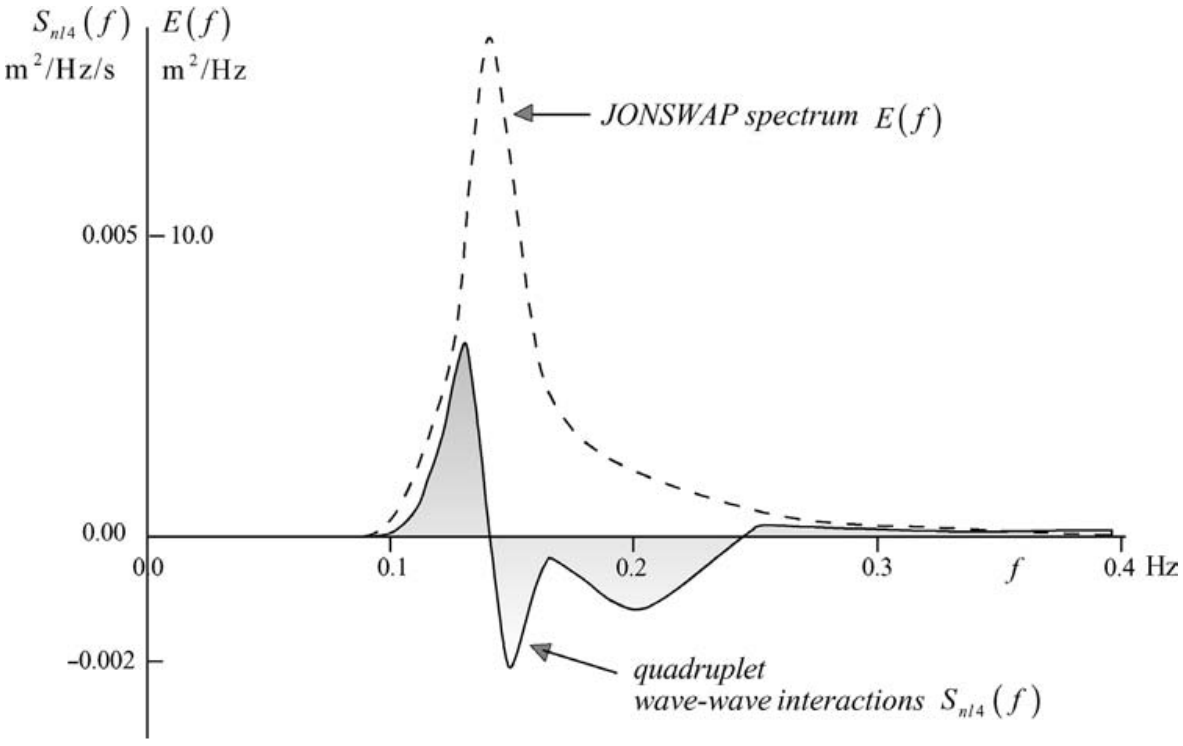

Figure 2.5: The source term for quadruplet wave-wave interactions (Holthuijsen, 2007).

Table 2.2: Main methods for solving the collision integral (quadruplet).

Method*	References	Remarks
DIA	Hasselmann et al. (1985).	Preserves important characteristic of the full solution. Computationally efficient.
GMD	Tolman (2013) and Tolman and Grumbine (2013).	Moderate improvement of the DIA method. Not yet completely validated.
WRT	Resio and Perrie (1991), Tracy and Resio (1982), van Vledder (2006), and Webb (1978).	Solves the original six-dimensional integral of Hasselmann (1962). Computationally expensive.
TSA	Perrie and Resio (2009) and Resio and Perrie (2008).	Significant improvement over the DIA. Reduces the computational time by a factor of 250 to 500 in respect to WRT. Not yet implemented in any operating numerical model.

* Legend: DIA = Discrete Interaction Approximation, GMD = Generalized Multiple DIA, WRT = Webb-Resio-Tracy, TSA = Two-scale approximation.

1. Deep water processes are relevant on a spatial scale from tens to thousands of kilometres. Modelling waves at this scale is computationally feasible by means of spectral models only, which describe the evolution of the wave field through the variation of the energy density spectrum in time and space.

2. Deep water processes are generally presented as source or sink terms representing the effect of each physical process on the wave energy spectrum.

3. Wind input source term (S_{in}) and whitecapping sink term (S_{ds}) are usually calibrated and validated as a unique parameterization ($S_{\text{in}}+S_{\text{ds}}$). Among the presented source terms, TC and AR resulted the most interesting for practical applications. However, both source terms show negative biases for significant wave heights and periods.

4. Quadruplet nonlinear interactions cause a shifting of the frequency peak of the wave spectrum from the mid-range to lower frequencies. This phenomenon is generally computed by means of the *collision integral*. Since its solution is computationally expensive, an approximation is needed. The Discrete Interaction Approximation (DIA) method provides a good compromise between accuracy and computational cost. Furthermore, DIA has been used as the reference term for quadruplet nonlinear interactions during the calibration and validation of the main $S_{\text{in}} + S_{\text{ds}}$ source terms.

2.2 Intermediate and shallow water waves

The main processes affecting sea waves in intermediate and shallow water are summarised as follows:

- Nonlinear triad wave-wave interactions
- Dissipation due to bottom friction

- Shoaling
- Refraction
- Reflection
- Diffraction
- Depth-induced breaking

All the processes are due to the interaction of waves with the ocean floor, except wave reflection and diffraction those are due to the interaction of waves with natural or artificial obstacles, and they can occur also in deep water. Depth-induced breaking is treated in Section 2.3 (i.e. Nearshore processes) since this wave process is strictly related with hydrodynamics and morphodynamics of the nearshore zone.

The aforementioned processes become relevant when waves approach on the continental shelf, which usually has an extension variable from 10 to 200 kilometres. For computational reason, this scale implies the use of a spectral model. Therefore, the formulations described in the following subsections are already implemented in at least one spectral model.

2.2.1 Nonlinear triad wave-wave interactions ($S_{\mathbf{nl3}}$)

When sea waves propagate from deep to shallow water, frequency dispersion diminishes and nonlinear wave-wave interactions evolve from cubic resonance (quadruplet) to quadratic near resonance (triad). This transition produces a change in the dispersion relation (Eq. 2.10), from a frequency dispersive regime to a frequency non-dispersive regime, where all wave components of the same amplitude travel with the same speed. Therefore, nonlinear triad interactions occurs only in very shallow water, where waves are non-dispersive.

The resonance conditions in shallow water occur between three wave components as presented in Nwogu (1994):

$$\begin{aligned} \vec{k}_1 + \vec{k}_2 &= \vec{k}_3 \\ \sigma_1 + \sigma_2 &= \sigma_3. \end{aligned} \tag{2.11}$$

An example of triad nonlinear interactions is the *self-self* interaction, that occurs when a unidirectional harmonic wave interacts with itself ($\sigma_1 = \sigma_2$) to create a second harmonic at twice its frequency ($\sigma_3 = 2\sigma_1$). The effect of the self-self interaction is that waves entering in shallow water transform their shape from quasi-sinusoidal to sharper crests and flatter troughs.

The magnitude of the energy transferred between the three wave components (*triad*) can be quantified with the biphase model $\beta_{1.2}$ (Holthuijsen, 2007):

$$\beta_{1.2} = \alpha_1 + \alpha_2 - \alpha_3 \tag{2.12}$$

where α_1, α_2 and $\alpha_3 = \alpha_1 + \alpha_2$ are the phases of the three interacting wave components. Since the biphase depends on the evolution of the wave energy and vice versa, triad wave-wave interactions are determined by means of a coupled model for the biphase and for the wave energy.

Nowadays, the most frequently formulation used in operational model is the lumped-triad approximation (LTA) of Eldeberky (1996). This method estimates the biphase from the spectrum and the local water depth, without a biphase evolution equation. The LTA method ensures that energy is always transported to higher frequencies and that no restitution of energy to lower frequency occurs. This simple approximation for triad wave-wave interactions seems to give reasonable results until the offshore edge of the surf zone, since in the surf zone it is proved that triad interactions transfer energy also at lower frequency (creating infra-gravity waves).

2.2.2 Wave dissipation due to bottom friction ($S_{\mathbf{bfr}}$)

When waves reach shallower water and interact with the bottom, the dominant dissipation mechanism is the bottom friction. Bottom friction occurs in a relatively thin layer, compared with the water depth, where water particles switch from orbital motion to turbulent motion. The rate of energy transferred from the orbital motion of the water particles to the turbulent bottom layer depend on the characteristic of the wave field and bottom. Mirfenderesk and Young (2003) expressed this quantity of energy (at wave number k) as:

$$S_{\mathrm{bfr}}(k) = -\overline{\tau_b u_{\mathrm{bk}}} \tag{2.13}$$

in which τ_b is the bed shear stress and u_{bk} is the orbital velocity of the wave with wave number k. However, it is not easy to determine the values of the parameters τ_b and u_{bk}. Reliable values are only obtained in laboratory conditions. Therefore, a general form of the sink term for dissipation due to bottom friction can be obtained directly from the wave energy $E(f, \theta)$

$$S_{\mathrm{bfr}}(f,\, \theta) = -C_f \frac{k}{\sinh{(2kd)}} E(f, \theta) \tag{2.14}$$

where C_f is the dissipation coefficient. Several formulation of the dissipation coefficient were developed (e.g. Bouws and Komen, 1983; Collins, 1972; Hasselmann and Collins, 1968; Madsen et al., 1988), but it is not clear which is the most accurate.

However, this term is relevant only in quite shallow water and the choice of C_f is strictly dependent on the nature of the bottom substrate (e.g. mud, rocks, sand, algae or marine plants). Therefore, the dissipation coefficient C_f is site specific and a calibration is needed for nearshore applications.

The effect of the bottom dissipation on the spectrum energy is to dissipate energy in the peak and intermediate frequency, whereas no significant modification is observed for higher frequency (see Fig. 2.6).

2.2.3 Wave shoaling

The variation of the wave height in the direction of propagation due to a changing in the group velocity is called *shoaling*. In fact, when waves propagate into shallow water, the phase speed c approaches to the group velocity c_g and waves become *less dispersive*. The physical effect of shoaling over a flat sloping bottom is that waves interacting with the bottom initially decrease their height, but then continuing to propagate into shallow water the wave height increases. In spectral wave models, this phenomenon can be accounted in the nonlinear triad parameterization.

2.2.4 Wave refraction

The shifting of the wave direction in according to the pattern of depth contours is called *refraction*. This phenomenon is due to the variation of the phase speed along the wave crest, when the water depth varies along the wave crest. In fact, waves turn towards the region of shallower water, where the phase speed decreases.

Figure 2.7 shows an example of refracting waves analysis by means of a graphical method for regular waves (wave refraction diagram). The solid line arrows represent the wave rays those indicate the direction of wave propagation. In deep water or in water with constant depth, the distance between rays remain constant, but approaching to the shoreline the rays converge or diverge depending on the local bottom features.

Spectral models account the phenomenon of refraction in the spectral propagation terms of the balance equation (Eq. 3.4).

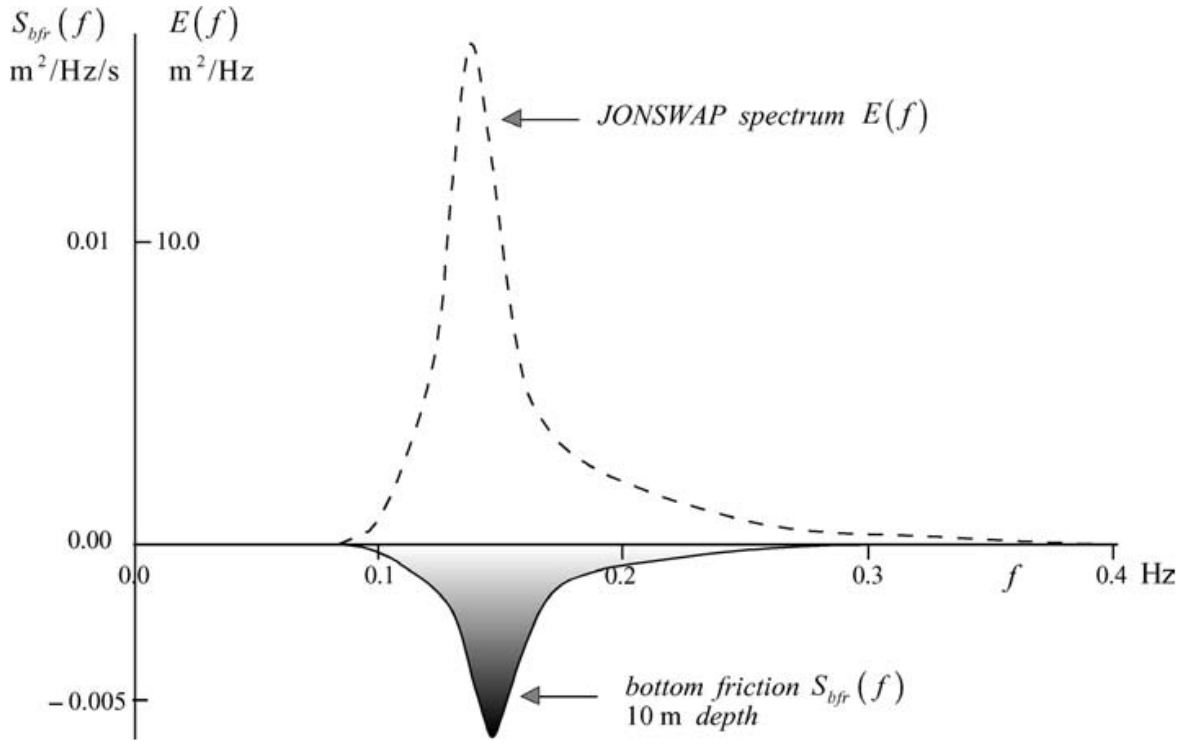

Figure 2.6: The sink term for bottom friction (Holthuijsen, 2007).

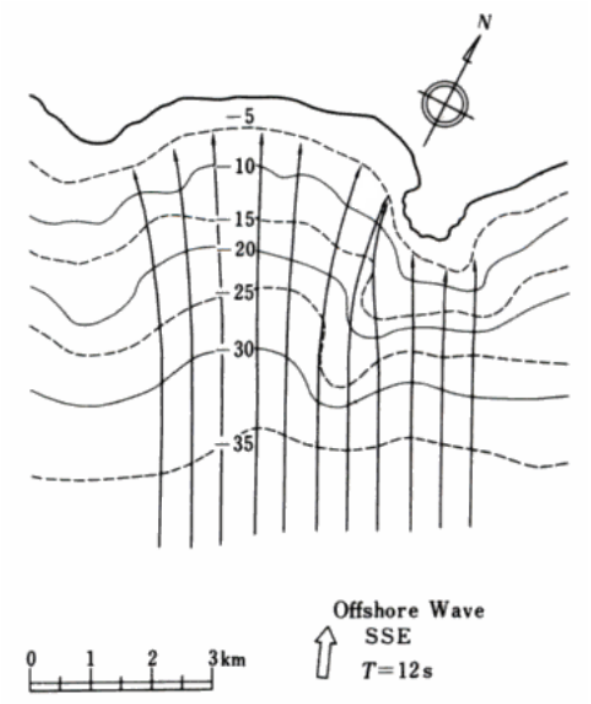

Figure 2.7: Refraction diagram of regular waves (Goda, 2000).

2.2.5 Wave reflection

When waves approach the shoreline, they can encounter different kind of coast, e.g. beaches, cliffs, man-made structures. Each kind of coastline reflects waves with different rates, for example a cliff can reflect the total of wave energy, whereas a beach with a gentle slope will barely reflect energy. The coefficient of wave reflection K_R is given by the ratio of reflected wave height H_R to incident wave height H_I:

$$K_R = H_R/H_I \tag{2.15}$$

In spectral wave wave models, wave reflection is possible only for small K_R coefficients, since it is simply treated as diffusion of the incident energy over different directions. However, the study of wave reflection over vertical structure (i.e. higher values of K_R) is not an objective of the present PhD thesis.

2.2.6 Wave diffraction

When waves travelling through the ocean encounter an obstacle such as breakwater, small island, or headland, they propagate around that obstacle in the shadow area and their amplitude vary rapidly in the horizontal space.

Some spectral models (e.g. SWAN) can be qualitatively represent this phenomenon. In cases where diffraction is the dominant processes (e.g. harbour, gap in a breakwater), phase-resolving models are necessary. However, the study of situations in which diffraction is the dominant process is not an objective of the present PhD.

1. Intermediate and shallow water processes modify waves approaching on the continental shelf, which usually has an extension variable from 10 to 200 kilometres. For computational limitations, this scale implies the use of a spectral model.
2. Nonlinear triad interactions transform wave entering in shallow water from quasy-sinusoidal shape to sharper crest and flatter trough shape (shoaling). The only formulation for triad implemented in current spectral models is the LTA.
3. The behaviour of the different formulations for bottom friction still needs to be clarified. The tuning of this term can be used to calibrate the model where bottom friction has a dominant role.
4. In spectral models, wave refraction is represented as a term of the action balance equation.
5. Spectral models are unable to well simulate strong wave diffraction and reflection. However, the study of cases where these processes are dominant lie outside the objective of the present study.

2.3 Nearshore processes

The term *nearshore* indicates the last portion of the sea next to the shore (see Fig. 2.8). It includes the zone where waves start to break induced by the bottom (i.e. the breaker zone), the zone where the breaking waves continue to move onshore (i.e. the surf zone), and the zone where waves cause a variation of the water level on the beach (i.e. the swash zone). The limits among the nearshore zones are not fixed and depend on the characteristics of the incident waves (i.e. wave height, wavelength and wave shape).

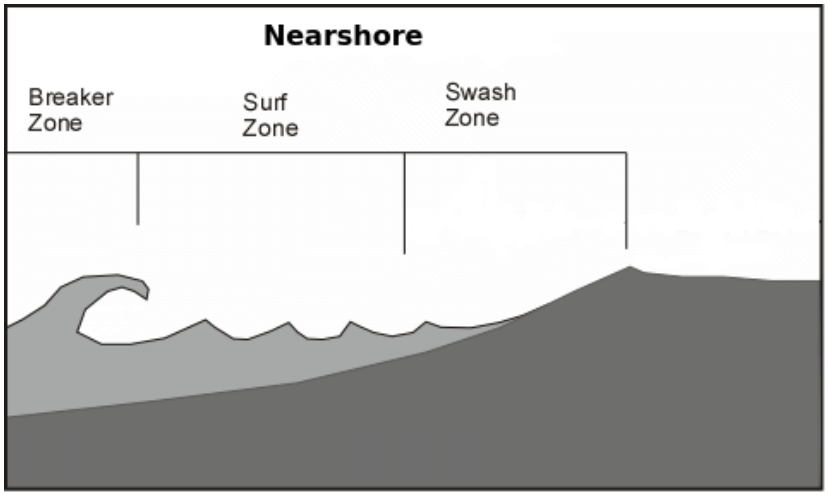

Figure 2.8: The nearshore, with the breaker zone, the surf zone, and the swash zone (modified from `www.tulane.edu`).

The dominant wave process in the nearshore is *breaking*, which activates nearshore currents and sediment transport, with a consequent modification of the seabed and shoreline. These processes are strictly connected, since the modification of the bathymetry implies a possible cross-shore shifting of the breaker zone and thus, modifying nearshore currents and sediment transport. The aforementioned nearshore system is summarised in Fig. 2.9.

In the prospective of operational modelling, that is one of the objectives of the present research, the use of a nearshore model (i.e. a model able to properly simulate the system of Fig. 2.9) is suggested only in the area where there are effective modifications of the bathymetry. This choice is justified by the overall high computational demand of nearshore models. Therefore, for the aim of the present research, the nearshore zone is intended as the area limited offshore by the closure depth, where the latter is defined (for a given time on interval) as the most landward depth seaward of which there is no significant change in bottom elevation, and no significant net sediment transport occurs between the nearshore and the offshore (Kraus et al., 1998).

2.3.1 Wave breaking ($S_{\mathbf{br}}$)

The physics of wave breaking induced by depth is very complex and not yet well understood. However, it can be defined as the process limiting wave height in shallow water.

The most known formulation for depth-induced wave breaking was developed by Battjes and Janssen (1978). The dissipation rate is estimated utilizing a turbulent bore model, while the breaking probability is estimated by means of a Rayleigh distribution of wave height with an upper cut-off determined by the local depth. This simplified model defines for each depth d a maximum possible wave height $H_{\max}$. The mean dissipation rate per area (integrated over all frequencies and direction) proposed by Battjes and Janssen (1978) is

$$\bar{D}_{\mathrm{br}} = -\frac{1}{4}\alpha_{\mathrm{BJ}} Q_b \bar{f}_0 \rho g H_{\max}^2 \tag{2.16}$$

where Q_b is the probability of breaking at a given point, $\bar{f}_0$ is the mean zero-crossing frequency of the breaking waves and α_{BJ} (breaker index) is a constant of order one.

The mean dissipation $\bar{D}_{\mathrm{br}}$ barely affects the shape of the wave energy spectrum (see Fig. 2.10). Therefore, the related dissipation term is proportional to the energy spectrum $E(f,\theta)$ (Holthuijsen, 2007):

$$S_{\mathrm{br}}(f,\theta) = \bar{D}_{\mathrm{br}} E(f,\theta)/m_0 \tag{2.17}$$

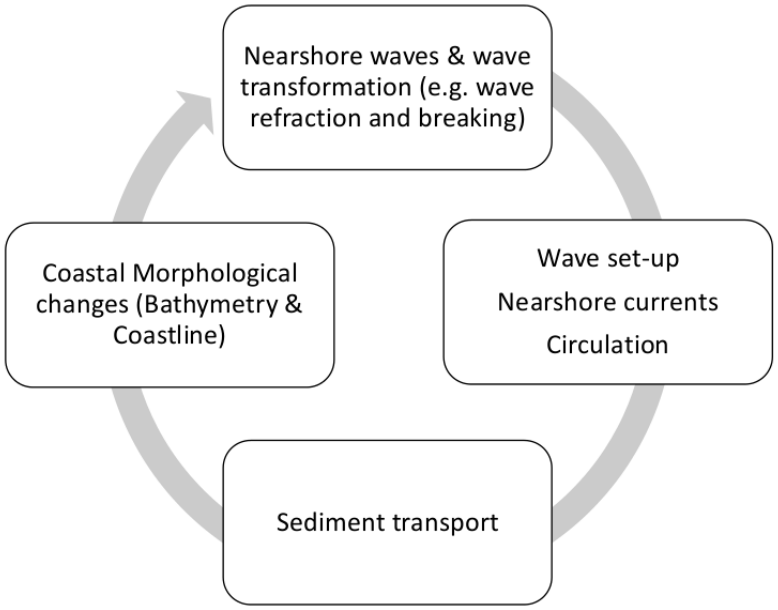

Figure 2.9: Flow chart summarizing the nearshore processes producing morphological changes.

where m_0 is the zero-order moment of $E(f, \theta)$:

$$m_o = \int_0^\infty E(f)\, df \tag{2.18}$$

During the years, several authors proposed different formulations for Q_b and $\bar{D}_{\mathrm{br}}$ (e.g. Baldock et al., 1998; Daly et al., 2010; Janssen and Battjes, 2007; Roelvink, 1993), but none of them have improved the physics representation of a breaking wave. No comparison between the different formulations has been conducted yet. However, the aforementioned formulations provide a good quantitatively representation of wave breaking, resulting in a shape-conserving dissipation of the wave energy spectrum in the surf zone. For the aim of the present research, this quantitative analysis is sufficient for a good estimation of the wave energy spectrum in order to model hydro- and morphodynamics processes.

2.3.2 Hydrodynamics processes

The wave processes summarised in the previous sections are mainly described by means of wave energy transport and transformation. However, waves also transport momentum, which is defined as the radiation stress (Longuet-Higgins and Stewart, 1964). Nearshore, in particular in the surf zone, the horizontal gradient of the radiation stress generates currents and changes in the mean sea level.

Radiation stress

The flux of momentum is formed by two contributions, the first due to the wave-induced velocities of the water particles and the second due to the hydrostatic pressure (Fredsøe and Deigaard, 1992). The components of the *radiation stress* (S_{xx}, S_{xy}, S_{yy}) can be calculated from the wave energy spectrum $E(f)$.

Water set-up

The water set-up induced by waves is a phenomenon on a horizontal scale larger than a wave period. Wave-breaking in the surf zone leads in a decreasing of the radiation stress

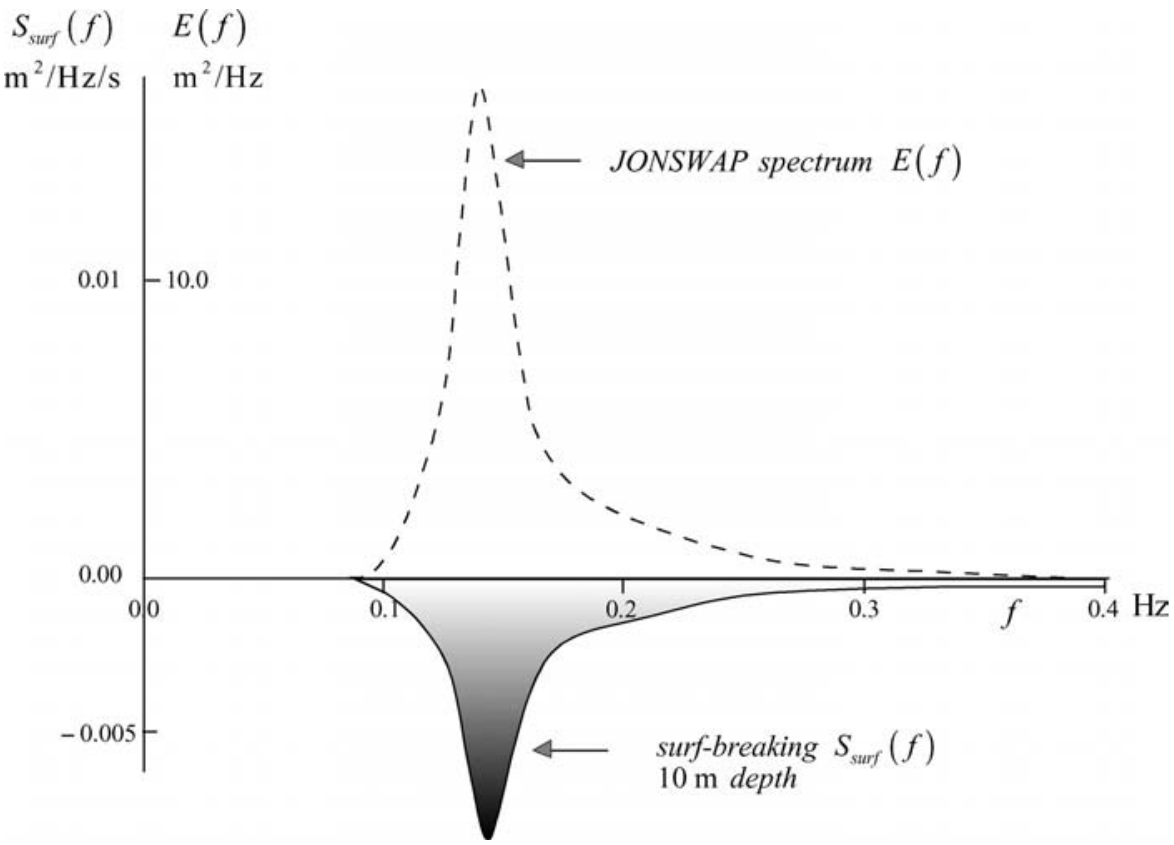

Figure 2.10: The dissipation term for depth-induced breaking (Holthuijsen, 2007).

in the shore direction. This gradient is balanced by changes in the level of the mean water surface (Fig. 2.11).

The momentum balance equation is given by

$$\frac{dS_{xx}}{dx} = -\rho g D \frac{d\bar{\eta}}{dx} \tag{2.19}$$

Eq. (2.19) implies that if the radiation stress gradient is positive ($dS_{xx}/dx > 0$), the slope of the mean surface $\bar{\eta}$ is negative ($d\bar{\eta}/dx < 0$) giving in a *set-down*, whereas if the radiation stress in negative ($dS_{xx}/dx < 0$), the slope of the mean surface is positive ($d\bar{\eta}/dx > 0$) giving in a *set-up* (Holthuijsen, 2007).

In the surf zone, wave-breaking causes a prevalent onshore flow. In order to balance this onshore discharge of water, an offshore flux of water is necessary. Since the onshore flow due to wave breaking is dominant near the mean water level, the offshore flow reaches its maximum at the bottom. This offshore near-bed flux is called *undertow*.

Circulation

The change of the flux of momentum toward the shore is usually not totally balanced by a pressure gradient from a sloping mean surface as described in the previous subsubsection (Fredsøe and Deigaard, 1992). Therefore, a shear stress associated with a mean current is necessary to balance the flux of momentum. One of the most studied current phenomenon occurs when wave direction is not normal to the shore, resulting in a current propagates parallel along the shoreline (*longshore current*).

The current dynamics can be strongly modified by irregularities in the cross-shore profile. Generally, the sandbar developing along the coast is interrupted by cross-shore rip channel. Therefore, the wave-breaking induced by the sandbar results less intense in the rip channel

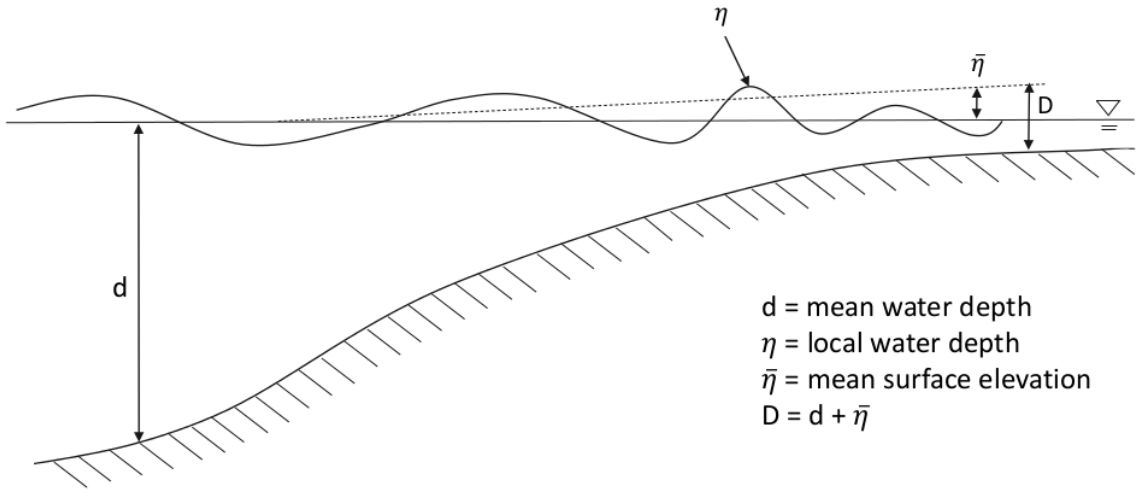

Figure 2.11: Sketch illustrating the different water levels.

due to higher water depth. Hence, the breaking induced water set-up inshore of the bar is balanced by an offshore flux in the rip channel (i.e. *rip current*).

The main methods for the calculation of velocity component are summarised in Table 2.3.

2.3.3 Morphodynamics processes

Sediment transport are mainly forced by waves and currents. Longshore currents transport the sediment along the coast, determining the development of the coastline, whereas cross-shore currents causes a net sediment transport in the wave direction, determining the beach profile. In the surf zone, waves produce also an offshore undertow velocity near the bottom, that may cause an offshore sediment flow affecting the beach profile as well.

Hence, the transport of sediment produces changes in the bathymetry and in the evolution of the coastline, and thus a modification of the nearshore wave dynamics, e.g. wave breaking, radiation stress and wave-induced currents (Fig. 2.9).

The sediment transport can be defined as the sum of three processes (Fredsøe and Deigaard, 1992):

- Wash load
- Suspended load
- Bed load

Table 2.3: Equations for the calculation of velocity component implemented in numerical modelling.

Method*	References	Remarks
BT	Chen (2006)	Implemented in FUNWAVE
GLM	Andrews and McIntyre (1978) and Walstra et al. (2000)	Implemented in XBeach
NLSW	Zijlema et al. (2011)	Implemented in SWASH
RANS	Warner et al. (2008b)	Implemented in ROMS

* Legend: BT = Boussinesq-type equations, GLM = Generalised Lagrangian Mean, NLSW = Nonlinear Shallow Water equations, RANS = Reynolds Averaged Navier-Stokes equations.

The *wash load* is represented by very fine sediment particles (< 0.06 mm) suspended in the water and usually not included in the "total sediment discharge". Therefore, the total sediment load is given mainly by two contribution: suspended and bed load. The *suspended load* is the contribution due to the sediment particles transported without contact with the bed due to the agitation of water turbulence. The *bed load* is the contribution due to the sediment particles in contact with the bed, transported by rolling, sliding or jumping. Bed and suspended load transport non-cohesive sediment only, i.e. the particles ranging from sand (0.06 mm to 2mm) to gravel (2 mm to 20 mm).

Sediment particles start to move over the seabed when the forces due to waves and/or currents exceed the threshold of motion. The threshold of motion is usually expressed in terms of critical bed shear-stress.

1. In the framework of the present research, the processes affecting the seabed and shoreline are classified as nearshore processes.
2. The dominant wave process in the nearshore is wave breaking. Its physics is not well understood, but it is generally implemented in the current wave models with source term based on statistical parameters. These models assure only a quantitative representation of the energy dissipated during the depth-induced breaking that is sufficient for the aim of the present research.
3. The momentum flux induced by waves is defined as *radiation stress*. The horizontal gradient of the radiation stress generates currents and changes in the mean sea level.
4. The main wave-induced currents are the *longshore current*, the *rip current* and the *undertow*.
5. These processes lead the sediment transport, which is the main cause of changes of seabed and shoreline.
6. There is an iterative process between waves inducing nearshore currents driving sediment transport, and bathymetry changes that affect wave processes such as wave shoaling, wave refraction and wave breaking.

2.4 Review and discussion of available models

Several models have been developed and implemented in operational wave modelling by institutes, universities, private company, etc. These models differ in physics, numerical solutions

Table 2.4: Sediment transport formulations implemented in common models.

References	Remarks
Soulsby (1997) and van Rijn (1984)	Implemented in XBeach. Consider the same critical velocity of motion U_{cr} for waves and currents.
van Thiel de Vries (2009) and van Rijn (2007a,b)	Implemented in XBeach. Two separate U_{cr} are considered for waves and currents.
Soulsby and Damgaard (2005)	Implemented in ROMS. Suitable also for coarse materials.

and range of application areas (offshore, nearshore, harbours, etc.). The most used wave models by oceanographers, coastal engineers or scientists are listed in Table 2.5. The column "type" of Tab. 2.5 indicates the governing equations of the models, as explained in the footnotes.

For the selection of the most suitable models in the present study, the current wave models will be evaluated using the following seven criteria:

1. Code with open source licence
2. Appropriateness of the implemented physics
3. Efficiency of numerical schemes
4. Easiness of nesting with other models
5. Number, expertise and experience of developers
6. Size and type of the users' community
7. Applicability to the present research

An open source code is necessary to eventually improve (or optimize) the code of the software according to the purpose of the present study. Furthermore, an open source code represents the spirit of academy research (transparency) rather than a (closed) software with proprietary licence.

The appropriateness of the implementation of the physics in the model is crucial because it is strictly related with the reliability of the results. The physics of the models is evaluated on the basis of the governing equations.

The numerical schemes adopted in the different models define the accuracy of the results and also the computational time of the algorithms. The computational time and efficiency are fundamental for any operational model.

The property of a model to be easily nested in others models with different range of application is very important in order to achieve the purpose of building a consistent operational numerical model system.

The term "easy nesting" means:

- The source code must be written in a language common to the majority of the models (e.g. Fortran)
- The openness of the source code that allows the nesting between models
- The availability of previous experience/studies using the model nested with other models

The expertise and experience of the developers of the source code guarantee frequently new releases of the software package, up-to-date with the state of the art of physics and numerical schemes.

A large community of users guarantees an extensive literature and implementations of the model.

The applicability of the models in the present research is evaluated considering:

- The accuracy of the physics in relation to deep and intermediate/shallow water processes, and nearshore processes
- The computational time and efficiency of the models applied to deep and intermediate/shallow water waves, and nearshore processes

Table 2.5: Most relevant wave model types available and web links.

Model name	Type*	Licensed	Website
BOUSS-2D	BT	Yes	http://www.aquaveo.com/software/sms-bouss2d
CGWAVE	MS	Yes	http://www.aquaveo.com/software/sms-cgwave
COULWAVE	NLSW + BT	No	http://isec.nacse.org/models/coulwave_faq.php
Delft3D WAVE**	AB	No	http://oss.deltares.nl/web/delft3d/home
FUNWAVE	BT	No	http://chinacat.coastal.udel.edu/programs/funwave/funwave.html
MIKE21	AB	Yes	http://www.mikebydhi.com/
MOHID**	WR + BT	No	http://www.mohid.com/
REF/DIF	MS	No	http://chinacat.coastal.udel.edu/programs/refdif/refdif.html
ROMS**	AB + BT	No	http://www.myroms.org/
SPHysics	SPH	No	https://wiki.manchester.ac.uk/sphysics/index.php/Main_Page
STWAVE	AB	No	http://chl.erdc.usace.army.mil/chl.aspx?p=s&a=software;9
SWAN	AB	No	http://swanmodel.sourceforge.net/
SWASH	NLSW	No	http://swash.sourceforge.net
TOMAWAC	AB	No	http://www.opentelemac.org/
WAM	AB	N.d.	N.d.
WAVEWATCH III	AB	No	http://polar.ncep.noaa.gov/waves/wavewatch/
XBeach**	AB + NLSW	No	https://oss.deltares.nl/web/xbeach/

* Type legend: BT = Boussinesq type equations, MS = Mild slope equation, NLSW = Nonlinear Shallow Water equations, AB = Action balance equation, WR = Semiempirical wind-wave relationships, SPH = Smoothed Particle Hydrodynamics.
** Includes also formulations for sediment transport.

Therefore, the column "Applicability" in Table 2.6 specifies the suitability of the model for deep water (DW), intermediate/shallow water (ISW), or nearshore (NS) applications.

As shown in the third column of Tab. 2.5, the wave models MIKE21, BOUSS-2D and CGWAVE are distributed with commercial licence. Though WAM was the first wave models of the third generation developed (WAMDI Group, 1988) and used by a large part of researchers, nowadays the code is maintained and developed by some institutes (e.g. ECMWF, KNMI) or private companies (e.g. Mike21 by DHI). Therefore, the aforementioned models have been excluded *a priori* from the evaluation.

The evaluation matrix illustrated in Tab. 2.6 is drawn on the basis of the technical manual of the models, the official website of the models and several scientific papers. Manuals and scientific papers are summarized in Tab. 2.7 and website addresses are listed in Tab. 2.5.

The highest scores in physics have been assigned to the phase-resolving models, describing the evolution of the water surface for each individual waves. For relatively large scale (i.e. more than 10-15 wavelength), it is not realistic the application of this type of models, and spectral models become the alternative. For this reason, phase-resolving models have been gathered in the category of Applicability (criterion 7, see Tab. 2.6) NS (for weakly-dispersive models) or ISW (for fully-dispersive models). Otherwise, spectral models have been gathered in the category DW and ISW.

Among DW models, TOMAWAC and WAVEWATCH III (hereafter WWIII) have been obtained the best scores. However, due to the big community of developers, WWIII implements the most recently formulations for deep water source terms (see Sec. 2.1). Furthermore, a new version of WWIII software package is released with about two-years frequency, assuring an up-to-date software.

WWIII accounts for ISW source terms (see Sec. 2.2) as well, but the employment of explicit schemes (fixed time step) makes WWIII unsuitable for coastal applications, where the use of high resolution grids is required. Therefore, a model like SWAN that implements implicit numerical schemes (variable time step) is more appropriate for ISW applications.

ROMS and Delft3D are comprehensive software packages, which include several modules (e.g. circulation, sediment transport, biogeochemical diffusion). In particular, ROMS is a framework of open source models, with modules that allow the user to couple the atmospheric, ocean circulation and wave models. Delft3D is a software able to couple different models, but currently only few of them are open source. The module for waves simulation is SWAN-based for both models. Since the present work represents a first effort toward the building of a wave model system, the focus is on the modelling of wave processes at different scales. Therefore, the use of a software composed of several coupled multi-physics models falls outside the scope of the present research. Thus, ROMS and Delft3D have been excluded from the final choice. However, the two models may be evaluated for future research since the excellent scores obtained in Tab. 2.6.

Among NS models (see Tab. 2.6), SPHysics seems to be very time-consuming and its use is excluded from this study. SWASH and XBeach are very similar in the part of the code related with NLSW equations. The advantage of XBeach is that it has the possibility of using also the AB equation instead of NLSW equations for simulating waves. This can lead to a speed up of the simulation. Furthermore, XBeach implements a coupling between the wave model, the NLSW equation model for hydrodynamics processes, and the advection-diffusion equation model for sediment transport. As discussed in Section 2.3, sediment transport processes are essential to achieve the objective of this study.

Considering the evaluation matrix of Tab. 2.6 and the relative discussion, WW3 has emerged as the best option to simulate waves in open ocean, SWAN for the propagation of deep water waves in intermediate/shallow water, and XBeach for simulating nearshore processes. Moreover, all of the selected models are written in Fortran 90 language that could facilitate modifications of the source code.

Table 2.6: Evaluation matrix of wave models. Scale: ● → best, ○ → worst.

Models	2. Physics	3. Numerics	4. Nesting	5. Developers	6. Users	7. Applicability*	**Score**
COULWAVE	◕	◕	◔	◒	◔	ISW	●●◒
Delft3D	◒	●	●	●	◕	ISW	●●●●◔
FUNWAVE	◕	◕	◔	◒	◒	ISW	●●◕
MOHID	◔	◔	●	◔	○	DW	●◕
REF/DIF	◒	◒	◔	◒	◔	ISW	●●
ROMS	◒	●	●	●	◒	ISW	●●●●
SPHysics	◕	◕	◒	◕	◒	NS	●●●◔
STWAVE	◒	◒	◒	◕	◒	ISW	●●◕
SWAN	◒	●	◕	●	●	ISW	●●●●◔
SWASH	◕	●	◒	◕	◒	NS	●●●◒
TOMAWAC	◒	●	◕	◕	◒	DW	●●●◒
WAVEWATCH III	◒	●	◒	●	●	DW	●●●●
XBeach	◕	●	◒	●	●	NS	●●●●◔

* Applicability legend: DW = Deep Water, ISW = Intermediate-Shallow Water, NS = Nearshore.

Table 2.7: List of references screened for the evaluation of the models.

Author-Year	Remarks
Abanades et al. (2014a)	Nesting of two SWAN grids plus one nearshore XBeach grid in Cornwall.
Abanades et al. (2014b)	Nesting of two SWAN grids plus nearshore XBeach beach profiles in Cornwall.
Breivik et al. (2009)	Nesting a series of telescoping grids using WAM and SWAN in order to simulate nearshore wave field in the Southwest of Norway.
Chini et al. (2010)	Application of TOMAWAC coupled with a surge model in East Anglia (England).
Deltares (2014)	Delf3D-WAVE User Manual.
EDF (2011)	TOMAWAC user manual.
Gomez-Gesteira et al. (2010)	SPHysics user manual.
Gomez-Gesteira et al. (2012b)	Theory and formulations of the model SPHysics.
Gomez-Gesteira et al. (2012a)	Validation of the model SPHysics.
Gonçalves et al. (2012)	Evaluation of the wave models SWAN and STWAVE in shallow water using nested schemes.
Kirby and Dalrymple (1994)	REF/DIF user manual.
Kirby (2003)	Presentation and validation of a wave/hydrodynamic model based on Boussinesq-type equation.
Lynett et al. (2008)	COULWAVE user manual.
Massey et al. (2011)	STWAVE user manual.
Mendonça et al. (2009)	Coastal application of FUNWAVE in São Pedro do Estoril, Portugal.
Rusu and Guedes Soares (2013)	Coastal application (Portugal) of SWAN forced with boundary conditions obtained from WAM. Moreover, REFDEF and FUNWAVE were compared in two nearshore areas, forced with boundary conditions obtained from SWAN.
Shi et al. (2013)	FUNWAVE user manual.
The SWAN Team (2016a)	Description of physics and numerics of SWAN.
The SWAN Team (2016c)	SWAN user manual.
SWASH Team (2014)	SWASH user Manual.
Tolman et al. (2013)	Describe the project entitled "Improving Wind Wave Prediction: Global to Regional Scales", with a state of the science of operational wave modelling.
Tolman (2014)	User manual and system documentation of WAVEWATCH III.
Uchiyama et al. (2010)	Description of ROMS with comparison of different model setup to the surf zone (North Carolina).
Veeramony et al. (2014)	Short description of Delft3D implemented in the US Navy waves and circulation forecast in the coastal regions.
Warner et al. (2008b)	Development of a three-dimensional, regional, coupled wave, current, and sediment-transport model. Two-way nesting between SWAN and ROMS.
Zijlema et al. (2011)	Description and validation of SWASH.

1. Seven criteria have been selected for the evaluation of the current numerical models as a possible candidate models for the prospective Operational Wave Model System (OWMS).
2. These models have been evaluated by means of an evaluation matrix (Tab. 2.6) using the selected criteria.
3. WAVEWATCH III, SWAN and XBeach have been selected for simulating deep water, intermediate/shallow water and nearshore processes, respectively.

2.5 Nesting approaches

The study of environmental phenomena involves various spatial and temporal scales. A number of numerical models are needed to forecast or hindcast the phenomena at the different scales considered.

For example, in Earth System Modelling (ESM), the scales of processes varying from global, simulated with Global Circulation Models (GCM), to regional and local, simulated with Limited-Area Models (LAM), down to Large-Eddy Simulation Models (LES) (Warner et al., 2008a). Each model must be able to represent the processes corresponding to the scale of the studied phenomena that implies also the use of grids with appropriate resolution.

Modelling waves from the open ocean to the shoreline, which is the main aim of the present research, implies the use of models with different grid resolutions able to represent the physics of sea waves at different scales. In particular, high resolution grids are necessary to have a better representation of waves dynamics in coastal water, where the spatial variation of the topographic features is high.

Generally, the increasing of the grid resolution leads to a significant reduction of the model time step, with an enhancement of the computational cost of the model. To avoid this problem, modellers use high resolution grids only in the specific areas of interest, limiting the computational cost.

A crucial point of this approach is the definition of initial and boundary conditions as treated in the seminal papers of Bryan (1969) and Bryan and Cox (1967). They developed a relative high resolution model for ocean circulation (Primitive Equation, PE) that produces consistent results also in case of open lateral boundaries by means of the definition of appropriate boundary conditions.

A first application of an ocean circulation model on regional scale was carried out by Spall and Robinson (1989), who modify and tested the model of Bryan (1969) and Bryan and Cox (1967). The advantage of the model proposed by Spall and Robinson (1989) is the inclusion of additional physics compared with the quasigeostrofic (QC) model, that extend the application of the PE model to the case of steep or tall topography. On the other hand, the computational cost of the PE model allows its use for regional applications only.

For regional applications of the PE model, the problem is to find satisfactory values for initial boundary conditions. Spall and Robinson (1989) evaluated the possibility of obtaining initial conditions values for the open boundaries from:

- numerically generated data
- measurements

The choice was to employ data numerically generated by a large scale QG model, since they are widely used in ocean modelling. Furthermore, data can be generated all along the boundaries of the PE regional model whereas measurements are generally spurious. Data numerically generated are still the most commonly used for boundary conditions in ESM, but in some cases can be integrated with measurements (i.e. data assimilation process).

Since the publication of the paper of Spall and Robinson (1989) that represents the first implementation of the one-way nesting approach, significant progresses have been made in the nesting approach including one-way and two-way algorithms/techniques.

The *nesting* (or embedding) of two or more grids consists in a high resolution grid (HR or child grid) embedded in a coarse resolution grid (CR or parent grid), enabling communication between the joint boundaries (Debreu et al., 2012; Onken et al., 2005). If the communication is carried out from HR grid to CR grid only, the nesting technique is called *one-way interaction*, otherwise if the communication is allowed in both direction (updating), the nesting is *two-way interaction*. In this section, only the most relevant journal articles dealing with the nesting of wave models as listed in Table 2.8 are analysed and discussed.

Chawla et al. (2007) present the setup of multi-grid WWIII operating at NCEP, where the computational domain is represented by an arbitrary number of grids with different resolution (Fig. 2.12). The wave model system produces results at three different scales: deep ocean, offshore and coastal. However, the resolution of the finer grids (about 6 km) is far from the resolution needed to represent wave dynamics in shallow water. Furthermore, the use of an explicit model like WWIII with high resolution grids (e.g. for shallow water applications) is computationally too expensive.

Grids are ranked according to their resolution, with the coarse resolution grids having a lower rank, the high resolution grids having a higher rank, and grids with similar resolution having the same rank. Each grid runs as a separate wave model, with the boundary conditions to initiate the HR model obtained from the CR model. Therefore, each model can be set up with its own time step, physics parameterization etc. The only message passing through the models will be the wave boundary conditions, defined at the *Active Boundary Points* (ABPs) on the overlapping edge of each grid.

In case of spectral models, such as WWIII, SWAN and XBeach, boundary conditions are transferred by spectral information only. Spectral output files produced by WWIII can be read directly from SWAN. This is true operating over regular grid only, since the passage of spectral files from WWIII to SWAN over unstructured grid is not yet possible.

Spectral output files produced by SWAN can be read from XBeach without any effort (in case of stationary modelling only), if the same coordinate reference system in both models are used. Usually, the reference system in regional applications (such in case of SWAN) is latitude/longitude based, whereas nearshore models (like XBeach) apply a reference system in metres. This implies a rearrangement of the spectral information during the communication between the models.

The multi-grid version of WWIII (from 3.xx) is described in detail by Tolman (2008). The model implements a two-way nesting algorithm that allows the user to resolve wave dynamics on grids with different resolutions. Different grids are considered as separate wave models, hence it implies consecutive computations of individual grids. Since the boundary conditions for HR grid are provided by CR grid, wave conditions of CR grid must to be computed before HR grid. In order to ensure absorption of outgoing wave energy and introduce incoming wave energy into HR grid, the first-order scheme is employed to solve the action balance equation (Eq. 3.4) at the cell boundaries between ABPs and regular grid points.

The two-way nesting technique needs that the information come back from HR grid to CR grid. This is done in Tolman (2008) by replacing the spectra at the grid point in the CR grid with the average spectral values of that part of the HR grid that covers the corresponding coarse resolution grid cell.

In nearshore applications, many wave models highlight "shadow zones" propagating from the lateral boundaries through the domain in the direction of wave propagation. In order to avoid this problem, in XBeach at the lateral boundaries, for wave components entering the domain, the along-shore or along-crest gradient is set to zero (Roelvink et al., 2009).

A multigrid management algorithm was defined by Tolman (2008) (Tab. 2.9), consisting in different sequential steps to be taken for each individual grid. The steps shown in Table 2.9

Table 2.8: List of the main references screened for illustrating the state-of-the-art of nesting techniques in wave modelling. The advantages and disadvantages in the framework of the present research are highlighted.

References	Description	Pros	Cons
Chawla et al. (2007)	Presentation of a multi-grid WWIII operating at NCEP/NOAA.	Each spatial grid runs as independent model.	The use of an explicit model like WWIII is computational expensive for grid resolutions requested in coastal water.
Tolman (2008)	Presentation of the algorithm for the two-way nesting of the multi-grid WWIII.	The nesting algorithm is described in detail.	The two-way nesting technique is not necessary in the present research.
Guedes Soares et al. (2011)	Development of a forecast system composed by a meteorological model (MM5) and two wave models (WAM and SWAN).	The forecast system includes an implicit model (SWAN) that allows to reach a spatial resolution appropriate for coastal areas.	Nearshore hydro and morphodynamic processes are excluded.
Paramygin et al. (2017)	Development of an operational forecast system for the Florida coast.	The system includes a coupling of an hydrodynamic model (CH3D) and a wave model (SWAN).	Nearshore hydro and morphodynamic processes are excluded.
Baart et al. (2009)	Development of a forecast system with three Delf3D nested models (large scale, regional scale and nearshore) and one XBeach (local model) in the framework of the MICORE project.	The forecast system includes a nearshore model (XBeach) that takes into account for hydro- and morphodynamics processes.	The modelling system lacks in a large scale model. Task manager programmes are written in MATLAB (Licensed programme).
Baart et al. (2016)	The forecast system of the MICORE project is updated with a WWIII global model and applied to a real case on the Dutch coast (Egmond, the Netherland).	The system takes into account for all the processes that affect wave from the open ocean to the nearshore.	Calibration and validation of the system for deep and intermediate water is not presented. No details on the nesting methodology are described.
Cheung et al. (2003)	Coastal flooding alert system in Hawaii, composed by three levels of nesting, a WAM ocean model, a coastal SWAN model and a nearshore Boussinesq-type model.	The system includes a phase-resolving model for the nearshore.	The system does not take into account for morphodynamic processes. Phase-resolving models are computationally expensive.
Vousdoukas et al. (2012)	XBeach application in an operational early-warning system in Algarve (Portugal).	XBeach is calibrated and nested in an operational forecast system.	The study is focused on the calibration of XBeach in a specific area of Algarve. No details on the nesting methodology are described.
Barnard et al. (2014)	Development of a numerical modelling system for predicting storm-induced coastal flooding, erosion, and cliff failures over the coast of South California (USA).	The system takes into account for all the processes those affect wave from the open ocean to the nearshore.	Boundary conditions are provided to XBeach by means of synthetic wave parameters.

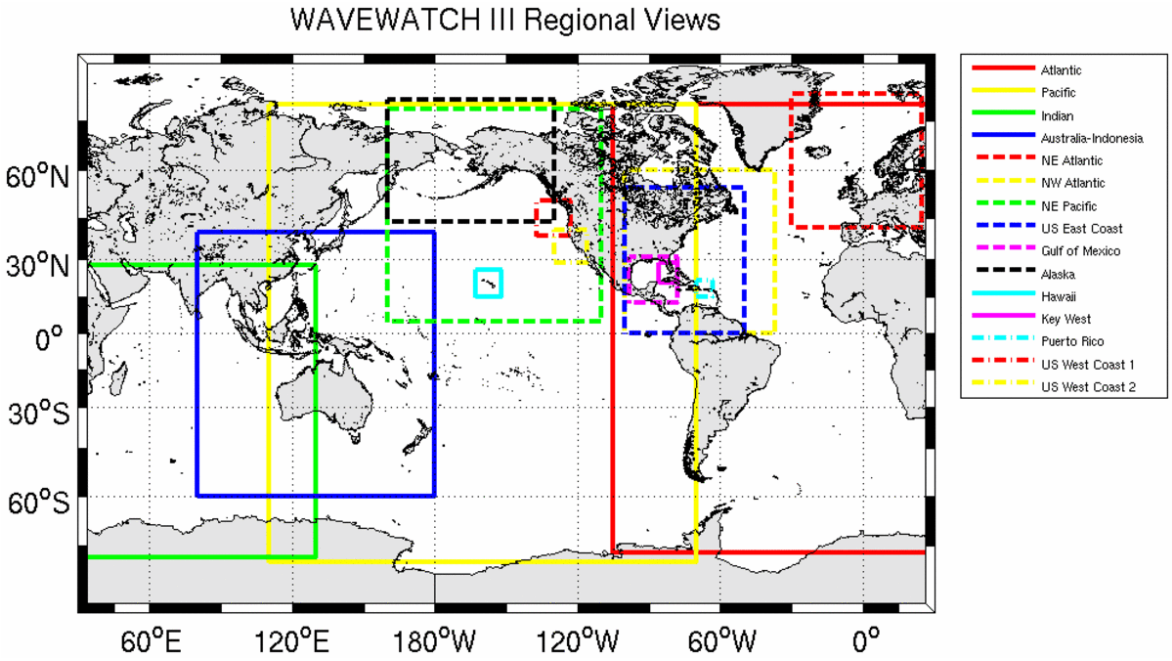

Figure 2.12: Summary of the different display views available for WW3 (`http://polar.ncep.noaa.gov/waves/`).

Table 2.9: Multigrid management algorithm developed by Tolman (2008).

Step	Action
1.	Update input fields for the grid as needed
2.	Update boundary data from lower resolution grid
3.	Update the model time step and the next synchronization time for the relevant grids
4.	Run the wave model up to its next synchronization time
5.	Reconcile the grid with grids with identical rank
6.	Stage boundary data to be provided to higher grid ranked grids
7.	Apply data from higher ranked grids to complete two-way nesting
8.	Stage data to be provided to lower ranked grids
9.	Perform output if requested

are repeated until all requested model integration and output have been completed. For one-way nesting step 7 and 8 are excluded.

The next synchronization time is determined by the availability of boundary data, maximum time of each model and time for output. The algorithm is greatly simplified if a global synchronization time is adopted. Obviously, this implies that the time step of CR grid will be chosen.

However, this algorithm could lead to a not optimal distribution of the computer resources. For example, in the case of a nested model with two grids (CR and HR) running on a multicore machine, the user must assign for each model a number of cores. If one of the models finish to run before the synchronization time, it must to wait for the end of the other model and viceversa, with a waste of computational resources. With only two grids, could be easy to find an optimal assignment of the resources in order that the models finish to run simultaneously, but with more than two grids (especially a cascade of grids) the problem could be very tricky.

Moreover, the algorithm of Tab. 2.9 must be applied inside the code of each model, leading to an important modification of the source code. This techniques is much closer to a *coupling* between models.

The two-way nesting technique could be useful to properly simulate the hurricane development. The area near the core of the hurricane is generally modelled with a low resolution grid that cannot catch up the time and spatial scale of the phenomenon. In the two-way nesting case, a high resolution model near the hurricane core (that should ideally be relocatable) can be used to obtain the spectral data for the boundary conditions of the low resolution grid, suitable to simulate the swell travelling away from the hurricane.

Since the aim of the present research is to model waves travelling from the open ocean to the shoreline and not viceversa, there are not advantages in the use of a two-way nesting algorithm. In particular, at the shoreline (i.e. the focus area for the final results of the present study) no implications of the non-consideration of the feedback from HR to the CR solution are reported in literature. Therefore, the one-way nesting interaction is preferred. Moreover, this choice is justified by the relatively small extension of the Mediterranean Sea (i.e. the test case area) compared to oceans. In fact, in the Mediterranean Sea, waves travelling away from the area of stronger wind reach the continental shelf in a relatively few time, and it does not makes sense to enlarge the resolution of the computational grid between the core of the storm and the coastline as described for the example of hurricane tracking.

One-way nesting allows the user to save computational time, avoiding the back communication from HR grid to CR grid. The last operation implies that CR model waits results from HR model, that usually is time consuming.

In one-way nesting the models could run in series, saving in an archive a sequence of boundary conditions at a chosen time. When the next model starts to run, it will read the stored boundary conditions at the right time (off-line performing of the models). Therefore, each model can run taking advantage of all the available computational resources.

A tentative algorithm for the management of a cascade of telescoping nested grids is shown in Table 2.10. Each step implies the fulfillment of a number of operations. For example,

Table 2.10: Tentative algorithm for the management of a cascade of telescoping grids.

Step	Action
1.	Run lower raked model
2.	Save boundary data with a chosen time step
3.	Perform output to obtain boundary data for higher raked model
4.	Run the higher ranked model with updating of the boundary conditions at the chosen time step

step 1 may include operations of data collection for bathymetry and forcing fields data and pre-processing operations to prepare bathymetry and forcing field files. Step 2 includes the individuation of the overlapping boundary area between CR grid and HR grid. Step 3 is part of the post-processing operations (those may include visualization of results), whereas step 4 may need a preparation of boundary conditions files for HR grid (i.e. pre-processing).

Guedes Soares et al. (2011) built an operational forecasting system for the coastal area of Portugal in the framework of the project MARPORT (Development of a Wave Prediction System for the Portuguese Ports). The system is composed by a meteorological model (MM5) that provides wind data, a large scale wave model (WAM), and a coastal wave model (SWAN). The WAM model operates on five nested grids in the North Atlantic, whereas the SWAN grid covers the West Iberian coast. The use of an implicit model like SWAN could allow the forecasting system to work with high resolution grids in coastal water with a reasonable computational effort, but up to now the two coastal grids implemented in the system have a resolution of 4.1 km.

The peculiarity of the system is that computations are spread over two machines with different Operative System, MM5 and WAM run on a Linux cluster, whereas SWAN runs on a Windows machine. Data collection and running of the models are achieved by developed programmes, whereas pre- and post-processing are achieved by MATLAB scripts.

In the present study it is preferred to run the model system on a single machine in order to assure the portability and reproducibility of the wholesystem. Furthermore, open source Operative Systems and free software will be favoured for the developing of pre- and post-processing programmes.

Paramygin et al. (2017) developed an operational model system for the Florida Coast (ACMS). The core of the system is a coupling between a hydrodynamic model (CH3D) and a wave model (SWAN). Wind, surge and waves at the open boundaries are acquired by low ranked models. The workflow of the model system is shown in Figure 2.13. It is fully automated by a job management module (task manager) that initiates the simulation and manages the module developed to carry out the steps of Tab. 2.11.

Baart et al. (2009) described in detail a real-time system for forecasting morphological impacts due to wave storm, developed during the EU project MICORE. The system is composed by three Delft3D models and one XBeach model, operating at different scales: large, regional, coastal and nearshore. Successively, the system has been updated with a global WWIII model instead of the large scale Delft3D (Baart et al., 2016), and tested in Egmond, the Netherland (see Fig. 2.14).

Baart et al. (2009) summarized the operations for the building of a general forecast model in six steps (see Table 2.11). The aforementioned steps are automated by task manager programmes written in MATLAB, with the exception of step 1 that is carried out manually. Baart et al. (2009) suggested the use of scripts to fully automate step 2 to 6, in order to

Table 2.11: The six steps for the building of a general forecast model as proposed by Baart et al. (2009).

Step	Name	Description
1	*Model setup*	Installation of the model and setting of parameters.
2	*Data collection*	Download of raw data for model initiation.
3	*Pre-processing*	Conversion of raw data in files readable by the model.
4	*Running model engines*	Running of the model previously set up.
5	*Post-processing*	Processing raw output data to generate human readable data.
6	*Publishing*	Results obtained from post-processing are automatically published to a webserver.

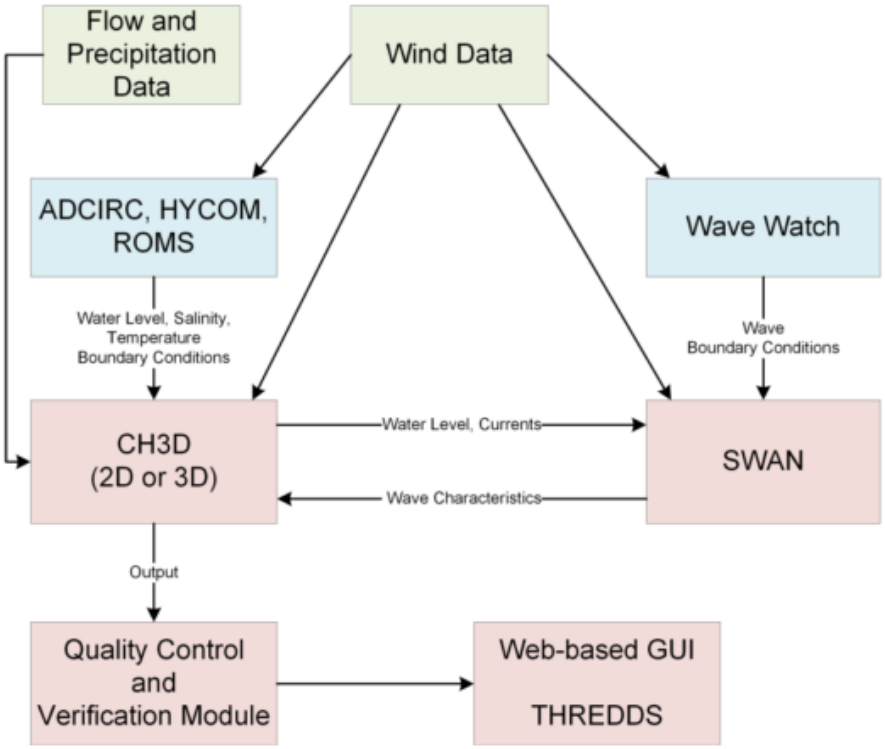

Figure 2.13: Workflow diagram of ACMS (modified from Paramygin et al., 2017). ADCIRC, HYCOM and ROMS are large scale hydrodynamics models, whereas Wave Watch is the large scale wave model. THREDDS is a protocol for Data Server.

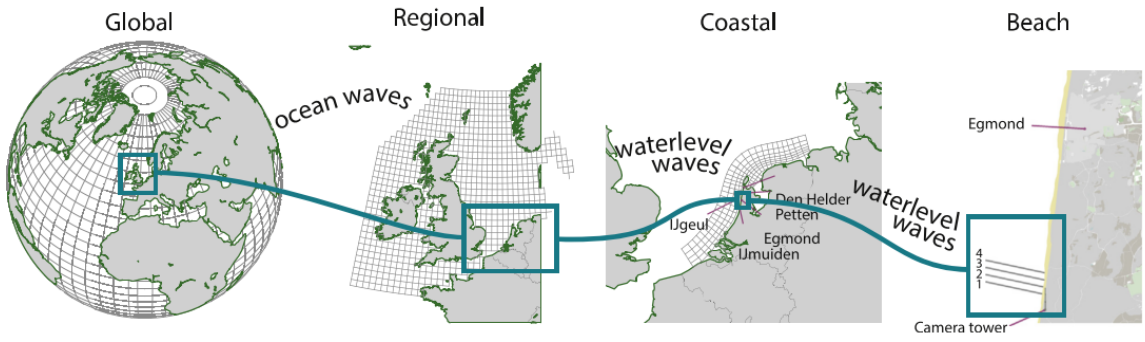

Figure 2.14: Schematization of the nested grids used in the model system as described by Baart et al. (2009) (Baart et al., 2016).

avoid human related errors. Furthermore, this technique guarantees the reproducibility of the system in case of update of the model version. In this case, only a little or no modification of the scripts is necessary to maintain the system, without any annoying modification of the source code.

Model setup consists of the download and compilation of the source code and the set up of model options and parameters (e.g. numerical scheme, time step, physics parameterization, grid setup). This step is generally carried out manually by the user, since it is machine-dependent and site-specific. It means that the installation of a model depends on the Operative System and version, compilers, etc. Model options and parameters are site-specific and depending by the geographical scale of the processes that will be simulated.

Data collection includes the operations needed to download environmental data (wind, pressure, wave, etc.). During the *pre-processing* phase, raw data are transformed in a file format readable by the numerical model. These data are used to force the model or provide initial and boundary conditions.

The fourth step (*running model engines*) consists in runnning the main executable file of the numerical model that generally produce raw output data (i.e. binary files).

During the *post-processing* phase the raw output data are elaborated in text files as table, image files, input files for graphs, etc. In case of a model system that implies the use of nested grids, input files providing initial and boundary conditions for high ranked grids must be produced.

In case of sharing of the model results as described by Baart et al. (2009), a phase of *publishing* on a webserver can be included. Otherwise, the model products can be saved in a storage disk.

In the framework of the MICORE project Vousdoukas et al. (2012) applied a SWAN/XBeach system on the coast of Faro (Algarve, Portugal). The calibrated SWAN/XBeach models are added as an extension to the operational WAVEWATCH-III/SWAN nested system operating in Portugal by the Portuguese Hydrographic Institute (`http://www.hidrografico.pt/previsao-operacional.php`). The modelling system is proposed as a part of a coastal early warning system following the methodology based on Specific Impact Indicators (SII) (Van Koningsveld et al., 2007), with warnings issued when pre-defined threshold values are exceeded. For example, Vousdoukas et al. (2012) selected as SII for the case of Faro beach (a) the maximum wave run-up height during storms, and (b) dune-foot horizontal retreat at the end of storms. No details on the nesting methodology were described by Vousdoukas et al. (2012), and no tools for automating the nesting procedure were developed during the research (M. Vousdoukas, personal communication, 20 March, 2017).

Another example of nested model system was presented by Barnard et al. (2014), who developed the Coastal Storm Modeling System (CoSMoS) for predicting the impact of storms on the coast of South California. The modelling system is inspired from that of MICORE project (e.g. Baart et al., 2016; Vousdoukas et al., 2012) with a global wave model (WWIII) nested with a series of Delf3D models for the downscaling of the wave field, and a series of XBeach cross-shore profile models spread over a 500 km coast selected as test case area. The system is integrated with a probabilistic Bayesian model for cliff failure. The choice of using XBeach as 1D model (cross-shore profile) is justified by the assumption that long-period waves, those cause high water levels and coastal flooding along the US West Coast, are refracted on the inner shelf and often approach normal to the shore and therefore, cross-shore processes result dominant. Wave conditions were transferred from Delft3D to XBeach by means of the synthetic wave parameters, with a lost of spectral information. Since the goal of the CoSMoS project is to consider variations in coastal hazards at a regional scale, the calibration of XBeach at specific sites was not carried out. Few validation cases were presented by Barnard et al. (2014), especially for nearshore processes (e.g. wave runup, shoreline change) due to the lack of measures.

Cheung et al. (2003) described a model system that simulates coastal flooding due to storm

surge and waves. The system consists in four models nested at three levels of geographical scale. A long-wave model for storm surge (SSM) is coupled with a wave model (WAM) on ocean scale, a nested wave model (SWAN) run on coastal scale, and a Boussinesq-type model (COULWAVE) run on nearshore scale. The system is automated through a preprocessor programme written in Octave language (i.e. a programme for Linux environment similar to MATLAB).

Figure 2.15 illustrates the structure of the model system described in Cheung et al. (2003). The bin and src directories store the executable files of the models and the source code of models and scripts, respectively. The term *frontend* contained in the src directory represents the scripts that automates the simulation process with minimal user intervention (Cheung et al., 2003). The support directory stores all the raw data files provided by the user and used by the system as initial and boundary conditions. The work directory stores the main input files, the shell script that controls the entire simulation process, the internally generated files, and the output files.

The model system runs automatically until the end of the SWAN simulation, when the user can check results and initiate manually a COULWAVE simulation at a selected time. Cheung et al. (2003) confirms that the presented modular structure is prone to update the models version with little or no change of the source code or the system structure itself.

The model system described by Cheung et al. (2003) has the limit to be not fully automated. Moreover, the nearshore model COULWAVE does not take into account for the important processes related to the sediment transport (e.g. changing in time of the seabed) which may modify the behaviour of waves in coastal water.

The review and analysis of the current nesting methods/techniques/algorithms carried out in this section revealed that the most important and up-to-date nested wave models are (i) the model system described in Baart et al. (2009, 2016) and applied by Vousdoukas et al. (2012) for a potential coastal warning system in Algarve, and (ii) the similar model system described by Barnard et al. (2014).

The former model system was developed in the framework of the MICORE project (Ciavola et al., 2011a,b) whereas the latter is a similar model system applied to the coast of South California. The MICORE system has been described and applied in several journal and conference papers but a comprehensive description, calibration and validation of the whole model system has never been carried out. Moreover, some parts of the software code of the model system have been written in MATLAB (licensed programme).

For these reasons, a new wave model system is developed and described in detail in the present study. The new wave model system is calibrated and validated (see 3), and applied (see 5) in a stretch of coast in the Mediterranean Sea (i.e. Tuscany, Italy). The calibration, validation and application of the model system in the Mediterranean Sea is particularly important since the peculiar characteristic of this sea, i.e. short fecth, complex topographic features of the coastline. In fact, the aforementioned model systems were applied in Atlantic Ocean (Vousdoukas et al., 2012) and Pacific Ocean (Barnard et al., 2014). Therefore, the present study represents the first application of a fully automated wave model system in the Mediterranean Sea.

In order to reach the goal of the present study of building an operative system able to simulate wave dynamics from the open ocean trough the beach, the three models selected in Section 2.4 (i.e. WWIII, SWAN and XBeach) will be nested following the tentative algorithm in Tab. 2.10. For the execution of the tentative algorithm, the six step in Tab. 2.11 proposed by Baart et al. (2009) will be carried out. The structure of the model system will be similar to that proposed by Cheung et al. (2003) (see Fig. 2.15).

In Figure 2.16, the general workflow of the proposed model system is shown. The development of the workflow will be carried out by means of the steps in Table 2.11. The step of *models setup* will be done manually, whereas *data collection* of wind data is automated by programmes. Initial and boundary conditions will be prepared in the phases of *pre-* and

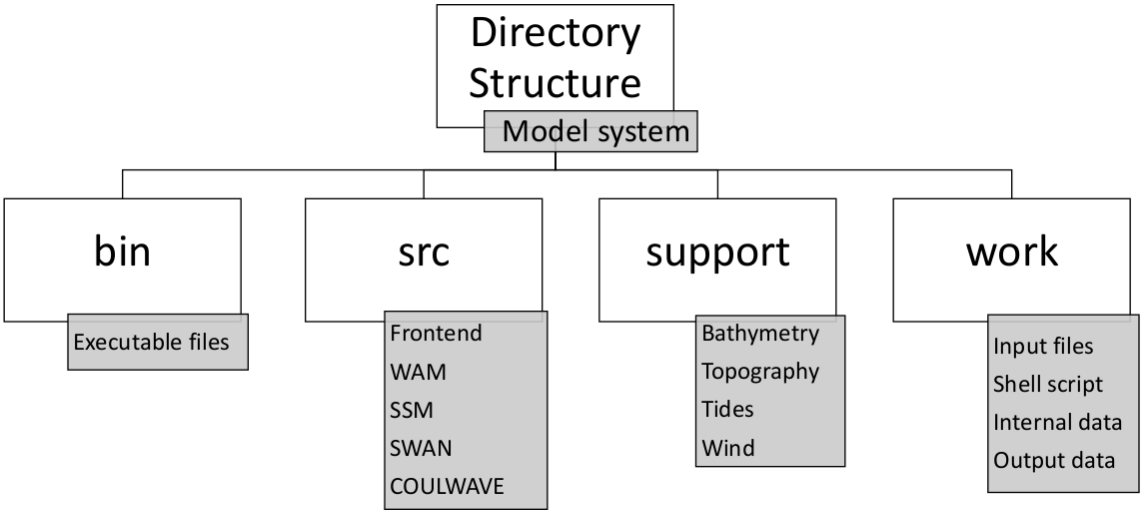

Figure 2.15: Directory structure of the model system described by Cheung et al. (2003) (modified from Cheung et al., 2003).

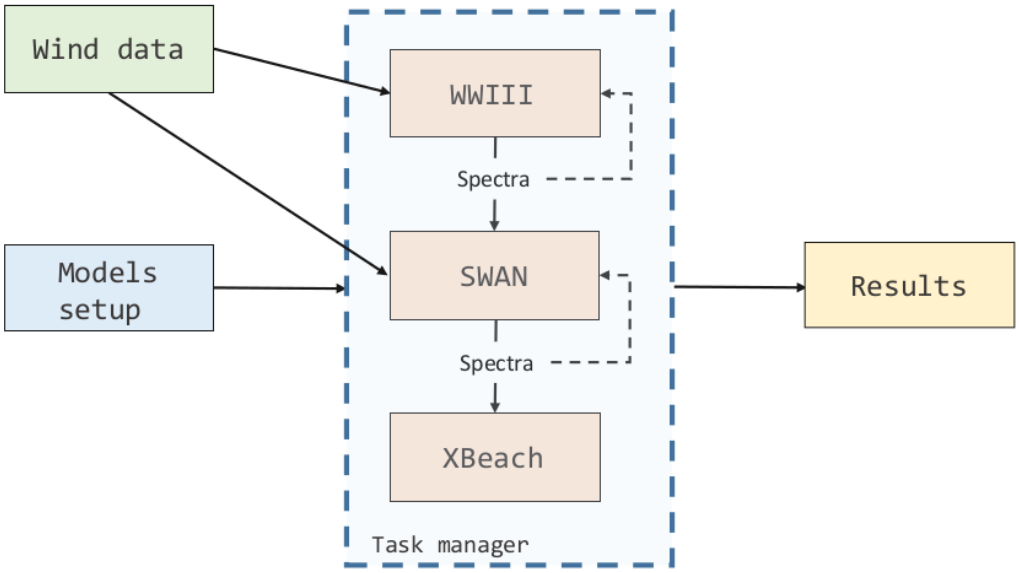

Figure 2.16: General workflow proposed for the building of the operational wave model system (OWMS).

post-processing, whereas a *task manager* programme will manage the running of the models. Finally, post-processing programmes will prepare the results in a readable format for analysts and decision makers (e.g. tables, figures, graphs).

Since the three selected programmes were developed to run mainly in a Linux environment, the auxiliary programmes that will be developed for the automation of the model system will be mainly written in Bash language, i.e. the basic language of Linux OS. Hence, the portability of the system will be ensured for any Linux machine.

Following this procedure, modifications of the source code of the models are reduced to the minimum, and future updating of each individual model will not affect the task manager programme, which represents the core of the model system.

1. The nesting of models with different grid resolutions is a technique for modelling physical processes occurring at different scales (and therefore different grid resolutions).
2. The models selected for building the Operational Wave Model System (OWMS) can be linked to each other sharing only spectral information.
3. Since the aim of the present research is to model waves travelling from the open ocean to the shoreline and not viceversa, spectral information are transferred only from CR model to HR model (one-way interaction). In particular, at the shoreline no implications of the non-consideration of the feedback from HR to the CR solution (two-way interaction) are reported in literature.
4. In order to exploit all the available computational resources it seems reasonable to run the models in series (off-line performance), saving the boundary conditions in an archive, and to transfer data between models at the right time.
5. Codes need to be developed as a task manager programme to prepare the boundary conditions in a format readable by the models (pre- and post-processing operations) and to manage the execution of the models.
6. The model system will be developed to run in a Linux environment. The codes for the task manager programme will be mainly written in Bash language.

2.6 Specification of objectives and methodology

As a main result of the review and analysis of the current knowledge on water waves mechanics and models, and considering the available resources of time and workforce, the objectives and methodology of the present study are specified in the following subsections.

2.6.1 Specification of objectives

Strong wind blowing over the sea surface is usually associated with severe wave conditions, and sometimes with hazardous coastal sea states and beach inundation. In order to prevent the lost of human life and the damage of beach facilities associated to the aforementioned hazards, wave numerical models can be used as tools for supporting Coastal Early Warning System (CEWS). However, the current numerical models are focused only on simulating waves in a specific spatial domain (e.g. deep ocean, continental shelf, coastal areas). Therefore, the main objective of the present study is the building of an Operational Wave Model System (OWMS), linking different models with different grid resolutions for simulating waves from the open ocean to the shoreline, in order to predict hazardous sea states in the nearshore and coastal erosion.

The new model system composed of three numerical models (WWIII, SWAN and XBeach) should overcome the limitations of each individual model, summarised as follow:

WWIII the explicit numerical scheme does not allow higher resolution grid and thus smaller time steps, necessary for nearshore applications.

SWAN the combined source term for wind generation and dissipation due to white-capping is not well formulated as in WWIII and does not account for morphodynamic changes and their effect on wave propagation.

XBeach the application is restricted to nearshore waves.

2.6.2 Specification of methodology

The methodology proposed in Fig. 2.17 is adopted in the present study, in order to achieve the aforementioned objectives. The study is approached by means of four work packages (WP):

WP1 A comprehensive review and analysis of available knowledge about water waves mechanics, existing wave models, and nesting techniques is carried out. Hence, the most suitable models for reaching the aim of the study are selected, on the basis of seven criteria of evaluation.

WP2 Performance of the three selected models, including data collection, calibration and validation of each model. For the validation of the models, a statistical analysis and comparison between model results and measure is conducted.

WP3 Development of the Operational Wave Model System (OWMS). A protocol of communication among the selected models is developed, in order to transfer wave boundary conditions from the lowest resolution grid (parent grid)/model to the higher resolution grid (child grid)/model.

WP4 The new Operational Wave Model System (OWMS) is applied to a case study in the Tuscany coast.

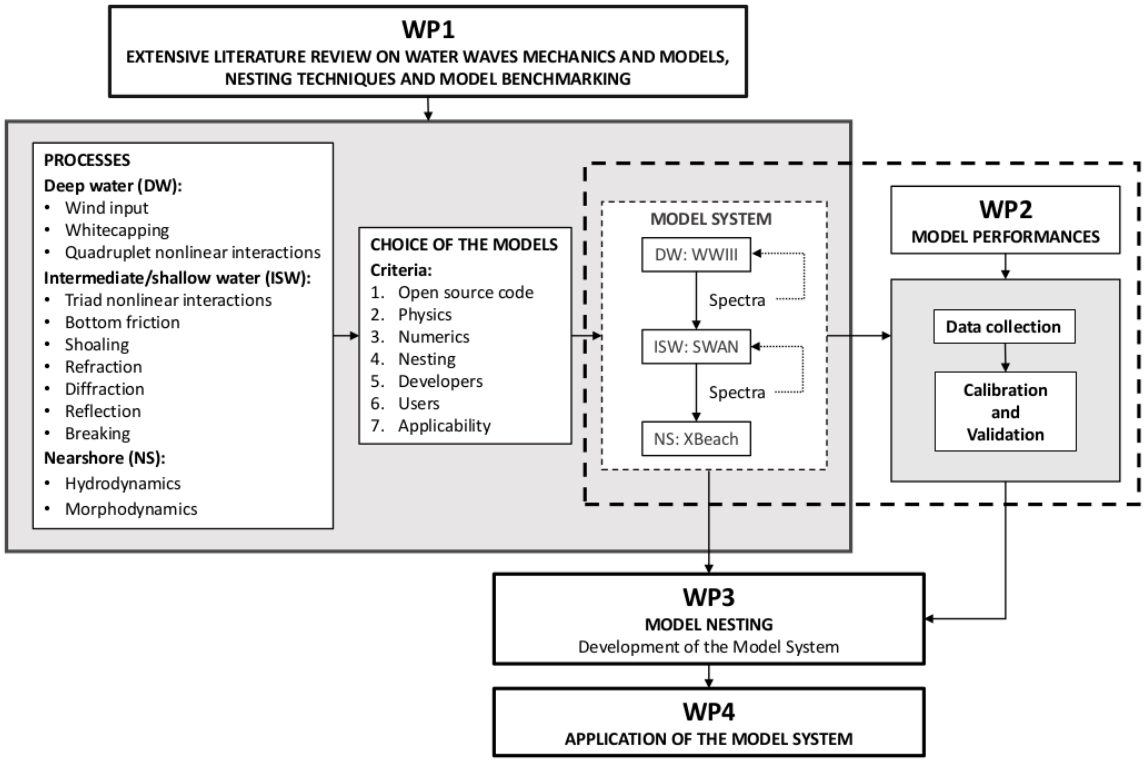

Figure 2.17: Flow chart of the proposed methodology.

3

Numerical Wave Modelling

In the previous chapter, three models have been selected in order to simulate the wave processes at different spatial scales. In particular, WAVEWATCH III (WWIII) has been selected for simulating wave processes in deep water, SWAN for intermediate/shallow water processes, and XBeach for nearshore processes. In this chapter, the performances carried out with the three models are described.

The aim of this chapter is to validate the three models in the North Tuscany (Italy), i.e. the area where the system will be applied in Chapter 5. Therefore, WWIII is calibrated and validated in the Western Mediterranean Sea, and SWAN is calibrated and validated in the Ligurian Sea. A sensitivity analysis is conducted with XBeach applied to typical profile of the beach object of study in the test case of Chapter 5. Furthermore, the main physical and numerical features of the models are presented in order to introduce the reader in the calibration and validation sections.

Sections 3.1 and 3.2 are organised in three subsections describing the governing equations, calibration, and validation for WWIII and SWAN, respectively. Section 3.3 is organised in three subsections describing the governing equations, validation, and sensitivity analysis for XBeach.

3.1 Wave modelling in deep water: WAVEWATCH III

WAVEWATCH III (Tolman, 2015) is a third generation spectral model that has been developed at the Marine Modeling and Analysis Branch (MMAB) of the National Centers for Environmental Prediction (NCEP). The source code is written in Fortran 90 and distributed with open licence. The version adopted in the present study is the 5.08, released in 2015.

3.1.1 Governing equations

To describe the model, a distinction is necessary between the relative or intrinsic radian frequency σ, which is observed in a frame of reference moving with the mean current, and the absolute radian frequency ω, which is observed in a fixed frame of reference:

$$\omega = \sigma + \vec{k} \cdot \vec{U} \tag{3.1}$$

where the dispersion relation according to linear theory is:

$$\sigma^2 = gk \tanh(kd) \tag{3.2}$$

and $\vec{U}$ is the (depth- and time-averaged over the scales of individual waves) current velocity. In *deep water*, where $kd \to \infty$ and $\tanh(kd) \to 1$, the dispersion relationship becomes:

$$\sigma = \sqrt{gk} \tag{3.3}$$

The irregular wind waves are described by means of the variance density spectra $E(\vec{k}, \sigma, \omega; \vec{x}, t)$, with the assumption of slowly varying depths and currents, which implies large-scale bathymetry and ignoring the wave diffraction.

The basic spectrum for the computation is the wavenumber-direction spectrum $E(k, \theta)$, which has been selected because of its invariance characteristics with respect to the physics of wave growth and decay for variable water depths. However, the output consists of the more traditional frequency-direction spectrum $E(f, \theta)$.

Since the energy of a spectral component in presence of current is no longer conserved, the wave propagation is described by means of the *wave action density spectrum* $N(k, \theta) = E(k, \theta)/\sigma$, which is conserved also in case of a current.

The action balance (AB) equation for the spectrum $N(k, \theta, \vec{x}, t)$ is given as

$$\frac{\partial N}{\partial t} + \nabla_{\vec{x}} \cdot \tilde{\vec{x}} N + \frac{\partial}{\partial k}\tilde{k} N + \frac{\partial}{\partial \theta}\tilde{\theta} N = \frac{S}{\sigma} \tag{3.4}$$

where

$$\tilde{\vec{x}} = \vec{c}_g + \vec{U} \tag{3.5}$$

$$\tilde{k} = -\frac{\partial \sigma}{\partial d}\frac{\partial d}{\partial s} - \vec{k} \cdot \frac{\partial \vec{U}}{\partial s} \tag{3.6}$$

$$\tilde{\theta} = -\frac{1}{k}\left[\frac{\partial \sigma}{\partial d}\frac{\partial d}{\partial m} + \vec{k} \cdot \frac{\partial \vec{U}}{\partial m}\right] \tag{3.7}$$

in which $\vec{c}_g(c_g, \theta)$ is the group velocity vector, s is a coordinate in the direction θ, m is a coordinate perpendicular to s and d is the water depth. Eq. (3.4) is valid for a Cartesian grid.

For large-scale applications, Eq. (3.4) is transferred to a spherical grid, definite by longitude λ and latitude ϕ:

$$\frac{\partial N}{\partial t} + \frac{1}{\cos\phi}\frac{\partial}{\partial \phi}\tilde{\phi} N \cos\theta + \frac{\partial}{\partial \lambda}\tilde{\lambda} N + \frac{\partial}{\partial k}\tilde{k} N + \frac{\partial}{\partial \theta}\tilde{\theta}_g N = \frac{S}{\sigma} \tag{3.8}$$

where

$$\tilde{\phi} = \frac{c_g \cos\theta + U_\phi}{R} \tag{3.9}$$

$$\tilde{\lambda} = \frac{c_g \sin\theta + U_\lambda}{R\cos\theta} \tag{3.10}$$

$$\tilde{\theta}_g = \tilde{\theta} - \frac{c_g \tan\phi \cos\theta}{R} \tag{3.11}$$

in which R is the radius of the earth and U_ϕ and U_λ are the current components.

The general source terms used in WWIII is defined as

$$S = S_{\mathrm{ln}} + S_{\mathrm{in}} + S_{\mathrm{ds}} + S_{\mathrm{nl4}} + S_{\mathrm{nl3}} + S_{\mathrm{bfr}} + S_{\mathrm{br}} \tag{3.12}$$

The sources term S_{in}, S_{ds}, S_{nl4}, S_{nl3}, S_{bfr}, S_{br} are already described in Chapter 2. The linear input term S_{ln} provides a more realistic wave growth during the model initialization, instead of starting from calm condition. The available source terms of WWIII are summarised in Table 3.1, where the column Switch indicates the module code of WWIII.

Table 3.1: List of available formulations for source terms in WWIII (Eq. 3.12).

Source term	**Formulation**	**Reference**	**Switch**
S_{ln}	CMR	Cavaleri and Rizzoli (1981)	LN1
$S_{\mathrm{in}} + S_{\mathrm{ds}}$	WAM3	Komen et al. (1984) and Snyder et al. (1981)	ST1
	TC	Tolman and Chalikov (1996)	ST2
	ECWAM	Bidlot et al. (2005)	ST3
	AR	Ardhuin et al. (2010)	ST4
	BYDRZ	Rogers et al. (2012)	ST6
S_{nl4}	DIA	Hasselmann et al. (1985)	NL1
	WRT	Resio and Perrie (1991), Tracy and Resio (1982), van Vledder (2006), and Webb (1978)	NL2
	GMD	Tolman (2013) and Tolman and Grumbine (2013)	NL3
	Nonlinear filter	NLS	
S_{nl3}	LTA	Eldeberky (1996)	TR1
S_{bfr}	JONSWAP	Hasselmann et al. (1973) and WAMDI Group (1988)	BT1
	SHOWEX	Ardhuin et al. (2003) and Grant and Madsen (1979)	BT4
	D&L	Dalrymple and Liu (1978)	BT8
	Ng	Ng (2000)	BT9
S_{br}	BJ	Battjes and Janssen (1978)	DB1

Table 3.2: Type of computational grids implemented in WWIII.

Type	**Remarks**
Regular	Traditional rectangular grid, equally spaced in both directions. Widely used.
Curvilinear	Spherical Multiple-Cell (SMC) grid. It is an unstructured grid but retains the conventional latitude/longitude grid cells. Used in case of alternative grid projection, rotate grid, or grid with higher nearshore resolution.
Unstructured	Triangle based grid. Manly used in coastal applications.

WWIII supports the use of two coordinate systems, a 'flat' Cartesian coordinate system in metres, used only for small scale and idealized test applications, and a spherical (latitude/-longitude) system used for real applications. The different types of WWIII computational grids are summarised in Tab. 3.2.

Since the use of WWIII in the present research is limited to large scale applications, where bottom and coastal features are irrelevant, a regular spherical grid with latitude/longitude coordinate system results as the best option. The regular grid assures a constant global time step over the entire domain and fast computation. Furthermore, the regular grid facilitates to build the input bathymetry grid.

Eq. 3.8 is solved using a fractional step method (Tolman, 2015). The different fractional steps of the model allow the use of four different time steps (see Tab. 3.3)

The first step Δt_g considers the temporal variation in depth, and therefore changes in the wavenumber grid, but using the model in deep water makes this step irrelevant.

The second step Δt_p in the spatial propagation, which is described by the first terms of the left side of AB equation (Eq. 3.4 or Eq. 3.8). At the land-sea boundaries, wave action propagating toward the shore is assumed to be absorbed without reflection, and waves propagating seawards are assumed to have no energy at the coastline. A similar approach is adopted for the "active boundary point" (see Sec. 2.5). The available propagation schemes are summarised in Table 3.4. The QUICKEST scheme is the default propagation scheme for spherical grids. This scheme is sufficiently free of numerical diffusion for the so-called "Garden Sprinkler Effect" (GSE), which produces the disintegration of the swell due to the discrete description of the spectrum (Booij and Holthuijsen, 1987).

The third step Δt_k considers refraction and residual (current-induced) wavenumber shifts (Tolman, 2015), in which the last two terms of the left side of AB equation are solved. The numerical schemes available for solving intra-spectral propagation are summerised in Tab. 3.4.

The last step Δt_s consists in solving the source term part (right side) of the AB equation. A semi-implicit first order scheme is applied over a series of dynamic time step Δt_d, where the minimum dynamical time step is defined by the user with Δt_s (Tab. 3.3).

3.1.2 Model calibration

The WAVEWATCH III (WWIII) model consists of several routines representing the wave processes summarized in Subsection 3.1.1. Therefore, the model compilation and calibration is crucial to obtain consistent results.

The aim of the present subsection is to individuate the best model setup for WWIII applications in the Mediterranean Sea. The subsection is organised as follows:

- The first paragraph (a) illustrates the basic knowledge to set up the model.

Table 3.3: Time steps used in WWIII to solve the AB equation with a fractional step algorithm.

Time step	**Description**
Δt_g	Global time step by which the entire solution is propagated in time.
Δt_p	Time step for spatial propagation.
Δt_k	The time step for intra-spectra propagation. Generally this value vary from Δt_g only in shallow water.
Δt_s	The time step for the integration of the source terms. This time step allows WWIII to achieve more accurate results for rapidly chancing wind and wave conditions, and more economical integration for slowly varying conditions.

Table 3.4: List of available propagation schemes in WWIII.

Scheme	Reference	Remarks	Switch
First order	Tolman (2015)	Simple 1st order upwind scheme, mainly used for tests.	PR1
UNO2	Li (2008)	Upstream non-oscillatory 2nd order advection scheme. Used for Cartesian grids.	UNO
QUICKEST	(Davis and Moore, 1982; Leonard, 1979)	3rd order scheme combined with the ULTIMATE TVD (total variance diminishing) limiter (Leonard, 1991), accurate both in space and time. Used for spherical lat/lon grid.	UQ

- A sensitivity analysis is carried out in paragraph (b) on grid resolution and $S_{\text{in}} + S_{\text{ds}}$ source term.
- A further sensitivity analysis is carried out on $S_{\text{in}} + S_{\text{ds}}$ source term and wind input database, simulating 5 real storms which occurred in the Mediterranean Sea (paragraph (c)).

The sensitivity analysis on the three parameters may be justified as follows:

- A too coarse grid resolution can lead to a smoothing of the wave conditions, whereas a too fine grid resolution can result in very time-consuming computations. Hence, an optimal resolution of the grid is necessary for balancing the reliability of the results and computational costs.
- The source term $S_{\text{in}} + S_{\text{ds}}$ influences the greater part of the wave energy in deep water.
- Since the only external forcing of the model is the wind direction and intensity, the different wind sources have an important role in the results of the model.

(a) Model setup

The first operation using WWIII is the compilation of the source code. The different source terms listed in Tab. 3.1 are selected by means of the correspondent switches as well as the numerical schemes of Tab. 3.4. As discussed in Chapter 2, the main processes affecting waves in deep water are generation by wind, energy dissipation due to whitecapping and nonlinear quadruplet wave-wave interactions, represented in wave modelling by the source term $S_{\text{in}}+S_{\text{ds}}$ and S_{nl4}, respectively.

Whereas the DIA formulation it is emerged as the best option for S_{nl4}, for the source term $S_{\text{in}}+S_{\text{ds}}$ two formulations were selected, TC and AR (see Subsec. 3.1.1). Therefore, the model calibration implies the use of two versions of WWIII, the first compiled with TC source term and the second with AR source term. The methodology followed for the compilation of the model is depicted in Figure 3.1.

The spectral information is an important setting of WWIII, which consists in four parameter:

- Frequency increment factor (XFR)
- First frequency (FR1)
- Number of frequencies (NK)

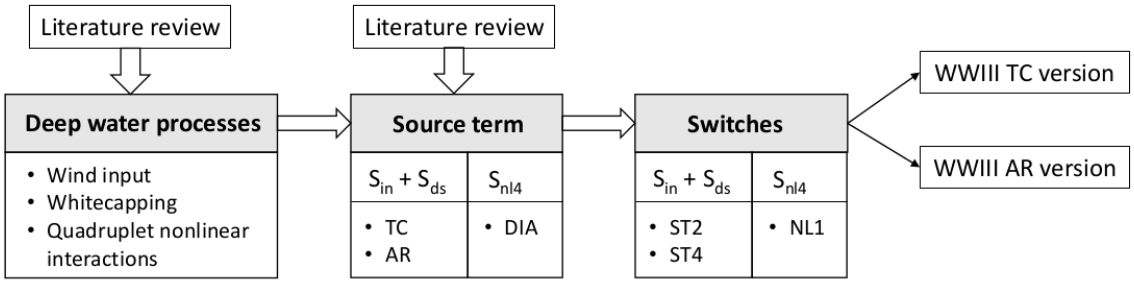

Figure 3.1: Methodology for the compilation of WWIII.

- Number of directions (NTH)

The code in brackets indicates the name of the variable as written in the source code. For large-scale applications, a spectral resolution with NK=25 ($\Delta f = 0.018$) and NTH=24 ($\Delta\theta = 15°$) is sufficient.

Otherwise, to fix the values of XFR and FR1, it is necessary to understand the range of frequency that exists in the area of study. For example, waves storms occurring in the Mediterranean Sea are characterized by peak period (T_p) ranged from 12s to 4s, corresponding to about 0.083Hz and 0.25Hz (f_p). Considering the normalised JONSWAP spectrum of Figure 3.2, almost the total of energy is comprised from $0.6f_p$ and $2.0f_p$, that means most of the energy ranges between 0.05Hz and 0.5Hz. Since WWIII provides the highest frequency considered in the model as

$$maxfreq = FR1 * XFR^{(NK-1)} \tag{3.13}$$

in the Mediterranean Sea, the maximum frequency is

$$maxfreq = 0.05 * 1.1^{24} = 0.492\text{Hz} \simeq 0.5\text{Hz}$$

The obtained spectral parameter for the application of WWIII in the Mediterranea Sea are summarised in Tab. 3.5.

Further important setting parameters are the four time steps (see Tab. 3.3). The first time step that should be determined is the spatial propagation time step Δt_p, which must satisfy the Courant-Friedrichs-Levy (CFL) criterion, i.e. the speed of fastest waves in the model must be less than or equal to the grid spacing in degrees (Δx) divided by Δt_p. Therefore, the computational grid has its own Δt_p determined by grid resolution, maximum latitude in

Table 3.5: Spectral parameter of WWIII applied in the Mediterranea Sea.

Parameter	**Code**	**Value**
Frequency increment factor	XFR	1.1
First frequency	FR1	0.05 Hz
Number of frequencies	NK	25
Number of directions	NTH	24

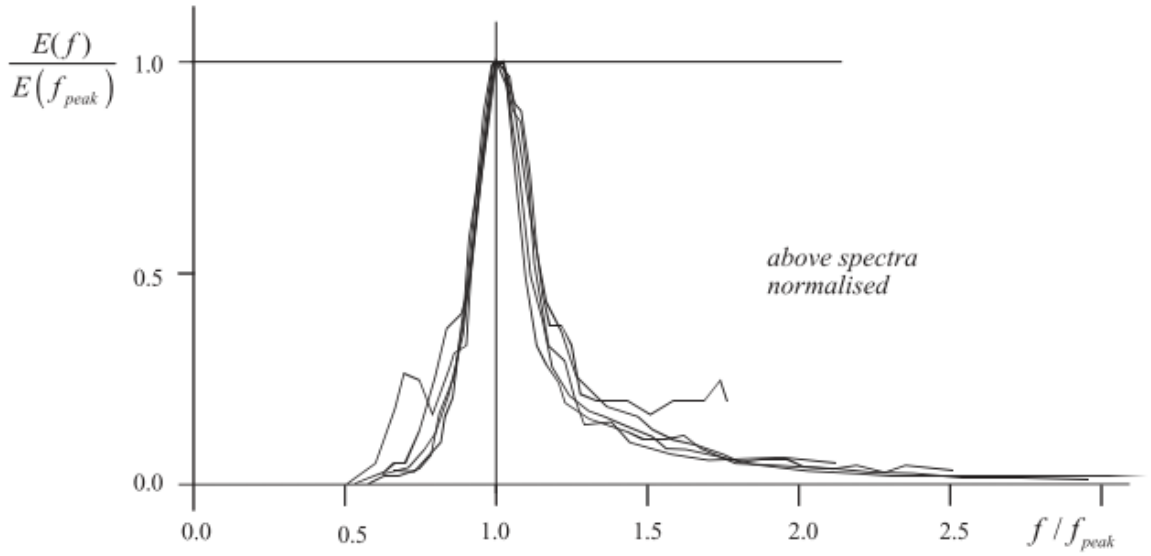

Figure 3.2: Normalised spectra observed by the JONSWAP under idealised, deep-water conditions (Holthuijsen, 2007).

the grid, and the first spectral frequency (FR1):

$$\begin{aligned}\Delta t_p &= \frac{\Delta x}{c_g} \\ &= \frac{\frac{40*10^6}{360} * \Delta x * \cos(\text{maxlat})}{\frac{1.15*g}{4\pi} * \frac{1}{\text{FR1}}} \\ &= \frac{40 * 10^6 * \Delta * \cos(\text{maxlat}) * 4\pi * \text{FR1}}{360 * 1.15 * g} \\ &= 123766 * \Delta x * \cos(\text{maxlat}) * \text{FR1} \end{aligned} \tag{3.14}$$

where cos(maxlat) is the cosine of the maximum latitude in degrees. Eq. (3.14) gives the maximum allowable time step for spatial propagation. The global time step Δt_g, by which the entire solution is propagated in time, can be set to approximately 2 or 3 times the Δt_p. Hence, the directional time step is set to $\Delta t_k = 1/2\Delta t_g$. Δt_k and Δt_g differ only in intermediate/shallow water conditions. The source term time step is adjusted internally and $\Delta t_s = 15$ seconds is the minimum allowed value (see Subsec. 3.1.1).

(b) Sensitivity analysis

A sensitivity analysis was performed in order to identify the most appropriate parameterization for the source term $S_{\text{in}} + S_{\text{ds}}$, in terms of its reliability to reproduce the wave field in the Mediterranean Sea. Furthermore, the feasibility to run the model with different grid resolution is evaluated.

As implied from the literature review (see Sec. 2.1), two parameterizations have been considered, the Tolman and Chalikov (1996) parameterization (TC) and the Ardhuin et al. (2010) parameterization (AR). The TC and AR formulations are discussed in detail in Pelli et al. (2015b).

A wind input, constant in space and time, was used and the model results were also compared, with the results obtained by means of the Young and Verhagen (1996) formula (YV).

Three computational grids covering the Mediterranean Sea were considered with respectively 0.025°, 0.05°, and 0.1° resolution both in latitude and longitude. The 0.025° grid has

1881x721 nodes, the 0.05° grid has 941x361 nodes, and the 0.1° grid has 471x181 nodes. The resolutions expressed in kilometres are respectively about 10km, 5km, and 2.5km at the latitude of the Western Mediterranean Sea. The time steps for each grid calculated with Eq. (3.14) are summarised in Table 3.6.

The basic test consisted in forcing the whole domain with 50km/h wind (constant in speed and direction) for three days. Several tests were performed by varying grid resolution, wind direction (SW, NW, NE, SE), wind input and dissipation source term ($S_{\text{in}} + S_{\text{ds}}$).

Results of the tests for significant wave height (H_{m_0}) and peak period (T_p) at points with different fetches were compared to the results obtained by means of the empirical formula given by Young and Verhagen (1996) and modified by Breugem and Holthuijsen (2007). The three different fetches (see Fig. 3.3) were defined as the maximum fetch for storm events respectively in the Eastern Mediterranean Sea (700 km), Western Mediterranean Sea (400 km), and Adriatic Sea (160 km). The output values were requested in three points located respectively offshore of Zante Island, North Sardinia and Pescara.

As shown in Table 3.7, a matching of the order of 10% between parameters obtained by empirical formula (YV) and WWIII model using any grid resolution with exception for the values obtained using TC parameterization and 0.01° grid resolution. The smallest difference is shown between the maximum value of empirical H_{m_0} (700 km fetch) and the ones modelled using TC parameterization, computed with both 0.025° grid (+1.1%) and 0.05° grid (+1.5%). Peak periods obtained with AR parameterization match better with the empirical peak periods than with the peak periods obtained with TC parameterization.

1. A sensitivity analysis is carried out for three grid resolutions and two $S_{\text{in}} + S_{\text{ds}}$ source terms.
2. A comparison between the wave parameters H_{m_0} and T_p modelled by WWIII and calculated with the Young and Verhagen (1996) formula is carried out for three idealised cases.
3. For the finer grid, a minor discrepancy between the wave parameters modelled and calculated is obtained. However, the difference between the intermediate and finer grids is relatively small. Hence, the intermediate grid is selected as the best option to ensure the reliability of the results and reasonable computational costs.
4. The effect of the two source terms is not clear. Therefore, a further analysis is carried out in the next paragraph by hindcasting five major storms of the last decade recorded in the Mediterranean Sea.

(c) Storm simulations

Given the similar behaviour of TC parameterization and AR parameterization to hindcast H_{m_0} and T_p, the latter are evaluated by simulating different real storms which occurred in

Table 3.6: Time steps in seconds for the different grid resolutions.

Grid	Δt_g	Δt_p	Δt_k	Δt_s
0.025°	201	105	105	15
0.05°	430	215	215	15
0.1°	860	430	430	15

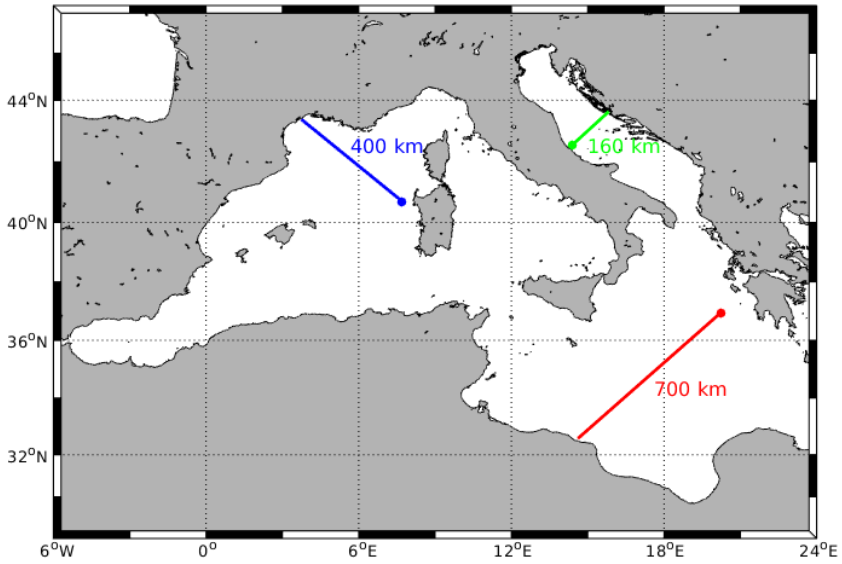

Figure 3.3: Location of the output points with different fetch.

Table 3.7: Comparison between wave parameters (H_{m_0} & Tp) obtained by WWIII model with different grid resolutions using TC parameterization, AR parameterization, and calculated by Young and Verhagen (1996) formula (YV). In bracket the deviations in percentage (%) of WWIII model result (TC, AR) from the value obtained by the YV-formula: $100 * (WWIII - YV)/YV$.

Wave parameter	**Test**	**Fetch (km)**		
		700	**400**	**160**
$H_{m_0}(m)$	YV	4.58	4.15	3.09
	$TC_{0.01}$	4.42 (−3.5)	3.13 (−24.6)	1.44 (−53.4)
	$AR_{0.01}$	4.16 (−9.2)	3.66 (−11.8)	2.62 (−15.2)
	$TC_{0.05}$	4.65 (+1.5)	3.82 (−8.0)	2.68 (−13.3)
	$AR_{0.05}$	4.15 (−9.4)	3.66 (−11.8)	2.70 (−12.6)
	$TC_{0.025}$	4.63 (+1.1)	3.83 (−7.7)	2.70 (−12.6)
	$AR_{0.025}$	4.22 (−7.9)	3.66 (−11.8)	2.72 (−12.0)
$T_p(s)$	YV	10.5	9.4	7.5
	$TC_{0.01}$	8.9 (−15.2)	7.1 (−24.5)	4.7 (−37.3)
	$AR_{0.01}$	9.8 (−6.7)	8.9 (−5.3)	7.1 (−5.3)
	$TC_{0.05}$	9.3 (−11.4)	8.2 (−12.8)	6.4 (−14.7)
	$AR_{0.05}$	9.8 (−5.3)	8.9 (−5.3)	7.1 (−5.3)
	$TC_{0.025}$	9.3 (−11.4)	8.2 (−12.8)	6.4 (−14.7)
	$AR_{0.025}$	9.8 (−6.7)	8.9 (−5.3)	7.2 (−4.0)

Table 3.8: List of storms simulated by WWIII and max H_{m_0} recorded at three locations: La Spezia buoy, Gorgona buoy (See locations in Fig. 3.4). Both buoys are moored in about 100 depth.

Case study	**Start date**	**End date**	**Max** $H_{m_0}(m)$
October 2003[1]	2003/10/02	2003/10/10	6.03
December 2008[2]	2008/12/03	2008/10/09	4.96
October 2012	2012/10/24	2012/11/08	6.39
December 2012	2012/12/02	2012/12/10	5.12
March 2013	2013/03/17	2013/03/28	6.13

[1] Only La Spezia
[2] Only Gorgona

Figure 3.4: Locations of La Spezia, Gorgona and Ancona buoys (Google Earth).

the Mediterranean Sea. To achieve a reasonable computational time and accuracy of the results, simulations are carried out over a 0.05° resolution grid, corresponding in the Western Mediterranean Sea to about 5 km. The computational grid has 941x361 nodes covering the whole Mediterranean Sea, but the analysis has been done for Western Mediterranean only.

Five of the main storms which occurred in the last decade are hindcasted and analysed (Tab. 3.21). WWIII was forced with two wind input databases (for AR parameterization only), the ERA-Interim (Dee et al., 2011) from ECMWF and the CFSR (Saha et al., 2010) from NCEP. Era-Interim has a 6-hour step data, whereas CFSR has a data step of 1 hour. Therefore, storm simulations are performed with the setups of WWIII, as shown in Table 3.9. The TC model setup was forced by only CFRS wind because first storm simulations performed with AR model setup highlighted a systematic underestimation of H_{m_0} values obtained forcing the model with ECMWF wind than those obtained from the model forced by the CFSR wind.

A first evaluation of the results is carried out mapping H_{m_0} over the computational domain. For example, Fig. 3.5 shows the different wave fields obtained with the three model setups. The wave field obtained using the model setups 1 and 3 (ECMWF wind forcing) generally results in lower H_{m_0} values than those obtained with the model setup 2 (CFSR wind forcing). The figure shows also that model setup 3 (TC source term) results in lower H_{m_0} values than those obtained from the model setups 1 and 2 (AR source term). The behaviour as described above is observed for all the storms analysed.

To assess the reliability of the model results, the hindcasted and measured data are compared by plotting the development of H_{m_0} over time. Typical results, exemplary shown for La Spezia station in Fig. 3.6, reveal that the hindcasted H_{m_0} peak values obtained with the model setup 2 underestimate all H_{m_0} measured peak values. Further examples for Gorgona and Ancona spots are shown in Appendix A. This trend is observed over all the considered storms. Some underestimations (negative bias) can also be observed for the H_{m_0} values obtained with the model setups 3. The best agreement between H_{m_0} modelled and measured was observed for the simulations carried out with WWIII setup 1 (AR+CFSR), even though a little underestimation can be observed.

The performance of WWIII is evaluated through comparison of measured and hindcasted H_{m_0} values obtained by the three model setups. Differences between measured and modelled H_{m_0} are evaluated using the statistical indicators listed in Table 3.10, selected for their large use in wave modelling.

A statistical analysis carried out for three different spots, Gorgona, La Spezia, and Ancona. The analysis for La Spezia is presented in Table 3.11. The tables of the statistical analysis for Gorgona and Ancona are presented in Appendix A. Statistical indicators confirm that a negative bias exists for all the model settings. Differences between hindcasted and measured H_{m_0} are greater by forcing the model with ECMWF wind than those by forcing the model with the CFSR wind. The more reliable results are obtained for the model setups 2 and 2*. In fact, values in the order of few centimetres are observed for bias, MSE and standard deviation for the model setup 2 and 2*. The setup 2* consists in a modification of the AR source term, it will be successively explained.

In general, the statistical analysis shows satisfying results for the simulations performed

Table 3.9: The three model setups used during the storm simulation tests depending on the source term parameterization and on the wind input dataset.

Setup	**Description**	**Acronyms**
1	AR source term forced with ERA-Interim wind data	AR+ECMWF
2	AR source term forced with CFSR wind data	AR+CFSR
2*	AR* source term forced with CFSR wind data	AR*+CFSR
3	TC source term forced with CFSR wind data	TC+CFSR

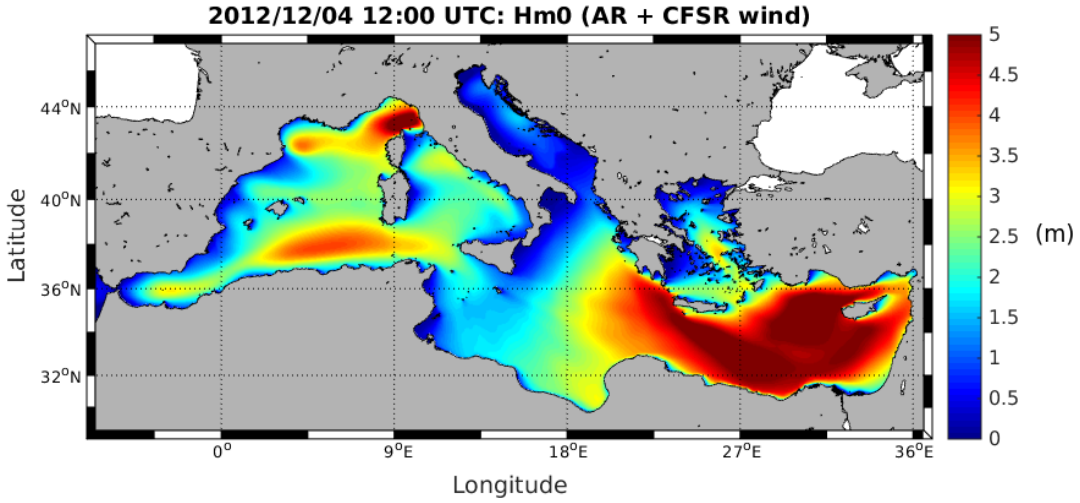

(a) *CFSR wind (AR parameterization).*

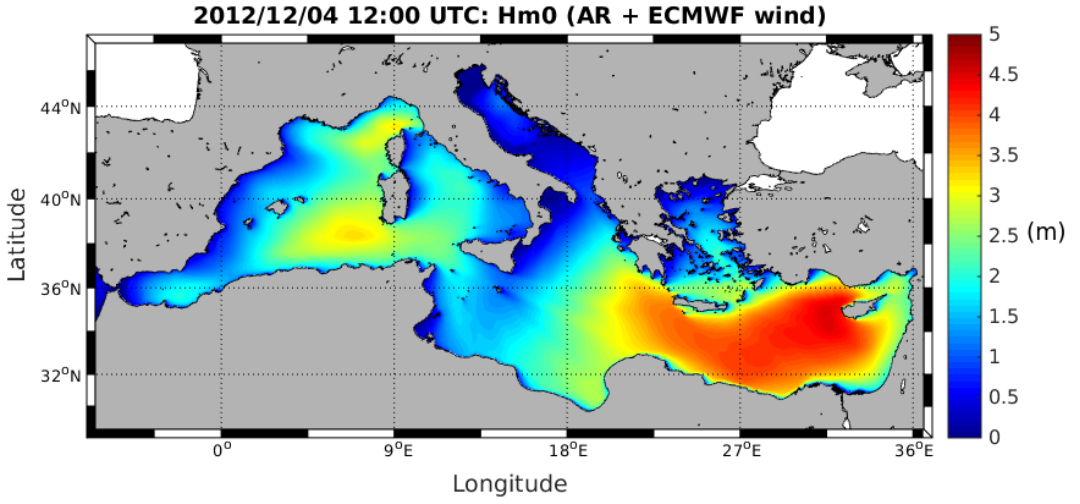

(b) *ECMWF wind (AR parameterization).*

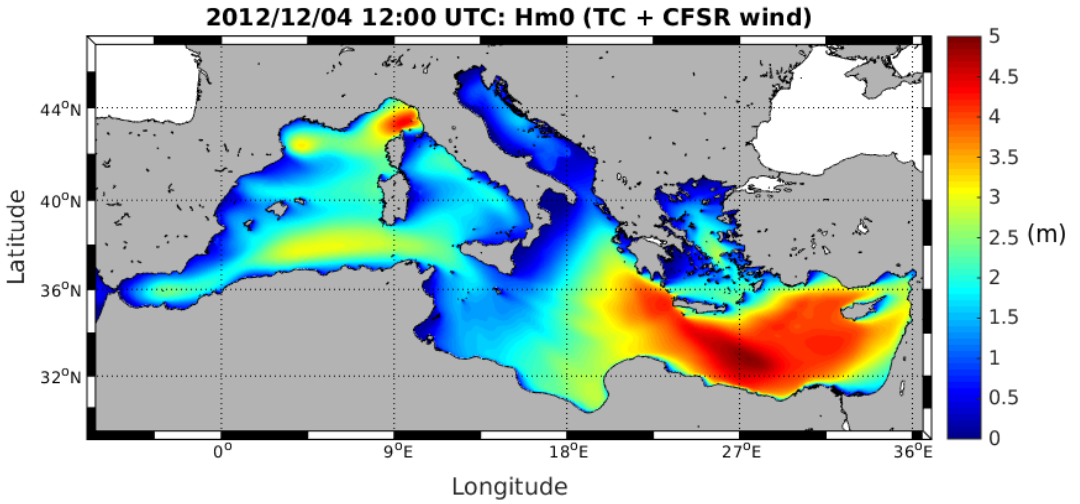

(c) *CFSR wind (TC parameterization)*

Figure 3.5: Wave field at the peak of the December 2012 storm in Ligurian Sea. $H_{m_0}(m)$ obtained by the three model setups.

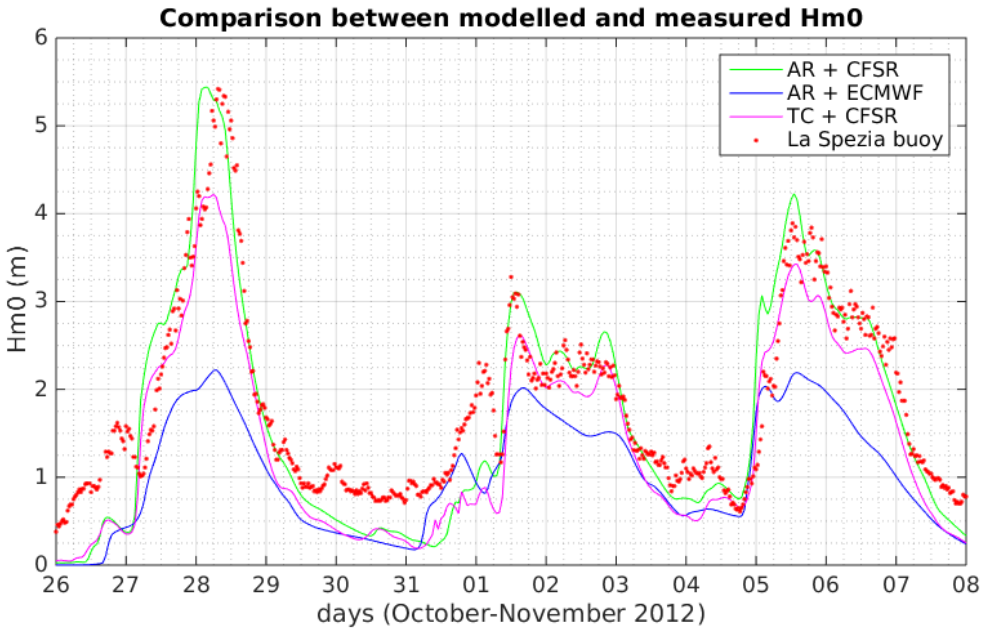

Figure 3.6: Comparison of H_{m0} time series obtained with the three model setups and measured at La Spezia.

Table 3.10: Statistical indicators for the evaluation of the WWIII model performance.

Statistical indicator	**Formula**
Bias	$\text{bias} = \frac{1}{n}\sum_{i=1}^{n}(y_i - x_i)$
Mean Square Error	$\text{MSE} = \frac{1}{n}\sum_{i=1}^{n}(y_i - x_i)^2$
Normalised Bias	$\text{NBI} = \frac{\sum_{i=1}^{n}(y_i - x_i)}{\sum_{i=1}^{n} x_i}$
Normalised Root Mean Square	$\text{NRMSE} = \sqrt{\frac{\sum_{i=1}^{n}(x_i - y_i)^2}{\sum_{i=1}^{n} x_i^2}}$
Scatter Index	$\text{SI} = \frac{RMSE}{\bar{x}}$
Standard deviation of difference	$\sigma_d = \sqrt{\frac{1}{n-1}\sum_{i=1}^{n}(y_i - x_i - bias)^2}$

Table 3.11: Summary of the statistical error indicators obtained from the comparison between hindcasted and buoy data for H_{m_0} at La Spezia spot.

Storm	**Setup**	**bias (m)**	**MSE (m)**	**NBI**	**NRMSE**	**SI**	σ_d **(m)**
Oct 2003	AR + ECMWF	-1.27	2.45	-1.273	0.567	0.401	0.87
	AR + CFSR	-0.54	0.57	-0.313	0.265	0.261	0.46
	TC + CFSR	-0.64	0.76	-0.395	0.318	0.261	0.59
Oct-Nov 2012	AR + ECMWF	-0.77	0.96	-0.726	0.463	0.335	0.61
	AR + CFSR	-0.13	0.27	-0.074	0.244	0.275	0.50
	TC + CFSR	-0.41	0.32	-0.290	0.267	0.213	0.39
	AR*+ CFSR	-0-03	0.31	-0.020	0.265	0.307	0.56
Dec 2012	AR + ECMWF	-0.68	0.64	-0.739	0.451	0.271	0.43
	AR + CFSR	-0.16	0.13	-0.115	0.205	0.205	0.33
	TC +CFSR	-0.45	0.30	-0.393	0.308	0.197	0.31
	AR*+ CFSR	-0.08	0.12	-0.053	0.196	0.214	0.34
Mar 2013	AR + ECMWF	-0.61	0.61	-0.835	0.463	0.367	0.49
	AR + CFSR	-0.23	0.17	-0.210	0.243	0.251	0.34
	TC + CFSR	-0.44	0.33	-0.485	0.342	0.277	0.37
	AR*+ CFSR	-0.16	0.14	-0.131	0.222	0.253	0.34

with the model setup 2 (AR+CFSR), except for the more early storms, the storm of December 2008 and the storm of October 2003. However, bias and MSE decrease considerably for the more recent years, where statistical parameters indicate smaller deviations between model and measures. This behaviour could be explained with an increment of the CFSR wind resolution after April 2011 from about 30km (0.31°) to about 20km (0.21°).

Results of the present study are also compared with results obtained by Casaioli et al. (2014) and Mentaschi et al. (2013). Both works illustrate a wave model setup for forecasting waves in the Mediterranean Sea, the former using WAM model and the latter using the WWIII model. Both wave models were forced with quite higher resolution wind data (about 10km). For Ligurian Sea, Casaioli et al. (2014) found values of bias ranging from 0.91m to 1.23m, and MSE ranging from 0.21m to 0.64m. In the present study, for model setup 1, it was found values of bias between -0.58m and -0.14m, and MSE ranging from 0.13m to 0.57m. It is worth to highlight that in the present study a general underestimation of wave high is observed (negative biases), whereas Casaioli et al. (2014) reported an important general overestimation using the WAM model.

A comparison between the present results for NBI and NRMSE with the ones obtained by Mentaschi et al. (2013) show that whereas NRMSE values are quite similar, the obtained NBI values are sensibly larger than those shown in Mentaschi et al. (2013). The NBI values for AR+CFSR (setup 2) range from -0.578 to -0.074, whereas Mentaschi et al. (2013) reported NBI values from -0.110 to 0.053.

Further storm simulations were carried out in order to improve the results of the statistical indicators. Following Mentaschi et al. (2015), the non-dimensional growth parameter β_{max} of AR parameterization was tuned from the default value of 1.52 to 1.75. This parameter represents the fraction of wind energy transferred to sea waves. The AR parameterization is described in detail in Pelli et al. (2015b).

The model setup 2* is referred in figures and tables with the acronym AR*+CFSR, that means AR parameterization with modified $\beta_{max} = 1.75$ and CFSR wind forcing. An example of the development of H_{m_0} measured and hindcasted (with the model setups 2 and 2*) over time is shown in Fig. 3.7 for Gorgona, in which the model setup 2* fits better the higher values than model setup 2. Further examples for La Spezia and Ancona spots are shown in Appendix A. The behaviour as aforementioned described is observed for all the storms analysed. Table 3.11 shows values of bias (absolute) and NBI for model setup 2* generally

lower than model setup 2, whereas no substantial variation of the other indicators is observed.

The decision of modifying the values of β_{max} in the AR parameterization has been taken since the final goal of the whole forecast system is to predict hazardous sea state in coastal zones. Therefore, the WWIII prediction of the sea state at the storm peaks is more important than the prediction of average sea states, which generally do not represent any hazard for the coastal zone. On the basis of the sensitivity analysis conducted by Mentaschi et al. (2015), the values of β_{max} is increased to 1.75 instead of $\beta_{max} = 1.52$. The test conducted applying this value highlighted the capacity of the model to capture the higher significant wave heights and therefore, to provide reliable high storm boundary conditions to the next module of the system.

Given the results presented in this section, model setup 2* emerged as the best option to simulate the wave field in the Mediterranean Sea. Hence, WWIII with model setup 2* will be validated in the next paragraph.

1. Among the tested model set up, the one set with AR parameterization in combination with CFSR wind dataset provides the best agreement between hindcasted and observed significant wave heights. In particular, the modified version of the AR parameterization using $\beta_{max} = 1.75$ instead $\beta_{max} = 1.52$ better hindcast the sea state at the peak of the storms.

2. The final objective of the present study is too predict hazardous sea state in coastal zones. The role of WWIII is to simulate the development of the storms that potentially evolve to hazardous sea states on the coast. Therefore, the model has been calibrated with particular attention on the reliability of the results under severe storm conditions.

3.1.3 Model validation

In order to provide a strong validation of the WWIII model, the H_{m_0} parameter has been compared with the observations of 8 stations of the RON buoys network (see Fig. 3.9), available from the 1st December 2009 to the 31st July 2014. Records with H_{m_0} lower than 0.5m were excluded from the database, since they are affected by noise (Mentaschi et al., 2015). The wave climate recorded by each station is illustrated in Figure 3.10.

A first comparison of measured and hindcasted H_{m_0} is conducted by means a linear regression analysis, exemplary shown in Figure 3.8 for Alghero and La Spezia spots. A little underestimation of the values of H_{m_0} modelled is present in general. However, the values of the correlation coefficient is high for all the stations (i.e. 0.9), except for the spot in the Adriatic Sea. The limitation of the model in the Adriatic Sea is treated later.

A quantitative comparison of measured and hindcasted H_{m_0} is carried out by means of the statistical indicators listed in Table 3.12. MSE is excluded from the analysis since its behaviour is identical of that of the bias, whereas the standard deviation is excluded because its values are spurious in the present context. A new indicators (i.e. HH) is introduced in order to compare the results of the present validation which those obtained in Mentaschi et al. (2015).

The values of error indicators summarised in Tab. 3.13 demonstrate a good agreement between H_{m_0} measured and simulated. In particular, the values of bias ranges from -0.26m of Monopoli to -0.04 of Alghero and Civitavecchia. Also the values of NBI and HH are very encouraging and close to the values obtained in the study of Mentaschi et al. (2015). The higher differences between H_{m_0} measured and modelled are emerged for the buoys located in the Adriatic Sea, i.e. Ancona and Monopoli (see Fig. 3.9). This fact is probably due to the quite poor resolution of wind data (from 20km to 30km) that can't capture the complex mesoscale features occurring in the Adriatic Sea, where some wave directions are short fetched.

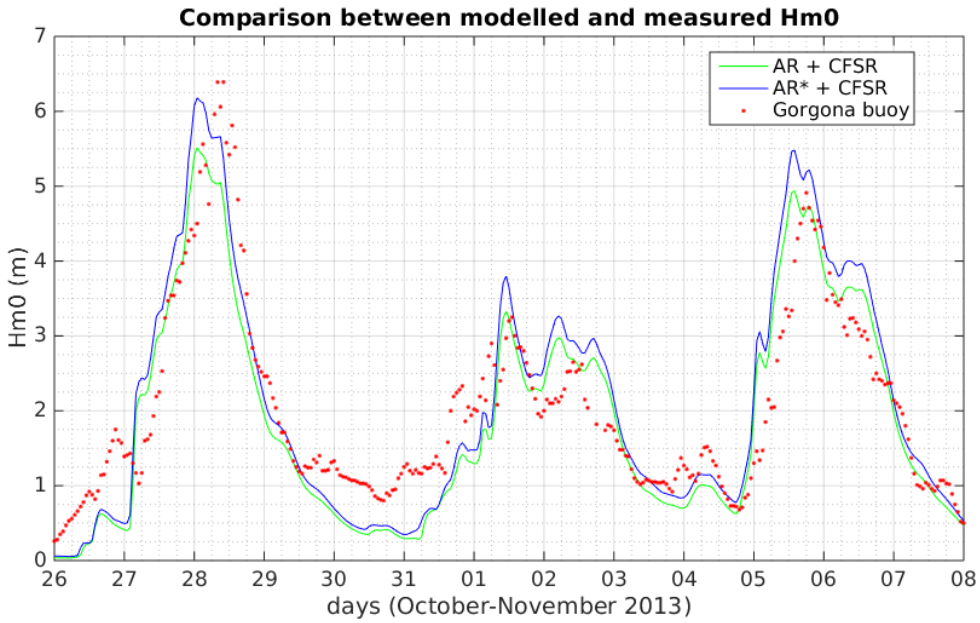

Figure 3.7: Comparison of H_{m0} time series obtained with the three model setups and measured at Gorgona.

Table 3.12: Statistical indicators for the evaluation of the WWIII model performance.

Statistical indicator	**Formula**
Bias	$\text{bias} = \frac{1}{n}\sum_{i=1}^{n}(y_i - x_i)$
Normalised Bias	$\text{NBI} = \frac{\sum_{i=1}^{n}(y_i - x_i)}{\sum_{i=1}^{n} x_i}$
Root Mean Square Error	$\text{RMSE} = \sqrt{\frac{1}{N} * \sum_{i=1}^{n}(x_i - y_i)^2}$
Normalised Root Mean Square	$\text{NRMSE} = \sqrt{\frac{\sum_{i=1}^{n}(x_i - y_i)^2}{\sum_{i=1}^{n} x_i^2}}$
Symmetrically Normalised Root Mean Square Error	$\text{HH} = \sqrt{\frac{\sum_{i=1}^{n}(x_i - y_i)^2}{\sum_{i=1}^{n} x_i * y_i}}$

Table 3.13: Summary of the statistical indicators obtained from the comparison between hindcasted and buoy data for H_{m_0} at 8 RON spots.

Buoy	**Observations**	**bias (m)**	**NBI**	**RMSE (m)**	**NRMSE**	**HH**
Alghero	12956	-0.04	-0.023	0.36	0.173	0.177
Ancona	4525	-0.18	-0.146	0.40	0.289	0.309
Civitavecchia	14085	-0.04	-0.045	0.32	0.287	0.290
Crotone	17244	-0.16	-0.141	0.34	0.264	0.281
La Spezia	20636	-0.11	-0.098	0.32	0.247	0.258
Monopoli	17503	-0.26	-0.267	0.39	0.361	0.415
Palermo	16063	-0.07	-0.075	0.29	0.224	0.234
Ponza	19092	-0.16	-0.136	0.36	0.252	0.269

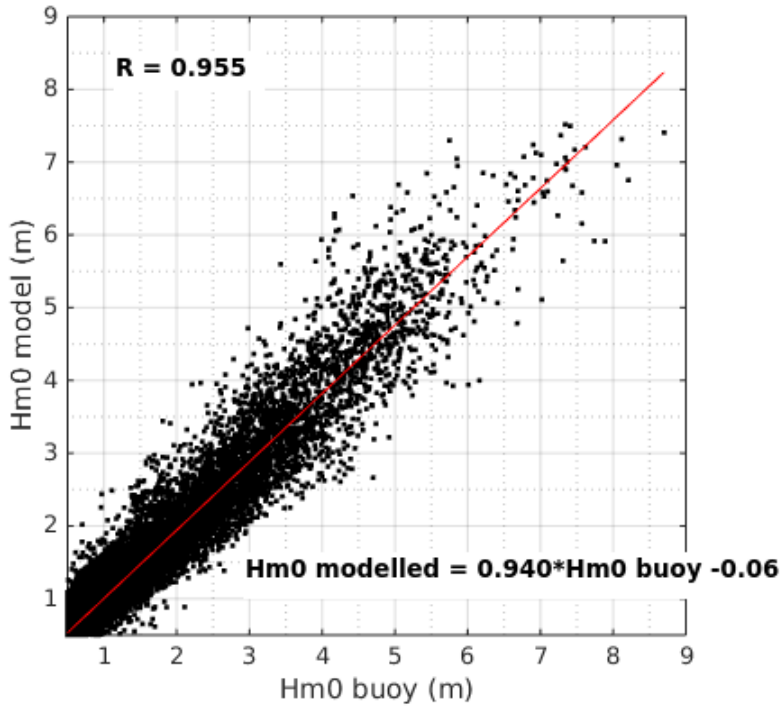

(a) *Alghero.*

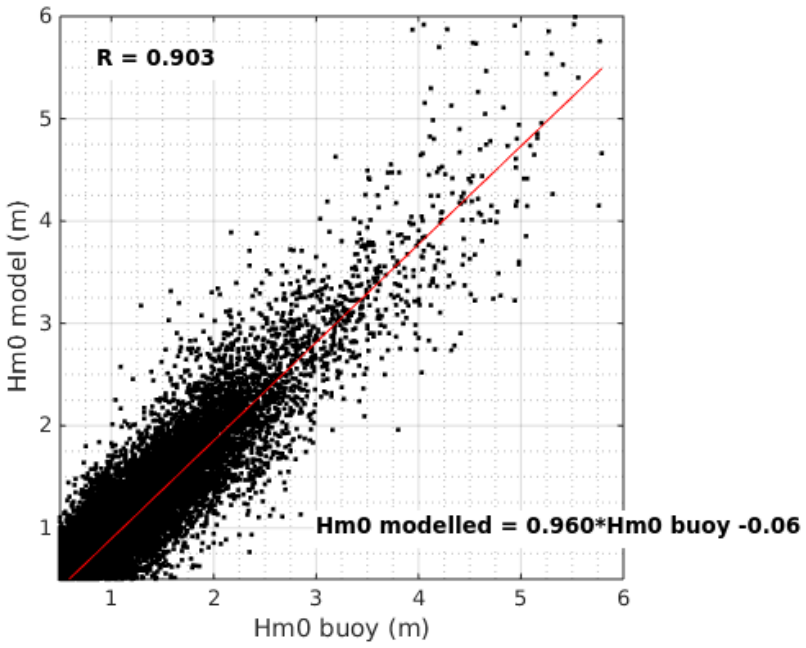

(b) *La Spezia.*

Figure 3.8: Linear regression graphs for modelled and observed H_{m_0} at (a) Alghero and (b) La Spezia.

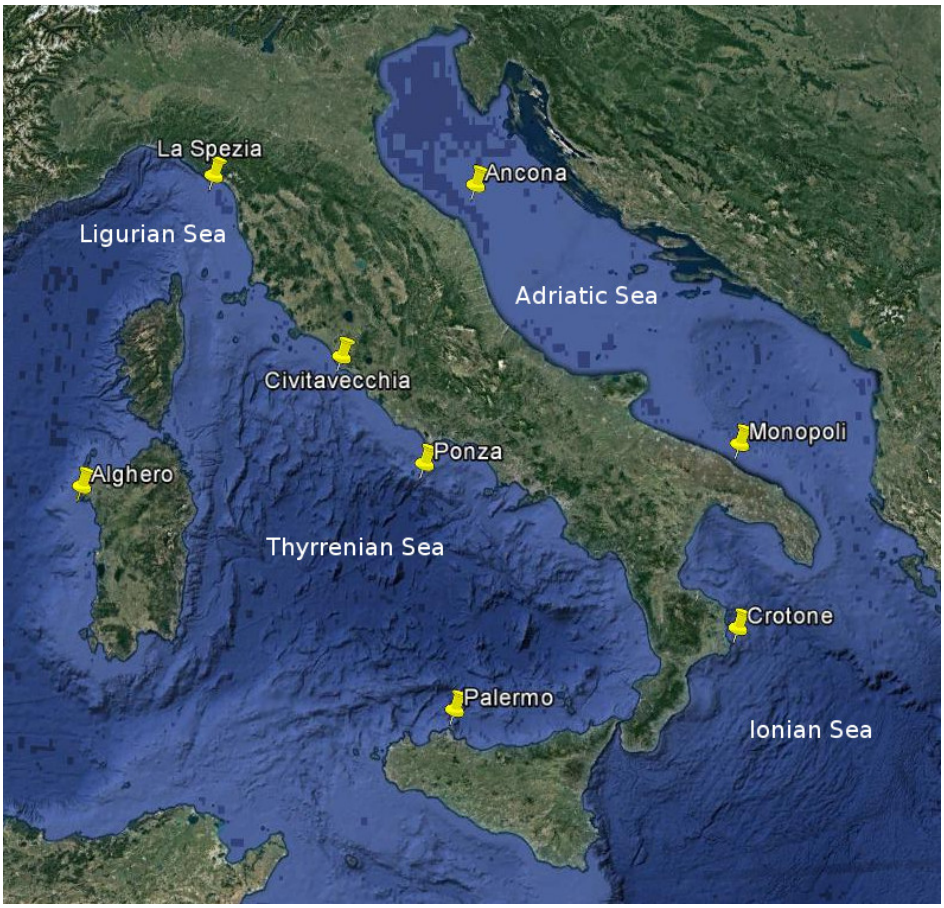

Figure 3.9: Location of the buoys of the RON network used for the validation of the model.

Table 3.14: Summary of the statistical indicators obtained from the comparison between hindcasted and buoy data for H_{m_0} at Crotone and Monopoli spots for all data and data filtered on direction.

Buoy	**Dataset**	**Observations**	**bias (m)**	**NBI**	**RMSE (m)**	**NRMSE**	**HH**
Crotone	All	17244	-0.16	-0.141	0.34	0.264	0.281
Crotone	Southern dir.	9390	-0.13	-0.130	0.32	0.245	0.262
Monopoli	All	17503	-0.26	-0.267	0.39	0.361	0.415
Monopoli	Northwest dir.	8635	-0.20	-0.207	0.32	0.322	0.385
Ancona	All	2404	-0.19	-0.118	0.46	0.260	0.275
Ancona	Southest dir.	1943	0.01	0.005	0.33	0.236	0.236

Table 3.15: Summary of the statistical error indicators obtained from the comparison between hindcasted and buoy data for H_{m_0} at 8 RON spots with a high-pass filter of 2m for measured H_{m_0}.

Buoy	**Observations**	**bias (m)**	**NBI**	**RMSE (m)**	**NRMSE**	**HH**
Alghero	3844	-0.14	-0.044	0.52	0.152	0.155
Ancona	560	-0.29	-0.114	0.61	0.234	0.249
Civitavecchia	706	0.04	0.017	0.50	0.197	0.195
Crotone	1623	-0.24	-0.090	0.62	0.221	0.232
La Spezia	1973	-0.19	-0.070	0.50	0.180	0.186
Monopoli	733	-0.47	-0.191	0.69	0.274	0.305
Palermo	2295	-0.21	-0.077	0.51	0.181	0.188
Ponza	2808	-0.28	-0.103	0.57	0.205	0.217

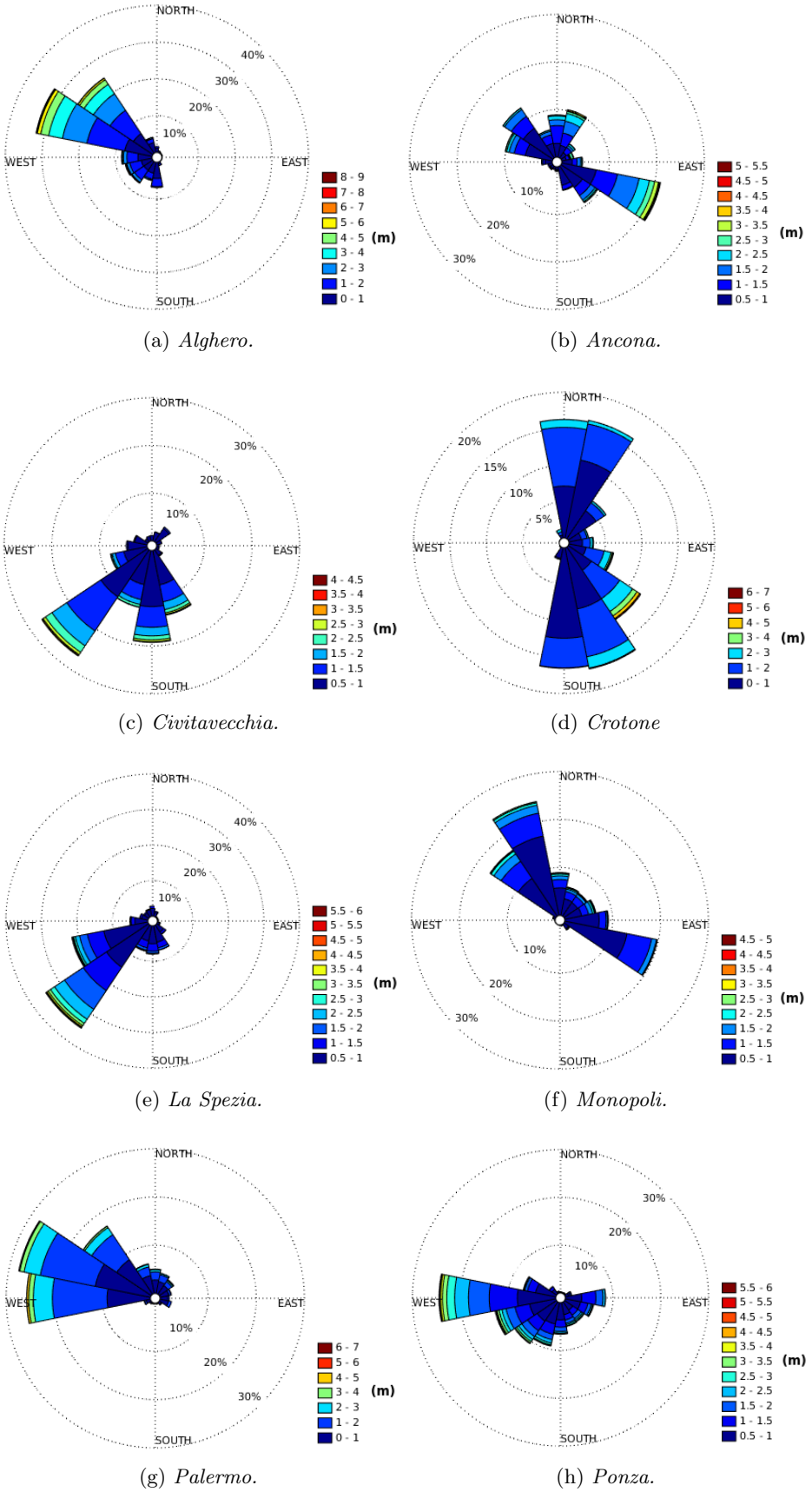

(a) *Alghero.* (b) *Ancona.*

(c) *Civitavecchia.* (d) *Crotone*

(e) *La Spezia.* (f) *Monopoli.*

(g) *Palermo.* (h) *Ponza.*

Figure 3.10: Wave climate for the 8 buoys of the RON network. Values of H_{m_0} lower than 0.5m are excluded.

This thesis is confirmed observing the measures at Crotone station, where two dominant wave directions are observed (see Fig. 3.10), one from Northern quadrant (short fetch) and the other from South quadrant (long fetch). Filtering the measurements in order to obtain a wave direction from Southern quadrant only, the correspondent error analysis (see Tab 3.14) shows a better agreement between measures and model than considering all the dataset.

The same operation was carried out for Ancona and Monopoli stations, where a long fetch component (Southeast and Northwest for Ancona and Monopoli, respectively) and a short fetch component (Northwest and Southeast for Ancona and Monopoli, respectively) of the wave rose can be observed in Fig. 3.10. The statistical analysis for the dataset filtered on the long fetch direction (Tab 3.14) shows better results than considering the complete dataset, in particular for Ancona.

In order to investigate the behaviour of the model in storm conditions, the statistical analysis were carried out filtering the significant wave height with a threshold of 2m (Tab. 3.15). A supplement analysis applying a threshold of 1m is presented in Annex (Tab. 4). The statistical values of Tab. 3.15 confirm the ability of the model to hindcast H_{m_0}, even in storm conditions.

The negative biases for all dataset became more negative for the threshold of 2m with the exception of Civitavecchia measurements, where the bias moves from -0.04m (all dataset) through +0.04 (2m threshold).

The NBI indicator confirms the good behaviour of the model. In general, NBI slightly decreases enhancing the threshold of H_{m_0}, with the exception of Palermo where NBI remains almost constant and Alghero where NBI slightly increases.

The trend of RMSE indicator is similar of the bias trend with an increasing of the values from Tab. 3.13 to Tab. 3.15, with the exception of Civitavecchia and Monopoli where the RMSE for 1m threshold is less than considering all dataset.

The behaviour of the NRMSE and HH indicators is similar and decrease from Tab. 3.13 to Tab. 3.15, with the exception for Monopoli that is fluctuating.

Concluding, the WWIII model, opportunely calibrated, is able to well hindcast H_{m_0} in the Mediterranean Sea, even in severe storm conditions. However, due to the spatial resolution of about 20-30km of CFSR wind data, the model underestimates wave height in case of short-fetch storms, where the wind velocity and direction can vary a lot in short space (i.e. less than 20km). This problem might be avoided in two suggested way: (1) to enhance the spatial resolution of wind data; (2) working on a fetch-depending $\beta_{\max}$ parameter.

For future improvements, it is primarily suggested to adopt in the model higher resolution wind data, usually provided by regional environmental agency. Unfortunately, these dataset are not open-source and agreements with the agencies are required. However, these choice seems to be the more reasonable for the first approach.

The choice of working on a new fetch-depending $\beta_{\max}$ parameter might be improve as well the results for severe waves associated with short-fetch storms since it revealed that higher values of $\beta_{\max}$ work well for short-fetch waves, whereas lower values of $\beta_{\max}$ work well in case of long-fetch waves. With a fixed value, this parameter needs a calibration for the typical fetch of the test case area, i.e. the Mediterranean Sea in the present study. The presence of different basins with different fetches in the area (e.g. Adriatic Sea, Aegean Sea) may be a limit of the model.

However, the final scope of the present study is to applied the model in the Tuscany area, supporting a Coastal Early Warning System (CEWS) associated with higher waves. In this area, higher waves are always associated with medium-fetch storms (i.e. the typical fetch of the Mediterranean Sea). Therefore, the value of $\beta_{\max}$ calibrated in Subsection 3.1.2 is specific for the Tuscany coast and no or few implications are expected for the final results. The application of the model in areas where higher waves are associated also with short-fetch storms (e.g. Adriatic Sea) needs particular attention, and the aforementioned improvements are highly suggested.

Concluding, the main finding of this section is that WWIII forced with CFSR wind can be adopted for hindcasting the offshore wave field, with the exception of short-fetch storms where recommendations are suggested. The results presented in Tab. 3.13 are comparable with those presented in Mentaschi et al. (2015), excluding the stations of Adriatic Sea (i.e. Ancona and Monopoli). It is worth to note, that CFSR wind data are freely available at the NCEP website and thus, without any computational effort due to the running of an atmospheric model such in the case of Mentaschi et al. (2015).

1. The validation of WWIII is carried out through the comparison of measured and hindcasted H_{m_0} based on about five years of observations at eight locations in the Italian seas.
2. The statistical analysis revealed that the model is able to hindcast wave height H_{m_0} at all considered locations with sufficient accuracy.
3. A limitation of the model is the underestimation of higher waves originated from short-fetch storms, that usually occur in the Adriatic Sea. This behaviour is related to the wider spatial resolution of the CFSR wind data.

1. The WWIII model set up 2* in Section 3.1 is able to generate and propagate the wave field in the Mediterranean Sea with sufficient accuracy.
2. Even for severe storm conditions, WWIII highlights relatively good results. This is crucial for transferring reliable storm wave conditions to the intermediate water module (i.e. SWAN).
3. Since the development of the wave field is strictly related to the wind forcing field, the choice of the wind database represents a crucial step.
4. Two datasets with different resolution are tested in Subsection 3.1.2: the ERA-Interim from ECMWF (resolution: about 57km), and the CFSR from NOAA (resolution: about 32km). Even though the CFSR database highlight the best results, the relatively coarse resolution of the dataset represents a limitation during short-fetch storms, in which high variations in wind direction and intensity might occur within a grid cell.
5. The limitation of wind database implies that in case of severe short-fetch storms, the model could fail, and to provide poor boundary conditions to the wave model in intermediate water depth.
6. However, in the present study the Operational Wave Model System (OWMS) will be applied for the coast of North Tuscany (see Chapter 5), where the validation of WWIII provides relatively good results (see La Spezia spot).

3.2 Wave modelling from deep to shallow water: SWAN

SWAN is a third generation spectral wave model, developed at Delft University of Technology. It includes the formulations for the deep water processes from the WAM model (Komen et al., 1994) integrated with the formulations for intermediate/shallow water. The code has been written in Fortran 90 programming language, and the version adopted in the present study

is the 41.10, released in 2016. The main advantage of SWAN compared to WWIII is the employment of implicit numerical schemes, which are more robust and economic in shallow water than the explicit ones (The SWAN Team, 2016a).

The objective of this section is the calibration and validation of the SWAN model to be implemented as the second module of the system, that simulates the evolution of waves in intermediate water. The model is forced with CFSR wind dataset (Saha et al., 2014; Saha et al., 2010), and the wave boundary conditions are provided from the WWIII model at the Mediterranean scale as described in Section 3.1.

The first subsection describes the governing equations of SWAN and the criterion for the selection of the computational grid. The second and third subsection describes the model calibration and validation, respectively.

3.2.1 Governing equations

The evolution of the wave field in space and time is described by means of the action balance (AB) equation, in the form:

$$\frac{\partial N}{\partial t} + \nabla_{\vec{x}} \cdot [(\vec{c}_g + \vec{U})N] + \frac{\partial c_\sigma N}{\partial \sigma} + \frac{\partial c_\theta N}{\partial \theta} = \frac{S}{\sigma} \tag{3.15}$$

where c_σ and c_θ representing the propagation velocities in the spectral space (σ, θ). The formulation for the general source term S is the same expressed in Eq. (3.12). The source terms for each process (see Tab. 3.18) have already been described in Chapter 2.

SWAN supports the use of two coordinates system, a 'flat' Cartesian coordinate system in metres for small scale applications, and a latitude/longitude coordinate system for applications on the continental shelf or quite large scale. In spherical coordinates, Eq. (3.15) is expressed as:

$$\frac{\partial N}{\partial t} + \frac{\partial c_\lambda \tilde{N}}{\partial \lambda} + \frac{\partial c_\phi \tilde{N}}{\partial \phi} + \frac{\partial c_\sigma \tilde{N}}{\partial \sigma} + \frac{\partial \tilde{c}_\theta \tilde{N}}{\partial \theta} = \frac{S}{\sigma} \tag{3.16}$$

with action density $\tilde{N} = NR^2 \cos\phi$ with respect to longitude λ and latitude ϕ. The propagation velocities in geographical space c_λ and c_ϕ are calculated as:

$$c_\lambda = \frac{d\lambda}{dt} = \frac{1}{R\cos\phi}\left[\frac{1}{2}\left(1 + \frac{2|\vec{k}|d}{\sinh(2|\vec{k}|d)}\right)\frac{\sigma|\vec{k}|\cos\theta}{|\vec{k}|^2} + U_\lambda\right] \tag{3.17}$$

$$c_\phi = \frac{d\phi}{dt} = \frac{1}{R}\left[\frac{1}{2}\left(1 + \frac{2|\vec{k}|d}{\sinh(2|\vec{k}|d)}\right)\frac{\sigma|\vec{k}|\sin\theta}{|\vec{k}|^2} + U_\phi\right] \tag{3.18}$$

with U_λ and U_ϕ the current velocities in longitude and latitude, respectively. The propagation velocity in θ-space (with assumption of deep water and without currents) is given by

$$\tilde{c}_\theta = c_\theta - \frac{c_{g_x}\cos\theta + c_{g_y}\sin\theta}{R}\cos\theta\tan\phi \tag{3.19}$$

SWAN is able to simulate the intermediate/shallow water processes as described in Table 3.16. It supports three types of computational grid, as summarised in Table 3.17. In the present study, simulations are carried out using regular grids with spherical coordinate system. The desired spatial resolution in the coastal region is reached by means of two telescoping grids with increasing resolution. The use of a triangular grid with increasing resolution in coastal water is excluded, since the bathymetry information in SWAN must be given as a regular grid. Therefore, in order to have consistency between the unstructured computational grid and the regular bathymetry grid, the size of the bathymetry grid must be equal to the size of the smallest triangle of the computational grid. This means to build a relative large bathymetry grid with high resolution, and consequent computing problems

Table 3.16: The ability of SWAN to simulate intermediate/shallow water processes.

Processes	**Ability**	**Remarks**
Nonlinear triad wave-wave interactions	Good	Accounted in a specific source term.
Dissipation due to bottom friction	Good	Accounted in a specific source term.
Shoaling	Poor	Quantitatively accounted in triad source term.
Reflection	Sufficient	A reflection coefficient can be specified for an obstacle.
Diffraction	Poor	Accounted in the left side of Eq. (3.15). Diffraction cannot be used in harbours or in front of reflecting breakwaters or cliff walls.
Depth-induced wave breaking	Sufficient	Quantitatively accounted in a specific source term.

Table 3.17: Type of computational grids implemented in SWAN.

Type	**Remarks**
Regular	Traditional rectangular grid, equally spaced in both directions. Widely used.
Curvilinear	Not well documented in SWAN manual.
Unstructured	Triangle based grid. SWAN accepts only grids generated with the software ADCIRC (commercial), TRIANGLE and EASYMESH. Supported only by Cartesian coordinate system in metres.

related to the big amount of data. Moreover, the CPU cost per grid point in triangular grid is often relatively higher than regular grids (The SWAN Team, 2016a). Therefore, this shortcoming could be greater than the advantage represented by the reduction in the number of grid points.

Resolving the AB equation in grids with relatively small resolution, such in the present study, leads to numerical problems related to the requirement of a very small time step that is impractical for an operational model. In order to employ a relatively larger (pseudo) time step by preserving numerical stability, SWAN employs an action density limiter (Hersbach and Janssen, 1999) that restricts the rate of change of the energy spectrum at each time step. The use of a larger (pseudo) time step is justified because most of the wave energy is transported by low-frequency waves. However, it is worth to mention that de Waal (2001) suspected that the limiter could be a hidden sink term in the AB equation.

In the latest version of SWAN, the balance between pseudo time step and minimizing the error due to the limiter is accounted with the frequency-dependent under-relaxation approach (The SWAN Team, 2016a). The principle of this techniques is to reduce the high rate of change of energy at higher frequency by means of the employ of a smaller pseudo time step (Ferziger and Perić, 2002). Therefore, the pseudo time step used in SWAN depends on which frequency region of the spectrum the AB equation is solved.

Time discretization is carried out by means of the implicit Euler scheme. The discretization in geographical space can be accounted with different method as summarised in Table 3.19. The discretization in the spectral space (σ, θ) is approximated with a hybrid central/upwind scheme (The SWAN Team, 2016a).

The stopping criterion of the iterative process uses the second derivative of succesive iterations of the calculated wave height.

1. SWAN is a spectral wave model that includes formulations for deep water processes integrated with the formulations for intermediate/shallow water.
2. The main advantage of using SWAN for intermediate/shallow water applications is the employment of implicit numerical schemes, which are more robust and economic in intermediate/shallow water than the explicit ones, such as those in WWIII.
3. In the present study, simulations are carried out using regular (rectangular) computational grids with spherical coordinates system. This implies the use of two telescoping grids in order to reach the requested coastal resolution.

3.2.2 Model calibration

The objective of this subsection is the calibration of SWAN for applications in the continental shelf of the North Tuscany, where the model system will be tested in Chapter 5. Wave boundary conditions are provided from WWIII running at Mediterranean scale as described in the previous subsection. Wind forcing field is obtained from CFSR database.

A first set of preliminary tests is carried out in paragraph (a) simulating the most intense storms observed by a wavemeter buoy in intermediate water (i.e. Carrara). The aims of these tests is to evaluate the behaviour of SWAN in intermediate water. Then, assuming that the bottom friction process is the most important in intermediate water, a sensitivity analysis is conducted on this source term in paragraph (b).

(a) Preliminary tests

The most severe storms observed by the Carrara wavemeter buoy (Autorità Portuale di Marina di Carrara, 2005) (see Fig. 3.11) are simulated in order of evaluate the behaviour of

Table 3.18: List of available formulations for source terms in SWAN.

Source term	**Formulation**	**Reference**	**Switch**
S_{ln}	CMR	Cavaleri and Rizzoli (1981)	AGROW
$S_{\text{in}} + S_{\text{ds}}$	WAM3	Komen et al. (1984)	KOMEN
	JANS	Janssen (1991) + Komen et al. (1984)	JANSSEN
	WEST	Yan (1987) + van der Westhuysen (2007)	WESTH
S_{nl4}	DIA	Hasselmann et al. (1985)	QUAD (1,2,3,8)[1]
	MDIA	Hashimoto and Kawaguchi (2001)	QUAD 4
	WRT	Resio and Perrie (1991), Tracy and Resio (1982), van Vledder (2006), and Webb (1978)	QUAD (51,52,53)[1]
S_{nl3}	LTA	Eldeberky (1996)	TRI 1
	SPB	Becq-Girard et al. (1999)	TRI 2
S_{bfr}	JONSWAP	Hasselmann et al. (1973) and WAMDI Group (1988)	JON
	COLLINS	Collins (1972)	COLL
	MADSEN	Madsen et al. (1988)	MAD
	RIPPLES	Smith et al. (2011)	RIP
	Ng	Ng (2000)	MUD
S_{br}	BJ	Battjes and Janssen (1978)	BRE

[1] The switch depends on which numerical scheme is adopted

Table 3.19: List of available propagation schemes in SWAN.

Scheme	**Reference**	**Remarks**	**Switch**
First order	Rogers et al. (2002)	Simple 1st order upwind scheme. Numerically diffusive over large scale.	BSBT
SORDUP	Rogers et al. (2002)	Second order scheme. Only for stationary computation.	STAT
S&L	Stelling and Leendertse (1992)	Second order scheme. Less diffusive that First order scheme.	NONSTAT

SWAN in intermediate water with wave boundary condition provided by WWIII.

The SWAN model is more "user friendly" than WWIII. All the settings (e.g. physics, numerical schemes) are given by means of a unique input file. The first model setup (see Tab. 3.20) is given following the work of Pelli (2011), who calibrated the model for applications in the Ligurian Sea.

Eleven storms (or storminess periods) selected in the period 2006-2011 (see Table 3.21) are simulated. All storms show observed peaks of H_{m_0} higher than 3.5m. Since the observed T_{m01} ranges from 7.1s to 9.1s, assuming that $T_p = 1.2 * T_{m01}$, the values of kd ranges from 1.01 and 0.75. Therefore, the condition of intermediate water ($\pi > kd > \pi/10$) is satisfied.

Two telescoping rectangular grids are employed (see Fig. 3.11) to downscale the wave field from deep water to the intermediate water of the Tuscany coast, with 800m and 100m of resolution, respectively. Wave conditions at the 800m grid boundaries are provided from the Mediterranean hindcasting performed with WWIII, whereas boundary conditions for the finer resolution grid (100m) were directly obtained from the coarser resolution grid (800m).

Even though the first order scheme for spatial propagation is numerically quite diffusive, it is applied for simulations since the effect of numerical diffusion in continental shelf application is negligible (Cavaleri et al., 2007; Rogers et al., 2002; The SWAN Team, 2016a). This is confirmed by tests conducted applying the S&L propagation scheme (second order), which revealed the same values of H_{m_0} obtained with the employment of the first order scheme. Moreover, a significant enhancement of the computational time was observed.

The hindcasted and observed data are compared by plotting the development of H_{m_0} over time. Typical results, are exemplary shown in Fig. 3.12 for storm 4 and 11. Three hindcasted curves are shown, the Mediterranean model (WWIII) in blue, the SWAN coarser resolution model (800m) in red, and the SWAN finer resolution model (100m) in cyan. Measured data at Carrara are plotted in green. Fig. 3.12 shows that the hindcasted H_{m_0} peak values often underestimate the observed H_{m_0} peak values, especially for the higher peaks. This trend was observed over all the analysed storms of Tab. 3.21.

For H_{m_0} peaks greater or equal to 3m, WWIII shows the worst agreement with the measurements, whereas the SWAN finer model (SWAN 100) shows the best agreements, mainly due to the relevance of bottom induced wave transformation and bottom friction in intermediate water, the latter being better reproduced in finer grid. However, results for WWIII and SWAN are very close, but the application of SWAN is justify by its lower computing demanding in higher resolution grids.

Further verifications are required due to the underestimation of H_{m_0} revealed by SWAN, particularly high for severe storm conditions.

Table 3.20: The first setup of SWAN as used for the simulation of the storms in Tab. 3.21.

Process	**Source term**	**Formulation**	**Switch**
Linear wind input	S_{ln}	CMR	AGROW
Exponential wind input + Whitecapping	$S_{\text{in}} + S_{\text{ds}}$	JANS	JANSSEN
Quadruplet	S_{nl4}	semi-explicit DIA	QUAD 1
Triad	S_{nl3}	LTA	TRI 1
Bottom friction	S_{bfr}	JONSWAP	JON
Wave breaking	S_{br}	BJ	BRE

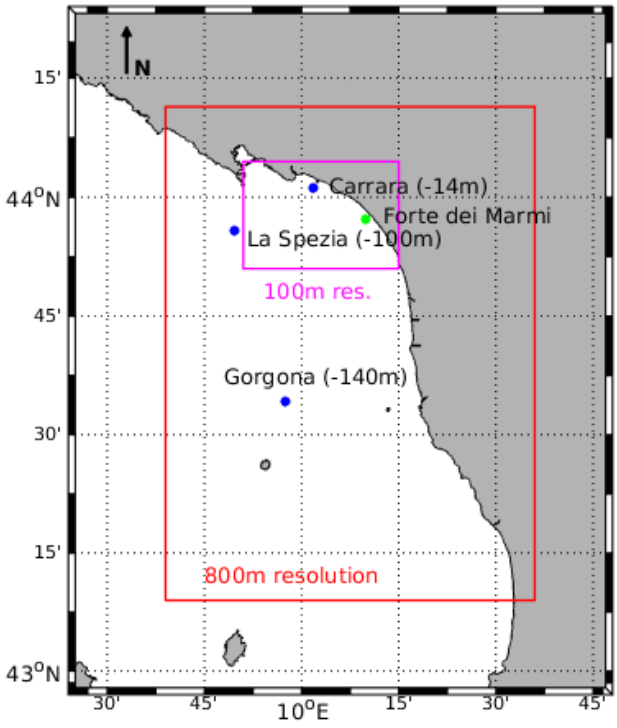

Figure 3.11: Location of La Spezia, Gorgona and Carrara buoys (blue dots) with mooring depth in brackets, Forte dei Marmi anemometer (green dot) and computational grids.

Table 3.21: List of the storms simulated between 2006 and 2011 in the Ligurain Sea with the maximum H_{m_0} recorded at Carrara (depth -14m) and the associated $T_{m_{01}}$.

Storms	**Initial date**	**End date**	$\mathbf{H_{m_0}}$	$\mathbf{T_{m_{01}}}$
1	2006-12-30	2007-01-04	4.34	7.4
2	2007-01-21	2007-01-26	4.42	7.4
3	2007-02-05	2007-03-05	3.82	7.1
4	2007-03-18	2007-03-22	4.83	7.6
5	2007-12-02	2007-12-12	5.00	7.9
6	2008-03-01	2008-03-27	5.37	8.3
7	2008-04-05	2008-04-24	3.96	8.3
8	2008-10-29	2008-11-02	5.09	7.9
9	2008-11-20	2008-12-09	5.30	8.6
10	2009-12-20	2010-01-12	4.11	7.3
11	2010-11-25	2010-12-01	4.43	9.1

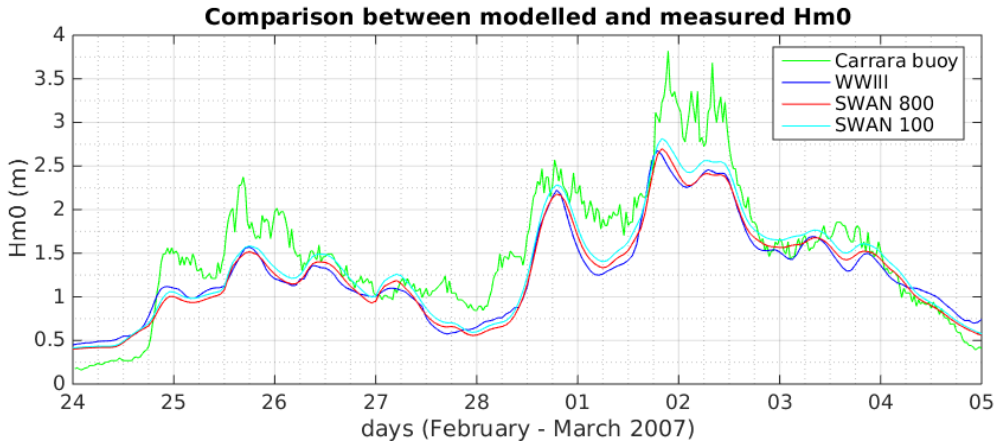

(a) *Storm 4.*

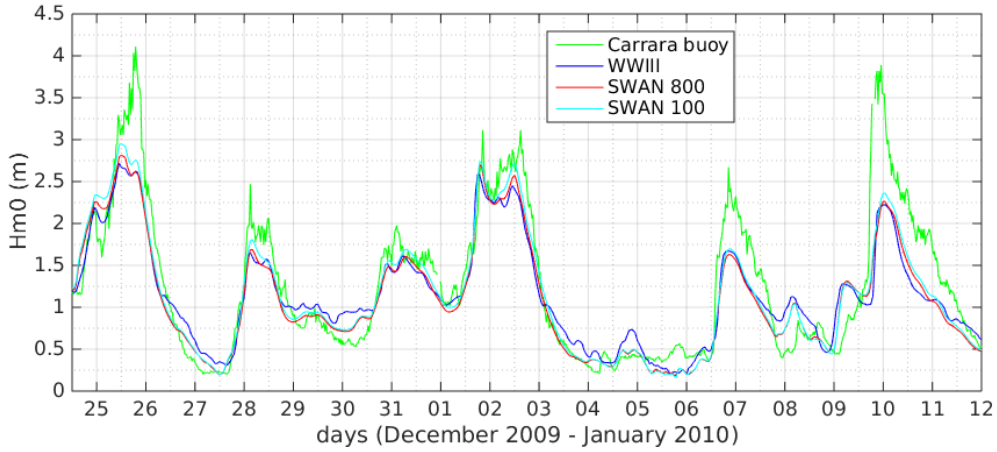

(b) *Storm 11.*

Figure 3.12: Comparison of H_{m_0} time series obtained with the first setup of SWAN and measured at Carrara (d=-14m) (see Table 3.21 for storm definitions).

(b) Sensitivity analysis

In order to decrease the gap between hindcasted and observed H_{m_0}, a sensitivity analysis is carried out on the bottom friction sink term (S_{bfr}), that is assumed to be the most important term affecting energy dissipation in intermediate water. Seven storms (listed in Tab. 3.22) are chosen with the purpose of comparing the hindcast and measured data both in deep (La Spezia buoy) and shallow water (Carrara buoy). The storms listed in Table 3.22 show observed peaks values of H_{m_0} higher than 2m. As shown in Fig. 3.11, the two wavemeter buoys are aligned on the dominant wave direction (i.e. South-West, see La Spezia station in Fig. 3.10) and thus, the effect of bottom friction can be analysed observing the evolution of waves propagating between the two locations.

The tested bottom friction sink term formulations and friction parameters are summarised in Tab. 3.23. The values of parameters shown in Tab. 3.22 were chosen following the SWAN user manual (The SWAN Team, 2016c) and the work of Padilla-Hernandez and Monbaliu (2001).

The development of the measured and simulated H_{m_0} over time is exemplary shown in Fig. 3.13 for Storm 1. In particular, panel (a) shows the comparison of measured data (green), WWIII hindcast (blue), and SWAN 800 hindcast at La Spezia spot, located about 20km offshore of Carrara buoy in SW direction. Only the SWAN 800 jon 0.019 is shown in panel (a), since the results for the different friction formulations present similar values of H_{m_0} at La Spezia spot (i.e. the effect of bottom friction is not relevant in deep water, see Chapter 2). Panels (a) of Fig. 3.13 shows that SWAN generally underestimates the H_{m_0} peaks as compared to WWIII. This behaviour is typical for all the hindcasted storms.

Since La Spezia buoys is moored in deep water, the differences between SWAN and WWIII are mainly due to differences in the formulations of deep water processes (i.e. wind input, whitecapping and quadruplet nonlinear interactions). However, all the storms simulated have highlighted differences in the order of few centimeters with exception of some isolated case.

Observing the measured wind velocities at Forte dei Marmi station, located about 13km from Carrara buoy (see Fig. 3.11), it is turned out that in case of strong wind the difference between WWIII and SWAN is slight, whereas in case of light wind this difference is generally larger. The aforementioned trend was observed in the majority of the storm simulated.

Therefore, in case of strong wind WWIII and SWAN works well both (at least for the spatial scale considered), whereas in case of waves propagating with light or no wind (swell) SWAN dissipates too much energy as compared to WWIII. This might be probably due to the numerical diffusion of the first order propagation scheme of SWAN, since in case of swell (i.e. waves propagating with no wind) deep water processes are not significant for the evolution of the energy spectrum. Another possible cause of this slight but systematic underestimation might be due to the different spectral resolution used in the two models,

Table 3.22: List of the storms simulated for evaluating the behaviour of the bottom friction sink term, with the maximum H_{m_0} recorded at La Spezia (-100m) and Carrara (-14m).

Storms	**Initial date**	**End date**	**La Spezia**		**Carrara**	
			$\mathbf{H_{m_0}}$	$\mathbf{T_{m_{01}}}$	$\mathbf{H_{m_0}}$	$\mathbf{T_{m_{01}}}$
1	2009-12-27	2010-01-12	4.48	7.7	3.82	6.9
2	2010-02-03	2010-02-22	3.48	6.6	2.62	6.4
3	2010-07-23	2010-07-29	3.10	5.8	2.62	6.0
4	2010-08-14	2010-08-20	2.97	6.0	2.33	5.7
5	2010-09-07	2010-09-30	2.89	5.8	2.52	5.5
6	2010-10-03	2010-10-07	2.30	5.7	1.72	5.6
7	2010-10-19	2010-12-28	2.67	6.5	2.30	6.7

Table 3.23: Bottom friction sink term formulations and friction parameters used for the simulation of the second set of storms.

Formulations	**Parameters**	**Acronyms**
JONSWAP	cfjon = 0.038	def
JONSWAP	cfjon = 0.019	jon 0.019
COLLINS	cfw = 0.030	col 0.030
MADSEN	kn = 0.003	mad 0.003

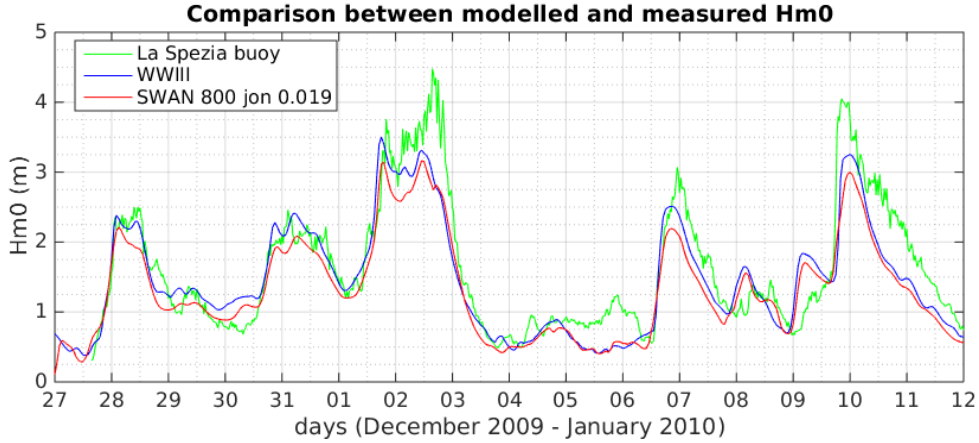

(a) *La Spezia spot.*

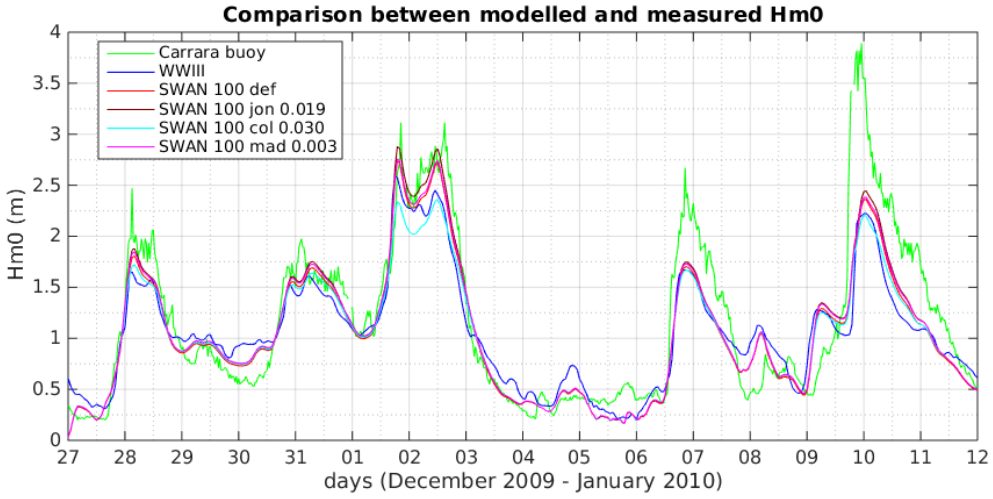

(b) *Carrara spot.*

Figure 3.13: Comparison of H_{m_0} time series modelled and measured at La Spezia (a) and Carrara (b) for Storm 1 of Tab 3.22.

i.e. 25 frequencies and 24 direction for WWIII, and 30 frequencies and 36 direction for SWAN. More investigation are needed in future research, in order to understand the origin of this systematic underestimation that affects the final results.

Panels (b) of Fig. 3.13 shows the comparison of measured data (green), WWIII hindcast (blue), SWAN def (red), SWAN jon 0.019 (brown), SWAN col 0.030 (cyan), and SWAN mad 0.003 (magenta). The best agreement between observations and hindcasting is given by the SWAN 100 jon 0.019 setup. Wave development of H_{m_0} for the default setup and for SWAN mad 0.003 are similar, but the gap between observation increases a little. Results for SWAN 100 col 0.030 are similar of those of WWIII, highlighting the biggest gap from observations, especially in correspondence of wave peaks. The trend as aforementioned described is typical for all the hincasted storms.

The objective of the comparison between measured and hindcasted H_{m_0} both in La Spezia and Carrara, as exemplary shown in Figs. 3.13, is to individuate the reasons for the underestimation by SWAN of some H_{m_o} peaks at Carrara spot. If the bias between H_{m_0} peaks observed and hindcasted remains constant between La Spezia and Carrara, it means that the cause of the underestimation should be an inaccuracy of the wave boundary conditions. On the other hand, if the biases at Carrara are larger than La Spezia, the cause of the underestimation is a poor performance of SWAN.

The development of H_{m_0} over time observed for the hindcasted storm of Table 3.22, and exemplary shown in Fig. 3.13 can be summarised as follows:

- There is a systematic negative bias of few centimeters between SWAN and WWIII at La Spezia for H_{m_0} around the storm peaks, with some exceptions in case of swell conditions, where the bias is larger.

- The best agreement between H_{m_0} observed and hindcasted at Carrara spot is obtained with SWAN 100 jon 0.019.

- The negative biases around the storm peaks between the SWAN hindcast and observations remain generally constant when waves travel from deep water (La Spezia) to shallow water (Carrara). This indicates that the model underestimation of some of the storm peaks is caused by an underestimation of the wave boundary conditions.

- Besides the described typical trend there are also some exceptions, such as the H_{m_0} peak of 10 January 2010 (Fig. 3.13), where the negative bias between model results and measurements is larger in Carrara than in La Spezia.

Hence, the uncertainties of the SWAN model are mainly related to the WWIII boundary conditions. As revealed in Section 3.1, the cause of the underestimation can be found in the poor grid resolution of forcing wind data (20km) that in some cases is not able to capture wind features at smaller scales. This explanation might also justify the exception of 10 January 2010, because waves travelling under underestimated wind conditions increase the deviations of the computed values from the measurements when moving from La Spezia to Carrara.

Therefore, the case of 10 January 2010 depicted in Fig. 3.13 is particularly analysed by comparing the forcing wind field obtained from CFSR with the wind measurements at Forte dei Marmi. Fig. 3.14 shows clearly the underestimation of the two main wind storms on 7 and 10 January by the CFSR database, leading to an underestimation of the hindcasted H_{m_0} peaks visible in Fig. 3.13.

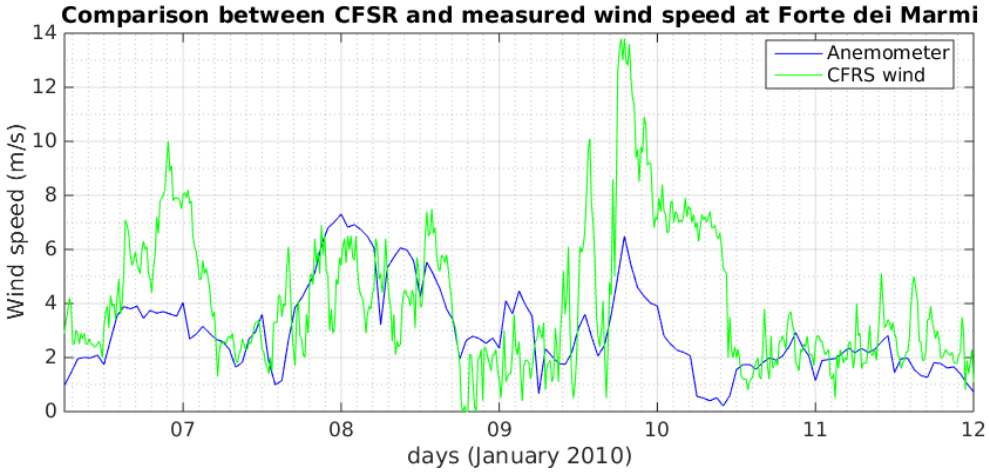

Figure 3.14: Comparison between CFSR forcing wind and measured wind at Forte dei Marmi spot.

1. The performance of the SWAN model is analysed in intermediate water by hindcasting eleven recorded storms, and comparing the hindcasted and observed significant wave heights H_{m_0}. The comparison has revealed a general underestimation of the hindcasted wave heights at the peak of the storms.

2. Assuming that the bottom friction represents the most relevant factor affecting dissipation in intermediate water, a sensitivity analysis has been conducted by varying this sink term.

3. From the results of the sensitivity analysis the best formulation for bottom friction is obtained (i.e. friction coefficient equal to 0.019 for JONSWAP parameterization).

4. However, it is noticed that the underestimation of wave peaks is mainly due to uncertainties of the wind forcing.

3.2.3 Model validation

The SWAN model chain (800m grid + 100m grid) has been validated for the best model setup (SWAN jon 0.019 as obtained from the model calibration) by using the main storms recorded in intermediate water at Carrara station (see Tab. 3.21) using the best model setup, as obtained from the model calibration (i.e. SWAN jon 0.019). Significant wave heights H_{m_0} computed with the finer grid resolution (100m) were compared with the measures at Carrara spot using the statistical indicators listed in Tab. 3.10. The results of the statistical analysis carried out over the complete set of measured data (a high-pass filter of 0.5m was applied to eliminate the noise of the instrument) and applying a threshold of 1m, 2m, are summarised in Tab. 3.24.

Considering all the dataset, the values of the statistical indicators are comparable with

Table 3.24: Summary of the statistical indicators obtained from the comparison between hindcasted and buoy data for H_{m_0} recorded at Carrara spot.

Threshold (m)	Observations	bias (m)	NBI	RMSE (m)	NRMSE	HH
0.5	3320	-0.16	-0.123	0.39	0.247	0.268
1.0	1833	-0.28	-0.150	0.49	0.244	0.267
2.0	610	-0.52	-0.189	0.72	0.256	0.281

the ones obtained from the WWIII model at La Spezia, located 20km offshore to Carrara (see Tab. 3.13). Applying the 1m filter, the values obtained from WWIII at La Spezia demonstrated a slightly better agreement as compared to those from SWAN.

Applying a filter of 2m over the recorded wave signals, the statistical indicators in Tab. 3.24 show a significant underestimation of wave heights obtained from the SWAN model as compared to those obtained from WWIII. The results of the statistical analysis carried out for WWIII at La Spezia and for SWAN at Carrara are compared in Tab. 3.25.

The possible reasons of this underestimation for severe storm conditions might be summarised as follows:

- Wave dynamics in intermediate/shallow water are generally more difficult to simulate than deep water dynamics, and higher values of the statistical indicators are expected.

- In case of swell, SWAN provides smoothed values of H_{m_0}, resulting in an underestimation of the wave height peaks.

- Some storms are heavily underestimated due to the uncertainty in the input wind data used in WWIII. In this case, the underestimation already observed in La Spezia (deep water) continues to increase in shallow water (Carrara).

Table 3.25: Statistical indicators obtained from the comparison between hindcasted and buoy data for H_{m_0} at La Spezia (WWIII) and Carrara (SWAN). A high-pass filter of 2m over the measured database was applied.

Station	Observations	bias (m)	NBI	RMSE (m)	NRMSE	HH
La Spezia (WWIII)	1973	-0.19	-0.070	0.50	0.180	0.186
Carrara (SWAN)	610	-0.52	-0.189	0.72	0.256	0.281

1. A SWAN model system with two telescoping grids and two grid resolutions (i.e. 800m and 100m) was applied to downscale the wave field from deep water to the intermediate water of Tuscany coast. Initial and boundary conditions were obtained from the WWIII model operating at the scale of the Mediterranean Sea.

2. Preliminary tests revealed a significant underestimation of H_{m_0} at the peaks of some severe storms.

3. Therefore, a sensitivity analysis is conducted on the bottom friction source term as the most relevant for wave energy dissipation in intermediate water. Hence, the best set for bottom friction has been found.

4. However, the model validation still revealed a general underestimation by the SWAN model of the wave field observed in intermediate water.

5. A statistical analysis is carried out for the validation of the SWAN model in intermediate water. Comparing the statistical indicators with those obtained for WWIII (Section 3.1), an increase of the underestimation of H_{m_0} is observed in intermediate water. However, a decrease of the model performance from WWIII to SWAN was expected, since modelling of wave processes in intermediate water (SWAN) is generally more difficult than in deep water (WWIII).

6. According to the results in Subsection 3.2.2, it is likely that the underestimation of H_{m_0} is partly due to the inaccuracy of the wave boundary conditions provided by WWIII using uncertain and low resolution wind input data. This would imply that a better and higher resolution wind forcing database is required in order to enhance the quality of the results.

3.3 Nearshore modelling of waves and effect of bathymetry changes: XBeach

XBeach is a numerical model for wave propagation, mean flow, sediment transport and morphological changes of the nearshore area, beaches, dunes and further coastal barriers. It is an open source and public-domain model that has been developed with major funding from the US Army Corps of Engineers, Rijkswaterstaat and the EU, supported by a consortium of UNESCO-IHE, Deltares, Delft University of Technology and the University of Miami (Roelvink et al., 2015).

The objective of this section is to briefly describe and validate the XBaech model in order to successively implement it as the third module of the Operational Wave Model System (OWMS), that simulates the evolution of waves in shallow water. Furthermore, a sensitivity analysis is conducted on the most relevant parameters to understand how to calibrate the model for the application case described in Chapter 5. Wave boundary conditions are provided from the SWAN model operating at a regional scale as described in Section 3.2.

The first subsection describes the governing equations of XBeach. The second subsection describes the model validation, and the third subsection describes the sensitivity analysis.

3.3.1 Governing equations

The description provided in this subsection is taken from the official XBeach website (`http://oss.deltares.nl/web/xbeach/home`), the official Technical Reference (Deltares, 2016), and the Internal Report Nr.1058 of Elsayed and Oumeraci (2015). The philosophy of XBeach regarding the model setup is similar to that of SWAN, i.e. all formulations and parameters

are specified in a unique input file that simplifies the use of the model. The model set-up are specified in the input file through a list of keyword/values.

The coordinate system of the XBeach computational grid is always oriented with the x-axis towards the coast and the y-axis alongshore (Fig. 3.15). Coordinates must be defined in world meter-based system (e.g. UTM), but in case of rectangular grid coordinates can be defined in a local coordinates system, oriented with respect to the world coordinates (x, y) by means an origin (defined by *xori* and *yory*) and orientation (*alfa* angle). The (nx) and (ny) values indicate the number of segments in x- and y-dimension, respectively.

XBeach can solve equations for wave propagation, flow, sediment transport and bottom changes over two types of grid:

1D single alongshore grid cell ($ny = 0$).

2DH more than three alongshore grid cells ($ny > 2$).

Depending on the time-scale considered by the user, XBeach can run in three modes:

- **Stationary mode**: Wave-group variations and infragravity waves are neglected. This mode can be used to model morphological changes during moderate waves conditions (when waves are generated by a local wind).

- **Surfbeat mode** (*nonstationary mode*): The variation of short-waves envelope on the scale of wave groups is solved, including infragravity waves. This mode can be used on dissipative beaches, in which short-waves are manly dissipated by depth-induced breaking.

- **Non-hydrostatic mode** (*wave resolving mode*): Depth-averaged flow due to waves and currents are solved using the Nonlinear Shallow Water (NLSW) equations. This is particularly important for the processes on steep beaches as short-wave runup and overwashing are included.

A sketch representing short and long waves, as well as short waves envelope and mean water level (MWL) is presented in Fig. 3.16.

The application of XBeach in this study mainly aims at the prediction of changes of the coastal morphology, including bathymetry changes and the associated wave dynamics on dissipative beaches. Furthermore, the process of inundation of the beach due to long-waves is also highlighted. Therefore, Xbeach should be used in *surfbeat mode*. This mode assures also a faster computational performance than the *non-hydrostatic mode*, a feature which is very important for a model supporting a Coastal Early Warning Systems (CEWS).

In the surfbeat mode, short-wave motion and the related shallow water momentum equation is accomplished from a time-dependent version of the stationary HISWA model (Holthuijsen et al., 1989). Thus, the action balance (AB) equation is given by:

$$\frac{\partial N}{\partial t} + \frac{\partial c_{g_x} N}{\partial x} + \frac{\partial c_{g_y} N}{\partial y} + \frac{\partial c_\theta N}{\partial \theta} = -\frac{S_{\mathrm{br}} + S_{\mathrm{bfr}} + S_{\mathrm{v}}}{\sigma} \tag{3.20}$$

where c_{g_x}, c_{g_y} and c_θ are propagation velocities in x, y and θ direction, respectively. The terms S_{br}, S_{bfr} and S_{v} represent the dissipation due waves breaking, bottom friction and vegetation, respectively.

For the nonstationary mode, the three different formulations for S_{br} listed in Tab. 3.26 are implemented. The default values of the coefficient γ and n are calibrated for the formulation of Roelvink (1993) (*roelvink1*). The other formulation needs a re-calibration of the coefficients. Therefore, *roelvink1* will be applied during the present research. The formulation of Roelvink

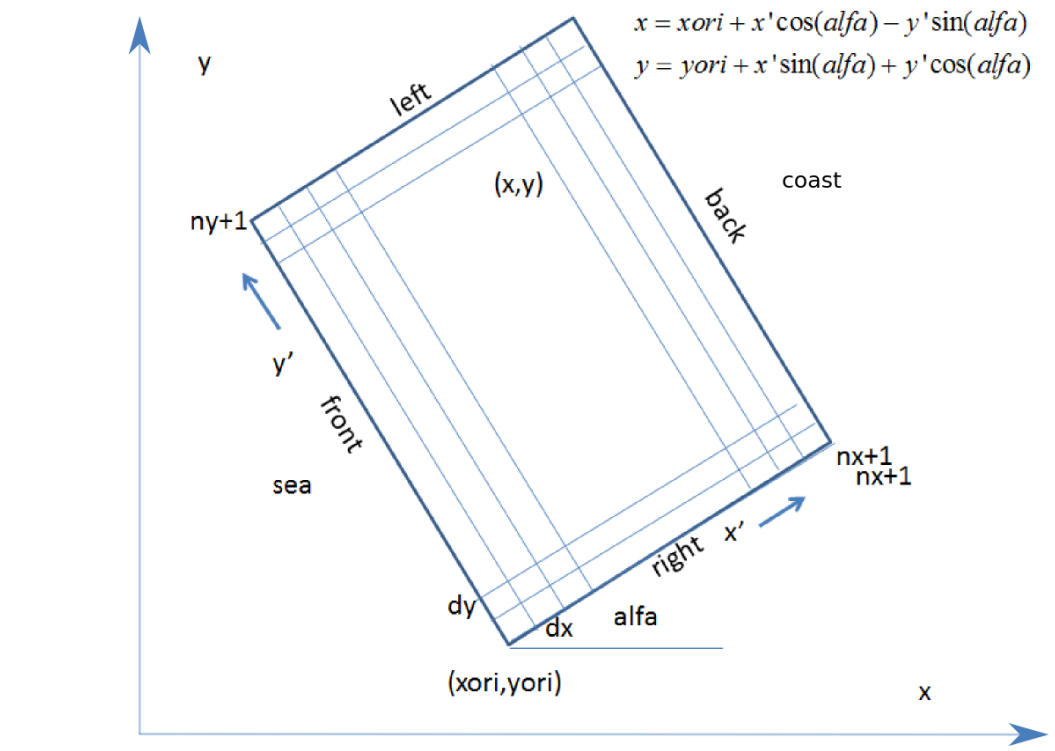

Figure 3.15: Example of rectangular coordinate system, with world coordinates (x, y), local coordinates (x', y') and *alfa* angle (Deltares, 2016).

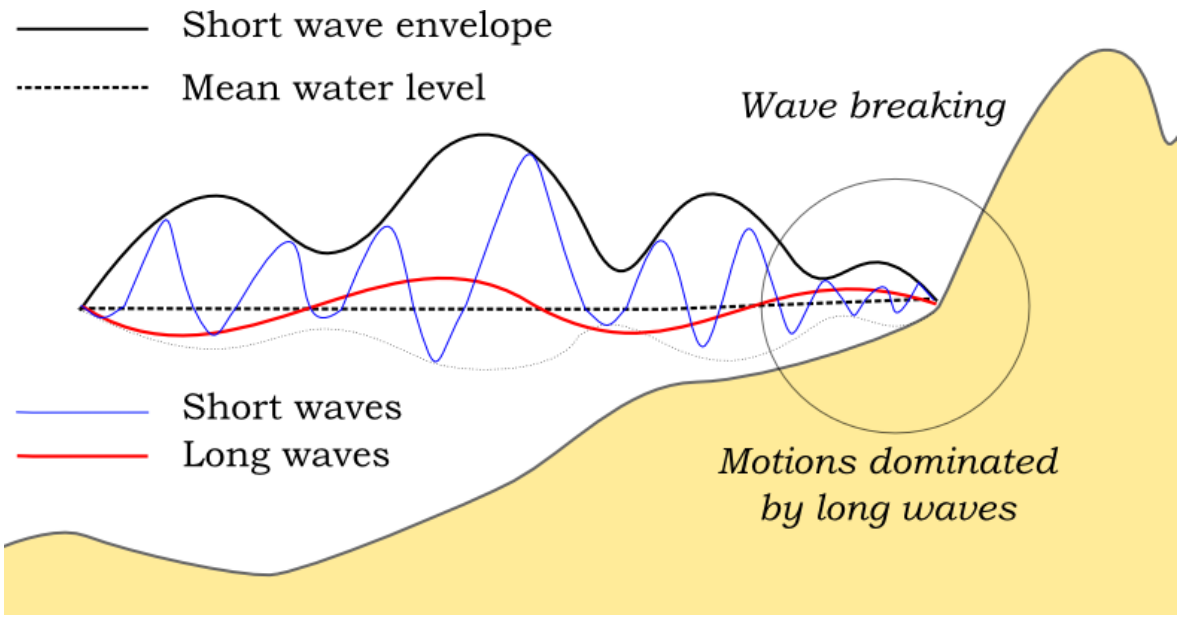

Figure 3.16: Relevant wave processes accounted for in XBeach (Deltares, 2016).

Table 3.26: The five formulations implemented in XBeach (instationary mode) for the dissipation term due to depth-induced wave breaking (S_{br}).

Wave breaking formula	keyword/value
Roelvink (1993)	(*break=roelvink1*)
Roelvink (1993) extended	(*break=roelvink2*)
Daly et al. (2010)	(*break=roelvink_daly*)

(1993) is summarised in the following equations:

$$\bar{S}_{\mathrm{br}} = 2\,\frac{\alpha}{T_{m01}}\,Q_b A_w \tag{3.21}$$

$$Q_b = 1 - \exp\left[\left(\frac{H_{\mathrm{rms}}}{H_{\mathrm{max}}}\right)^n\right] \tag{3.22}$$

$$H_{\mathrm{rms}} = \sqrt{\frac{8A_w}{\rho g}} \tag{3.23}$$

$$H_{\mathrm{max}} = \gamma\,(d + \delta H_{\mathrm{rms}}) \tag{3.24}$$

$$A_w(x,y,t) = \int_0^{2\pi} E_w(x,y,t,\theta)\,d\theta \tag{3.25}$$

where Q_b is the fraction of breaking waves, A_w the energy of the wave, H_{rms} the root-mean-square wave height, and H_{max} the maximum wave height. Other calibration coefficients in *roelvink1* are the wave dissipation coefficient α and the fraction of wave height in Eq. (3.23) δ.

The bottom friction sink term (S_{bfr}) is represented as

$$S_{\mathrm{bfr}} = \frac{2}{3\pi}\rho f_w \left(\frac{\pi H_{\mathrm{rms}}}{T_{m01}\sinh kd}\right)^3 \tag{3.26}$$

This term represents the short wave dissipation in Eq. (3.20), whereas the friction term associated to the momentum equation adopted to compute the mean currents, orbital velocities and surface elevation is treated separately in Eq. (3.33).

The wave energy dissipation due to vegetation is not relevant for this study and therefore, it is not accounted for in Eq. (3.20).

The instationary mode takes into account the radiation stress, that can be obtained from the wave energy (E) in accord with the linear wave theory (see Pelli et al., 2015a):

$$\begin{aligned}
S_{xx}(x,y,t) &= \int \left(\frac{c_g}{c}(1+\cos^2\theta) - \frac{1}{2}\right) E\,d\theta \\
S_{xy}(x,y,t) &= S_{yx}(x,y,t) = \int \sin\theta\cos\theta\,\frac{c_g}{c}E\,d\theta \\
S_{yy}(x,y,t) &= \int \left(\frac{c_g}{c}(1+\sin^2\theta) - \frac{1}{2}\right) E\,d\theta
\end{aligned} \tag{3.27}$$

The radiation stress terms due to roller are added to the Eqs. (3.27) (see Deltares, 2016).

The XBeach instationary mode solves wave skewness and asymmetry associated to non-linearity of waves in shallow water. Two possible wave form can accounted in the model, the formulation of Ruessink et al. (2012) and the formulation of van Thiel de Vries (2009). The latter is the default.

The model takes into account also the wave breaking-induced turbulence at the bottom in order to influence the sediment transport. Several models are implemented into XBeach (see Tab. 3.27). However, only the bore-averaged model can be used in combination with the waveform of van Thiel de Vries (2009).

Long-waves and mean flows are solved in the XBeach instationary mode by means of the Nonlinear Shallow Water (NLSW) equations. The wave induced mass flux and the succeeding flow are depth-averaged with the Generalised Lagrangian Mean (GLM) formulation (Andrews and McIntyre, 1978; Walstra et al., 2000). Thus, the momentum and continuity equations are formulated in terms of the Lagrangian velocities u_L and v_L, defined as the distance accounted from a wave particle in one wave period divided the wave period itself. These velocities are related to the Eulerian velocities u_E and v_E through the relationships:

$$\begin{aligned}
u_L &= u_E + u_S \\
v_L &= v_E + v_S
\end{aligned} \tag{3.28}$$

Table 3.27: The three formulations for turbulence variance at the bottom implemented in XBeach.

Bottom turbulence formula	keyword/value
Wave averaged	(*turb=wave_ averaged*)
Bore-averaged	(*turb=bore_ averaged*)
No turbulence	(*turb=none*)

in which u_S and v_S are the Stokes drift in x- and y-direction, respectively (Phillips, 1977). The Stokes drift is calculated from the short wave energy (E) obtained from Eq. (3.20):

$$\begin{aligned} u_S &= \frac{E\cos\theta}{\rho dc} \\ v_S &= \frac{E\sin\theta}{\rho dc} \end{aligned} \tag{3.29}$$

where ρ is the water density, d is the water depth and c is the phase speed. Thus, the GLM-momentum equations are resulted as:

$$\frac{\partial u_L}{\partial t} + u_L\frac{\partial u_L}{\partial x} + v_L\frac{\partial u_L}{\partial y} - f_c v_L - v_h\left(\frac{\partial^2 u_L}{\partial x^2} + \frac{\partial^2 u_L}{\partial y^2}\right) = \frac{\tau_{s_x}}{\rho d} - \frac{\tau_{b_x}}{\rho d} - g\frac{\partial \eta}{\partial x} + \frac{F_x}{\rho d} \tag{3.30}$$

$$\frac{\partial v_L}{\partial t} + u_L\frac{\partial v_L}{\partial x} + v_L\frac{\partial v_L}{\partial y} - f_c u_L - v_h\left(\frac{\partial^2 v_L}{\partial x^2} + \frac{\partial^2 v_L}{\partial y^2}\right) = \frac{\tau_{s_y}}{\rho d} - \frac{\tau_{b_y}}{\rho d} - g\frac{\partial \eta}{\partial y} + \frac{F_y}{\rho d} \tag{3.31}$$

$$\frac{\partial \eta}{\partial t} + \frac{\partial d v_L}{\partial x} + \frac{\partial d v_L}{\partial y} = 0 \tag{3.32}$$

in which τ_{s_x} and τ_{s_y} are the wind shear stresses, η is the water level, F_x F_y are the wave-induced stresses, v_h is the horizontal viscosity and f_c is the coefficient of Coriolis. The bottom shear stresses τ_{b_x} and τ_{b_y} are obtained as (Ruessink et al., 2001):

$$\begin{aligned} \tau_{b_x} &= C_f \rho u_E \sqrt{(1.16 u_{\mathrm{rms}})^2 + (u_E + v_E)^2} \\ \tau_{b_y} &= C_f \rho v_E \sqrt{(1.16 u_{\mathrm{rms}})^2 + (u_E + v_E)^2} \end{aligned} \tag{3.33}$$

Five formulations for the dimensionless bed friction coefficient c_f are implemented in XBeach, as listed in Tab. 3.28.

XBeach models the sediment transport applying to the concentration of sediments in the water column a depth-averaged advection-diffusion scheme, with a source-sink term based on the equilibrium sediment concentrations (Galappatti and Vreugdenhil, 1985) as follows:

$$\frac{\partial dC}{\partial t} + \frac{\partial dCu_E}{\partial x} + \frac{\partial dCv_E}{\partial y} + \frac{\partial}{\partial x}\left[Dd\frac{\partial C}{\partial x}\right] + \frac{\partial}{\partial y}\left[Dd\frac{\partial C}{\partial y}\right] = \frac{hC_{eq} - dC}{T_s} \tag{3.34}$$

Table 3.28: The five formulations for the dimensionless bed friction coefficient implemented in XBeach.

Formulation	Relevant coefficient	Keyword	Default value
Constant	C_f	cf	0.003
Chézy	C	chezy	$55 m^{-1/2} s^{-1}$
Manning	n	manning	0.02
White-Colebrook	K_s	white-colebrook	0.01
White-Colebrook grain size	D_{90}	white-colebrook-graisize	$0.0003 m$

In Eq. (3.34) C is the depth-averaged sediment concentration varying on the wave group scale and D is the sediment diffusion coefficient. The adaption time T_s, representing the entrainment of the sediment into the water column is given by:

$$T_s = max\left[f_{T_s}\frac{d}{w_s}, T_{s,min}\right] \tag{3.35}$$

where w_s represents the sediment fall velocity and the factor f_{T_s} is a calibration coefficient taking into account that w_s is depth-averaged. Small values of T_s mean an instantaneous sediment response. The entrainment or deposition of sediment is fixed through the difference between the sediment concentration C and the equilibrium concentration C_{eq}. Hence, the source term of Eq. (3.34) is represented by the equilibrium concentration C_{eq}.

The effect of waves nonlinearity in shallow water, represented by skewness and asymmetry, is accounted for advection-diffusion equation. Thus, Eq. (3.34) is modified as follows:

$$\frac{\partial dC}{\partial t} + \frac{\partial dC(u_E - u_a\sin\theta)}{\partial x} + \frac{\partial dC(u_E - u_a\cos\theta)}{\partial y} + \frac{\partial}{\partial x}\left[Dd\frac{\partial C}{\partial x}\right] + \frac{\partial}{\partial y}\left[Dd\frac{\partial C}{\partial y}\right] = \frac{dC_{eq} - dC}{T_s} \tag{3.36}$$

where u_a is calculated as

$$u_a = (f_{Sk}S_k - f_{As}A_s)u_{\text{rms}} \tag{3.37}$$

where S_k is the wave skewness, A_s is the wave asymmetry, u_{rms} is the root-mean square velocity, and f_{Sk} and f_{As} are two calibration factors. A unique value for both factors can be set with the parameter *facua*.

Bottom updating is accounted for sediment fluxes into water and dune erosion (avalanching). Bed level changes due to sediment fluxes are computed on the basis of the gradients in the sediment transport as follows:

$$\frac{\partial z_b}{\partial t} + \frac{f_{\text{mor}}}{1-p}\left(\frac{\partial q_x}{\partial x} + \frac{\partial q_y}{\partial y}\right) = 0 \tag{3.38}$$

where z_b is the bed level, p is the porosity, f_{mor} is a morphological acceleration factor of $O(1-10)$ (Reniers et al., 2004) and q_x and q_y are the sediment transport rates in x- and y-direction, respectively.

The generation of large shockwaves due to abrupt changes of the bed level are avoided limiting the maximum speed of bed changes to an imposed value ($v_{\text{av,max}}$).

The numerical schemes utilize a curvilinear (rectangular is a special case), staggered grid where depths, water levels, wave action and sediment concentrations are given in the cell centers and velocities and sediment fluxes at the cell boundaries (Fig. 3.17). In Fig. 3.17, quantities given at the cell center are represented with the letter z, whereas quantities given at the cell boundaries are denoted by the subscript u and v. The letter c indicates the corner

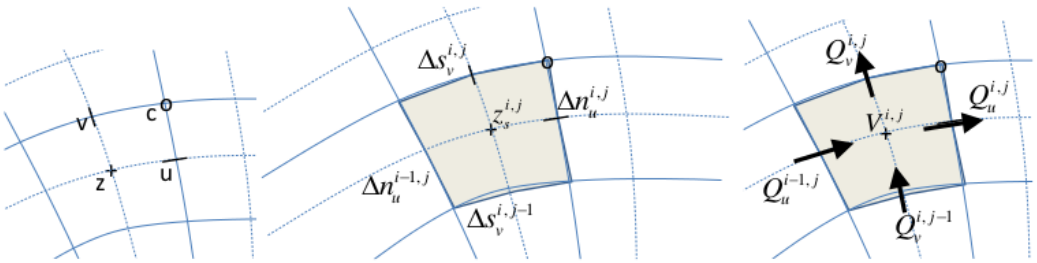

Figure 3.17: Location of staggered grid points (left), definition of grid distances (middle) and terms in volume balance (right).

of the cell, grid directions are indicated with s and n. Fluxes and volumes are indicated with Q and V, respectively. A finite-volume approach is utilized where mass, momentum and wave action are strictly conserved.

The XBeach instationary mode solve the AB equation (Eq. 3.20) with the second order upwind scheme. This scheme preserves the propagation of wave groups with little numerical diffusion.

For the NLSW equation (Eq. 3.30), the time integration of the mass and momentum balance equations is solved with an explicit second order leap-frog scheme.

1. XBeach is a numerical model for wave propagation, mean flow, sediment transport and morphological changes of the nearshore area, beaches, dunes and further coastal barriers. It can be used in 1D (profile) or 2DH mode.
2. The model can run in stationary mode, instationary mode, which is also called surfbeat (phase averaged) and non-hydrostatic mode (phase resolving).
3. For the purpose of the present research XBeach will be used in the surfbeat mode.

3.3.2 Model validation

The validation of a nearshore model able to compute wave propagation, hydrodynamics, sediment transport and morphological change is not an easy task due to lacks of field measurements. Especially, for morphological changes due to storms, a survey of the bathymetry and coastline pre- and post-storm should be needed. However, some validation tests are available in literature, where XBeach was calibrated both in laboratory and real case tests. Some of the available validation cases are summarised in the "XBeach skillbed report" (Deltares, 2016), other validation cases were published in journal articles, conference proceedings and thesis. The most relevant studies with implications for the present research are summarised in Table 3.29.

Table 3.29: Summary of the most relevant XBeach test cases for the present study.

Test case	Description	Remarks	References
Wave transformation	Laboratory test. Irregular waves over a concrete bar-trough beach.	Model results and measures are in good agreement for water set-up and short wave height. Poor agreement is observed for long wave height close to the shore.	Boers (1996) and Deltares (2016).
DELILAH	Field experiment at Duck, North Carolina. Simulation of 2DH hydrodynamics over a beach with boundary conditions consisting in directionally-spread short waves.	The slope of the roller model set to 0.05 (instead of 0.10) showed better results.	Birkemeier et al. (1997) and Deltares (2016).
Ningaloo Reef	Field experiment. Propagation of waves over a flat reef and into the onshore lagoon with 1D model and 2DH model.	The behaviour of the friction coefficient was investigated. A general good agreement with measures was observed, but infragravity (IG) wave height was slightly underestimated offshore the reef.	Deltares (2016) and Van Dongeren et al. (2013).

Continued on the next page

Continued from the previous page

Test case	Description	Remarks	References
Extreme conditions	Laboratory test. Extreme conditions with a raised water level at 4.6m above the flume bottom. 1D model with 1m of grid resolution.	Results for high- and low-frequency wave and wave setup were in agreements with measures. Beach and dune erosion were well estimated varying the underwater critical slope and the critical slope above water.	Arcilla et al. (1994) and Deltares (2016).
Dune overwash modelling	Simulation of the overwash on Santa Rosa Island, Florida, during Hurrican Ivan.	The effect of the morphological acceleration factor was discussed.	McCall (2008).
Ostend beach (Belgium)	1D and 2DH application and validation of XBeach during storm conditions.	The default settings were applied, except from the amount of onshore transport, which has been used as a calibration parameter.	Bolle et al. (2011).
Dziwnow Spit (Poland)	1D application and validation of XBeach during storm conditions.	A sensitivity analysis was carried out over 5 parameters. Good values of BSS were found for the best setup.	Bugajny et al. (2013).
Hurricane Sandy	Hindcast of the impact of Hurricane Sandy on New Jersey.	Wave asymmetry and bottom friction formulations were discussed.	Nederhoff (2014)
Storm-hazard forecast	Calibration of Xbeach for prediction of dune erosion and morphological changes. Faro beach (Portugal) was chosen as test case area.	A sensitivity analysis was carried out over several parameters. Poor values of BSS were generally observed. However, the most influence parameters were individuated.	Vousdoukas et al. (2012).
Attempt to overcome the erosion overestimation	After a review of literature, two new improvements were implemented in XBeach in order to overtake the erosion overestimation.	First improvement: the constant parameter *facua* is defined in relationship with the average seaward slope steepness. Second improvement: introduction of a calibration factor for (*facpi*) the grain-stabilization and Particle Interaction effect. The improved model was validated by means of three testing cases.	Elsayed and Oumeraci (2017)
Flood propagation	Evaluation of the XBeach performance for flood propagation in the hinterland. XBeach was compared with two other models for flood propagation by means of the simulation of three testing cases.	The real case study (Het Zwin) showed a good agreement between modelled and measured flow velocities and water levels, whereas the flood extent and flow levels predicted by XBeach are up to 40% larger than measured values.	Elsayed and Oumeraci (2016)

The "XBeach skillbed report" summarises the test cases carried out to calibrate and validate the model during its development. For the purpose of the present study, four test cases are highlighted: high- and low-frequency waves transformation over a concrete bar-

trough beach (laboratory test), field experiment at Duck (North Carolina), field experiment at Ningaloo Reef (Western Australia), and extreme conditions over beach and dune (laboratory test). Observing the results of these tests, it is emerged that Xbeach with the default setup simulates well high-frequency waves and coastal erosion, whereas an underestimation of low-frequency waves can occur. However, the results of the tests collected in the "XBeach skillbed report" are not described in detail.

Other studies found in literature are more helpful for the calibration of XBeach (see Tab. 3.29). In his Master Thesis, McCall (2008) developed a part of the Xbeach code ables to predict the phenomenon of dune overwash. The 2DH model was applied to the coast of Santa Rosa Island (Florida), during the Hurrican Ivan. The most interesting part of the thesis (for the purpose of the present work) is a sensitivity analysis carried out over the morphological acceleration factor (*morfac*) (see Tab. 3.30). The erosion obtained with *morfac* equals to 1, 5 and 10 demonstrates the little influence of this parameter on the XBeach results, except for boundary-related issues on the eastern side of the computational grid for *morfac*=10. The morphological acceleration factor speeds up the morphological time scale relative to the hydrodynamic timescale. It means that simulating a morphological evolution of one hour with *morfac*=6 takes only ten minutes of CPU time.

XBeach with default settings was used by Bolle et al. (2011) to evaluate the beach erosion in Ostend (Belgium) for the storm of 10 November 2007. The quantitative comparison between model and results was evaluated by means of the Brier Skill Score:

$$BSS = 1 - \frac{\overline{(z_{b,c} - z_{b,m})^2}}{\overline{(z_{b,i} - z_{b,m})^2}} \tag{3.39}$$

where $z_{b,c}$ in the computed profile, $z_{b,m}$ is the measured profile, and $z_{b,i}$ is the initial profile. A low value of BSS means poor agreement between model and measures, whereas a value close to 1 means excellent agreement (see van Rijn et al., 2003). An average value of $BSS = 0.53$ (fair) was observed for 1D computations.

A detailed study on the performance of XBeach during storm conditions on the beach of Dziwnow Spit (Poland) was carried out by Bugajny et al. (2013). The model was run in 1D mode over a total of 8 profiles along the coast of Dziwnow. They conducted a sensitivity analysis over 5 parameters. For the best setup, values of $BSS = 0.90$ were reached for a single profile, whereas the mean BSS for all the profiles was 0.64. The work of Bugajny et al. (2013) is particularly relevant because the storm hindcasted at Dziwnow Spit is very similar to the conditions observed at the site chosen as the test case area for the present research (i.e. North Tuscany coast), even though the mean slope of the Dziwnow Spit is steeper than North Tuscany (15.0% vs. 1.5%). Furthermore, for the profiles close to the point where offshore boundary conditions are provided, excellent value of BSS (i.e. $BSS > 0.8$) were presented.

Another important validation test case in real conditions was described in Nederhoff (2014), where XBeach was used to reproduce the morphological changes due to the impact of the Hurrican Sandy in October 2012. Nederhoff (2014) carried out a sensitivity analysis for the wave nonlinearity and bed friction formulation, finding the best results for *facua*$= 0.25 \div 0.30$ and bed friction formulation of Chézy with coefficient $C = 30 m^{1/2} s^{-1}$ (see Tab. 3.30).

Vousdoukas et al. (2012) calibrated XBeach in storm conditions in Algarve (Portugal) by means of a sensitivity analysis for several parameters. Even though the values of BSS obtained were generally poor, the behaviour of the model in relation of the changing of each parameter was well highlighted.

Hence, the most relevant parameters in XBeach are individuated and described in Table 3.30.

Table 3.30: List of the most important parameters affecting the results of XBeach in case of dissipative beaches.

Parameter	**Description**	**Default value**	**Suggested value**	**Remarks**
bedfriction	Bed friction coefficient formulation (NLSW)	chezy	chezy	A friction coefficient of $30m^{1/2}s^{-1}$ is recommended, instead the default value of $55m^{1/2}s^{-1}$.
break	Dissipation due to wave breaking formulation	3	1	A value of 1 corresponds to Roelvink (1993) formulation, a value of 3 corresponds to a modified version of Roelvink (1993) (see Deltares, 2016). The parameters α, δ and γ represent the calibration coefficients (see Subsection 3.3.1).
facua	Effect of wave nonlinearity	0.1		Values between 0.1 and 0.5 are proposed in literature. Elsayed and Oumeraci (2017) correlate values with the mean slope of the beach.
morfac	Morphological acceleration factor	1.0	10.0	Higher values of morfac speed up the morphological time scale relative to the hydrodynamic time scale.
turb	Enable short wave turbulence	2	0	A value of 0 deactivates the turbulence model, a value of 1 corresponds to the wave averaged model, a value of 2 corresponds to the bore averaged model. Activating this model, BSS values decrease.
wetslp	Critical bed slope for wet area	0.3	0.4	

3.3.3 Sensitivity analysis

This subsection describes the sensitivity analysis conducted on the most relevant parameters of the XBeach model listed in Table 3.31. The aim of this subsection is to understand the sensibility of the model to the variation of the relevant parameters.

The evolution of a beach profile after 10 hours of wave forcing is used to evaluate the model sensitivity. The initial beach profile represents the typical profile of a stretch of coast located at Marina dei Ronchi (North Tuscany, Italy), well described in Chapter 5. The mean slope of the beach is 1.5%, calculated from the closure depth (-8m) to the highest part of the dry beach. The closure depth is chosen as the offshore limit of this typical profile, since no modification of the seabed occurs at lower depth.

Two wave fields are used as wave boundary conditions, representing a beach erosion event and a beach accretion event, respectively, according to Dean (1973). Wave direction from 270°N is perpendicular to the shore, since XBeach profiles have the x-axis oriented to East by default (see Subsection 3.3.1).

The evolution of the beach profile is simulated with XBeach varying the most relevant parameters listed in Table 3.31, and described in detail in Subsections 3.3.1 and 3.3.2.

The tests performed adopting the turbulence model enabled (*turb=2*) result in a sensible higher erosion of the shoreline than the test carried out with the turbulence model disabled (see Fig. 3.19), for erosive wave boundary conditions. Vousdoukas et al. (2012) demonstrate that BSS values for XBeach with the turbulence model disabled are generally better than the ones obtained with the model enabled. Therefore, the rest of the tests will be carried out with the turbulence model disabled. A sketch summarising the tests carried out for the sensitivity analysis is shown in Figure 3.18.

It is interesting to note that even in wave conditions that should provide a nourishment of the emerged beach (according to Dean, 1973), XBeach simulates a little erosion. This behaviour is observed for all the tests carried out, and it represents a significant shortcoming of the model.

The evolution of the bottom profile simulated with XBeach for different value of *facua* are shown in Figure 3.20, that shows variations only in the part of the profile close to the shoreline since no appreciable changes are observed for depths lower than -2m. This behaviour seems not realistic for the erosive case, where an erosion of the offshore bar was expected.

The tested values of *facua* are suggested by literature and lay between 0.1 and 0.5 (e.g. Bugajny et al., 2013; Vousdoukas et al., 2012). The value of 0.02 is obtained from the formula proposed by Elsayed and Oumeraci (2017), who found a correlation between the mean slope of the beach and the value of *facua*. However, little differences are observed applying the

Table 3.31: The parameters tested in the sensitivity analysis.

Parameter	**Description**	**Default value**	**Tested value**
bedfriccoef	Bed friction coefficient	55 $m^{1/2}s^{-1}$	30 $m^{1/2}s^{-1}$
alpha*	Dissipation coefficient	1.0	0.5, 1.5, 2.0
gamma*	Breaker parameter	0.55	0.4, 0.45, 0.5, 0.6, 0.7, 0.8, 0.9
facua	Effect of wave nonlinearity	0.1	0.02, 0.2, 0.3, 0.4, 0.5
morfac	Morphological acceleration factor	1	5, 10
turb	Enable short wave turbulence	2	0 (Disabled)
D50 (mm)	D50 grain size	0.2	0.3, 0.4, 0.5, 0.6
wetslp	Critical bed slope for wet area	0.3	0.4

* Parameter of Roelvink (1993) formulation.

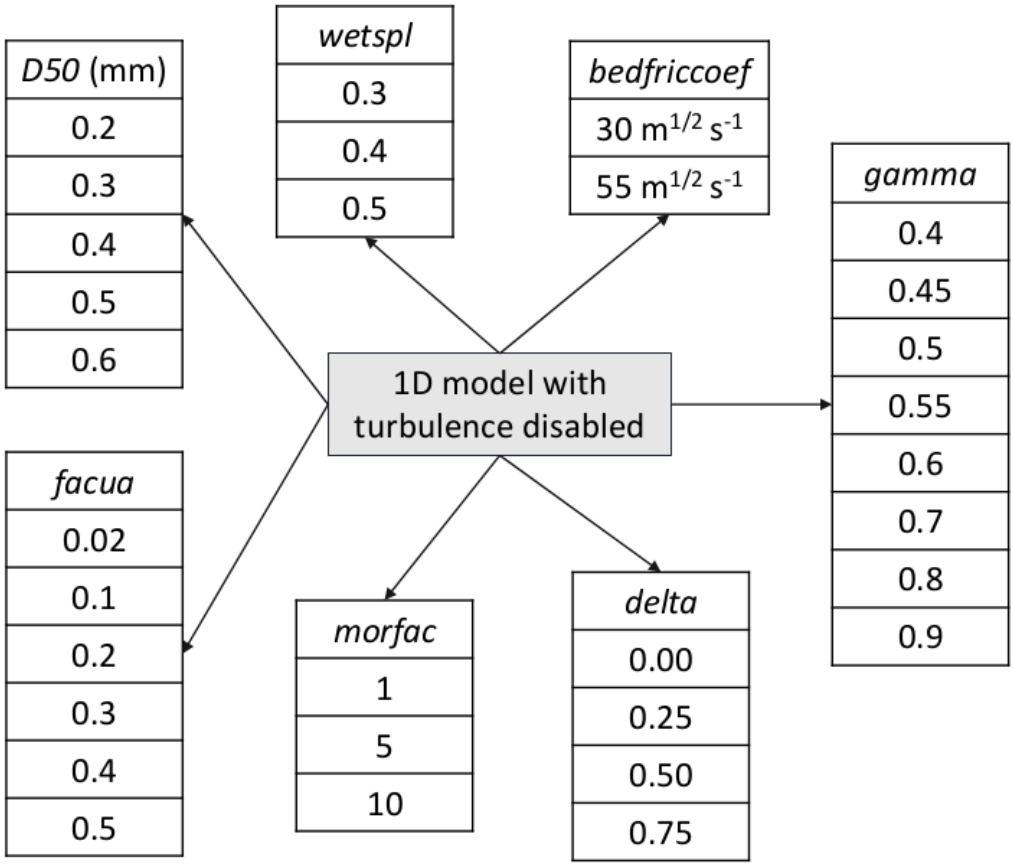

Figure 3.18: Sketch summarising the methodology followed to perform the sensitivity analysis.

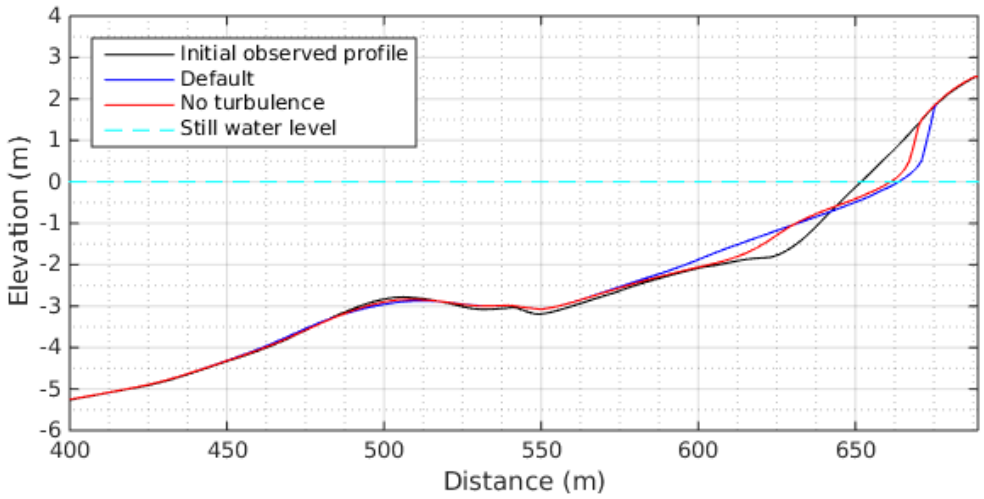

Figure 3.19: Elevation of the bottom profile simulated with XBeach with turbulence model enabled and disabled for erosion conditions.

default value of 0.1 and 0.02 for the erosion conditions, whereas for accretion conditions the profiles coincide.

From Figure 3.20 it can be noticed that the erosion of the emerged part of the beach is higher for lower values of *facua* for both erosive and accretion cases. In fact, higher values of *facua* simulate a stronger onshore sediment transport component. Panel (b) confirms that XBeach is unable to simulate the phenomenon of beach accretion.

A sensibility analysis on the breaking formulation is carried out varying the value of the parameters *gamma* (γ) of Eq. (3.23) and α of Eq. (3.21). The response of XBeach varying these parameters is still not clear in literature. The parameter γ determines the maximum wave height before breaking through the Eq. (3.24) and therefore, it moves the point of breaking waves. Figure 3.21 shows the evolution of the profile varying the value of γ in case of erosion conditions. The values of γ=0.4, 0.55, 0.7, 0.9 shown in Fig. 3.21 correspond to a $H_{\max}$ of 1.2m, 1.65, 2.1, 2.7, respectively, at the depth of the top of the offshore sandbar (about -3m). Moving offshore the breaker decreasing the default values of 0.55 to 0.4 does not produce a significant difference of the profile evolution. Moving onshore the breaker enhancing the values of γ to 0.7 and 0.9 results in a higher erosion of the emerged beach (especially for 0.9) and little erosion of the offshore bar.

The other parameter of the wave dissipation formulation tested is *alpha* (α), representing the wave dissipation coefficient of Eq. (3.21). A decreasing of this value results in a decreasing of the wave dissipation, whereas an increasing of the value results in an increasing of the wave dissipation. Changing the default value of α from 1.0 to 0.5, 1.5 and 2.0 produces an appreciable effect only in case of α=2.0, resulting in a higher recession of the shoreline and a gentler slope of the beach than applying α=0.5, 1.0, 1.5.

The evolution of the profile simulated by XBeach combining the effect of α and γ for erosion conditions is shown in Figure 3.22. The sensitivity of the model to α is little. In fact, only for the extreme combinations α=0.5,γ=0.7 and α=1.5,γ=0.4, the role of α is important resulting in a significant different evolution of the profile. These two combinations physically correspond to lower dissipation and breaker closer to the shoreline, and higher dissipation and breaker more distant from the shoreline, respectively.

The analysis of the parameter *D50* highlights only little differences for the emerged part of the beach. Six grain sizes are tested, 0.2mm (default value), 0.3mm, 0.4mm, 0.5mm, and 0.6mm. Less beach erosion is observed for the coarser diameters.

The variation of the Chezy coefficient (*bedfriccoef*) from the default value of 55 $m^{1/2}s^{-1}$ to the value suggested by Nederhoff (2014) of 30 $m^{1/2}s^{-1}$ results in not relevant differences of the profile evolution.

Three values of the *wetslp* parameter are tested, 0.3 (default value), 0.4 (suggested by Vousdoukas et al., 2012), and 0.5. The parameter *wetslp* is defined as the critical slope for wet area. Little differences are observed applying a values of 0.4 and 0.5, whereas an higher erosion of the emerged part of the beach is observed for the default value 0.3 (see Fig. 3.23).

The changing of the parameter *morfac* from 1 to 5 and 10 does not produce appreciable changing of the results.

An important aspect to highlight is that XBeach is not able to simulate the nourishment of the emerged beach that usually occurs during the periods of light swell (see Dean, 1973). This implies that XBeach cannot be used for long-term simulations, in which erosive events alternate with accretion events. Furthermore, it seem that erosion is too focused on the shoreline and affects too little the offshore sandbar, even tuning the coefficients of the wave breaking formulation.

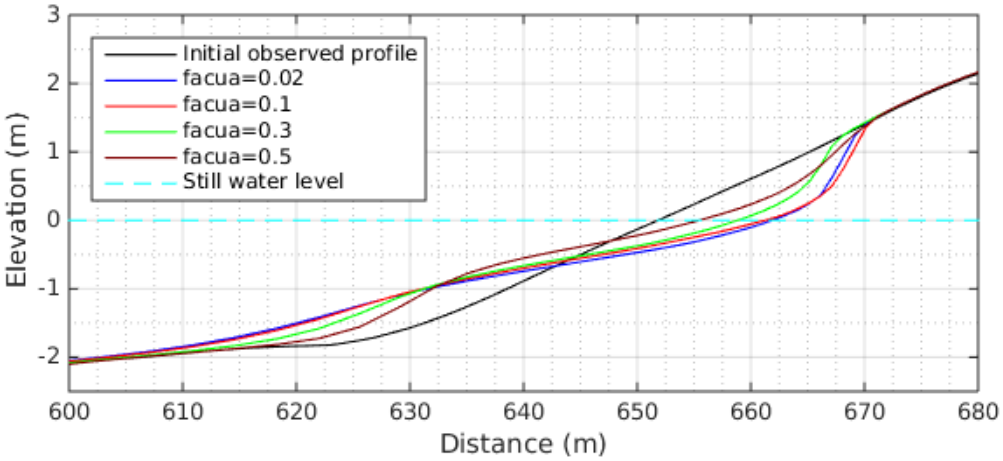

Figure 3.20: Elevation of the bottom profile for values of *facua*=0.02, 0.1 (default), 0.2, 0.3, 0.5, erosion conditions.

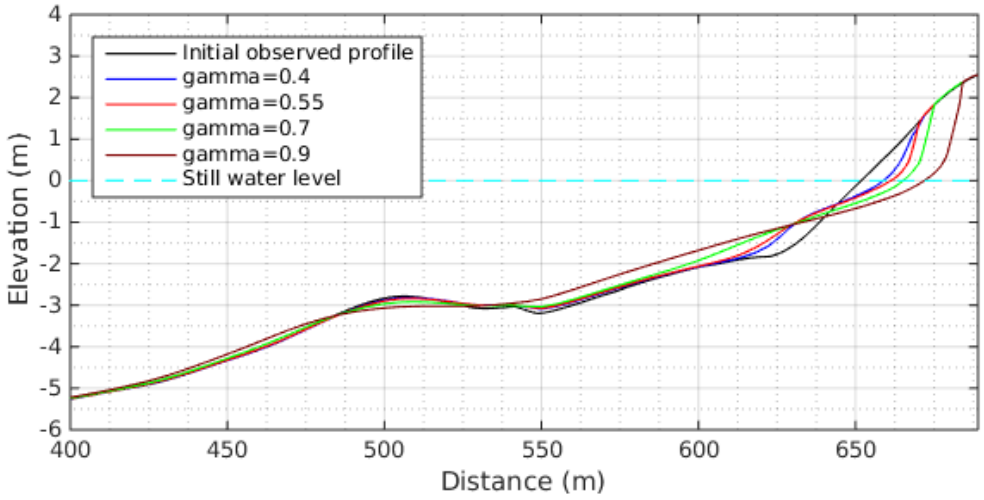

Figure 3.21: Elevation of the bottom profile for values of *gamma*=0.4, 0.55 (default), 0.7, 0.9 in case of erosion conditions.

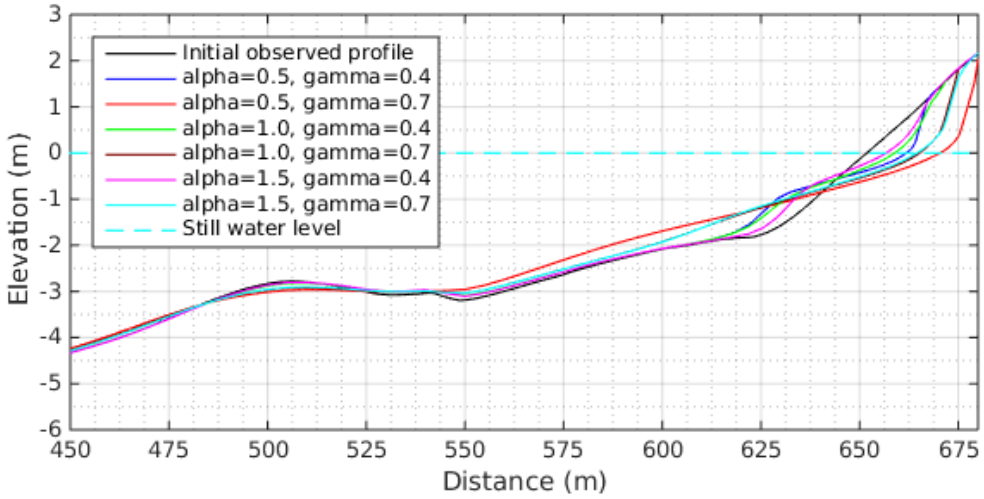

Figure 3.22: Elevation of the bottom profile combining the effect of the parameters *alpha* and *gamma* for erosion conditions.

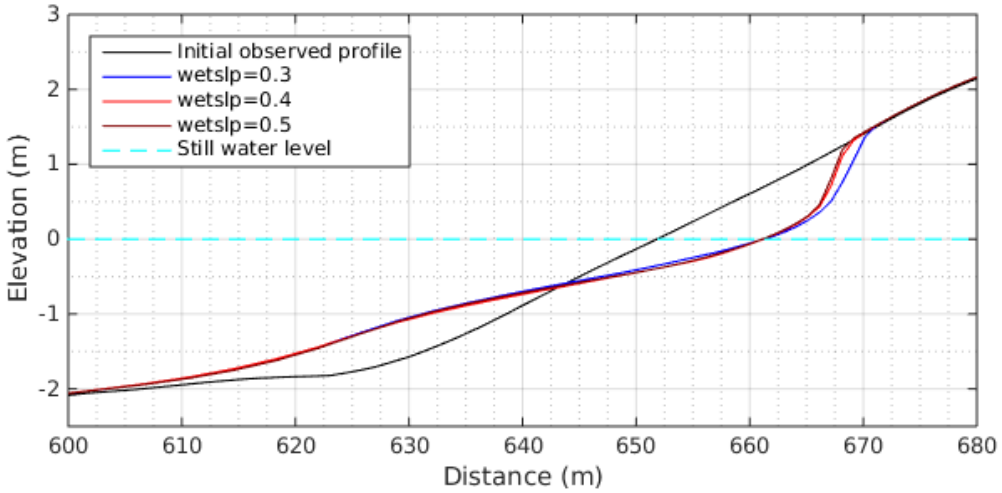

Figure 3.23: Elevation of the bottom profile for values of *wetslp*=0.3, 0.4, 0.5 for erosion conditions.

1. A sensitivity analysis is carried out by varying seven relevant parameters of XBeach.
2. The model is forced with two wave boundary conditions to reproduce two different modes: (1) beach erosion and (2) beach accretion according to Dean (1973).
3. The results of the simulations revealed that Xbeach is unable to simulate beach accretion conditions. This implies that XBeach cannot be used for long-term simulations, in which erosive events alternate with accretion events, but this is less relevant for the present study which focuses only on the hazardous sea state for coastal early warning.

3.4 Summary and implications

In Chapter 3 have been described the calibration and validation of the models selected for the building of the operational wave model system (i.e. WWIII, SWAN, and XBeach), which is the objective of the present study. Moreover, a brief description of the governing equations of each model has been presented.

Since the extensiveness and the importance of this chapter, the key results, their limitations and implications for the final results nearshore are summarised and discussed in the present section.

The most important achievements in this chapter is the calibration of the deep water wave model (WWIII) for the typical storms occurring in the Mediterranean Sea, and of the intermediate/shallow water wave model (SWAN) for the typical storms occurring in the North Tuscany. This is justified because both wave models were mostly calibrated for storms in the other seas/regions.

The WWIII model revealed that is able to well hindcast the significant wave height (H_{m_0}) in the Mediterranean Sea, but an underestimation of higher waves associated with severe short-fetch storms was observed. The possible causes of this underestimation has been individuated in (a) the wider resolution of the wind data which force the model that is unable to catch the features of regional storms with short fetches, (b) the constant value of the $\beta_{\max}$ parameter (it represent the fraction of energy transferred from wind to waves) that it was demonstrated to vary with the wind velocity. Therefore, future research might be carried out improving the spatial quality of the wind database and/or developing a function related to the wind velocity for the value of $\beta_{\max}$.

Also the performing of the intermediate/shallow water model (SWAN) revealed an underestimation in the order of few centimeters (only isolated cases highlighted greater underestimations) for higher waves both in deep and intermediate waters. These underestimations might be related to (a) uncertainties in the wave boundary conditions provided by WWIII, (b) uncertainties in the wind data. However, a decrease of the model performance from WWIII to SWAN was expected, since modelling of wave processes in intermediate water (SWAN) is generally more difficult than in deep water (WWIII).

For further research, more validation cases would be needed in order to understand the frequency of the higher underestimations which can affect the results nearshore. However, it seems reasonable to believe that an improving of the results for the deep water model could lead to an improving of the results for the intermediate/shallow water model.

XBeach is the wave model selected to forecast/hindcast waves nearshore. It was selected because its ability to simulate the two-way interaction between waves and seabed modifications. In fact, XBeach will start to operate at the closure depth, where waves and currents start to modify the seabed.

A sensitivity analysis was carried out varying seven relevant parameters of XBeach. The model was forced with two wave boundary conditions to reproduce two different modes: (1) beach erosion and (2) beach accretion, according to Dean (1973). The most relevant finding is the limitation of XBeach to simulate beach accretion conditions, as already reported in literature. This implies that the model cannot be used for long-term simulations, in which erosive events alternate with accretion events, but this is less relevant for the present study which focuses only on the hazardous sea state for coastal early warning.

For future development of the model system proposed in the present PhD study, an implementation of a model to account for beach accretion periods under moderate sea state is suggested. For example, van Rijn et al. (2011) carried out beach accretion tests with three numerical models, CROSMOR (van Rijn et al., 2007), UNIBEST-TC (Ruessink et al., 2007) and DELFT3D (see 2.4), but results were generally poor. In fact, van Rijn et al. (2011) suggested further research to improve all three models with respect to accretion conditions.

Moreover, since it is reported in literature that even under severe storm conditions, XBeach has the limitation to overestimate the erosion rate (e.g. De Vet, 2014; Mccall et al., 2010; McCall, 2008), possible improvements of the morphodynamic module of XBeach might be carried out, as suggested and performed by Elsayed and Oumeraci (2017).

It is worth to mention that XBeach was demonstrated to have a large potential for a wider range of applications (e.g. Elsayed, 2016), such as the assessment of beach/dune overwash, barrier breaching and inundation, thus making XBeach ideal for early warning of potential erosion and structural damages and mitigating threats to lives and properties. However, in the present PhD, it is was preferred to apply XBeach to a simply beach erosion test case for two reasons: (1) this study is a first attempt to integrate XBeach in a fully-automated model system with the final objective of supporting a coastal early warning; (2) the majority of the coast of the Italian peninsula (i.e. the focus area) presents mild-sloping beaches without dune system, such as the ones selected for the test case application (i.e. Marina dei Ronchi, North Tuscany). Therefore, the test case presented in Chapter 5 could be representative for a large part of the Italian coast.

4

Nesting of wave models

In the previous chapter, the three models selected in Section 2.4 were described for the building of a nested model system, which is the main aim of the present study. In particular, the most suitable models for simulating deep water processes, intermediate/shallow water processes and nearshore processes resulted WAVEWATCH III (WWIII), SWAN and XBeach, respectively.

The objective of this chapter is to link the selected models in order to build a seamless model system able to simulate wave processes from the open ocean to the shoreline. In Section 2.5, examples of available model systems were provided, following similar goals as in this PhD research (e.g. Baart et al., 2016; Barnard et al., 2014; Cheung et al., 2003; Vousdoukas et al., 2012). In all these studies different models were adopted to simulate the physical processes occurring at the different geographical scales (i.e. deep water, intermediate/shallow water, nearshore), and different levels of grid resolution depending on the bottom and coastline variability. The process of embedding two or more grids with different resolutions is called nesting. In wave modelling, the communication between grids is generally carried out transferring spectral information at the so-called Active Boundary Points (ABPs), i.e. the points where the grids overlap each other.

The three selected models have already the capability to produce output spectral files which can readily used as initial and boundary conditions for nested applications, even among different models. In fact, output files of WWIII can be read by SWAN by means of an easy post-processing operation, and output files of SWAN can be read directly by XBeach, but only for stationary simulations and not for the non-stationary mode as used in this PhD study. The most important condition is that coarse resolution model and high resolution model must have the same coordinate system.

The compatibility of the selected models in terms of nesting in each other is not accidental, since one of the selection criteria considered in Section 2.4 and shown in Table 2.6 is the "Easiness of nesting with other models". All the models are spectral and developed sharing the same structure and methodology (e.g. FORTRAN language, modular). In fact, the initial development of all three models was at the Delft University.

Among the articles cited and discussed in Table 2.8, only Cheung et al. (2003) and the researches related to the MICORE and CoSMoS projects (i.e. Baart et al., 2016; Barnard et al., 2014; Vousdoukas et al., 2012) presented a forecast system able to simulate wave processes from the open ocean to the shoreline, including a large scale model, a regional model, and a nearshore model. In particular, Cheung et al. (2003) implemented in their model system WAM as ocean wave model, SWAN as coastal wave model, and a Boussinesq-type model (COULWAVE) as nearshore wave model. The MICORE (and the similar CoSMoS) system

implements WWIII as ocean model and improved the model system using three levels of coastal model (Delft3D), and XBeach as nearshore model. Therefore, only the MICORE (and CoSMoS) system simulates also nearshore morphodynamic processes. The modelling chain was automated by means of programmes written in MATLAB (Baart et al., 2009).

The aim of this chapter is to link the three selected models by means of computer codes written in an open source language, building a seamless model system. In order to reach this objective, the six steps proposed by Baart et al. (2009) will be followed (see Tab. 2.11). The model system will be organized in a structure similar to that presented by Cheung et al. (2003). This chapter describes in detail (a) the methodology adopted for the building of the nested system, (b) the algorithms developed for the nesting of the wave models, and (c) the programmes developed to support the nesting methodology. An overview of the working principle of each wave model is presented in order to better understand the proposed nesting methodology. Therefore, the operations needed to set up and run each model are described. These operations can be generally summarized in six steps (modified from the six steps proposed by Baart et al., 2009) as shown in Table 4.1.

Model setup (MS) includes the download and compilation of the source code and the setup of model options and parameters (e.g. numerical scheme, time step, physics parameterization, grid setup).

Data collection (DC) includes the operations needed to download environmental data (wind, pressure, wave, etc.), which are necessary to force the model.

Grid pre-processing (GP) collects the operations needed to set up the integration grid and the grid of bathymetry data.

Initial and boundary pre-processing (IBC) collects the operations needed to set up initial and boundary wave conditions and input grids (e.g. wind, current).

Running model (RM) includes the operations needed to run the wave model and consequently, to obtain the requested output files (i.e. raw model results).

Post-processing (PP) collects the operations needed to transform raw output files in human readable files as tables, graphs and images, or to obtain input files for nested grids. An additional *Publishing* class can be supplemented, but in the first stage of the research it was preferred to store the results in an internal archive.

Section 4.1 illustrates the methodological approach adopted for the building of the nested system. Section 4.2 describes how to set up and run WWIII and SWAN as separate models and then, the methodology developed to nest the two models. Section 4.3 describes how to set up and run XBeach as a separate model and then, the methodology developed to nest SWAN and XBeach. Section 4.4 describes the methodology proposed for building and running the whole model system (i.e. WWIII, SWAN and XBeach). In the flowcharts of this chapter the programmes are presented by continuous line boxes, and files by dashed line boxes.

4.1 The methodological approach

The methodological approach adopted for the building of the nested model system is motivated from the analysis of the current knowledge on the nesting approaches carried out in Section 2.5.

One of the main characteristics of the proposed nesting methodology is the multi-grid approach as presented by Chawla et al. (2007) and Tolman (2008) for the multi-grid WWIII operating at NCEP. The three selected models (i.e. WWIII, SWAN, and XBeach) are implemented in the developed model system as three independent models and thus, each model can be set up with its own time step, physics parameterization etc. Each model is appropriate for modelling wave processes in specific conditions (i.e. deep water, intermediate/shallow water, and nearshore).

As already mentioned in the previous chapters, the main objective of the present research is to simulate the wave processes from the open ocean to the shoreline. For this purpose, the

Table 4.1: The six steps proposed for the building of a general hindcast/forecast model (modified from Baart et al., 2009).

Step	Name	Description	Abbreviation
1	Model setup	Installation of the model and setting of parameters	MS
2	Data collection	Download of raw data for model initiation	DC
3	Grid pre-processing	Set up of integration grid and bathymetry grid	GP
4	Initial and boundary condition pre-processing	Set up forcing files	IBC
5	Running model	Running of the model previously set up	RM
6	Post-processing	Processing raw output data to generate human readable data or forcing files for nested grids	PP

use of grids in coastal areas with a resolution much finer than the one adopted by Chawla et al. (2007) in the multi-grid WWIII is necessary. Therefore, the SWAN model with a much finer resolution is implemented in the model system.

The advantage of SWAN as compared to WWIII (which uses explicit schemes) is the employment of implicit schemes, which are computationally more robust and more economic for high resolution applications. For example, the same choice was made by Guedes Soares et al. (2011) and Paramygin et al. (2017) during the development of their forecast wave system.

In order to downscale the wave field from the open ocean to the nearshore, several independent models running over grids with different resolutions can be implemented in the system. For example, four models are implemented in the system applied to the Marina dei Ronchi test case in Chapter 5: (1) a WWIII model works over a large scale grid covering the Mediterranean Sea, (2) a SWAN model over a regional scale grid covering North Tuscany, (3) another SWAN model over a grid covering the coast of Versilia, and finally (4) an XBeach model is applied on a cross-shore profile of Marina dei Ronchi beach.

The implementation of XBeach in the model system for simulating wave processes in the nearshore is motivated by:

- In nearshore areas, hydrodynamic processes due to waves induce a modification of the bathymetry and of the shoreline;
- These morphological changes may crucially modify the wave parameters and dynamics as well as the wave-induced nearshore currents, water levels and other associated processes.

Therefore, to predict reliable indicators for coastal hazard (e.g. wave runup, beach erosion), a model that takes into account the updating of the bathymetry changes due to waves is necessary. For example, XBeach was adopted also from Baart et al. (2009), Barnard et al. (2014), and Vousdoukas et al. (2012) to predict coastal hazard in the nearshore.

The nesting of different models implies that the boundary conditions transferred from the coarse resolution model (parent grid) to the finer resolution model (child grid) share the same information. This is the reason why all the selected models are spectral. Spectral information can be easily transferred from WWIII to SWAN, and from SWAN to XBeach. For the present research, the nesting of the three selected wave models consists in the management of all operations needed to transfer spectral information between the models at the right time and geographical space (i.e. pre- and post-processing operations).

Since the aim of the present research is to model waves travelling from the open ocean to the shoreline and not vice versa, the one-way interaction between models is sufficient, i.e. spectral information are transferred only from coarse resolution grid to high resolution grid and not back. The primary advantage of the one-way nesting is that the single models can be implemented independently. It is therefore well-suited for operational forecast.

Following Baart et al. (2009), all the operations needed to set up and run a wave model, including the management of spectral information, are collected in six steps (see Tab. 4.1). It is worth to note, that the six steps of Table 4.1 represents a general methodology for set up and run any numerical model and thus, the proposed nesting methodology may be applied in different fields to solve problems of downscaling.

The steps related to the management of spectral information (3 to 6 of Tab. 4.1) are automated by programmes specifically developed. Then, a software manager programme executes in sequence the different modules of the model system (those consist in the three wave models and the developed programmes). The task manager programme, called NEMO, represents the core of the model system. All the codes are open source, including the code of the wave models. The choice of using only open source codes is motivated by:

- The system have to be *reproducible*: new implementation of the source code can be easily updated.
- The single models have to be *replaceable*: new versions of the models can be easily implemented in the system.

Moreover, these two characteristics allow any users to implement in the system new models for the simulation of additional physical processes (e.g. tides, offshore currents).

The characteristics of reproducibility and replaceability are ensured by the modular nature of the NEMO system schematized in Figure 4.1. The different modules are represented by:

- 4 wave models: (1) WWIII Mediterranean Sea, (2) SWAN North Tuscany, (3) SWAN Versilia, (4) XBeach Marina dei Ronchi profile.
- Pre- and post- processing utility programmes package.

The modules are managed by a task manager programme. With the modular approach the system can be easily modified, improved, or adapted for different areas of application.

In Figure 4.2 are summarised the methodological approach described in the present section, with the problem statements formulated during the development of the model system, the methodologies adopted to reach the intermediate goals, and the practical solutions adopted for the development of the methodology.

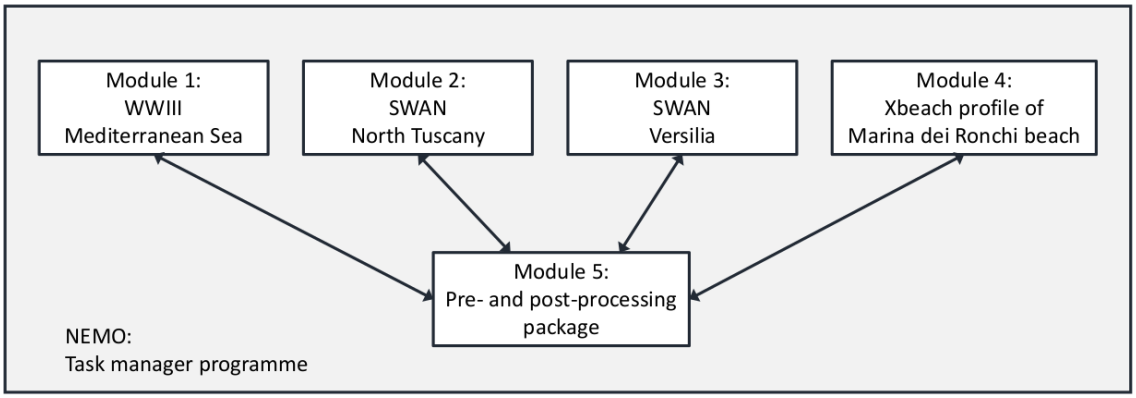

Figure 4.1: Flowchart of the modular approach of the NEMO system.

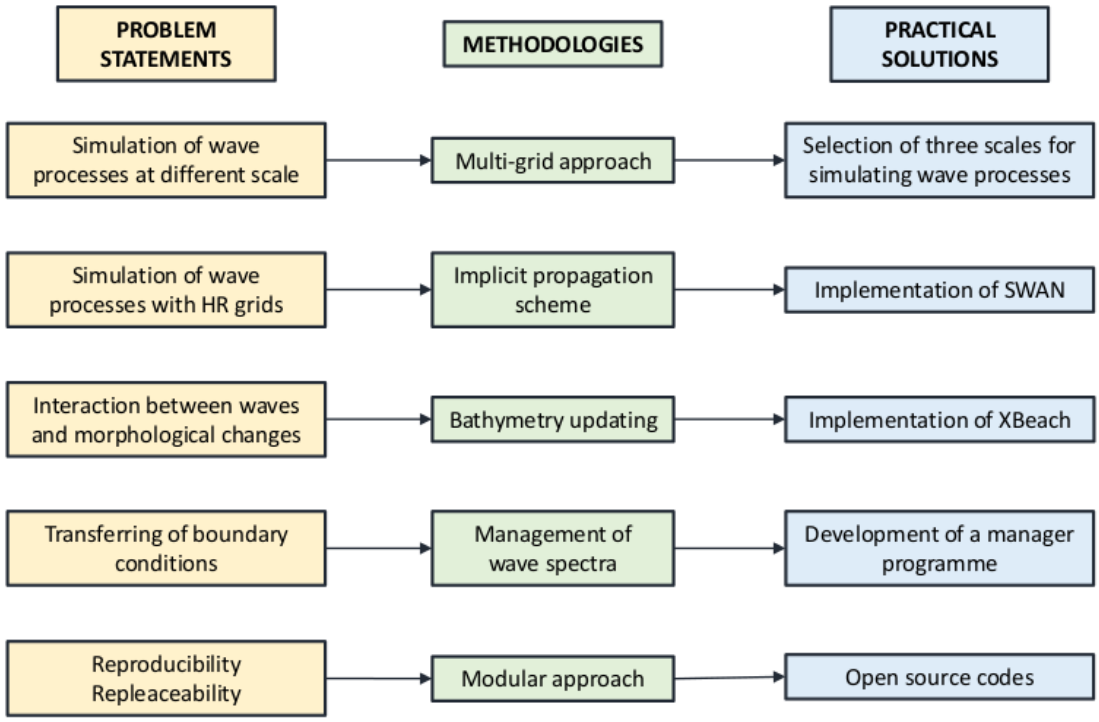

Figure 4.2: Flowchart of the nesting approach adopted for the development of the NEMO system, with Problem Statements, Methodologies, and Practical Solutions.

The works describing the development of a model system similar to NEMO for structure (WWIII, SWAN and XBeach) and aim (support to Coastal Early Warning System) (e.g. Baart et al., 2009; Vousdoukas et al., 2012) lacks in motivations for the nesting methodology and practical solutions adopted. Therefore, the characteristics of reproducibility and replaceability were not guarantee. Moreover, the utilities and manager programmes for the automatization of the model system were written in a licensed programming language, i.e. MATLAB (Baart et al., 2009).

In order to allows the scientific community to reproduce and improve the NEMO system, in the next three sections, the methodological approach will be integrated with an in-depth analysis of the practical solution adopted.

1. A multi-grid approach is adopted for simulating wave processes at different scales.
2. Three spectral models are implemented in the system in order to simulate the wave processes at the different scales. Boundary conditions are transferred only from coarse resolution grid to high resolution grid by means of spectral information.
3. The nested system is built with a modular approach: each grid represents a module, with an utilities package module for nesting operations. The modules are managed by a task manager programme that represents the core of the nesting system.

4.2 Nesting of WAVEWATCH III and SWAN

As already mentioned in Section 2.5, the most used technique to transfer boundary conditions from coarse resolution grid to high resolution grid is sharing spectral information at the Active Boundary Points (ABPs), i.e. at the points where the grids overlap each other. In

case of using WWIII and SWAN, this operation is simplified because the raw output of WWIII, opportunely pre-processed, can be directly used as boundary conditions for SWAN. A detailed description of pre-processing operations will be illustrated in Subsection 4.2.3.

The general six steps for setting and running a simulation with a numerical model summarized in Table 4.1 are specified for WWIII and SWAN in Figure 4.3. The dark grey box highlights the steps implicated in the nesting procedure. At each selected time step, WWIII must transfer boundary conditions to SWAN, resulting in multiple iterations of the highlighted steps. In order to achieve the transfer of boundary conditions, two strategy may be adopted:

- to carry out a file transfer at each time step.
- to carry out a complete simulation of WWIII, saving the results at each time step and then, to execute SWAN that reads the boundary conditions from the stored file.

The first strategy is more tricky (similar to *coupling*) and implies an important modification of the source code of both models. The second strategy is generally adopted for *one-way nesting* and requires no or only slight modifications of the source code of the models. Moreover, the second strategy respects the philosophy of the modular approach, that implies that each model works independently as a single module.

After a discussion on the strengths and limitations of the aforementioned strategies carried out in Section 2.5, the one-way nesting is adopted for the nesting of WWIII and SWAN. Follow the modular approach, new improvements/updates of the numerical models can be easily implemented into the model system.

The steps of Figure 4.3 highlighted in light grey are described in Subsection 4.2.1 and Subsection 4.2.2 for WWIII and SWAN, respectively. The nesting steps highlighted in dark grey and the utilities developed for the building of a seamless WWIII-SWAN system are described in Subsection 4.2.3.

4.2.1 Using WAVEWATCH III

The steps for carrying out a complete simulation with the WWIII model are summarized in Figure 4.4.

The phase of model setup (step 1) includes the model installation and the settings of the model options and parameters. For the model installation, reference is made to the WWIII user manual (Tolman, 2015), and the internal report Pelli (2016). The settings of the model options (e.g. physics formulations) and parameters were already described in Section 3.1.

In the present application, bathymetry data and wind data are collected (step 2) in order to obtain the files of bathymetry and the file of forcing wind field. The files of bathymetry are generated with the support of GRIDGEN (step 3), an open source MATLAB package (Chawla and Tolman, 2007). Two files of data are furnished with GRIDGEN, ETOPO2 and ETOPO1 (`https://www.ngdc.noaa.gov/mgg/global/global.html`) which represent the global relief model of Earth's surface integrating land topography and ocean bathymetry with 2 arc-minute and 1 arc-minute of resolution, respectively.

In order to improve the bathymetry resolution, two other databases are freely available for the Mediterranean Sea, the General Bathymethry Chart of the Oceans (GEBCO) (`www.gebco.net`) with 1/2 arc-minute resolution, and the European Marine Observation and Data Network (EMODnet) (`www.emodnet-hydrography.eu`) with 1/8 arc-minute resolution. Data files obtained from both database can be used by GRIDGEN after an easy operation of pre-processing. In particular, the use of the EMODnet database is described in the next subsection. Grid pre-processing operations (step 3) are also carried out by the programme ww3_grid collected in the WWIII package. The aforementioned steps cannot be implemented in the nesting algorithm, since they are site-specific and are carried out only once for each

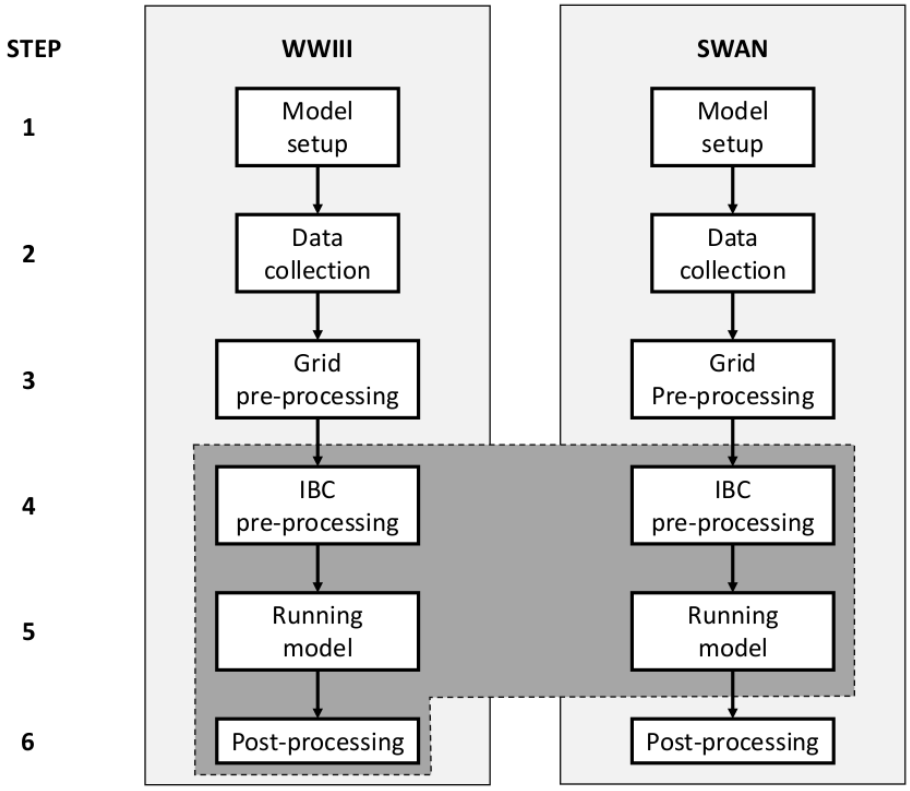

Figure 4.3: Workflow with the steps described in Table 4.1. The light grey box enclose the six steps needed to carried out a complete simulation with a numerical wave model. The dark grey box encloses the steps implicated in the nesting procedure.

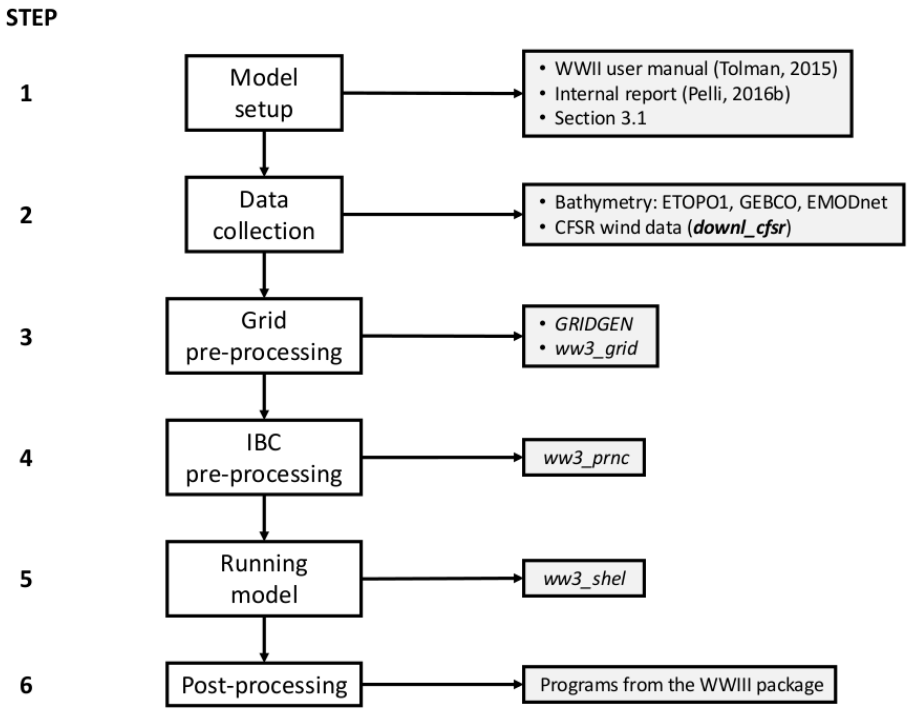

Figure 4.4: Workflow for WWIII. New codes are in italic, original codes are in bold.

computational domain (with exception of the collection of forcing data that can be optionally implemented).

Step 4 in the WWIII workflow (Fig. 4.4) is the pre-processing of the initial and boundary conditions (Fig. 4.5). In the case of the Mediterranean Sea, the main boundary condition is represented by the forcing wind field, since the boundaries of the integration domain are represented by land (i.e. no waves entering the domain). In the present study, wind data were obtained from CFSR database (Saha et al., 2014; Saha et al., 2010). The Bash programme downl_cfsr was developed in order to simplify the download and cropping of the data for the area of interest. The cropping of CFSR data is necessary since they cover the whole earth surface and may require several Gigabytes.

Once the CFSR file is obtained, the programme ww3_prnc must be used to transform the CFSR file (wind_cfsr.nc) in binary format (wind.ww3). If the model starts from calm sea conditions, the programme ww3_strt can be used to warm up the model with the linear wind growth of Cavaleri and Rizzoli (1981), whereas if initial sea conditions are supplied from a previous run of WWIII, the file restartN.ww3 can be directly used as initial conditions (N indicates the number of the restart file).

The operations summarised in Fig. 4.5 are implemented in the nesting procedure, but they can be optionally excluded depending on the purpose of the simulation (e.g. forecast, long-term hindcast, single storm hindcast).

The programme ww3_shel represents the wave model of the WWIII package (step 5) and it needs at least four files to run, mod_def.ww3 (produced by ww3_grid), restart.ww3, wind.ww3 and ww3_shel.inp, as shown in Fig. 4.6. The file ww3_shel.inp specifies the time frame of calculations and output parameters, and its setup is crucial for the success of the nesting procedure between coarser and higher resolution model (i.e. WWIII and SWAN, respectively). The use of this file is described in Subsection 4.2.3. The output files out_pnt.ww3 and out_grd.ww3 (see Fig. 4.6) contain spectral data at requested points and for each grid node, respectively.

Step 6 can be carried out using the programmes supplied by the WWIII package. Post-processing operation for nesting purpose will be described in Subsection 4.2.3.

4.2.2 Using SWAN

The steps for carrying out a complete simulation with SWAN are summarized in Figure 4.7. Model setup (step 1) includes the installation of the model and the setting of model options and parameters. For model installation, reference is made to the SWAN implementation manual (The SWAN Team, 2016b) and the SWAN user manual (The SWAN Team, 2016c) since it is not object of the present work. The setting of model options and parameters have been already described in Section 3.2. Bathymetry data and wind data are collected (step 2) from the same sources described for WWIII in the previous subsection.

Preparing a SWAN running is relatively easier than WWIII, since it needs few files:

`file.bot`	File with bottom depths
`wind.inp`	File with wind input (optional)
`file.swn`	Input file for the programme
`file.spc`	Spectral boundary conditions (optional)

In the present study, the files of bottom depths have been built (step 3) with the GRIDGEN software for the intermediate resolution grid (800m), or using a number of MATLAB functions for the high resolution grid (100m) (see Fig. 4.15). The intermediate resolution grid has been built by means of the EMODnet database with 1/8 arc-minute resolution (about 300m). The EMODnet files (NetCDF format) needs a complex operation of pre-processing to be used by

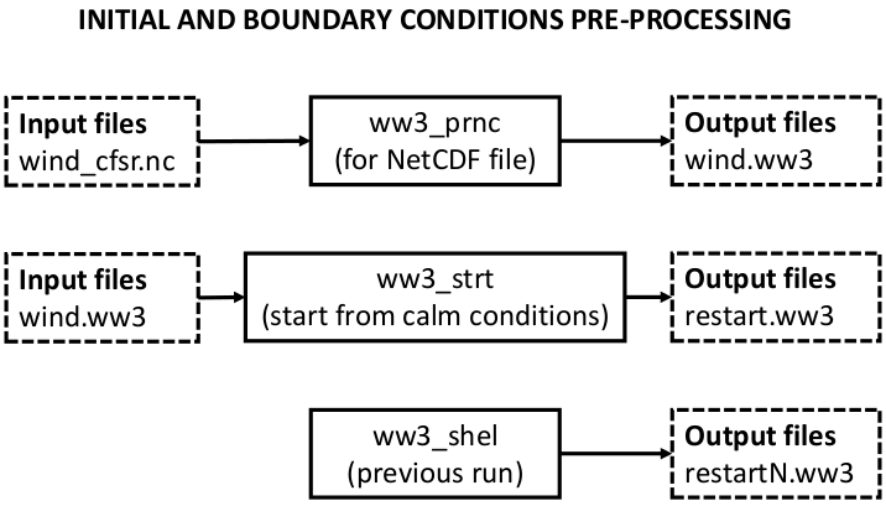

Figure 4.5: Flowchart for the preprocessing of initial and boundary conditions.

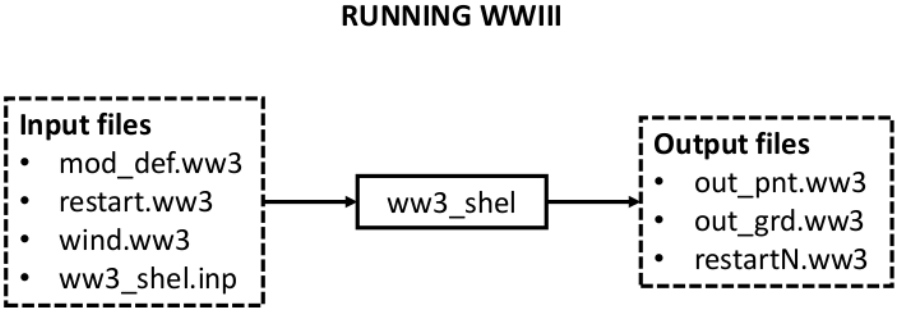

Figure 4.6: Flowchart for the input/output process of the ww3_shel programme.

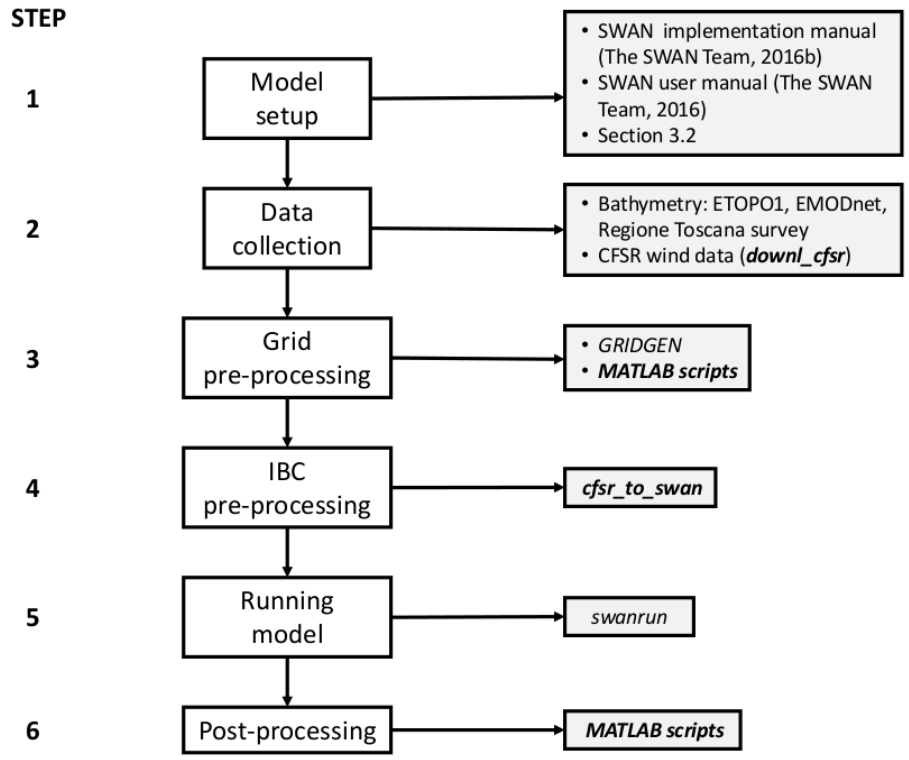

Figure 4.7: Workflow diagram of SWAN. Programmes are in italic, original programmes are in bold.

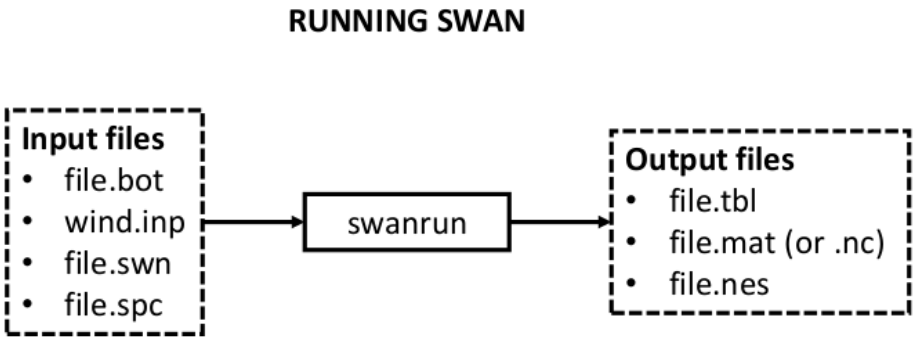

Figure 4.8: Flowchart describing the input/output process of the swanrun programme.

GRIDGEN, as summarized in Table 4.2. The high resolution grid has been built integrating the EMODnet database with the bathymetry data provided by the Tuscany Region. This operation has been carried out in the MATLAB environment.

The wind input file can be built with the Bash programme cfsr_to_swan, developed during the present study (step 4). This programme uses in input the same CFSR wind data used to force WWIII, and it produces in output an ASCII file with wind vectors, ready to use as wind input for SWAN. The file *.swn contains all the settings about grids, physics and numerics of the model. The file *.spc contains the spectral boundary conditions provided from the parent grid (coarser resolution model). The last file is crucial for the success of the nesting procedure, and it is described in detail in Subsection 4.2.3.

The programme swanrun initiates the wave model (step 5) and produces three possible files of output (Fig. 4.8):

`file.tbl`	Table of wave parameters at requested points
`file.mat`	MATLAB grid file of requested wave parameters
`file.nes`	Spectral boundary conditions for child grids

Optionally, a NetCDF output for grid file (instead of MATLAB) can be requested, but few wave parameters are supported. If boundary conditions for a child grid (higher resolution model) are requested, a file *.nes will be generated. This file is involved in the nesting procedure, and its use will be described in detail in the next subsection.

Post-processing operations (step 6) can be carried out by means of script written in MATLAB language. Post-processing operation for nesting purpose will be described in Subsection 4.3.2.

4.2.3 Nesting procedure

The wave models WWIII and SWAN are run as coarse (CR) and high (HR) resolution model, respectively (see Fig. 4.9). The general nesting approach adopted in the present study is to install and set up each model as separate modules, and to develop a *task manager* programme that runs the models in sequence, i.e. modular approach (see Section 4.4). Nesting operations, which are mainly the processing of spectra files, are carried out by a number of programmes collected in an utilities package. This choice is justified because, independently of the model version considered for the model system, no or only slight modifications of the source code of the wave models would be required. The methodology for running in sequence WWIII and SWAN is summarised in the flowchart of Figure 4.10.

Table 4.2: Steps for the pre-processing of the EMODnet bathymetry file.

Step	Description	Remarks
1.	Unpack the file and extract only bathymetry data*	The file is packed and contains additional data.
2.	Round data to integer*	GRIDGEN needs integer data.
3.	Transform the file from NetCDF format to ASCII	The FORTRAN programme emodnet_to_XYZ was developed to carry out this operation.
4.	Load the ASCII file in MATLAB-GRIDGEN environment	The MATLAB programme load_grd_emodnet was developed to carry out this operation.

* Operation carried out with the NCO tools (`http://nco.sourceforge.net/`)

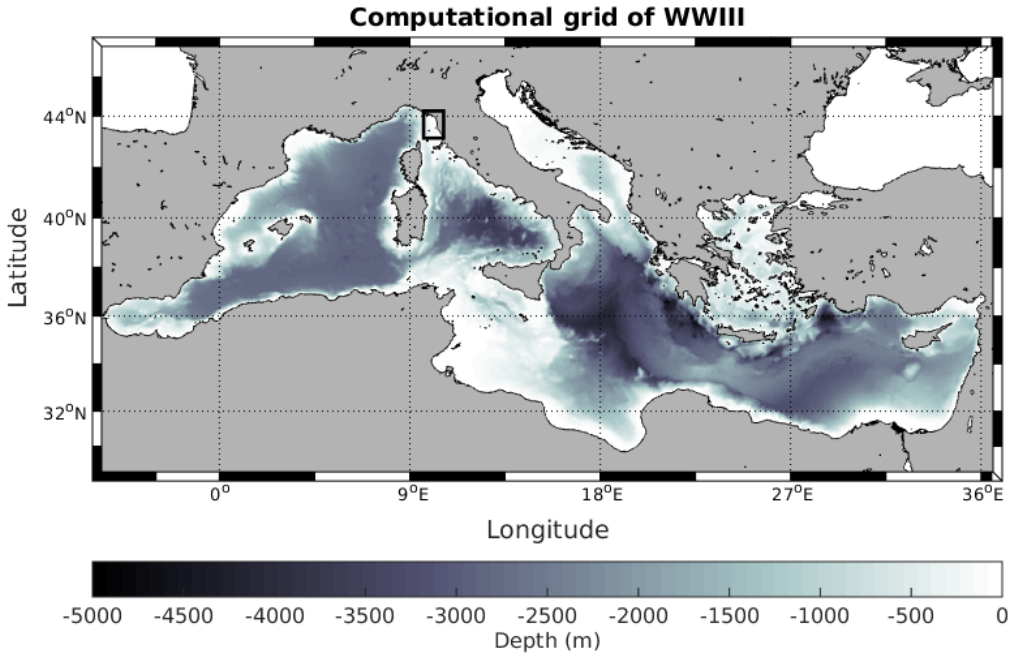

Figure 4.9: Computational grid of WWIII with bathymetry. The box on the Ligurian Sea represents the computation domain of SWAN. Black Sea and Atlantic Ocean are excluded from the domain.

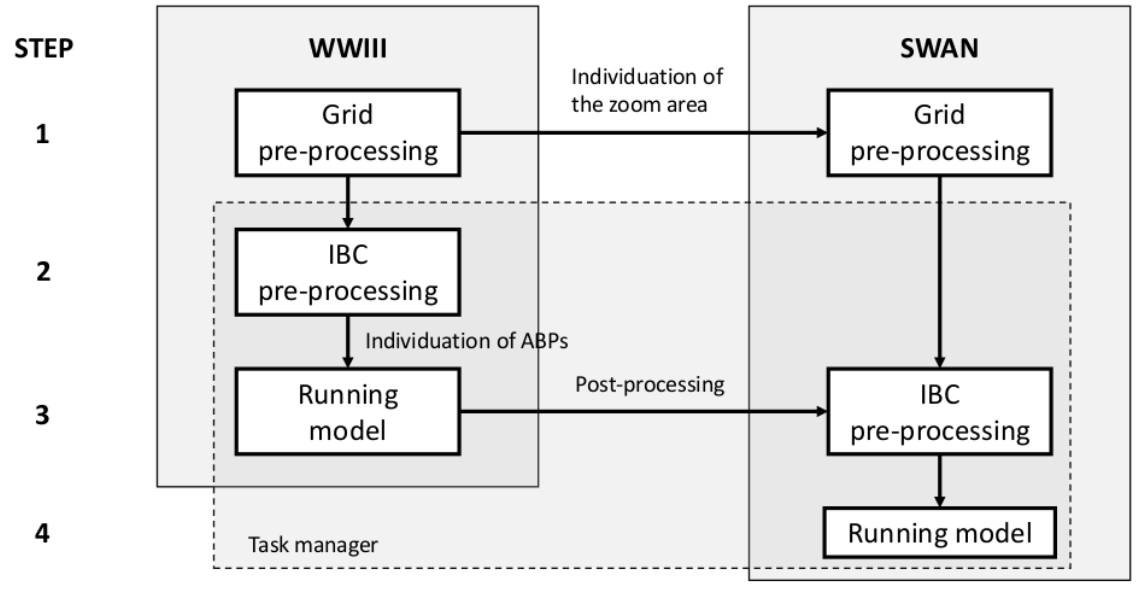

Figure 4.10: Flowchart of the methodology for running in sequence WWIII (CR model) and SWAN (HR model). The dashed box encloses the steps carried out by the task manager programme.

Step 1 includes the grid preprocessor (GP) operations as illustrated in Subsections 4.2.1 and 4.2.2. These operations are site-specific and cannot be implemented in the model system. The main operation of GP is the building of the bathymetry file(s).

In step 2, initial and boundary conditions pre-processing (IBC) for CR model (WWIII) are built as illustrated in Fig. 4.5. In order to support the execution of step 2, the Bash programme ww3_make_mrun was developed to set up multiple simulations of one month of duration.

Between step 2 and step 3, it is necessary to individuate the *Active Boundary Points* (ABPs), i.e. the grid points where spectral data are passed from CR grid to HR grid. When APBs are written in ww3_shel.inp (i.e. the input file of the WWIII wave module), WWIII stores spectral data at ABPs in the file out_pnt.ww3. In the present study, the management of ABPs is assigned to the original Bash programme wwswan_prep. This programme needs a file of input (wwswan_prep.inp), where the user indicates the full paths of the three files read by the programme, i.e. swan.swn, ww3_grid.inp and ww3_shel.inp (Fig. 4.11).

The programme wwswan_prep reads the coordinates of the origin and the length of the axes of the SWAN grid, and it calculates the minimum and maximum latitude and longitude. Then, the grid resolution for each axis of the WWIII computational grid are read. Using the information of the WWIII and SWAN grids, the programme calculates two arrays containing the longitude and latitude of the points laying over the boundary of the SWAN grid, spaced by the resolution of the WWIII grid (Fig. 4.12).

For a successfully nesting between the two models, SWAN needs that ABPs lie (nearly) on the boundary of its computational grid. In particular, the SWAN user manual (The SWAN Team, 2016c) specifies that the SWAN boundary needs to lies within a rectangle with a width equal to 0.1 times the distance between two consecutive ABPs. In order to avoid any numerical error, the computational grids of WWIII and SWAN have been built with the overlapping boundaries lie on the same longitude or latitude. Then, ABPs are selected respecting the criterion that they must lie perfectly on the boundary of the SWAN computational grid. Where spectral information miss (i.e. at the boundary points of HR grid between two consecutive ABPs, see Fig. 4.12), spectra are obtained by means of interpolation of the ABPs spectra. This operation is executed directly by SWAN. ABPs are stored in a file called abp_PROJ.txt, where PROJ is the project name of the swan model, and successively written in ww3_shel.inp.

The use of ABPs is preferred to the alternative technique of providing wave boundary conditions by means of wave parameters (i.e. H_{m_0}, T_p, peak direction, and directional spreading) supplied along the active segments. The active segment is defined as a portion of the boundary where incoming waves are constant.

The shortcoming of using the active segments is represented by the annoying operation of pre-processing of the wave parameter files as well as the setup of the SWAN input file.

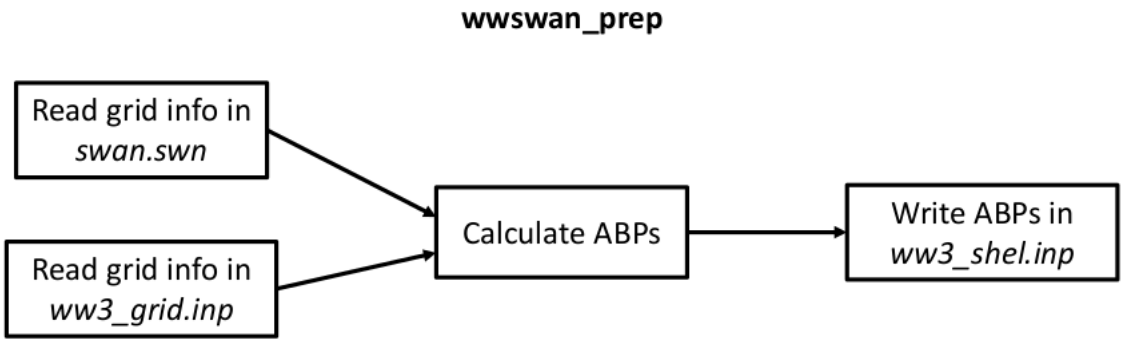

Figure 4.11: Workflow diagram of the wwswan_prep programme. File names are written in italic.

Moreover, a lost of information occurs since WBC are provided to SWAN by means of a parametric spectrum assumed to be a priori with a JONSWAP shape.

The advantages of using the ABPs are:

- The high number of ABPs spread along the boundary of HR grid assures the spatial variability of wave conditions, those are smoothed using the active segments.

- The real spectrum (instead of a parametric spectrum) guarantees the reliability of the wave boundary conditions.

Usually, active segments are used in case of lack of wave data, e.g. only one wave gauge available (see Gaeta et al., 2016).

Steps 3 and 4 of Fig. 4.10 are carried out by the original Bash programme wwswan_shel as illustrated in Figure 4.13. Like the preparation programme, wwswan_shel needs a file of input (wwswan_shel.inp) where are specified the full paths of the directory of WWIII programmes, the file of ABPs, ww3_outp.inp and the executable of SWAN. The programme wwswan_shel allows to run in sequence WWIII and SWAN.

The first operation of the programme is the execution of ww3_shel (i.e. the wave model of the WWIII package) that produces the binary file out_pnt.ww3, where the spectral data at the ABPs are stored. Then, the programme of the WWIII package ww3_outp allows to extract spectral data from the binary file, and writes them in an ASCII file with extension *.spc. Thus, the tag numbers of ABPs must to be written in the input file of the programme (ww3_out.inp). This operation is carried out by the Fortran function search_abp, developed during the present study. This function compares the coordinates of the output points listed in ww3_shel.out with the coordinates of ABPs listed in abp_PROJ.txt. Then, only the target number of ABPs are written in the input file ww3_outp.inp (see Fig. 4.14). This operation is necessary when the CR model provides several output points for different purpose, e.g. output at the stations of measurement or points of interest, ABPs for other HR grids.

The next step is the execution of the programme ww3_outp that produces the ASCII file ABP.spc, ready to use as wave boundary conditions of SWAN.

The last step is the running of the SWAN model with HR grid. Depending on the nearshore resolution needed, wwswan_shel can be set up to run the wave models more than once over grids with increasing resolution. This are necessary since it is good practice to reduce the resolution between CR and HR grids at least for a factor of 10, in order to avoid numerical errors.

For example, in the test case presented in Chapter 5, the model system includes three nested WWIII/SWAN modules: (1) a WWIII model running on a domain covering the whole Mediterranean Sea with about 5km of grid resolution (Fig. 4.9), (2) a SWAN model covering the North Tuscany with resolution of 800m, (3) and a SWAN model covering the Versilia coast with a resolution of 100m (see Fig. 4.15).

The running of the two SWAN models is simply carried out by executing in series swanrun in the directories where the models with 800m and 100m of resolution have been set up. Specifying into the input file (800m.swn) the features of the 100m resolution grid (i.e coordinates of the origin and length of the axis), the file of spectral boundary conditions (file.nes) for the 100m model is automatically produced by the 800m model. Then, the *.nes file saved in the 800m model directory is linked in the directory of the 100m model, and swanrun is executed again in last directory.

It is worth to note that the programme wwswan_shel is written to run both WWIII and SWAN with OpenMP parallelization strategy. The numbers of threads must to be set up in the user environment.

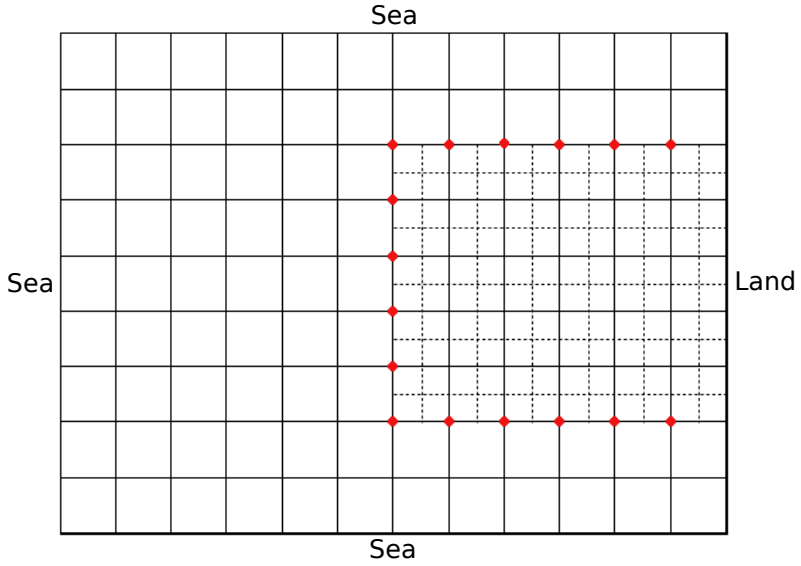

Figure 4.12: Selection criterion for Active Boundary Points (ABPs). Filled lines represent Coarse Resolution grid, dashed lines represent High Resolution grid, and red dots are ABPs, where the data are passed from CR grid to HR grid. The interpolation of the spectra on the HR boundary points is carried out by the SWAN model.

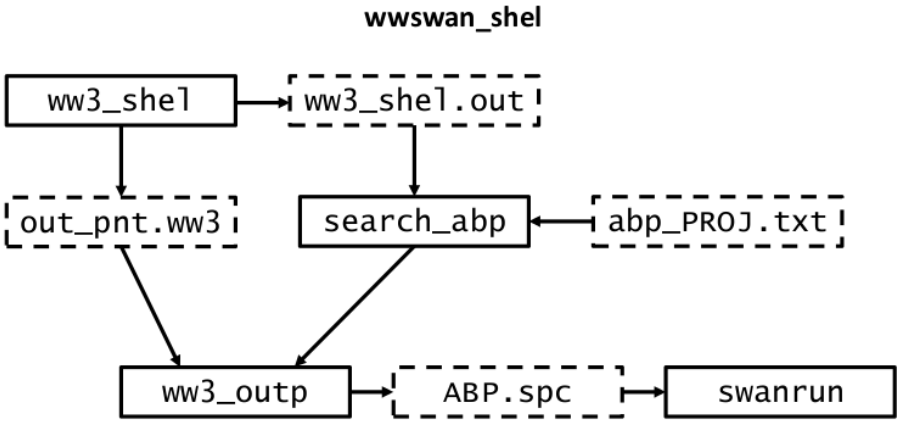

Figure 4.13: Workflow diagram of the wwswan_shel algorithm. Programmes are in the continuous line boxes, files in the dashed line boxes.

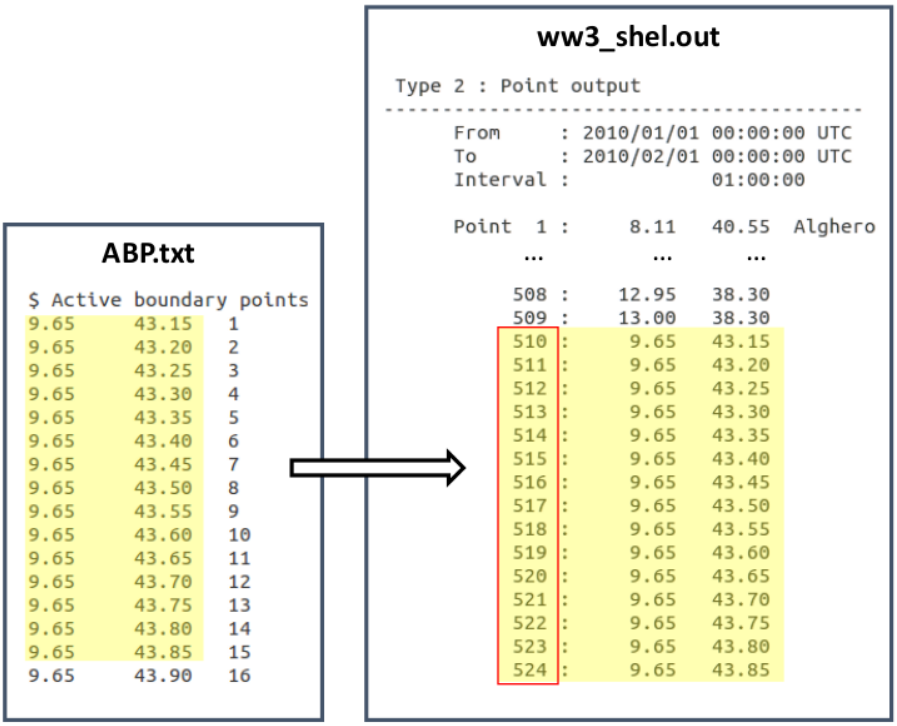

Figure 4.14: Example of a selection of output points carried out by the function search_abp. The yellow highlight indicates the correspondence between coordinates. The red box indicates the target numbers.

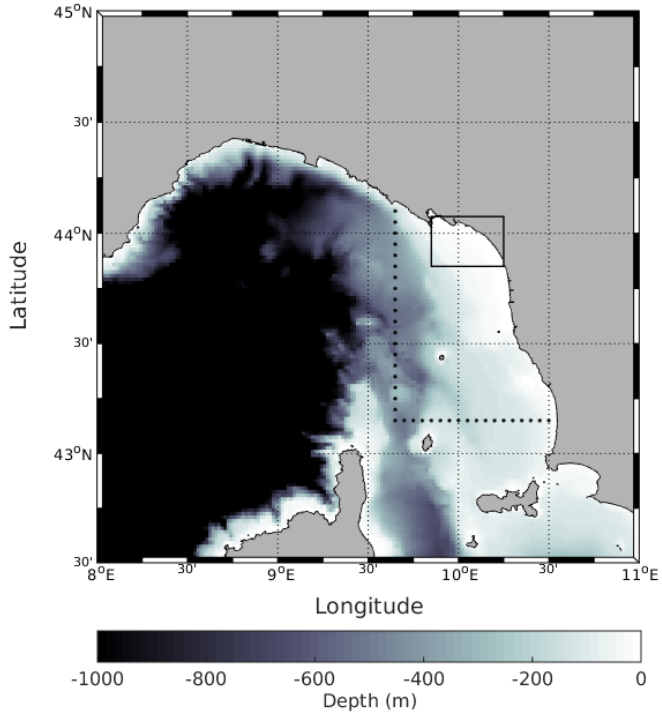

Figure 4.15: Active Boundary Points (ABPs) of the SWAN 800m grid (black dots). The black box represents the SWAN nested model with 100m resolution for the Versilia coast.

1. The processes for carrying out a complete simulation with a wave model may be summarised in six steps:
   (a) Model setup (MS)
   (b) Data collection (DC)
   (c) Grid pre-processing (GP)
   (d) Initial and boundary conditions pre-processing (IBC)
   (e) Running model (RM)
   (f) Post-processing (PP)

   Steps (c) to (f) are an integral part of the nesting procedure.
2. The *one-way nesting* technique is used to link WWIII and SWAN. The main advantage of this technique is that no or only slight modifications of the model source code is required.
3. The Bash programme wwswan_prep is developed to set up a nested simulation using WWIII as coarser resolution (CR) model and SWAN as higher resolution (HR) model.
4. The Bash programme wwswan_shel executes WWIII and SWAN in sequence, as a seamless model system. Initial and boundary conditions of the SWAN model are extrapolated from the output files of WWIII.

4.3 Nesting of SWAN and XBEACH

Like for the nesting of WWIII and SWAN, the focal point of the nesting of SWAN and XBeach is the transfer of wave boundary conditions (WBC) between the models. For 1D applications of XBeach (i.e. cross-shore profile), as described by Baart et al. (2016), Barnard et al. (2014), and Vousdoukas et al. (2012), it is necessary to provide WBC to XBeach only at the offshore point of the profile.

The question is more complex for 2DH applications of XBeach, but in case of a relatively small computational domain with contour depth parallel to the shore, offshore wave conditions can be considered constant along the boundary. Thus, one active boundary point (ABP) can be sufficient to provide WBC to XBeach.

WBC can be provided to XBeach in two ways: (1) by means of wave spectrum, and (2) by means of wave parameters (i.e. H_{m_0}, T_p, and direction). The representation of WBC by means of wave parameters simplifies the wave spectrum hindcasted by SWAN in a spectrum with a pre-defined shape, with a lost of information. In this case, XBeach provides WBC with a JONSWAP spectrum defined by two parameters, the peak enhancement factor γ, and the directional spreading coefficient s. The definition of these two parameter is not an easy task, since they have to be extrapolated from the SWAN spectrum.

The only advantages of using wave parameters as WBC (this is the choice of Barnard et al., 2014) is the possibility by default to carry out Xbeach time-varying simulation. However, a new utility programme was developed in order to adapt the spectral output of SWAN for providing time-varying WBC to XBeach. Therefore, in the present research WBC are transferred from SWAN to XBeach by means of spectral files.

Figure 4.16 shows the workflow for SWAN and XBeach. The light grey box highlights the 6 steps necessary to carry out a complete simulation with each model, whereas the dark grey box highlights the steps implicated in the nesting procedure. The step 5 of SWAN (i.e. running model) lie outside the nesting procedure since it has been already implemented

in the WWIII-SWAN system.

The one-way nesting strategy is adopted to link SWAN and XBeach. The main advantage of this technique is that no or little modification of the source code of the models is necessary.

The steps for carrying out a complete simulation with XBeach are described in Subsection 4.3.1. The nesting steps of Fig. 4.16 highlighted in dark grey and the utilities developed for the building of a seamless SWAN-XBeach system are described in Subsection 4.2.3.

4.3.1 Using XBeach

The steps for carrying out a complete simulation with XBeach are summarized in Figure 4.17. The methodology regarding the setup of XBeach (step 1) is similar to that of SWAN, i.e. all settings are specified in a unique text file (params.txt) that simplifies the use of the model. Details about model setup can be found in Deltares (2016) and Elsayed and Oumeraci (2015) (`https://www.researchgate.net/publication/304539209_Modelling_Strategies_with_XBeach_XBeach_Manual`), and in Section 3.3 of the present thesis.

In the present study, bathymetry data are provided from a survey carried out by the Region of Tuscany (step 2). Bathymetry and boundary conditions are supplied by means of separate files. Bathymetry files and params.txt can be built with the support of the MATLAB Toolbox released with the XBeach package (step 3). A detailed tutorial on the use of the Matlab Toolbox can be found in Elsayed and Oumeraci (2015). A basic model folder contains at least 5 files:

`params.txt`	File with model settings.
`bed.dep`	File with bathymetry information.
`x.grd`	File with x-coordinates of the grid. This file is only used with a non-equidistant grid.
`y.grd`	File with y-coordinates of the grid. This file is only used with a non-equidistant two-dimensional grid.
`jonswap.txt`	File with wave boundary conditions. In the default case the description of a JONSWAP spectrum.

In the present study, initial and boundary conditions for incoming waves (WBC) are provided from a SWAN coarser model instead of the default WBC specified in jonswap.txt. The pre-processing of output file of SWAN (step 4) is carried out by the program split_spc and will be described in the next section.

If the coordinates of an output point are specified in the input file of SWAN, it will generate a file *.spc in which a time-varying spectrum at one location is stored. This type of WBC can be used for 1D XBeach applications (i.e. cross-shore profile), or in case of 2DH applications where depth contours are parallel to the shore and thus, WBC are constant over the offshore boundary.

If the features of the XBeach grid are specified in SWAN, a file *.nes will be generated. This file contains the time- and space-varying spectrum along the XBeach grid boundaries, useful to obtain WBC for 2DH applications over complex bathymetry, where the WBC may vary along the offshore boundary. A shortcoming of this strategy is that the file *.nes could be very big and it needs a complex operation of post-processing.

Another possibility to obtain WBC, in the case of XBeach 2DH model with complex offshore bathymetry, is that a series of output points with coordinates laying on the offshore edge of the XBeach grid would be requested to SWAN.

The three strategies for obtaining WBC from SWAN are summarised in Table 4.3. However, the output WBC files obtained from SWAN are "crude" and need a manipulation before

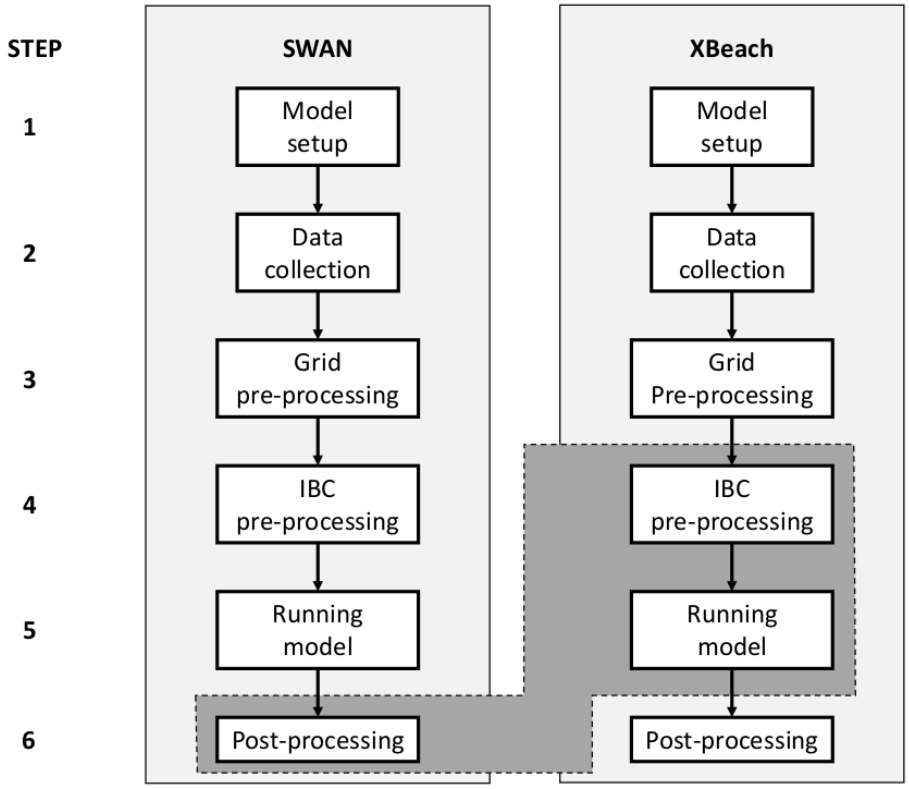

Figure 4.16: Workflow with the steps described in Table 4.1. The light grey box enclose the six steps needed to carry out a complete simulation with a numerical wave model. The dark grey box encloses the steps implicated in the nesting procedure.

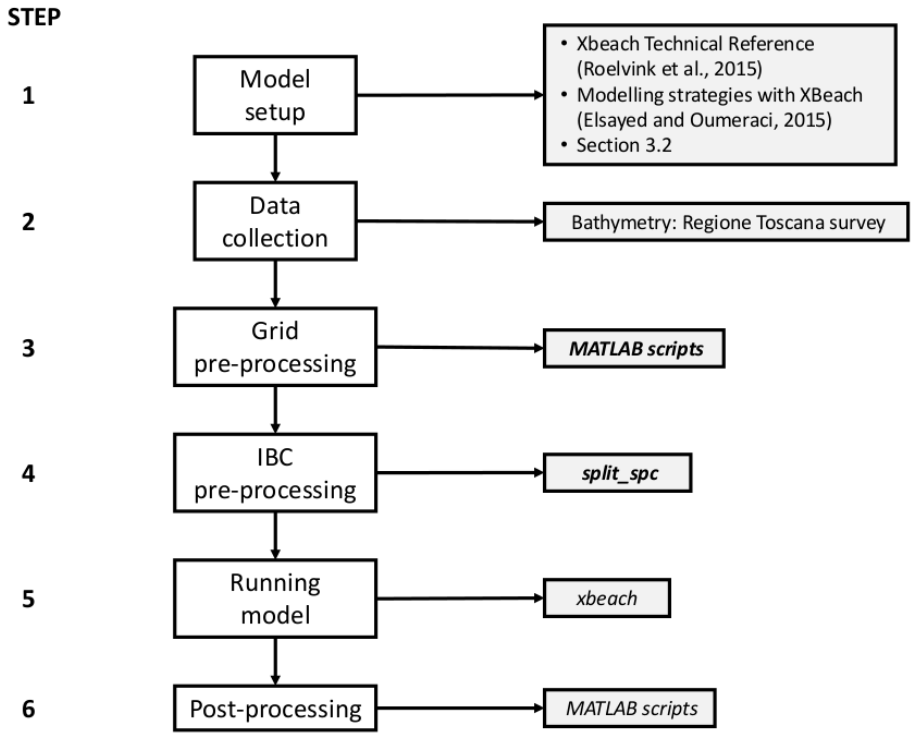

Figure 4.17: Workflow of XBeach. New codes are in italic, original codes are in bold.

Table 4.3: Strategies to obtain wave boundary conditions for XBeach, from SWAN running on a coarser grid.

XBeach features	**SWAN request**	**File of crude WBC**	**Remarks**
1D model or 2DH model with regular bathymetry	Single output point	file.spc	The XBeach WBC are constant over the offshore boundary
2DH model with complex bathymetry	Grid output	file.nes	This file contains also the lateral WBC, not requested in XBeach
2DH model with complex bathymetry or series of 1D models	Multiple output points	Series of file.spc	The output points lay only on the offshore edge of the grid

being used by XBeach. The manipulation of output files of SWAN is illustrated in Subsection 4.3.2

XBeach needs WBC as files containing a single spectrum for each time step and location. The list of spectrum files must be summarised in two files, one for times and one for location. In case of singleton location, the filelist of locations is not needed.

4.3.2 Nesting procedure

The methodology presented in this subsection is developed to nest SWAN and XBeach for the first case of Table 4.3, i.e. XBeach 1D or 2DH model with offshore depth contourlines parallel to the shore. The motivation of this choice is that the XBeach model is generally applied to simulate the evolution of cross-shore profiles (1D model), or small nearshore 2DH grids where depth contourlines are parallel to the shore and thus, WBC are constant over the offshore edge of the domain. However, the third case in Tab. 4.3 (i.e. 2DH model with complex bathymetry or series of 1D models) can be solved with a little improvement of the nesting procedure.

The use of a single point for providing WBC to XBeach implies that wave conditions will be constant along the offshore boundary of the domain. Furthermore, with only one point of WBC source, it is not important to specify the coordinates of the Active Boundary Point, since wave conditions are supplied all over the offshore boundary. This implies a great simplification of the nesting procedure since any difference in the reference coordinate system of the models becomes superfluous.

The one-way nesting strategy has been adopted to link the two models. WBC are transferred from SWAN to XBeach by means of spectral information provided at a selected time step. The models run in sequence: first, a SWAN model running over a coarser grid stores the wave spectrum for the selected location at each time step, and successively a cross-shore XBeach model runs reading WBC from the stored SWAN spectral files. This strategy requires no modification of the source code of the models. Furthermore, the sequential running of the models allows an easy management of the computer resources, i.e. each model can employs all the computer resources.

The general methodology for running in sequence SWAN and XBeach is shown in Fig. 4.18. Grid pre-processing operations (step 1) must be carried out for both XBeach and SWAN, with particularly attention to set in the input file of SWAN (swan.swn) an output point representative of the WBC for the XBeach model. Initial and boundary conditions for the SWAN model (step 2) are obtained from WWIII as described in Subsection 4.2.3.

The crucial point of the flowchart in Fig. 4.18 is associated with the post-processing of the output file of SWAN (file.spc, step 3), where spectral information are stored for all output

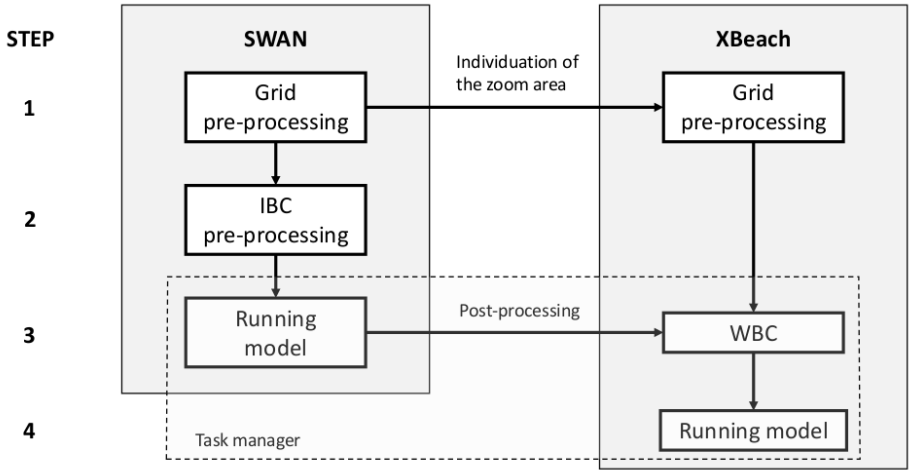

Figure 4.18: Flowchart of the methodology for running in sequence SWAN (CR model) and XBeach (HR model). The dashed box encloses the steps carried out by the task manager programme.

times. This file needs to be split in several files containing the wave spectrum for a single output time, which represent the WBC for the XBeach model. Then, the lists of all the WBC files must be written in the file filelist.txt. Step 3 allows XBeach to simulate time-varying wave conditions that is not possible using the default spectral output file of SWAN. It is worth to specify that in the present case, the post-processing of SWAN output and pre-processing of XBeach WBC are equivalent.

The manipulation of the spectral output file of SWAN is carried out by the Bash programme split_spc, developed during the present study. The flowchart of Fig. 4.19 describes the algorithm of the programme spilt_spc. The programme reads the file file.spc and copies the header in a temporary file. The header contains important information about the spectrum, such as the numbers and limits of the relative (or absolute) frequency bins, and the numbers and limits of the spectral directions.

Then, the file file.spc is split in multiple files containing the wave spectrum for a single output time and thus, the temporary header file is concatenate to each spectrum file. Finally, the list of WBC files is written in the file filelist.txt, together with the duration of WBC and the WBC time step in seconds. After the execution of split_spc, the XBeach simulation is ready to start (step 4). Step 3 and 4 are managed by a task manager programme as described in the next Section.

1. The nesting procedure presented in this section allows XBeach to run as 1D model (beach profile) or 2DH model of a beach with offshore depth contourlines parallel to the shore.

2. The default wave boundary conditions (WBC) are provided using a parametric JONSWAP spectrum. In the present study, WBC can be provided from a coarser model (i.e. SWAN) by means of a list of files containing spectral information at a given time.

3. The Bash programme split_spc has been developed in order to transform the output spectral file of SWAN in a list of files for providing WBC to XBeach. This operation allows XBeach to simulate time-varying wave conditions.

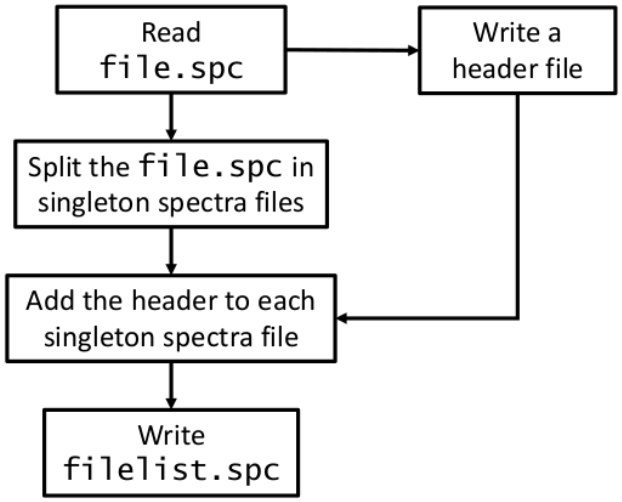

Figure 4.19: Flowchart of the algorithm executed by the programme split_spc.

4.4 The NEsted MOdel (NEMO) System with WWIII, SWAN and XBeach

This section presents an overview of the whole nested model (NEMO) system obtained by linking the two model systems described in Sections 4.2 and 4.3 (i.e. WWIII-SWAN and SWAN-XBeach, respectively) as illustrated in Figure 4.20. The methodology carried out for building and running the NEMO system is divided in 10 steps as summarised in Table 4.4.

Step 1 consists in the setup of the models WWIII, SWAN and XBeach. This step includes the installation of the models and the settings of model options and parameters. For the installation of the models, the reader is referred to Deltares (2016), Elsayed and Oumeraci (2015), Pelli (2016), The SWAN Team (2016b,c), and Tolman (2015) since it is not object of the present thesis. The settings of model options and parameters have been already described in Chapter 3.

The structure of the NEMO system is presented in Figure 4.21. The models are installed in the src folder, executable files and the programmes developed in the present work are stored in the bin folder, raw environmental data are stored in the data folder, and input, temporary and output files are stored in the work folder. A customization of the system structure is possible, but input files need to be set up.

Step 2 is the collection of bathymetry data for the building of the bathymetry files, and wind data for forcing the model system. In the present study, bathymetry data are downloaded from ETOPO1 and EMODnet databases, and obtained from the survey of the Tuscany Region.

Step 3 consists in building the bathymetry files for each computational grid. An overview of the methodology proposed for the building of the bathymetry files was given in Sections 4.2 and 4.3.

In Step 4, wind data are pre-processed in order to obtain the boundary conditions and forcing fields for the WWIII.

In Step 5, the coordinates of Active Boundary Points (ABPs) of the SWAN computational grid are calculated and requested to WWIII as output points. Therefore, spectral information at ABPs will be calculated and stored in a binary file by WWIII. These information will be used by SWAN as wave boundary conditions. This step is carried out by the original programme wwswan_prep.

Steps 6 to 8 are carried out using the original programme wwswan_shel. These Steps are the running of the WWIII model, the pre-processing of the initial and boundary conditions

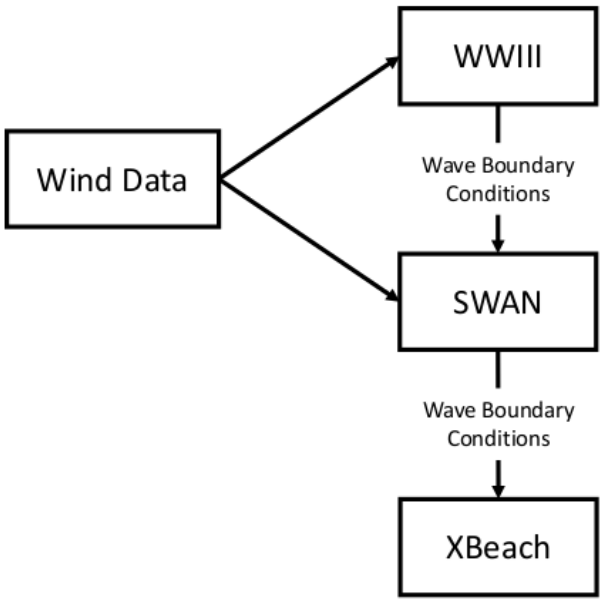

Figure 4.20: Workflow diagram of the NEsted MOdel (NEMO) system.

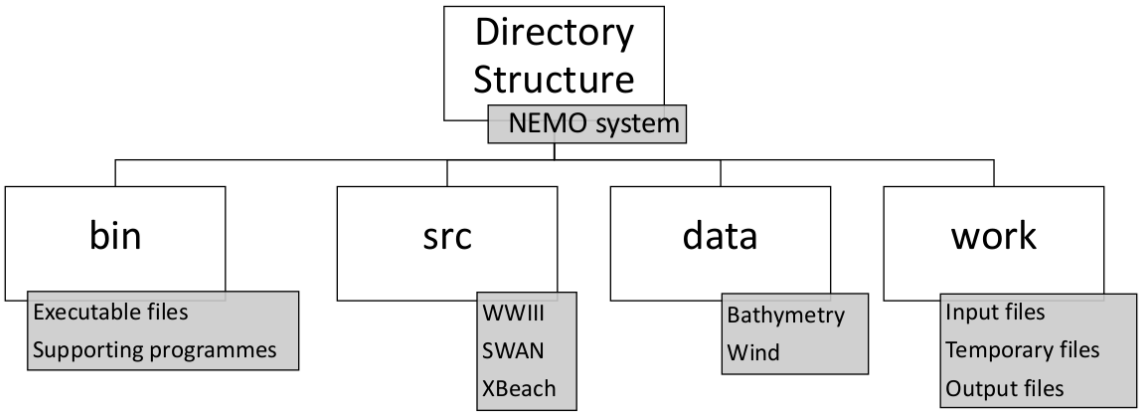

Figure 4.21: Directory structure of the NEMO system.

for the SWAN model, and the running of the SWAN model. Steps 2 to 8 are discussed in detail in Section 4.2.

In Step 9, wave boundary conditions for the XBeach model are extrapolated from the output of SWAN. This operation is carried out by the original programme split_spc. The last step consists in the execution of the XBeach model. Steps 9 and 10 are discussed in detail in Section 4.3.

Steps 4 to 10 are implemented in the model system and executed in sequence by the task manager programme nemo_system. The workflow diagram of the programme nemo_system is shown in Figure 4.22. This Bash programme is like a "box" where the programmes developed are called and executed in series, according to Table 4.4. The programme nemo_system allows the user to save time, avoiding annoying manually operations of data processing and mistakes related to the high number of files and programmes implicated in the nesting methodology.

1. The methodology proposed for building and running a seamless model system using WWIII, SWAN and XBeach is summarised in 10 steps as shown in Table 4.4.
2. Steps 1, 2, and 3 (i.e. models setup, data collection and grid pre-processing) are specific for each model and are not implemented in the model system.
3. Steps 4 to 10 are carried out by a number of programme developed during the present study. These programmes are managed by the task manager programme nemo_system, that represents the core of the model system.

4.5 Concluding remarks

This chapter describes the methodology developed to link the selected models (i.e. WWIII, SWAN and XBeach) in order to obtain a seamless model system. The models were selected evaluating some criteria, among them the most important are "Open source code", "Physics reliability" and "Easiness of nesting with other model" (see Section 2.4). Therefore, the codes of the models are open source, and each one has physics formulations appropriate for simulating waves at specific spatial scales and in specific relative water depths.

For example, WWIII is specific for simulating the development of sea waves in the deeper open ocean on a scale of thousands of kilometers, SWAN is specific for simulating waves dynamics on continental shelf (scale of tens to hundreds of kilometers), and XBeach is specific for simulating nearshore waves dynamics (including hydro- and morphodynamics that interact with waves) on a scale of tens to hundreds of meters.

The features of the three models adopted, which are all spectral models, are specific for simulating waves from an oceanographic to a coastal engineering scale. This indeed facilitates the nesting procedure since the only information required to transfer wave boundary conditions between the models is the spectral information. Furthermore, some efforts have already been done by the model developers in order to simplify the nesting procedure among the models. In fact, spectral output files of WWIII are in the same format of initial boundary conditions files for SWAN, and spectral output files of SWAN are in a similar format of initial boundary conditions files for XBeach.

However, some operations of pre-processing of the spectral output files are necessary. For example, the key points of the nesting between WWIII and SWAN is the selection of the Active Boundary Points (ABPs), i.e. the boundary points of the child grid where spectral information are provided by the parent grid. The programme wwswan_prep has been developed to select ABPs and manage the pre-processing of initial and boundary condition for the nested grid.

Table 4.4: Summary of the steps for building and running the model system NEMO.

	Steps	**Methodology**	**Remarks**
1.	Models setup	WWIII, SWAN and XBeach are installed as separate models	See Deltares (2016), Elsayed and Oumeraci (2015), Pelli (2016), The SWAN Team (2016a,b), and Tolman (2015).
2.	Data collection	Collection of bathymetry data and wind data	New codes have been developed to help the execution of this step.
3.	Grid pre-processing	Built the bathymetry files for each model	Site-specific. Individuation of the zoom area.
4.	WWIII initial and boundary conditions pre-processing	Programme ww3_prnc	New codes have been developed to help the execution of this step. Implemented in the model system.
5.	Individuation of SWAN Active Boundary Points	Programme wwswan_prep	Implemented in the model system.
6.	Run WWIII	Programme wwswan_shel	Implemented in the model system.
7.	SWAN initial and boundary conditions pre-processing	Programme wwswan_shel	Implemented in the model system.
8.	Run SWAN	Programme wwswan_shel	Implemented in the model system
9.	XBeach initial and boundary conditions pre-processing	Programme split_spc	Implemented in the model system.
10.	Run XBeach	Programme xbeach	Implemented in the model system.

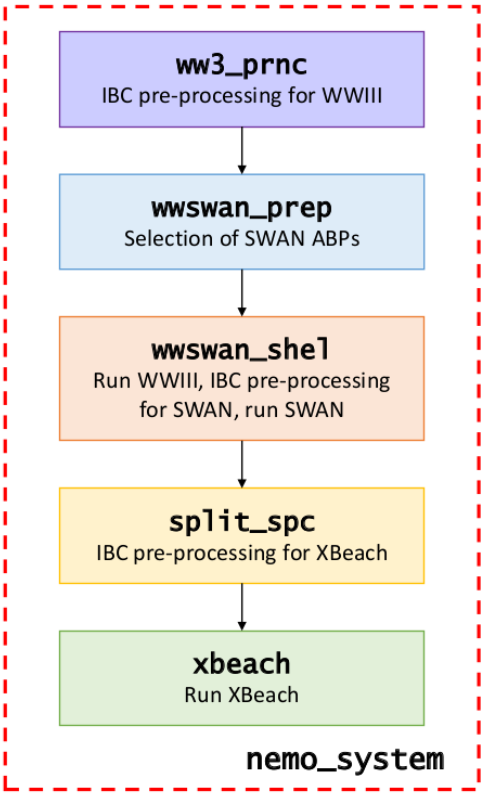

Figure 4.22: Workflow of the manager code nemo_system with the implementation of Steps 5 to 10 as the core of NEMO.

The strategy of providing wave boundary conditions (WBC) by means of ABPs was preferred to the possibility of providing WBC to SWAN by means of wave parameters (i.e. H_{m_0}, T_p,, peak direction and directional spreading) since the pre-processing of spectral file is straightforward. Furthermore, a lost of information occur when WBC are provided by means of a parametric spectrum assumed a priori with a JONSWAP shape. Moreover, wave parameters needs to be defined along the boundary by means of active segments (i.e. portions of the boundary where WBC are constant) with a further lost of information in respect to ABPs which provide WBC at each point of the computational domain.

The main problem of the SWAN-XBeach nesting is represented by providing WBC to XBeach in case of nonstationary simulations. In order to compute nonstationary simulations, XBeach needs that WBC to be provided as a list of files describing the wave spectrum at each time step. Therefore, the default single spectral output files of SWAN, in which spectral information are stored for all the output time, need to be pre-processed. This operation is carried out by the programme split_spc, developed to overcome the limitation.

The transfer of spectral information is carried out adopting the one-way nesting strategy. Information are transferred only from coarse resolution (CR) grid to high resolution (HR) grid and not vice versa. This choice is justified by the aim of the research which consists in modelling waves from deep water to the shoreline, i.e. from CR grid to HR grid. The one-way interaction allows to run the model in sequence and implies no or only slight modifications of the source code.

The building and running of the model system is summarised in Table 4.4 in 10 steps. Steps 1, 2, and 3 are specific for each model and are not implemented in the model system. Steps 4 to 10 are automated by means of a task manager programme (nemo_system), that represents the core of the model system.

The approach using a task manager programme that manages the original code of the models allows the user to easily update the single models by introducing improvements/exten-

sions, or fully new versions of the models without modification of the structure of the NEMO system. Furthermore, new models (e.g. atmospheric, tide, circulation) could be easily added to the model system.

5

Application of the nested model system

The nested model (NEMO) system proposed in Chapter 4 is applied to a real case. The test case area is the Versilia coast (North Tuscany), a stretch of coast with valuable tourism facilities developed on the beach, vulnerable to beach inundation. Two significant storms hit the the coast of North Tuscany between the 2nd December 2011 and the 20th December 2011 (see Fig. 5.7), causing considerable damages to the local tourism activities for beach recreation.

In particular, the storm of the 15nd-17th December, with a peak of significant wave height of about 6 meters observed in deep water, was one of the most intense and devastating in the last 20 years. The storm had an important impact on the regional media (see Fig. 5.1), where an erosion of the beaches of Marina dei Ronchi (northern Versilia) with a mean recession of 20m was reported.

The objective of this chapter is to hindcast the storm of December 2011 in the North Tuscany, and to evaluate the impact of the storm on the coast of Marina dei Ronchi by applying the proposed NEMO system.

The reliability of the model in deep water is evaluated by comparing the wave parameters observed and hindcasted. In order to assess the behaviour of the NEMO system on the shoreline, the observed and simulated beach profiles are compared. Two bathymetry surveys conducted in September 2011 and January 2012 are available for the coast of Marina dei Ronchi. Since the most important storm, which occurred in this period is that of December 2011, it is assumed that the main changes between the two surveys were caused by this storm. Moreover, the wave setup, the shoreline regression and the beach erosion hindcasted by the NEMO system are compared with the information extrapolated from the local newspapers, interviews to the owners of beach facilities, and photographs.

The application of the NEMO system to the Versilia coast is motivated by the goal of the present study to build a model system for the support of a Coastal Early Warning System (CEWS).

Currently, the alert system for wave storms of the Tuscany Region as shown in the following website `http://www.regione.toscana.it/allertameteo/il-sistema-di-allertamento` does not include a model that takes into account near shore wave dynamics and the wave risk is evaluated on the basis of deep water conditions only. Section 5.1 describes in detail the test case area in Marina dei Ronchi and Section 5.2 describes the NEMO application to the storm of December 2011 in this area.

IMPRESE IN GINOCCHIO

Il mare si mangia i bagni Ida e Delfino

Scalzate le verande: e oggi i bollettini del mare prevedono onde alte sei metri

MARINA MASSA. Il Bagno Ida, il Delfino, il Palmo rischiano di sparire. Ma persino alla Partaccia, dove l'arenile è più consistente, ieri ha vissuto nella preoccupazione. Il mare, con onde altissime, ha devastato la costa con furore. E i bagni di Ronchi, come è nella storia degli ultimi anni, hanno pagato subito un caro prezzo. Al momento in cui scriviamo i bollettini del mare indicano per la notte (ieri, ovviamente) e stamani l'apice della mareggiata. La speranza dell'oggi è di ritrovare ancora in piedi l'Ida, il Delfino e gli altri.

«Il pericolo è la lunghezza dell'onda - spiega Maurizio Ragaglini, del Consorzio balneare Riviera Apuana - Il vento forte in realtà schiaccia il mare, il pericolo è quando molla e l'onda si allunga. Le previsioni danno purtroppo mare agitato, ovvero onde alte fino a sei metri. Sarà una notte drammatica».

A Ronchi, dunque i problemi più grossi, seguiti anche dalla protezione civile.

«Mi hanno chiamato stanotte avvisandomi della mareggiata e sono venuto a vedere. La spiaggia non c'era già più ma la veranda sì, era solo un po' rotta. Ma ora guardi, non c'è più nulla!», racconta arrabbiato e amareggiato Luca Vece, bagnino e tuttofare, guardando quello che rimane del suo bagno: un casottino diventato ora una palafitta sul mare. E sì, perché i venti metri di spiaggia, corrispondenti a quattro file di ombrelloni più battigia, ora non ci sono più e là, dove prima c'era la veranda del bar che d'estate si riempie di tavolini, ora c'è uno strapiombo di due metri con sotto onde che non sembrano dare tregua. Uno scenario post-apocalittico: dove prima c'era il Bagno Ida, ora c'è solo un mare infuriato.

Anche la spiaggia della Partaccia ha perso decine e decine di metri di arenile Danni ingenti

Bagno Delfino, la forza delle onde ha scalzato le fondamenta

«La spiaggia - spiega Luca - non è a livello del mare, ma un po' rialzata. Così facendo però erode il terreno sotto e rischia di crollare tutto. Questa casettina domani rischia di non esserci più».

La mareggiata sarebbe iniziata nelle prime ore del mattino di ieri e avrebbe portato via la spiaggia dei bagni che vanno dal piccolo torrente che costeggia viale della Repubblica fino al Bagno Palmo; nel pomeriggio le onde si sono spinte oltre portandosi via anche il cemento del Bagno Ida. Il piccolo torrente che costeggia il viale della Repubblica e sfocia a due passi dai bagni invasi dalle onde, si è riempito d'acqua.

La situazione è critica anche per i bagni vicini.

Lì, le onde si sono mangiate già una grande fetta dell'arenile, lasciandogli giusto una striscia di sabbia; dune, costruite con la sabbia probabilmente in previsione di una mareggiata, cercano di difendere i loro chioschetti. Ma le previsioni meteorologiche per stanotte non sono rincuoranti: le onde potrebbero arrivare a sei metri e le dune di sabbia potrebbero non bastare.

Anche Palmo, Tropicana e Paradiso sono minacciati seriamente La polemica per i lavori non fatti

Non è la prima volta che la furia del mare travolge e stravolge quella zona. Solo due anni fa una mareggiata aveva inondato il Bagno Palmo e distrutto tutto la stabilimento. Ora la storia si ripete e inizia la "caccia al colpevole". «La colpa - continua Luca infuriato - è di questi Geotubi che dovrebbero avere la stessa funzione delle scogliere e invece non servono a nulla. Anzi. Non fanno defluire le correnti e questo è quello che succede. L'amministrazione pubblica avrebbe fatto bene a spendere il suo tempo e i suoi soldi in altro modo. Hanno sprecato soldi utili. E ora pretendiamo delle risposte».

«Noi speriamo - continua Luca - che questo faccia innescare un meccanismo di tutela dell'ambiente costante. Noi lavoriamo e sudiamo anni per poi vedere sparire i nostri risparmi in un giorno. Non è giusto. Non può pagare sempre chi lavora tutta la vita. E poi bisogna sfatare questo mito dei proprietari dei bagni che lavorano l'estate e tutto l'anno non fanno nulla. Guardate. Noi abbiamo sempre dei problemi da superare!».

Disperati i balneari. Che vedono una vita di lavoro, investimenti e speranze andare sott'acqua. Il problema sono i lavori anti erosione: soldi ma soprattutto un programma organico di intervento a levante come a ponente. Perchè il tempo, purtroppo, per il mare è scaduto.

Melania Carnevali

Figure 5.1: The news of the coast damages due to the storm of 15-16 December 2011 on a regional newspaper (courtesy of Il Tirreno, 2011).

5.1 Test case area

The shoreline of Marina dei Ronchi has been selected as test case area for the following reasons:

- The deep water wave climate observed at La Spezia (24km offshore in WSW direction) is available for the years 2010-2015.
- The near shore wave climate observed at Carrara (8km in NW direction) is available for the years 2006-2011.
- Two bathymetry surveys were conducted before the start of the storm season, in September 2011, and after two consecutive significant storms in January 2012.
- The typical incident storm waves have a direction perpendicular to the shore, thus limiting the wave-induced longshore transport.
- The beach of Marina dei Rochi is stable (i.e. no erosion or accretion) (Anfuso et al., 2011).

The position of the wave gauges, the area of the bathymetry surveys, and the other features of the North Tuscany coast are summarised in Figure 5.2a.

The wave climate at Marina dei Ronchi is well represented by observations of the wave buoys of La Spezia and Carrara, moored in a water depth of -100m and -14m, respectively (see Fig. 5.2a). Wave observations summarized in Figure 5.3 show a prevalent wave direction perpendicular to the shoreline (i.e. SW), limiting the longshore sediment transport due to waves in the test case area. The coast is located nearby the transition area of two opposite sediment drifts, the sediment supply of the Magra river from North and the sediment supply of the Arno river from South. In particular, the south part of Marina dei Ronchi is located in a transition zone between a northern erosion zone (Marina di Massa) and a southern accretion zone (Marina di Pietrasanta) (Anfuso et al., 2011).

The closure depth calculated with the Hallermeier formula (Hallermeier, 1980) by D'Eliso et al. (2006) using the wave observations at La Spezia for the period 1996-2005 was -7.63m. The value obtained in the present study using the observations at the same location for the period 2010-2015 is -11.05m. However, the real closure depth estimated by D'Eliso et al. (2006) comparing beach profiles from different surveys resulted in -7.20m. In fact, the comparison between the available surveys in September 2011 and January 2012 (Figs. 5.4-5.5) shows that no significant changes in the seabed elevation occurred for depth less than -6m. These values are summarised in Table 5.1. A reasonable value of the closure depth for Marina dei Ronchi may be $d_c = -8m$, that represents the average of the d_c values in Tab. 5.1.

An overview of the shoreline of Marina dei Ronchi is shown in Figure 5.2b, where the bathymetry surveys were carried out in September 2011 and January 2012. The dry beach lacks in dunes that were replaced by human facilities for beach recreation. The norther part is characterised by a series of groynes. Since XBeach does not account for the effect of porous media such as groynes, simulations are carried out in the coast free of groynes, i.e. between Poveromo creek and Versilia river (see Fig. 5.2b).

Table 5.1: Estimated values of the closure depth (d_c).

Data set	Type of calculation	Depth of closure (d_c) [m]
1996-2005	Hallermemier formula	7.63
2002-2005	From bathymetry surveys	7.20
2010-2015	Hallermemier formula	11.05
2011-2012	From bathymetry surveys	6.00

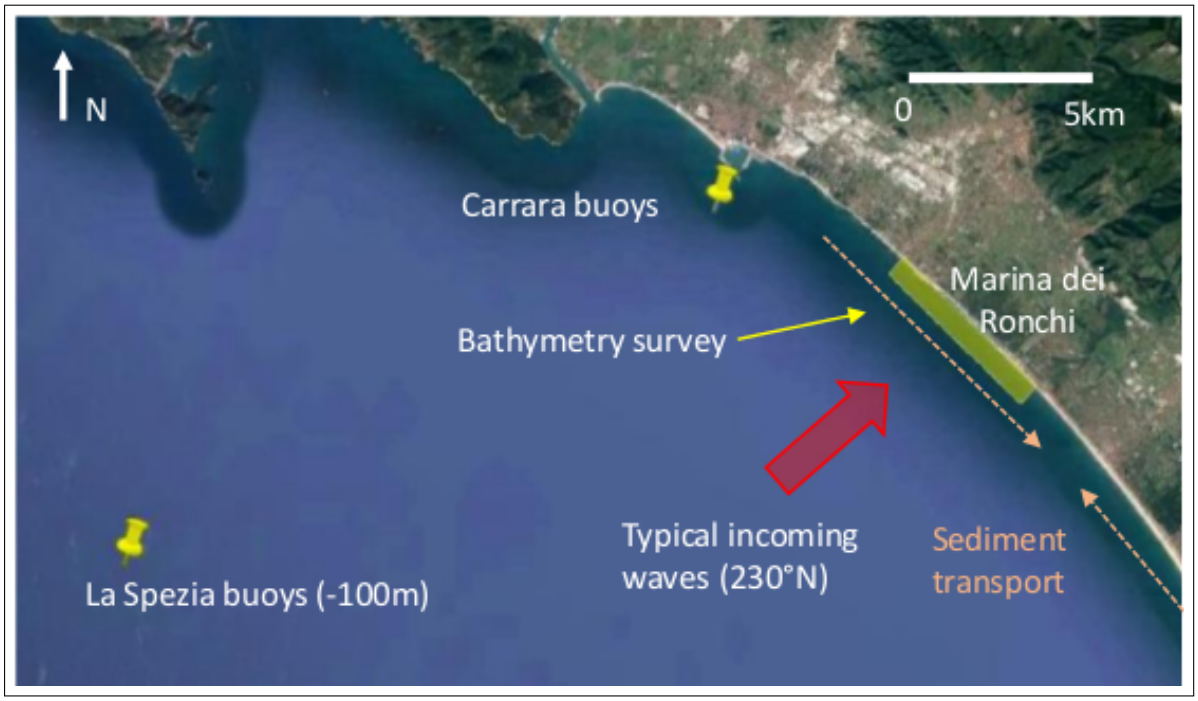

(a)

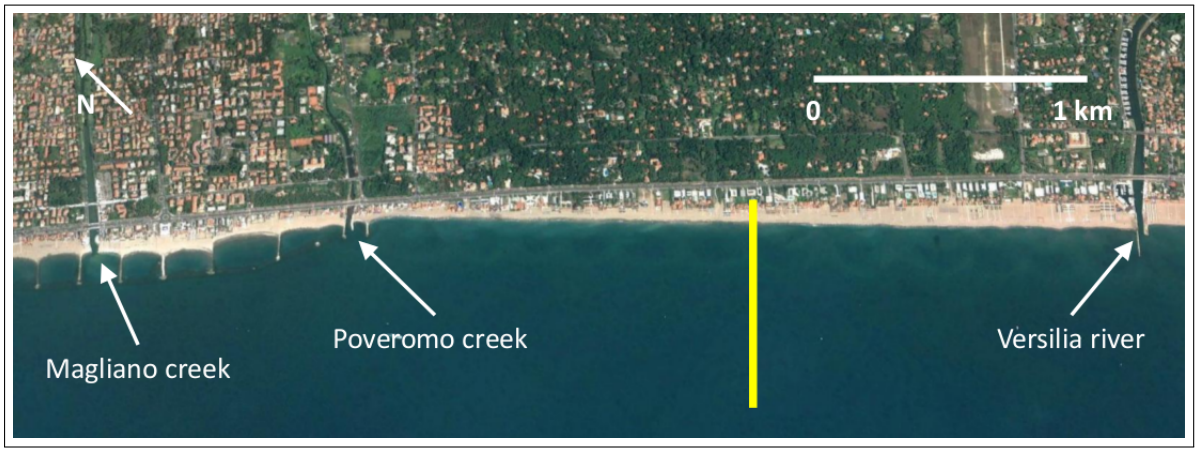

(b)

Figure 5.2: (a) North Tuscany coast with wave buoy locations (yellow marks), the area of the bathymetry surveys (yellow patch), and the direction of waves and sediment transport features (modified from Google Earth), and (b) detail of Marina dei Ronchi beach with highlighted in yellow the test case area (modified from Google Earth).

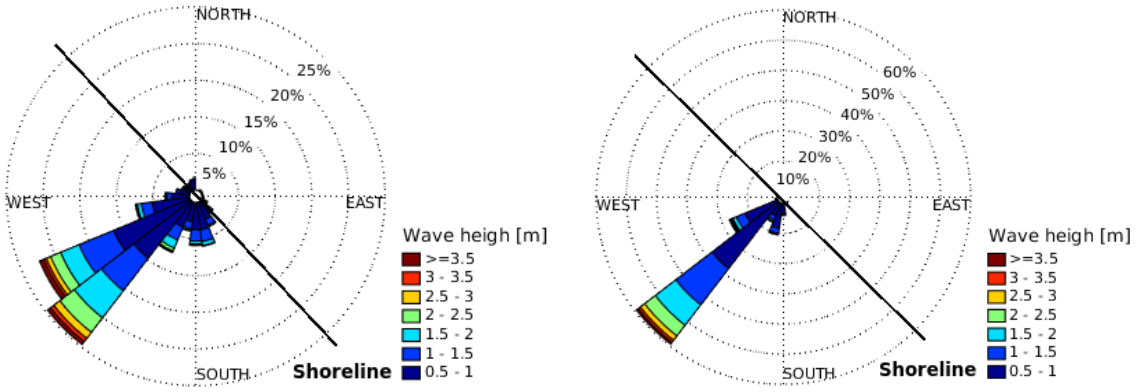

(a) La Spezia (b) Carrara

Figure 5.3: Wave rose for (a) La Spezia and (b) Carrara with the shoreline orientation of Marina dei Ronchi. H_{m_0} values are filtered at 0.5m.

Since 2DH simulations with XBeach are too time consuming for an Early Warning System, the application case will be carried out in 1D mode. Therefore, a homogeneous stretch of 50m of width (highlighted in yellow in Fig. 5.2b) is selected as representative profile for a 1D application with XBeach. The mean profiles of the selected area are shown in Figure 5.6 for the surveys of September 2011 and January 2012. The two profiles are represented as the area included between an interval of confidence of 95% of the standard deviation from the mean profile.

The mean slope of the profile is 1.5%, calculated from the closure depth to the highest part of the emerged beach. The mean grain size ($D50$) calculated according to a survey of October 1999 is 0.5mm (Aminti et al., 2004).

Figure 5.6 confirms that the test case area can be considered homogeneous since the maximum standard deviation is of few decimeters in correspondence of the sandbar, i.e. at 500m$<x>$550m for the survey of September 2011 and 450m$<x>$500m for the survey of January 2012. Furthermore, the gradient of the longshore sediment transport between 2011 and 2012 is close to 0, justifying a cross-shore application (i.e. 1D). Figure 5.6 proves also that no significant changes of elevation occurs for depths less than -6m.

5.2 Test case storm characteristics

An overview of the storm event simulated during the test case application is described in Figure 5.7, that shows the evolution of wave parameters H_{m_0} and mean direction (Dir) over time at La Spezia (depth -100m). The main features of the two storms are summarised in Table 5.2.

NEMO System simulates the wave climate of all the Mediterranean Sea by means of the deep water module WAVEWATCH III (WWIII) with a resolution of about 5km. Then, the

Table 5.2: Main features of the two storms simulated with XBeach occurred between December 2011 and January 2012. H_{m_0} is referred to the peak storm, T_p and Mean Dir are the corresponding values.

Storm	Start	End	La Spezia			Ronchi		
			H_{m_0}	T_p	Dir	H_{m_0}	T_p	Dir
1	2011-12-03 19:00	2011-12-08 19:00	5.08	10.0	238	3.49	10.9	230
2	2011-12-14 15:00	2011-12-18 17:00	5.87	11.1	229	3.64	11.1	230

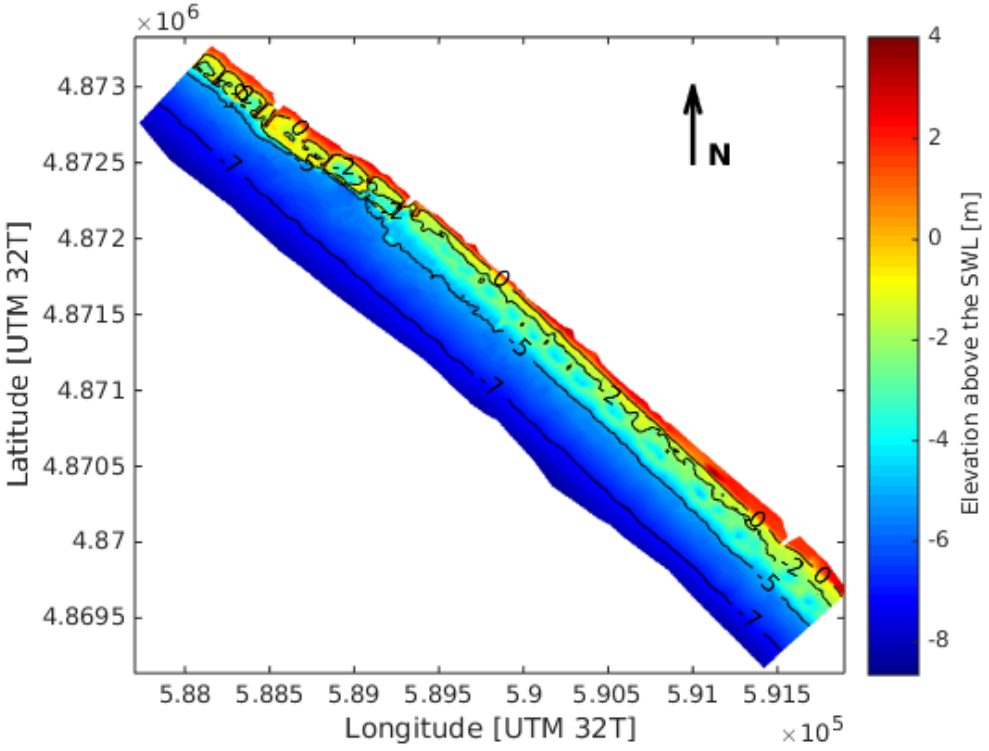

(a) September 2011

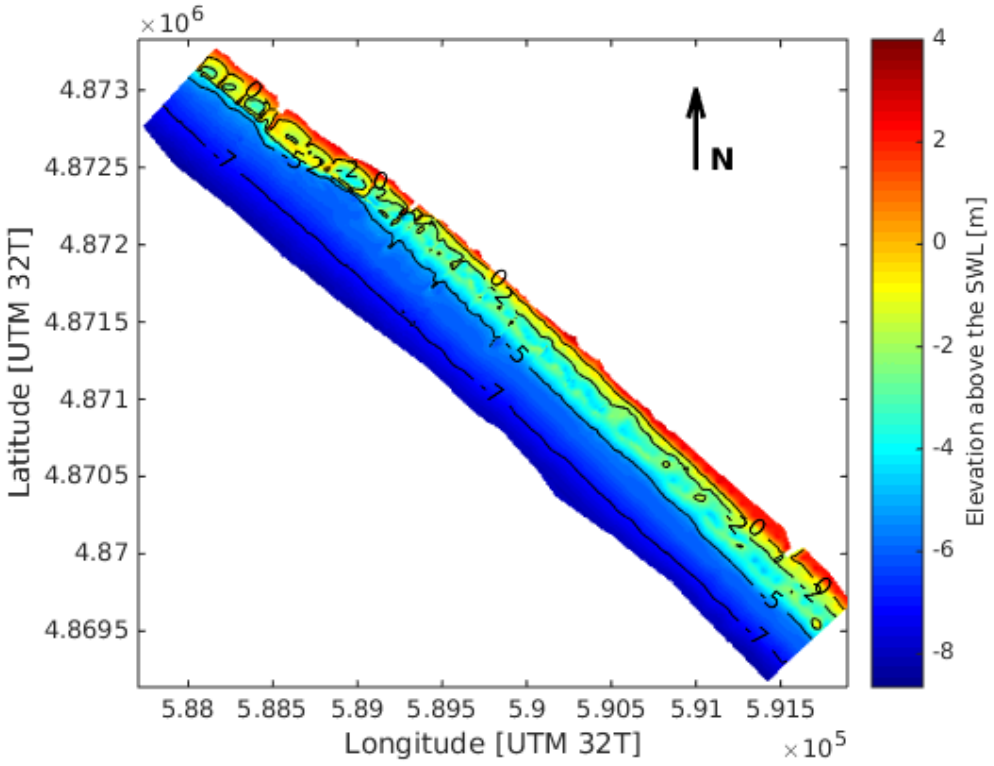

(b) January 2012

Figure 5.4: Bathymetry surveys of Marina dei Ronchi coastline, (a) September 2011, (b) January 2012.

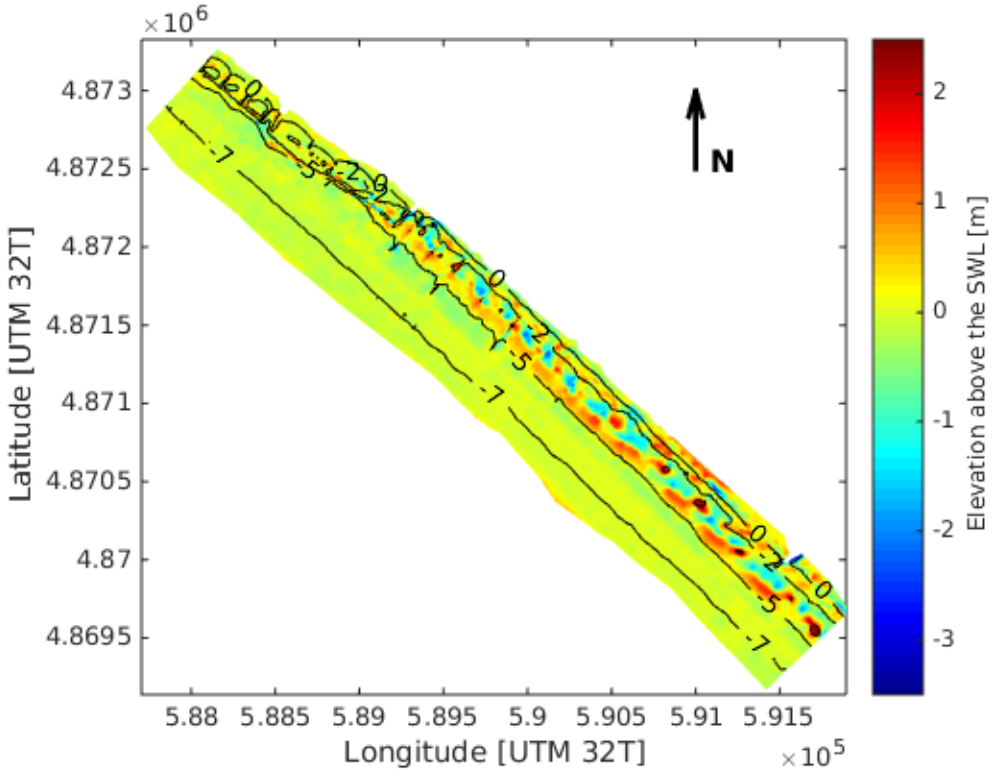

Figure 5.5: Elevation differences between the bathymetry survey of January 2012 and September 2011 at Marina dei Ronchi. Contourlines refer to 2012 data set.

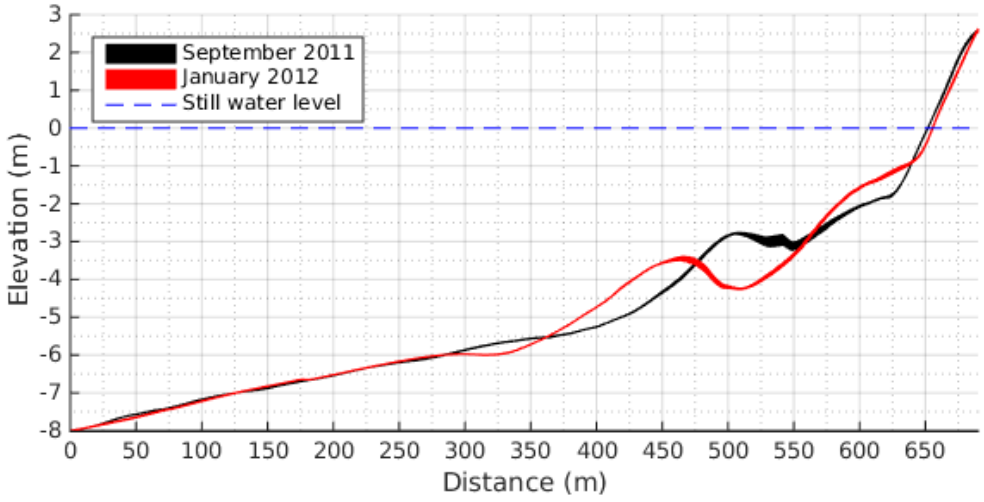

Figure 5.6: Mean beach profiles of the test case area for the surveys of September 2011 (before the storms) and January 2012 (after the storms). The profiles are represented with the area included between an interval of confidence of 95% of the standard deviation from the mean profile.

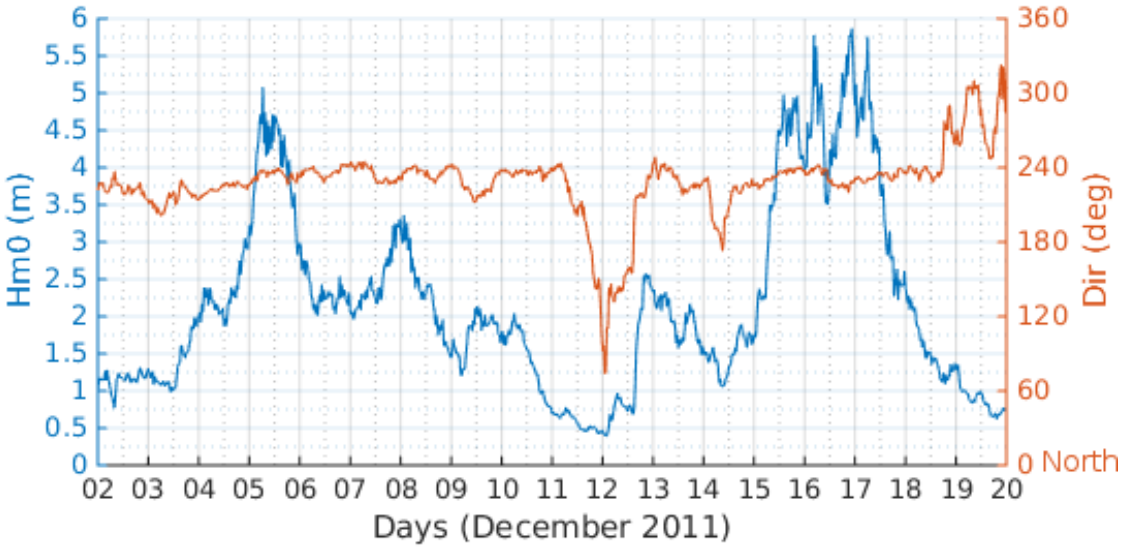

Figure 5.7: Time series of H_{m_0} and *dir* (mean direction) parameters observed at La Spezia (depth -100m) for the period 2 December 2011 - 20 December 2011.

downscaling of the wave field is carried out in the North Tuscany coast with the intermediate water module SWAN. Two telescoping SWAN grids cover the North Tuscany coast with a resolution of 800m and 100m, respectively (Figure 5.8).

The reliability of the hindcasted wave field in deep water is evaluated comparing the wave parameters observed at La Spezia with those hindcasted by WWIII. Figure 5.9 shows the evolution over time of the observed and hindcasted wave parameters H_{m_0}, T_p, Dir at La Spezia. A relatively good agreement is observed for all parameters. As shown in Fig. 5.9a, discrepancies between observed and hindcasted H_{m_0} occur on the first pulse of the second storm (15-16 December) as well as between the two storms.

It is worth to mention that even though the calibration and validation of WWIII (see Section 3.1) was carried out for the wave parameter H_{m_0}, the agreement between observed and hindcasted peak period (T_p) and direction (Dir) is largely satisfactory. Of course, as it revealed by Figure 5.9, it is not possible to well predict T_p and Dir for calm sea state (i.e. H_{m_0} close to zero).

Since the wave buoy of Carrara was inoperative in December 2011, it is not possible to compare the hindcasted and observed wave parameters in intermediate water. However, the wave parameters hindcasted by SWAN (with 800m grid resolution) are compared with observations at La Spezia in Figure 5.10. The comparison between observed and hindcasted wave parameters is comparable with the one shown for WWIII in Figure 5.9. Hence, no significant errors occur during the transfer of boundary conditions between WWIII and SWAN. Also in this case, a good agreement between observed and hindcasted peak periods (T_p) and directions (Dir) are observed.

The reliability of the NEMO system in intermediate water has been already shown in Section 3.2, where it was demonstrated for several storms that when wave parameters hindcasted by SWAN well match with observations at La Spezia, a good agreement between model and observations is also reported for the Carrara station. Therefore, the comparison of wave parameters shown in Figure 5.10 may be sufficient to prove that the NEMO system well hindcasts the storms of December 2011 in intermediate water.

The performance of the NEMO system in shallow water and shoreline is evaluated in two ways:

- Comparing the modelled cross-shore profile with the profile observed in January 2012.
- Comparing the modelled wave setup and the shoreline evolution with the information

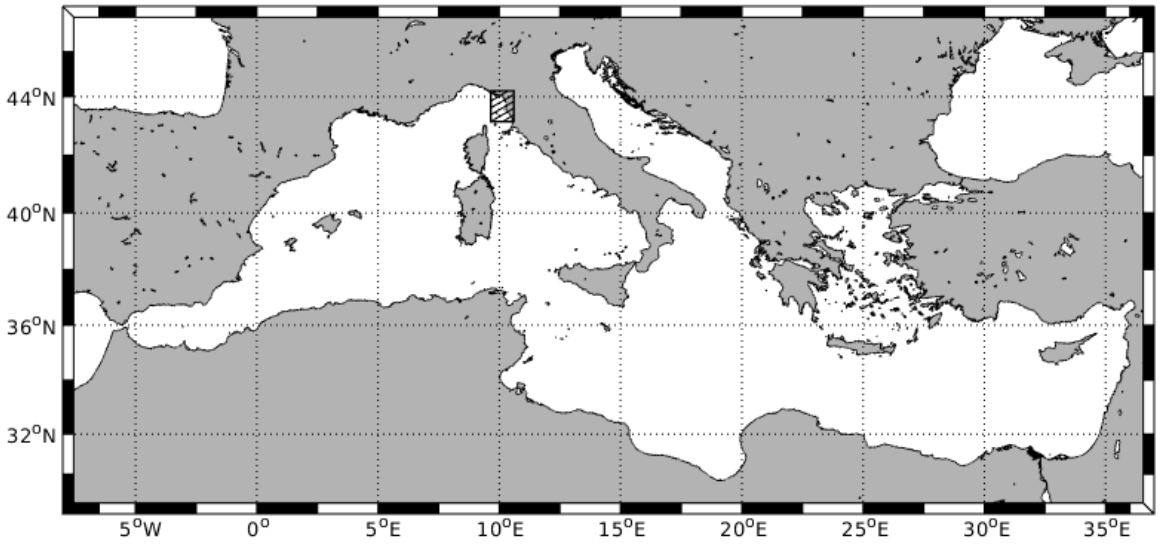

(a) WWIII grid

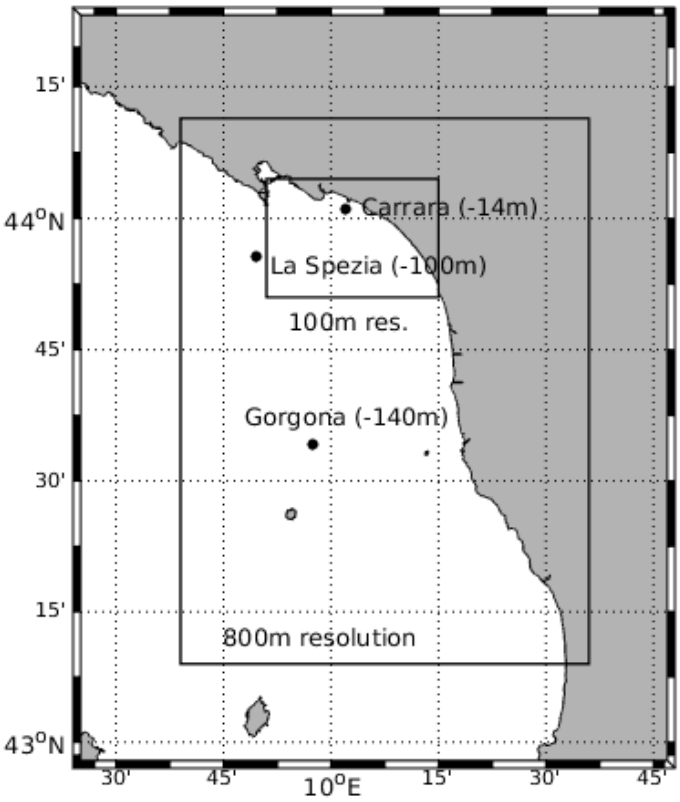

(b) SWAN grids

Figure 5.8: Computational grids of the NEMO system for (a) WWIII (Mediderranean Sea), and (b) SWAN (North tuscany 800m and 100m).

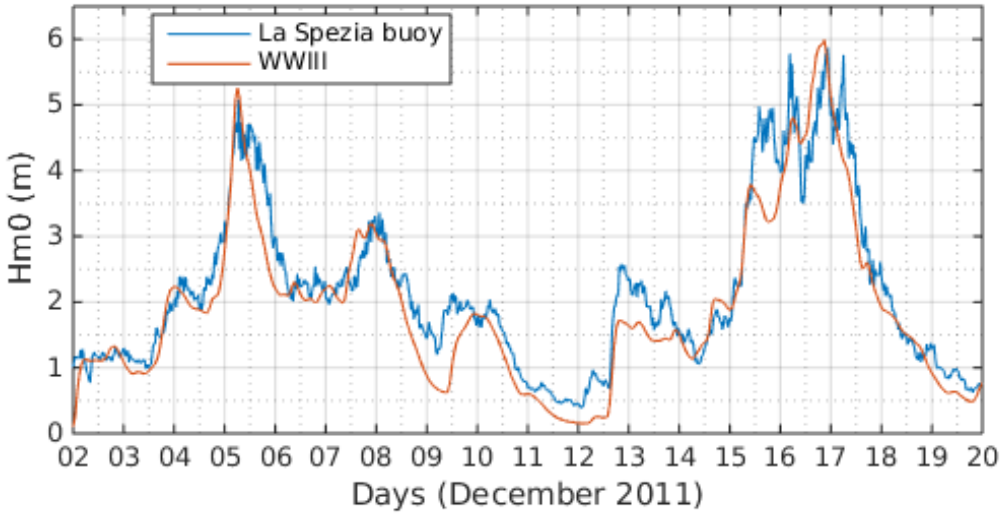

(a) H_{m_0} comparison

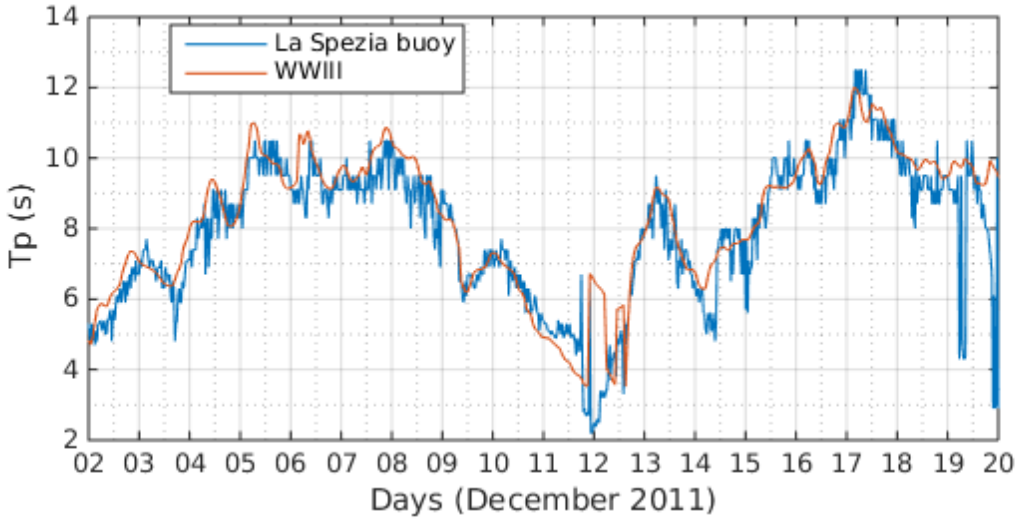

(b) T_p comparison

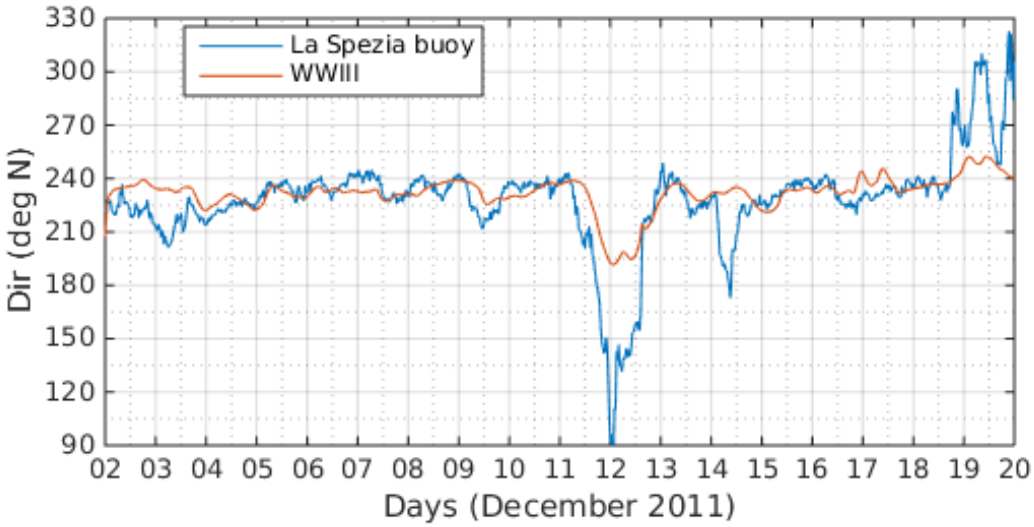

(c) *Dir* comparison

Figure 5.9: Comparison of the wave parameters H_{m_0}, T_p, *Dir* observed and simulated by WWIII at La Spezia.

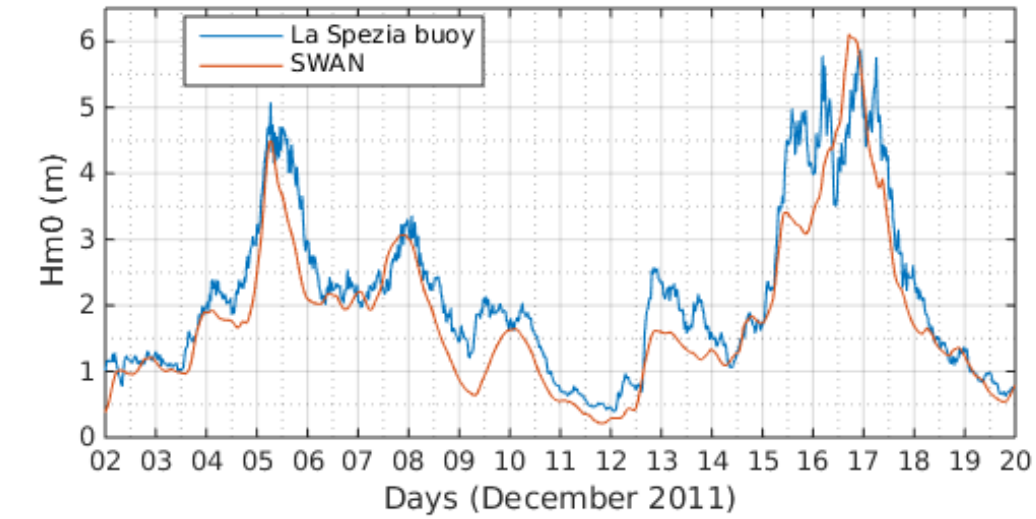

(a) H_{m_0} comparison

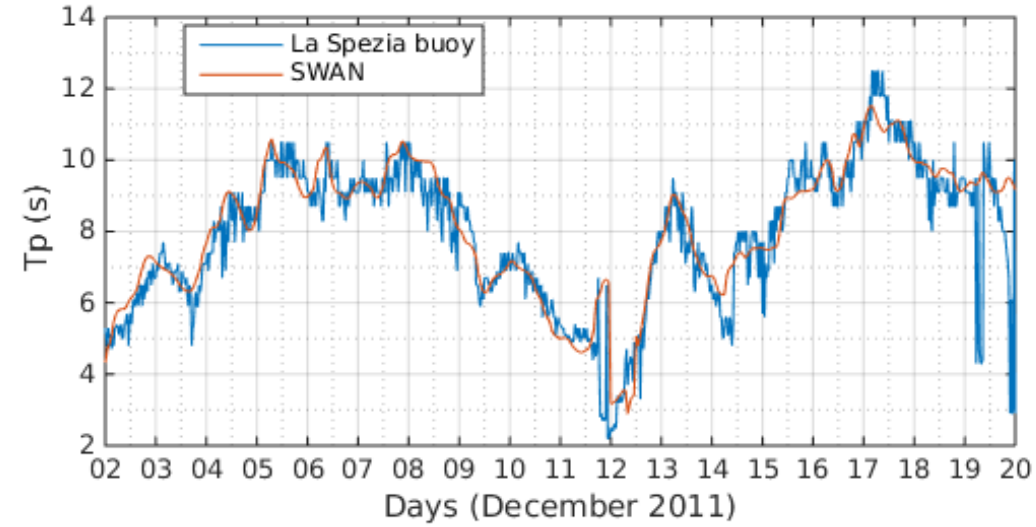

(b) T_p comparison

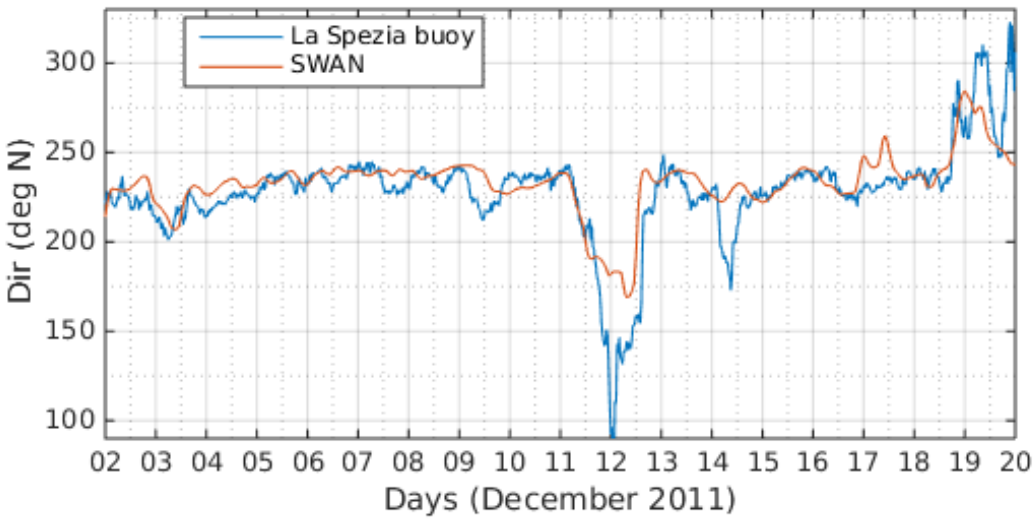

(c) *Dir* comparison

Figure 5.10: Comparison of the wave parameters H_{m_0}, T_p, *Dir* observed and simulated by SWAN at La Spezia.

collected on local newspapers and interviews to the owners of beach facilities, and photographs.

The profile observed in September 2011 is assumed as initial condition since no significant storms have been observed between September and December 2011. The survey of January 2012 was conducted about one month after the storm of 15-16 December 2011 and therefore, some discrepancies between hindcasted and observed profile would be expected.

5.2.1 Cross-shore profile analysis

The performance of the NEMO system in shallow water and shoreline is first evaluated comparing the profile modelled with XBeach with the profile observed in January 2012.

Two cases are considered:

- Simulating the morphodynamics only for the most significant storm (i.e. December 12 to December 20) of the two successive storms and therefore, assuming that only beach accretion occurred during the relatively calm period between the two storms.
- Simulating morphodynamics processes for both successive storms, i.e. from December 2 to December 20.

Figure 5.11 shows the comparison of the profile observed in September 2011 and January 2012, and the profile modelled with XBeach simulating the morphodynamic processes of only the main storm (Fig. 5.11a), and for the two consecutive storms (Fig. 5.11b). Significant differences between modelled and observed profiles (January 2012) are noticed in both cases. Therefore, carrying out a quantitative comparison (e.g. BSS) does not make sense. Qualitatively, the model is able to reproduce in both cases the zones where the profile was eroded or accreted, except the erosion in the offshore part of the profile (300m$>x<$350m). For example, the formation of a nearshore bar at x=600m is well-reproduced in both cases.

The only difference observed between Fig. 5.11b and Fig. 5.11a consists in the erosion of the upper part of the beach profile (called hereafter "dry beach") and the consequent size of the nearshore bar. Obviously, the dry beach is more eroded simulating morphodynamic processes of both storms. However, since both simulations give a profile significantly different from the profile observed in January 2012, it is not possible to evaluate what is the better modelling strategy.

From the information collected on local newspapers, interviews to the owners of beach facilities, and photographs, it is clear that the profile of the dry beach of Marina dei Ronchi on the 17th of December (i.e. after the second main storm) was significantly different from the profile observed in January 2012. Therefore, it seems more meaningful to compare qualitatively the results of the NEMO system with the information published directly after the storms.

In the next subsection, a qualitative evaluation of the performance of the NEMO system in the nearshore is conducted comparing the modelled wave setup and shoreline evolution with the information collected on local newspapers, interviews, and photographs.

5.2.2 Wave setup and shoreline evolution analysis

Since the scope of the NEMO system is to contribute in the assessment of the risk for human activities on the beach, it is very important that the wave setup and shoreline regression reported during, and immediately after the test case storm will be reliably predicted.

Based on the information collected on local newspapers (Il Tirreno, 2011), interviews to the owners of beach facilities, and photographs (Fig. 5.12) about the storms those hit the Versilia coast in December 2011, three certain conditions are summarised in Table 5.3.

The NEMO system was applied to the mean profile of Marina dei Ronchi beach shown in Figure 5.2b for four test cases, as summarised in Table 5.4. The choice of modelling the event

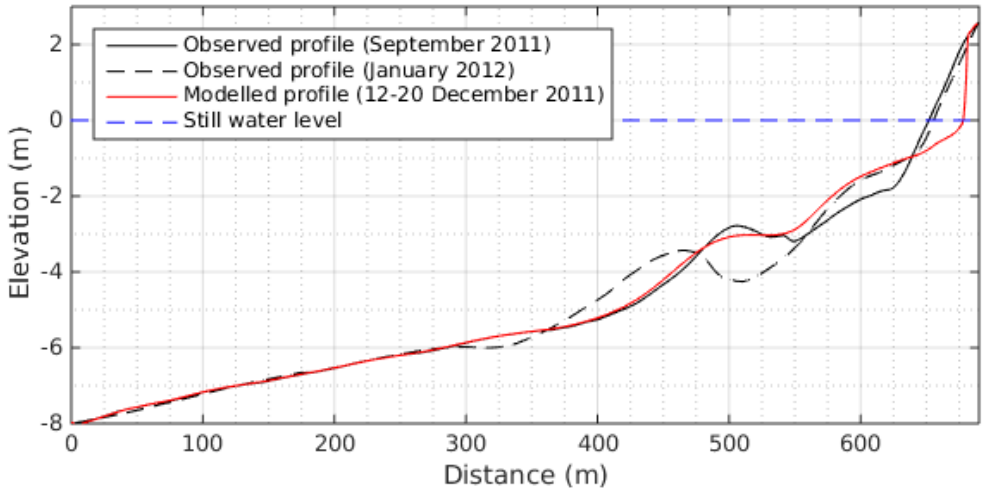

(a)

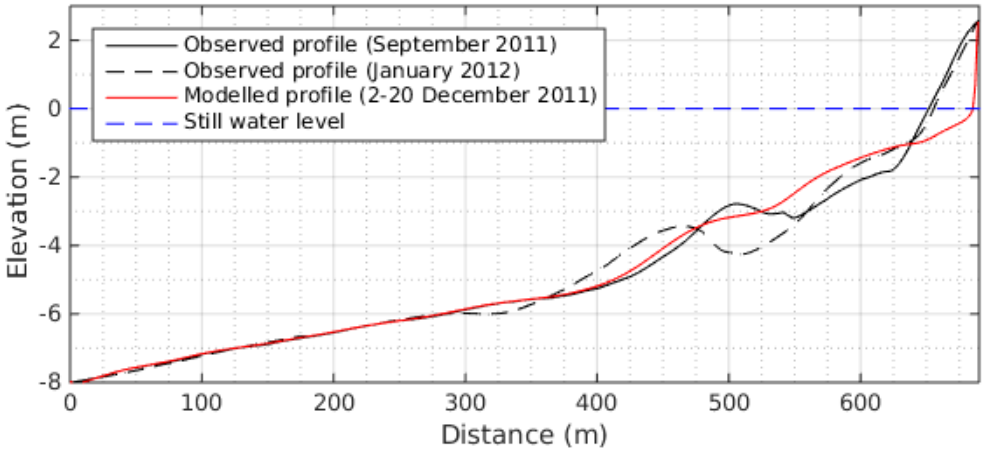

(b)

Figure 5.11: Elevation of the bottom profile observed in September 2011, January 2012 and modelled with XBeach simulating morphodynamic processes for (a) two storms (2-20 December 2011) and (b) one storm (12-20 December 2011).

Table 5.3: The three conditions extrapolated from the available information about the storms of December 2011 at Marina dei Ronchi beach.

Conditions	Description
1	The first storm (4-9 December, see Fig. 5.7) produced a significant erosion of the beach of Marina dei Ronchi. However, no damages to the beach facilities were reported.
2	The second storm produced a significant beach erosion in the area between Poveromo creek and Versilia creek (see Fig. 5.2b), leaving only few meters of the dry beach (see Fig. 5.12a).
3	During the peak of the second storm (15-17 December), the wave setup reached the level of the beach facilities along Marina dei Ronchi beach, causing significant damages in the north part of the beach (see Fig. 5.12b).

(a) South view

(b) Damages of beach infrastructures

Figure 5.12: The north part of Marina dei Ronchi beach on the 21th of December 2011.

excluding/including bottom and shoreline changes is motivated by the interest of evaluating the importance of morphodynamic processes in a nested model supporting Coastal Early Warning System (CEWS), since the current alert system of the Tuscany Region does not include the modelling of nearshore processes.

As indicated in Table 5.4, the decision to hindcast not only the second storm (12-20 Dec 2011) which represents the main storm, but also to consider the previous storm (2-12 Dec 2011), is motivated by the interest of investigating the effect of the first storm (no damages reported) on the main storm (damages and significant beach erosion reported).

Figure 5.13 shows the comparison between the maximum wave setup modelled for Test case 1 and Test case 2 from Table 5.4 that occurred on 2011 December 17, 04:00. In particular, Figure 5.13a shows that the maximum wave setup reaches a high of 1.27m above the still water level (SWL), in case of excluding bottom and shoreline changes. The shoreline regression due to wave setup is 16m. The situation observed in Fig. 5.13a is different from Condition 3 of Tab. 5.3 (i.e. the wave setup reached the the level of the beach facilities during the peak of the storm) since the beach facilities are positioned at the end of the profile ($x = 690m$, $y = 2.5m$).

Figure 5.13b shows that the maximum wave setup reaches a height of 1.29m above the SWL, in case of including bottom and shoreline changes. Even though the values of wave setup for both Test case 1 and 2 are very similar, the shoreline regression of 24m due to wave setup and beach erosion modelled for Test case 2 is higher than the shoreline regression of 16m modelled for Test case 1.

Therefore, the shoreline regression shown for Test case 2 (Fig. 5.13b) is closer to Conditions 3 of Tab. 5.3 than the shoreline regression shown for Test case 1 (Fig. 5.13a). However, the conditions modelled for Test case 2 does not match exactly with Condition 3 of Tab. 5.3, since the shoreline is still 14m far from the beach facilities.

Figure 5.14 shows the comparison between the maximum wave setup modelled for Test case 3 and Test case 4 of Table 5.4, that occurred on 2011 December 17, 07:00. In particular, Figure 5.14a shows that the maximum wave setup reached a height of 1.77m above the SWL, in case of excluding bottom and shoreline changes. The shoreline regression due to wave setup is 22m. In this case, the wave setup is 0.50m higher than the value reported for Test case 1, and 0.48m higher than the value reported for Test case 2. Hence, it is demonstrated that the first storm (4-9 December 2011) has a significant effect on the modelling of the second storm which finally caused much higher beach erosion and damages. However, the shoreline modelled in Test case 3 is positioned at $x = 674m$ (see Fig. 5.14a), which is still 16m far from the position of the beach facilities ($x = 690m$).

The results for Test case 4 are shown in Figure 5.14b. The maximum wave setup reached a height of 2.00m above the SWL. The beach erosion is 25m, and the shoreline regression is 30m. Also in this case, the importance of modelling the first storm is evident. In fact, the values of wave setup, beach erosion and shoreline regression are significantly higher than the values observed for Test case 2 (see Fig. 5.13b).

The situation shown in Figure 5.14b is very similar to the real conditions summarised in Table 5.3. In fact, the wave setup modelled in Test case 4 is 2.00m, close to the level of the beach facilities (about 2.50m). Also the erosion modelled in Test case 4 (i.e. 25m) is similar to

Table 5.4: The four test cases modelled in Subsection 5.2.2. The column "Morphodynamics" means that bottom and shorelines changes are excluded (No), or included (Yes) in the NEMO system.

Test case	Period	Morphodynamics	Description
1	12-20 December 2011	No	Modelling only the main storm
2	12-20 December 2011	Yes	Modelling only the main storm
3	2-20 December 2011	No	Modelling two storms
4	2-20 December 2011	Yes	Modelling two storms

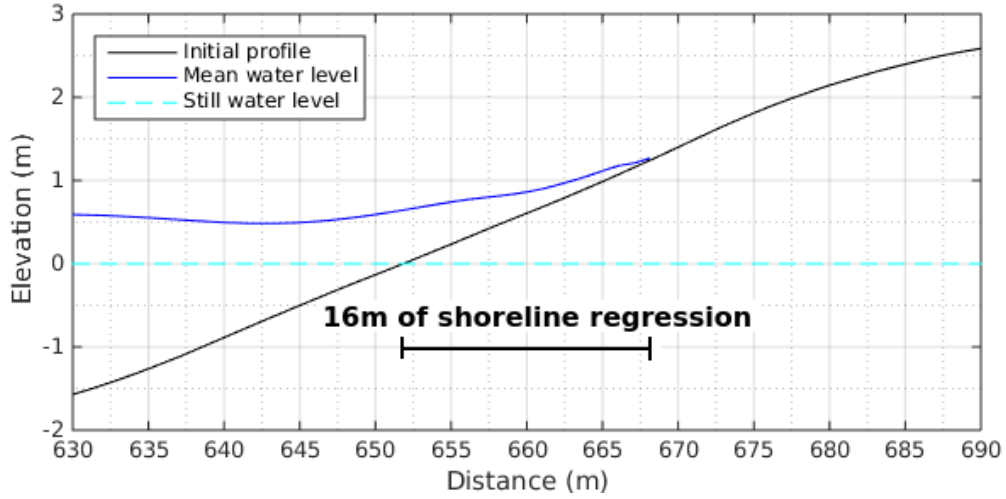

(a) Test case 1

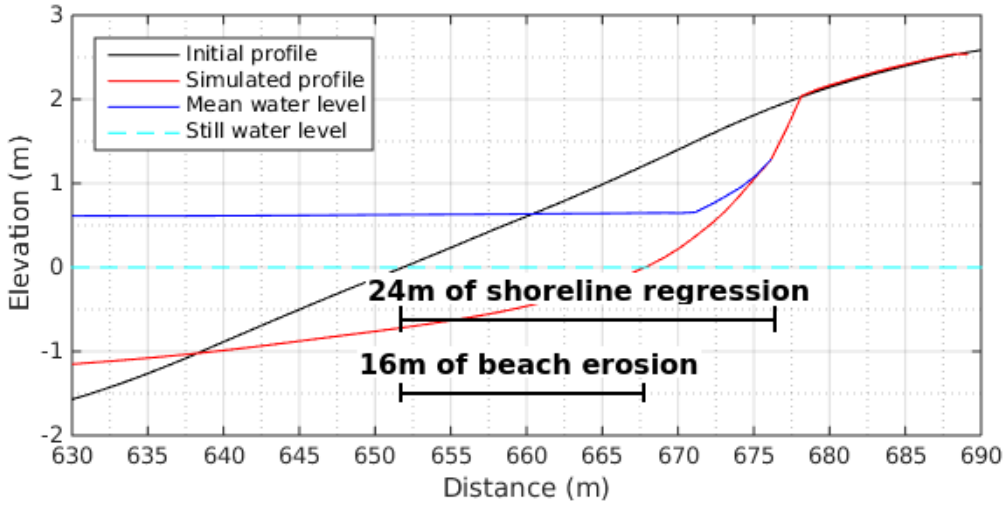

(b) Test case 2

Figure 5.13: The maximum water level modelled 2011 in Marina dei Ronchi beach for (a) Test case 1 (second storm without "morphodynamics changes") and (b) Test case 2 (second storm with "morphodynamics changes") from Table 5.4 (2011 December 17, 04:00).

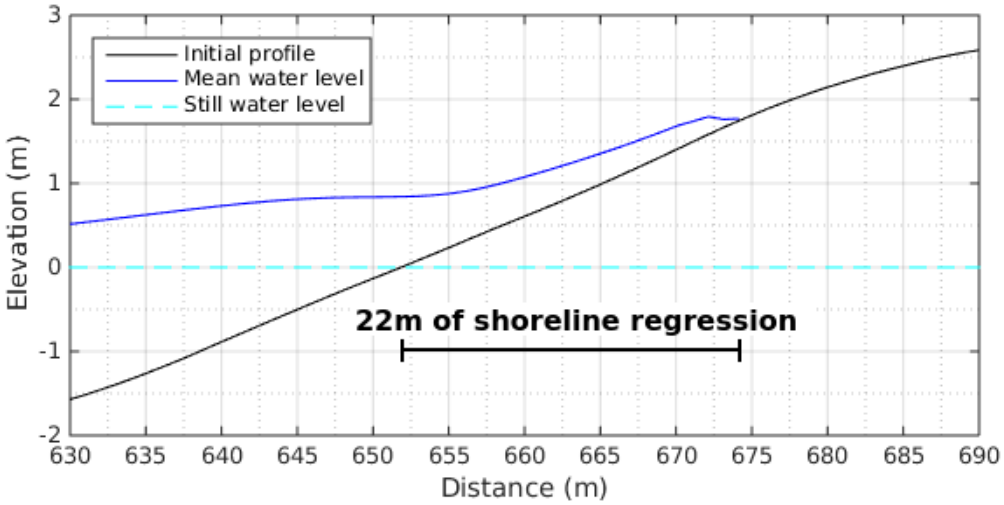

(a) Test case 3

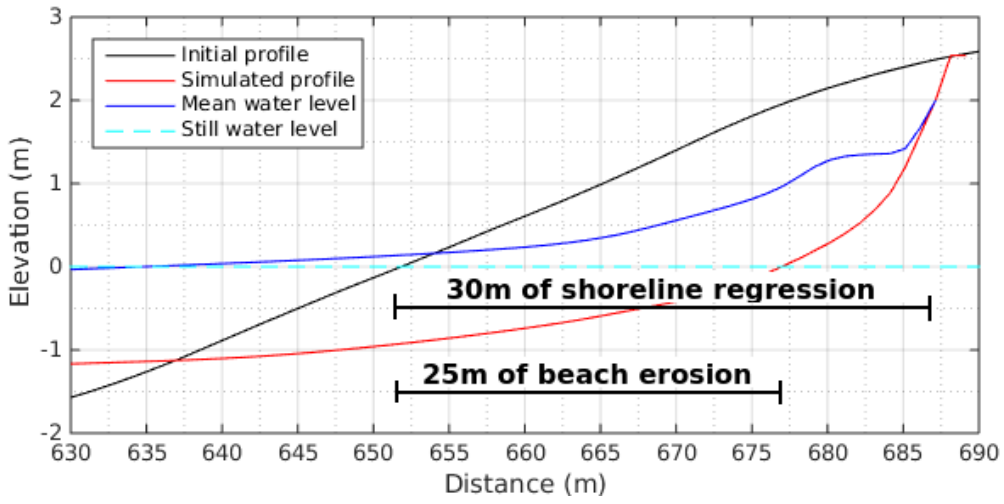

(b) Test case 4

Figure 5.14: The maximum water level modelled 2011 in Marina dei Ronchi beach for (a) Test case 1 (both storms without "morphodynamics changes") and (b) Test case 2 (both storms with "morphodynamics changes") from Table 5.4 (2011 December 17, 04:00).

that observed in southern part of the photograph shown in Fig. 5.12a. In fact, the observed beach extension is about 10-15 meters, and the modelled beach extension is 13 meters.

5.3 Summary and implications

The NEMO system described in Chapter 4 is applied to a real test case. The coast of Marina dei Ronchi (Versilia, North Tuscany) has been selected as test case area. This choice is justified by the touristic and economical importance of the activities developed on the backshore of the Versilia coast. Therefore, a system that takes into account nearshore dynamics could be a support of the Early Warning System already operative in the area.

One of the most severe storm, that actually occurred in this area between the 15th and 17th December 2011 is hindcasted with the NEMO system. This storm was preceded by another significant storm, that actually occurred in the same area between the 4th and the 9th December 2011. The impact of the main storm on the coast of Marina dei Ronchi is modelled by considering (1) the morphodynamic changes associated with the second (main) storm only, and (2) the morphodynamic changes associated with both storms.

The reliability of the NEMO system in deep water is proved by a comparison between the wave conditions observed offshore the Versilia coast (i.e. La Spezia) at a water depth of -100m and the hindcasted wave conditions. Since the buoy located in intermediate water was out of order in December 2011, a direct comparison between results and observations was not possible, but the reliability of the model in intermediate water was extensively demonstrated in Section 3.3.

The application of the system on the nearshore is performed by comparing (1) the modelled cross-shore profile with the profile observed in January 2012, and (2) the modelled wave setup and the shoreline evolution with the information collected on local newspapers, interviews with the owners of beach facilities, and photographs. The initial profile has been extrapolated from a survey of September 2011.

Though significant differences are observed between the modelled and the observed profiles, the NEMO system was able to predict the locations of the zones of erosion and accretion across the shore profile. It is worth to note, that the profile of the dry beach observed in January 2012 is very different from the ones observed immediately after the storm (see Fig. 5.12). This means that a new accretion of the beach occurred between the end of the storm (17 December 2011) and the beach survey (24-25 January 2012).

Hence, a further qualitative comparison is conducted between the modelled wave setup and shoreline recession with the information collected on local newspapers, interviews with the owners of beach facilities, and photographs. For Test case 4 from Table 5.3, in which the bottom and shoreline evolution of both storms was also considered in the modelling, the maximum wave setup and shoreline recession extrapolated from the available sources of information are similar to those hindcasted by the NEMO system.

However, further studies are needed in order to validate the NEMO system in the nearshore. In particular, the exclusion from the model system of the variability of the water level in the large scale model (WWIII) and regional model (SWAN) could lead to uncertainties of the nearshore water level and consequent underestimation of the damages. This might fully explain the damages observed at Marina dei Ronchi on the 15th and 17th December 2011.

Since the qualitative analysis conducted in the nearshore provided promising results, possible future applications to real test cases might be through comparative analyses of the model results with in situ photographs before and after storms. As demonstrated by Elsayed and Oumeraci (2016, 2017) and in the PhD thesis by Elsayed (2016), XBeach also represents an ideal hydro-morphodynamic model to simulate the erosion and breaching of beach/dune system and the subsequent inundation extent, flow depths and velocities, so that the damages can also be easily assessed. Therefore, for future improvements of the system, an extension

of the XBeach domain in the hinterland (i.e. considering the structure damaged) would be useful

1. The comparison of the hindcasted and observed wave parameters for the test case in deep water provided very good results. Therefore, the NEMO system can be definitely used as support for offshore activities, such us offshore industry, renewable offshore energy, sailing, etc.

2. A quantitative analysis cannot be carried out with the available bathymetry data. The qualitative analysis carried out comparing the modelled wave setup and shoreline recession with the available sources of information (e.g. local newspaper, interviews, photographs) reveals a relatively good performance of the NEMO system, that might be suitable to support existing Coastal Early Warning Systems (CEWS). However, for the nearshore area, more suitable field data for a systematic quantitative validation of the NEMO system would be required.

3. Further studies are needed to individuate the time necessary to recover the dry beach after an erosive event. This issue is crucial, since XBeach in the NEMO system is not capable to reproduce beach accretion after the storm. For this purpose, a morphodynamics module (e.g. Delft3D) might be added to the model system.

6

Summary, concluding remarks and outlook

6.1 Summary of key results

The present study focuses on the hindcast and forecast of sea waves dynamics in the nearshore by means of the use of numerical models. The main objective of the present study is to build a model system that support Early Warning System (EWS) for coastal hazard. Providing reliable wave conditions on the coast implies that the wave generation/evolution in deep water and in intermediate water are successfully and correctly modelled. Therefore, all the processes affecting waves from their generation in deep water to their energy dissipation on the coastline have been analysed. Depending on the space and time scale considered, different processes are dominant and thus, different formulations are needed for modelling these processes. To reach the objective of the study, a new model system is implemented by adapting and nesting three among the most appropriate existing models. As illustrated in Figure 6.1, the obtained system of nested models, called NEMO, is able to simulate the dominant processes at regional to local scale, i.e. from deep water to the nearshore. An overview of the methodology in this PhD study was provided in Figure 2.17 and the overall methodology of the applied nesting approach was summarized in Figure 4.2.

Even though the goal of this study was not the research on the improvements/extensions of the existing models, the limitations of each model have been identified and the implications for the present study have been highlighted in Chapter 3. In fact, the focus was rather the nesting of the three selected models that takes into account all the processes affecting waves from deep to shallow water. A list of the main processes modelled by the NEMO system is summarised in Table 6.1.

The model system was built by developing a main task manager programme that includes each model as separate module, with an utility module for executing the nesting operation. Furthermore, the main core of each model, which solves the equations of the underlying physics was not modified. However, future improvements of each single model can be easily integrated in the NeMo system by means of the proper installation of the new model version. This modular approach was described in Figure 4.1.

One of the main efforts in the present research was the calibration of the deep water model (WWIII) and intermediate/shallow model (SWAN) for the typical storms occurring in the Mediterranean Sea, since the wave model system presented in literature were applied in different seas (i.e. North Sea, Atlantic Ocean, Pacific Ocean). In particular, a significant focus was dedicated to the calibration of WWIII, since an erroneous wave field in deep water

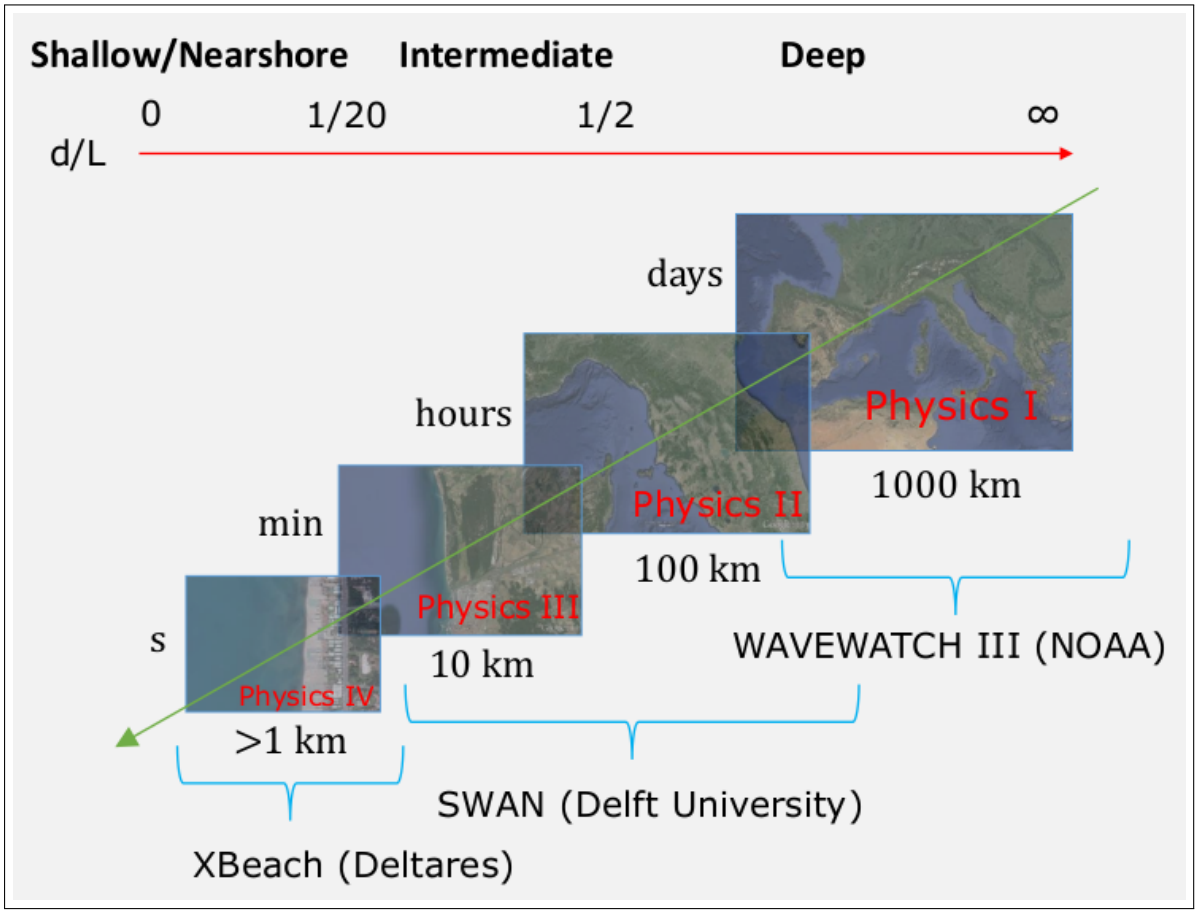

Figure 6.1: Model System NEMO with nested codes WAVEWATCH III, SWAN and XBeach for wave modelling from deep water to the shore.

Table 6.1: Summary of the key processes affecting sea waves at different scales from deep water (DW) to intermediate/shallow water (ISW) and nearshore (NS).

Scale	**Process**
Deep Water (DW)	Generation by wind Whitecapping Nonlinear quadruplet interactions
Intermediate/shallow water (ISW)	Nonlinear triad interactions Wave dissipation due to bottom friction Wave shoaling Wave refraction Wave reflection Wave diffraction Wave breaking
Nearshore (NS)	Radiation stress Wave set-up Circulation (current) Sediment transport Seabed/nearshore morphodynamic changes

may propagate the error through the other modules of the system. The calibration of WWIII was focused on the prediction of significant wave high in storm conditions that generally results in coastal hazard to the shoreline. Only the work of Mentaschi et al. (2015) described a calibration of WWIII in the Mediterranean sea, but focusing on average wave conditions.

The calibration of SWAN was conducted for the area of North Tuscany, (see Section 3.2) where the NEMO system was applied in the test case described in Chapter 5. Wave boundary conditions for SWAN were provided from the large scale model WWIII in terms of files of parameterized wave spectra. In Section 3.2, it was demonstrated that when WWIII hindcasts reliable wave height in deep water, SWAN also hindcasts reliable wave height in intermediate water. This implies that (a) the wave boundary conditions are correctly transferred by spectral files, and (b) the SWAN model properly simulates wave dynamics in intermediate water.

The other important goal of the present study is the application of the NEMO system to a real test case, in order to prove the reliability of the developed system. Hence, one of the most intense and devastating storms in the North Tuscany of the last 20 years, that actually occurred between the 15^{th} and the 17^{th} December 2011, was modelled.

The comparison of modelled and observed wave parameters in deep water has highlighted the good performance of the model. For the test case storm, a wave analysis in intermediate water was not possible due to the lack of wave observations due to a breakdowns of the buoy. However, the reliability of the NEMO system in intermediate water is extensively demonstrated for several storm in Section 3.2.

Furthermore, the reliability of the NEMO system was evaluated in the nearshore. The maximum wave set up and shoreline regression extrapolated from the available sources (i.e. local newspapers, interviews to the owners of beach facilities, and photographs) were compared with those modelled across a typical beach profile of the coast of Marina dei Rochi (Versilia).

This qualitative comparison showed that the system has the potential to predict the wave setup and the shoreline regression associated to the extreme event and therefore, the support of the system to Early Warning System could be possible.

6.2 Implications for practice and further research

Wave modelling in general, and multi-scale modelling in particular, is a wide topic, treating for example, the theoretical formulations of wave processes at different scale, the solutions for practical applications, the solutions for numerical problems, and the statistical analysis of the wave field. In the present study, a complete review of the current knowledge on water wave mechanics and its modelling from deep to shallow water was carried out, in order to building a model system able to simulate the wave evolution from the open ocean to the nearshore.

The results of the present study may be used in practice for:

- **Forecasting of hazardous sea states**: deep water wave models are usually developed and calibrated for simulating waves in a specific sea or ocean. The calibration of the NEMO system for the Mediterranean Sea (WWIII) and North Tuscany (SWAN) provides reliable forecast supporting economical activities such as shipping, fisheries and offshore industries.

- **Wave climate database**: a wave climate database has been produced for the whole Mediterranean Sea for the years 2000-2015. The wave climate at given specific location is crucial for coastal & offshore engineering since statistical wave parameters are still the basis for projects related to ports, jetties, dykes, wind and wave energy harvesting, etc.

- **Coastal hazard**: the NEMO system can be used to predict hazardous sea states at the shoreline as a supporting tool for the decision making in the context of coastal early-warning.

Further improvements of the system may be related to the following issues:

- **Limitations of the existing models**. The results of WWIII are highly dependent on the formulation of wind input and whitecapping processes. In particular, using the Ardhuin et al. (2010) formulation, it was shown that assuming the parameter $\beta_{\max}$ as a constant may represent a serious limitation. The formulation of this parameter as a function of the wind velocity might result in an improvement of the results.

  As expected, XBeach is not able to simulate the process of beach accretion as it was primarily developed for the erosion of beach/dune systems under severe storm surges. Therefore, this last module of the NEMO system needs to be activated only over a certain threshold of wave conditions. The incorporation of a more appropriate model to simulate beach behaviour during moderate (accretional) wave conditions into the NEMO system is easily possible.

- **Further validation** may be conducted for intermediate and shallow water waves; for this purpose, proper field data would be needed. This step is necessary in order to individuate the threshold for activating the XBeach module.

  Moreover, it is also important to understand and quantify beach accretion between successive storms. Indeed, the importance of modelling not only the main storm event, but also the previous storm event was clearly in Section 5.2.

- **Inclusion of more physics processes in the system**. Tide is not included in the model system. For example, an astronomical tidal range of 35cm plus an atmospheric component of +20cm and -18cm is observed in the test case area. Local wind set-up is also not included in the system. For example a value of 67cm for a 50-years return period was computed in the test case area (Anfuso et al., 2011).

- **2DH application of the XBeach module**. With the availability of an appropriate computing power an investigation on the applicability of XBeach in 2DH mode could be possible.

- **Improvement of forcing wind field**. The crucial importance of the forcing wind field has been demonstrated in Chapter 3. Improving the spatial resolution of the wind database could lead to an improvement of the results, especially for the case of short-fetch storms.

Appendix A

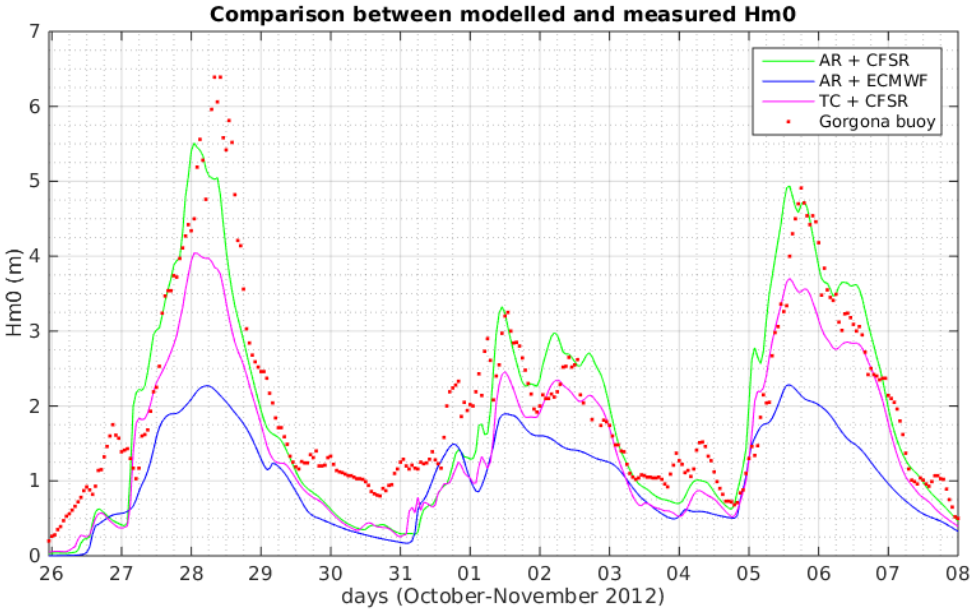

(a) *Comparison for the storm of October-November 2012 at Gorgona.*

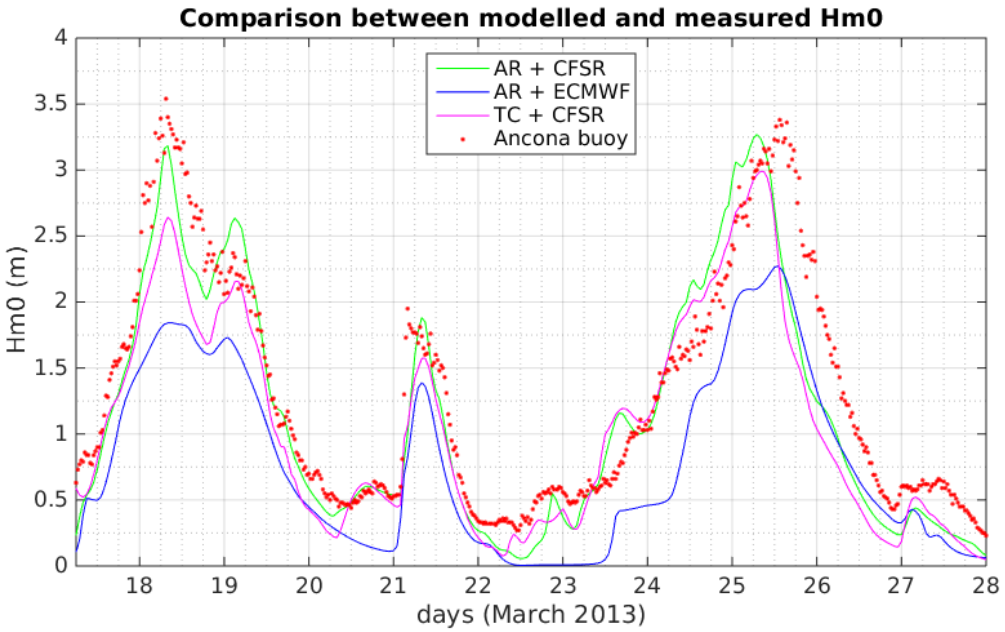

(b) *Comparison for the storm of March 2013 at Ancona.*

Figure 2: Comparison of H_{m0} time series obtained with the three model setups and measured at (a) Gorgona, (b) Ancona.

Table 2: Summary of the statistical error indicators obtained from the comparison between hindcasted and buoy data for H_{m_0} at Gorgona spot.

Storm	**Setup**	**bias (m)**	**MSE (m)**	**NBI**	**NRMSE**	**SI**	σ_d **(m)**
Dec 2008	AR + ECMWF	-0.93	1.34	-0.803	0.447	0.331	0.69
	AR + CFSR	-0.43	0.31	-0.257	0.215	0.170	0.36
	TC + CFSR	-0.75	0.83	-0.558	0.352	0.249	0.52
Oct-Nov 2012	AR + ECMWF	-0.97	1.52	-0.897	0.514	0.377	0.77
	AR + CFSR	-0.16	0.38	-0.084	0.257	0.293	0.60
	TC + CFSR	-0.52	0.53	-0.344	0.304	0.250	0.51
	AR*+ CFSR	0.06	0.45	0.027	0.279	0.328	0.67
Dec 2012	AR + ECMWF	-0.73	0.73	-0.690	0.435	0.245	0.44
	AR + CFSR	-0.15	0.25	-0.092	0.252	0.264	0.47
	TC + CFSR	-0.47	0.37	-0.355	0.310	0.217	0.39
	AR*+ CFSR	0.04	0.26	0.020	0.260	0.285	0.51
Mar 2013	AR + ECMWF	-0.82	1.10	-1.036	0.523	0.402	0.65
	AR + CFSR	-0.35	0.31	-0.278	0.279	0.269	0.44
	TC + CFSR	-0.60	0.55	-0.588	0.369	0.268	0.43
	AR*+ CFSR	-0.18	0.28	-0.123	0.263	0.312	0.50

Table 3: Summary of the statistical error indicators obtained from the comparison between hindcasted and buoy data for H_{m_0} at Ancona spot.

Storm	**Setup**	**bias (m)**	**MSE (m)**	**NBI**	**NRMSE**	**SI**	σ_d **(m)**
Dec 2008	AR + ECMWF	-0.58	0.42	-0.078	0.414	0.222	0.29
	AR + CFSR	-0.29	0.19	-0.279	0.276	0.244	0.32
	TC + CFSR	-0.43	0.29	-0.477	0.344	0.249	0.33
Oct-Nov 2012	AR + ECMWF	-0.81	0.84	-1.065	0.493	0.271	0.43
	AR + CFSR	-0.58	0.46	-0.578	0.364	0.226	0.36
	TC + CFSR	-0.67	0.61	-0.742	0.418	0.251	0.40
	AR*+ CFSR	-0.20	0.16	-0.182	0.255	0.262	0.34
Dec 2012	AR + ECMWF	-0.54	0.38	-0.679	0.382	0.229	0.30
	AR + CFSR	-0.14	0.13	-0.118	0.226	0.254	0.34
	TC + CFSR	-0.26	0.20	-0.242	0.279	0.279	0.37
	AR*+ CFSR	-0.06	0.13	-0.045	0.225	0.271	0.36

Table 4: Summary of the statistical indicators obtained from the comparison between hindcasted and buoy data for H_{m_0} at 8 RON spot with a high-pass filter of 1m for measured H_{m_0}.

Buoy	**Observations**	**bias (m)**	**NBI**	**RMSE (m)**	**NRMSE**	**HH**
Alghero	8193	-0.07	-0.033	0.41	0.162	0.165
Ancona	2404	-0.19	-0.118	0.46	0.260	0.275
Civitavecchia	5127	-0.00	-0.009	0.17	0.244	0.245
Crotone	7501	-0.19	-0.116	0.42	0.236	0.259
La Spezia	8928	-0.12	-0.074	0.38	0.210	0.218
Monopoli	5908	-0.06	-0.222	0.21	0.315	0.245
Palermo	8148	-0.15	-0.085	0.39	0.203	0.212
Ponza	10287	-0.22	-0.125	0.44	0.234	0.249

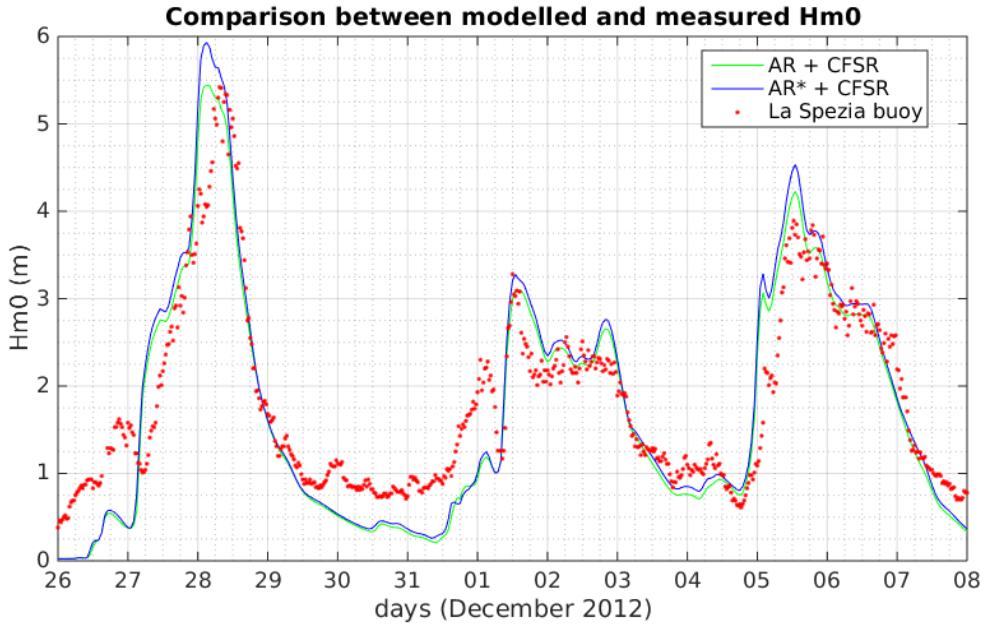

(a) *Comparison for the storm of October-November 2012 at La Spezia.*

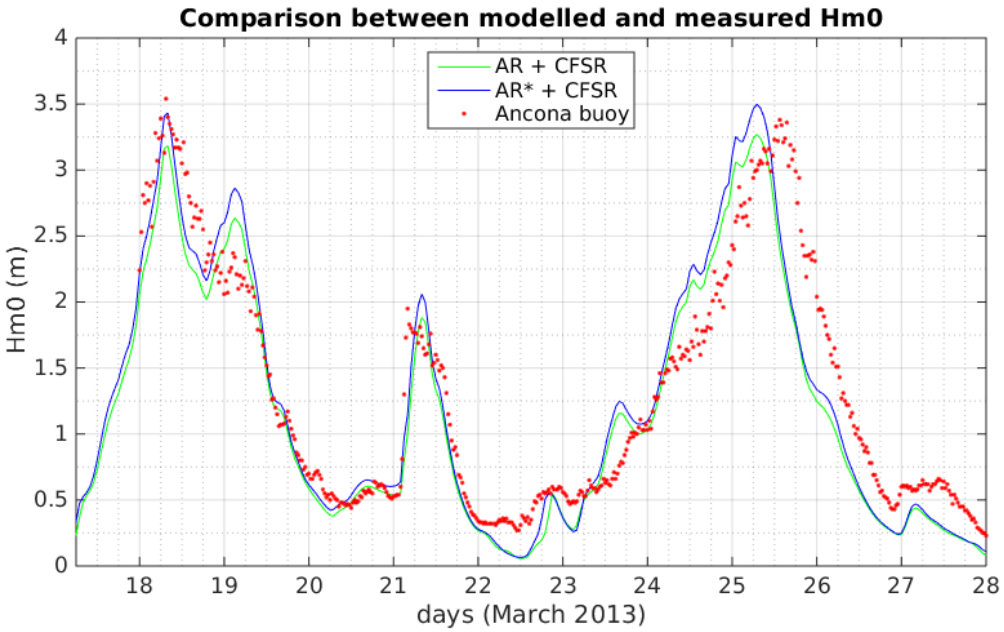

(b) *Comparison for the storm of March 2013 at Ancona.*

Figure 3: Comparison of H_{m0} time series obtained with the three model setups and measured at (a) La Spezia, (b) Ancona.

References

Abanades, J., D. Greaves, and G. Iglesias (2014a). "Coastal defence through wave farms". In: *Coastal Engineering* 91, pp. 299–307.

— (2014b). "Wave farm impact on the beach profile: A case study". In: *Coastal Engineering* 86, pp. 36–44.

Aminti, P., C. Cammelli, L. Cappietti, N.L. Jackson, K.F. Nordstrom, and E. Pranzini (2004). "Evaluation of Beach Response to Submerged Groin Construction at Marina di Ronchi, Italy, Using Field Data and a Numerical Simulation Model". In: *Journal of Coastal Research* (33), pp. 99–120.

Andrews, D.G. and M.E. McIntyre (1978). "An exact theory of nonlinear waves on Lagrangian-mean flow". In: *Journal of Fluid Mechanics* 89, pp. 609–646.

Anfuso, G., E. Pranzini, and G. Vitale (2011). "An integrated approach to coastal erosion problems in northern Tuscany (Italy): Littoral morphological evolution and cell distribution". In: *Geomorphology* 129 (3), pp. 204–214.

Arcilla, A. S., J. A. Roelvink, B. A. O'Connor, A. Reniers, and J. A. Jimènez (1994). "The Delta Flume '93 experiment". In: *Coastal Dynamics 1994*, pp. 488–502.

Ardhuin, F., W.C. O'Reilly, T.H.C. Herbers, and P.F. Jessen (2003). "Swell Transformation across the Continental Shelf. Part I: Attenuation and Directional Broadening". In: *Journal of Physical Oceanography* 33 (9), pp. 1921–1939.

Ardhuin, F., E. Rogers, A.V. Babanin, J.-F. Filipot, R. Magne, A. Roland, A. van der Westhuysen, P. Queffeulou, J.-M. Lefevre, L. Aouf, and F. Collard (2010). "Semiempirical Dissipation Source Functions for Ocean Waves. Part I: Definition, Calibration, and Validation". In: *Journal of Physical Oceanography* 40 (9), pp. 1917–1941.

Autorità Portuale di Marina di Carrara (2005). *Sistema di monitoraggio meteomarino del porto di Marina di Carrara*. Tech. rep. Marina di Carrara, Italy.

Baart, F., T. Van Der Kaaij, M. Van Ormondt, A. Van Dongeren, M. Van Koningsveld, and J.A. Roelvink (2009). "Real-time forecasting of morphological storm impacts: A case study in the Netherlands". In: *Journal of Coastal Research* 2009 (SPEC. ISSUE 56), pp. 1617–1621.

Baart, F., M. van Ormondt, J.S.M. van Thiel de Vries, and M. van Koningsveld (2016). "Morphological impact of a storm can be predicted three days ahead". In: *Computers and Geosciences* 90, pp. 17–23.

Baldock, T.E., P. Holmes, S. Bunker, and P. Van Weert (1998). "Cross-shore hydrodynamics within an unsaturated surf zone". In: *Coastal Engineering* 34 (3), pp. 173–196.

Banner, M.L., J.R. Gemmrich, and D.M. Farmer (2002). "Multiscale Measurements of Ocean Wave Breaking Probability". In: *Journal of Physical Oceanography* 32 (12), pp. 3364–3375.

Barnard, P.L., M. van Ormondt, L.H. Erikson, J. Eshleman, C. Hapke, P. Ruggiero, P.N. Adams, and A.C. Foxgrover (2014). "Development of the Coastal Storm Modeling System (CoSMoS) for predicting the impact of storms on high-energy, active-margin coasts". In: *Natural Hazards* 74 (2), pp. 1095–1125.

Battjes, J.A. and J.P.F.M. Janssen (1978). "Energy loss and set-up due to breaking of random waves". In: *Proceeding of the 16th International Conference on Coastal Engineering*. Hamburg, pp. 569–587.

Becq-Girard, F., P. Forget, and M. Benoit (1999). "Non-linear propagation of unidirectional wave fields over varying topography". In: *Coastal Engineering* 38 (2), pp. 91–113.

Berkhoff, J.C.W. (1972). "Computation of Combined Refraction - Diffraction". In: *Proceedings of the 13th International Conference on Coastal Engineering*. Vancouver, pp. 471–490.

Bertin, X., N. Bruneau, J.-F. Breilh, A.B. Fortunato, and M. Karpytchev (2012). "Importance of wave age and resonance in storm surges: The case Xynthia, Bay of Biscay". In: *Ocean Modelling* 42, pp. 16–30.

Bidlot, J.-R., S. Abdalla, and P.A.E.M. Janssen (2005). *A revised formulation for ocean wave dissipation in CY25R1*. Tech. rep. Research Dept. Tech. Rep. Memo. R60.9/JB/0516, ECMWF, Reading, UK.

Birkemeier, W.A., C. Donoghue, C.E. Long, K.K. Hathaway, and C.F. Baron (1997). *1990 DELILAH Nearshore Experiment: Summary Report*. Tech. rep. September, pp. 1–217.

Blake, E.S., T.B. Kimberlain, R.J. Berg, J.P. Cangialosi, and J.L. Beven II (2013). *Tropical Cyclone Report Hurricane Sandy (AL182012) 22 – 29 October 2012*. Tech. rep. National Hurricane Center (NHC), pp. 1–10.

Boers, M. (1996). *Simulation of a Surf Zone with a Barred Beach; Part 1: Wave Heights and Wave Breaking. Report No. 96-5*. Tech. rep. Delft University of Technology, Department of Civil Engineering.

Bolle, A., P. Mercelis, D. Roelvink, P. Haerens, and K. Trouw (2011). "Application and Validation of Xbeach for Three Different Field Sites". In: *Coastal Engineering Proceedings* 1 (32).

Booij, N. and L.H. Holthuijsen (1987). "Propagation of ocean waves in discrete spectral wave models". In: *Journal of Computational Physics* 68 (2), pp. 307–326.

Bouws, E. and G.J. Komen (1983). *On the Balance Between Growth and Dissipation in an Extreme Depth-Limited Wind-Sea in the Southern North Sea*.

Breivik, Ø., Y. Gusdal, B.R. Furevik, O.J. Aarnes, and M. Reistad (2009). "Nearshorewave forecasting and hindcasting by dynamical and statistical downscaling". In: *Journal of Marine Systems* 78 (SUPPL. 1), S235–S243.

Breugem, W. A. and L. H. Holthuijsen (2007). "Generalized Shallow Water Wave Growth from Lake George". en. In: *Journal of Waterway, Port, Coastal, and Ocean Engineering* 133 (June), pp. 173–182.

Brocchini, M. and N. Dodd (2008). "Nonlinear Shallow Water Equation Modelling for Coastal Engineering". In: *Journal of Waterway, Port, Coastal, and Ocean Engineering* 134 (April), pp. 104–120.

Bryan, K. (1969). "A Numerical Method for the Study of the Circulation of the World Ocean". In: *Journal of Computational Physysics* 4 (3), pp. 347–376.

Bryan, K. and M.D. Cox (1967). "A numerical investigation of the oceanic general circulation". In: *Tellus* 19 (1), pp. 54–80.

Bugajny, N., K. Furmańczyk, J. Dudzińska-Nowak, and B. Paplińska-Swerpel (2013). "Modelling morphological changes of beach and dune induced by storm on the Southern Baltic coast using XBeach (case study: Dziwnow Spit)". In: *Journal of Coastal Research* 65 (sp1), pp. 672–677.

Casaioli, M., F. Catini, R. Inghilesi, P. Lanucara, P. Malguzzi, S. Mariani, and A. Orasi (2014). "An operational forecasting system for the meteorological and marine conditions in Mediterranean regional and coastal areas". In: *Advances in Science and Research* 11, pp. 11–23.

Cavaleri, L., J.H.G.M. Alves, F. Ardhuin, A.V. Babanin, M.L. Banner, K. Belibassakis, M. Benoit, M. Donelan, J. Groeneweg, T.H.C. Herbers, P.A. Hwang, P.A.E.M. Janssen, T.T. Janssen, I.V. Lavrenov, R. Magne, J. Monbaliu, M. Onorato, V.G. Polnikov, D.T. Resio, W.E. Rogers, A. Sheremet, J. McKee Smith, H.L. Tolman, G.Ph. van Vledder, J. Wolf, and I.R. Young (2007). "Wave modelling - The state of the art". In: *Progress in Oceanography* 75 (4), pp. 603–674.

Cavaleri, L. and P.M. Rizzoli (1981). "Wind wave prediction in shallow water: Theory and applications". In: *Journal of Geophysical Research* 86 (C11), pp. 10961–10973.

Chalikov, D.V. and M.Yu. Belevich (1993). "One-dimensional theory of the wave boundary layer". In: *Boundary-Layer Meteorology* 63 (1-2), pp. 65–96.

Chalikov, D.V. and V.K. Makin (1991). "Models of the wave boundary layer". In: *Boundary-Layer Meteorology* 56 (1-2), pp. 83–99.

Chawla, A., D. Cao, V. Gerald, T. Spindler, H.L. Tolman, M. Modeling, and A. Branch (2007). "Operational Implementation of a Multi-grid Wave Forecasting System". In: *Proceeding of the 10th International Workshop on Wave Hindcasting and Forecasting & Coastal Hazards Symposium*. Oahu, Hawaii.

Chawla, A. and H.L. Tolman (2007). *Automated grid generation for WAVEWATCH III*. Tech. rep. MMAB - NOAA.

Chen, Q. (2006). "Fully Nonlinear Boussinesq-Type Equations for Waves and Currents over Porous Beds". In: *Journal of Engineering Mechanics* 132, pp. 220–230.

Cheung, K.F., A.C. Phadke, Y. Wei, R. Rojas, Y.J.-M. Douyere, C.D. Martino, S.H. Houston, P.L.-F. Liu, P.J. Lynett, N. Dodd, S. Liao, and E. Nakazaki (2003). "Modeling of storm-induced coastal flooding for emergency management". In: *Ocean Engineering* 30 (11), pp. 1353–1386.

Chini, N., P. Stansby, J. Leake, J. Wolf, J. Roberts-Jones, and J. Lowe (2010). "The impact of sea level rise and climate change on inshore wave climate: A case study for East Anglia (UK)". In: *Coastal Engineering* 57 (11-12), pp. 973–984.

Ciavola, P., O. Ferreira, P. Haerens, M. Van Koningsveld, and C. Armaroli (2011a). "Storm impacts along European coastlines. Part 2: lessons learned from the MICORE project". In: *Environmental Science & Policy* 14 (7), pp. 924–933.

Ciavola, P., O. Ferreira, P. Haerens, M. Van Koningsveld, C. Armaroli, and Q. Lequeux (2011b). "Storm impacts along European coastlines. Part 1: The joint effort of the MICORE and ConHaz Projects". In: *Environmental Science & Policy* 14 (7), pp. 912–923.

Collins, J.I. (1972). "Prediction of shallow-water spectra". In: *Journal of Geophysical Research* 77 (15), pp. 2693–2707.

Dalrymple, R.A. and P.L.-F. Liu (1978). "Waves over Soft Muds: A Two-Layer Fluid Model". In: *Journal of Physical Oceanography* 8 (6), pp. 1121–1131.

Daly, C., D. Roelvink, A.R. van Dongeren, and R.T. McCall (2010). "Short wave breaking effects on low frequency waves". In: *Proceeding of 30th International Conference on Coastal Engineering*. San Diego, pp. 1–13.

Davis, R. W. and E. F. Moore (1982). "A numerical study of vortex shedding from rectangles". In: *Journal of Fluid Mechanics* 116 (3), p. 475.

De Vet, P.L.M. (2014). "Modelling sediment transport and morphology during overwash and breaching events (M.Sc. Thesis)". PhD thesis. Delft University of Technology and National University of Singapore.

De Waal, J.P. (2001). "Wave growth limit in shallow water". In: *Ocean Wave Measurement and Analysis*. ASCE, pp. 560–569.

Dean, R.G. (1973). *Heuristic models of sand transport in the surf zone*.

Debreu, L., P. Marchesiello, P. Penven, and G. Cambon (2012). "Two-way nesting in split-explicit ocean models: Algorithms, implementation and validation". In: *Ocean Modelling* 49-50, pp. 1–21.

Dee, D. P., S. M. Uppala, A. J. Simmons, P. Berrisford, P. Poli, S. Kobayashi, U. Andrae, M. A. Balmaseda, G. Balsamo, P. Bauer, P. Bechtold, A. C M Beljaars, L. van de Berg, J. Bidlot, N. Bormann, C. Delsol, R. Dragani, M. Fuentes, A. J. Geer, L. Haimberger, S. B. Healy, H. Hersbach, E. V. Hólm, L. Isaksen, P. Kållberg, M. Köhler, M. Matricardi, A. P. Mcnally, B. M. Monge-Sanz, J. J. Morcrette, B. K. Park, C. Peubey, P. de Rosnay, C. Tavolato, J. N. Thépaut, and F. Vitart (2011). "The ERA-Interim reanalysis: Config-

uration and performance of the data assimilation system". In: *Quarterly Journal of the Royal Meteorological Society* 137 (656), pp. 553–597.

D'Eliso, C., L. Cappietti, and E. Pranzini (2006). "Field monitoring of a submerged groin system". In: *IAHR - 2nd international short course, workshop on coastal processes and port engineering*. Ed. by G.R. Tomasicchio and P. Veltri. Cosenza - Italia, pp. 189–200.

Deltares (2014). *Delft3D-WAVE. User manual, version 3.05.33643*.

— (2016). *XBeach skillbead report, revision 4917*. Tech. rep. Deltares.

Donelan, M.A. and Y. Yuan (1994). "Wave dissipation by surface processes". In: *Dynamics and Modelling Ocean Waves*. Ed. by G .J. Komen, L. Cavaleri, M.A. Donelan, K. Hasselmann, S. Hasselmann, and P.A.E.M. Janssen. Cambridge University Press, pp. 143–155.

EDF (2011). *TOMAWAC: Software for sea state modelling on unstructured grids over oceans and coastal seas - Release 6.1*. Tech. rep.

Eldeberky, L. (1996). "Nonlinear transformation of wave spectra in the nearshore zone". PhD thesis. Communication on Hydraulics and Geothecnical Engineering, Delft University of Tecnology, Faculty of Civil Engineering, Report No. 96-4.

Elsayed, S.M. (2016). "Breaching of Coastal Barriers under Extreme Storm Surges and Implications for Groundwater Contamination". PhD thesis. Technische Universitat Braunschweig, Germany.

Elsayed, S.M. and H. Oumeraci (2015). *Modelling Strategies with X-Beach (X-Beach Manual). Internal Report Nr. 1058*. Tech. rep. TU Braunschweig, LWI, Department of Hydromechanics and Coastal Engineering.

— (2016). "Combined Modelling of Coastal Barrier Breaching and Induced Flood Propagation Using XBeach". In: *Hydrology* 3 (4), p. 32.

— (2017). "Effect of beach slope and grain-stabilization on coastal sediment transport: An attempt to overcome the erosion overestimation by XBeach". In: *Coastal Engineering* 121, pp. 179–196.

Feng, H. and Y. Yeli (1992). "Theoretical study of breaking wave spectrum and its application". In: *Breaking Waves*. Ed. by M.L. Banner and R.H.J. Grimshaw. International Union of Theoretical and Applied Mechanics. Springer Berlin Heidelberg, pp. 277–282.

Ferziger, J.H. and M. Perić (2002). *Computational methods for fluid dynamics*. Springer-Verlag, Berlin.

Fredsøe, J. and R. Deigaard (1992). *Mechanics of coastal sediment transport*. Ed. by Philip L.-F. Liu. World Scientific.

Gaeta, M.G., A.G. Samaras, I. Federico, R. Archetti, F. Maicu, and G. Lorenzetti (2016). "A coupled wave-3-D hydrodynamics model of the Taranto Sea (Italy): A multiple-nesting approach". In: *Natural Hazards and Earth System Sciences* 16 (9), pp. 2071–2083.

Galappatti, G. and C.B. Vreugdenhil (1985). "A depth-integrated model for suspended sediment transport". In: *Journal of Hydraulic Research* 23 (4), pp. 359–377.

Gelci, R., H. Cazalé, and J. Vassal (1956). "Utilization des diagrammes de propagation à la prévision énergétique de la houle". In: *Bulletin d'information du Comité d'Océanographie et d'Etude des Côtes* 8, pp. 170–187.

— (1957). "Prévision de la houle. La méthode des densités spectroangulaires". In: *Bulletin d'information du Comité d'Océanographie et d'Etude des Côtes* 9, pp. 416–435.

Goda, Y. (2000). *Random Seas and Design of Marine Structures, Advanced Series on Ocean Engineering, vol. 15*. Singapore, World Scientific.

Gomez-Gesteira, M., A.J.C. Crespo, B.D. Rogers, R.A. Dalrymple, J.M. Dominguez, and A. Barreiro (2012a). "SPHysics – development of a free-surface fluid solver – Part 2: Efficiency and test cases". In: *Computers & Geosciences* 48, pp. 300–307.

Gomez-Gesteira, M., B.D. Rogers, A.J.C. Crespo, R.A. Dalrymple, M. Narayanaswamy, and J.M. Dominguez (2012b). "SPHysics – development of a free-surface fluid solver – Part 1: Theory and formulations". In: *Computers & Geosciences* 48, pp. 289–299.

Gomez-Gesteira, M., B.D. Rogers, R.A. Dalrymple, A.J.C. Crespo, and M. Narayanaswamy (2010). *User Guide for the SPHysics code.*

Gonçalves, M., E. Rusu, and C.G. Soares (2012). "Evaluation of the wave models SWAN and STWAVE in shallow water using nested schemes". In: *Maritime Engineering and Technology*, pp. 481–485.

Grant, William D. and Ole Secher Madsen (1979). "Combined wave and current interaction with a rough bottom". In: *Journal of Geophysical Research: Oceans* 84 (C4), pp. 1797–1808.

Guedes Soares, C., L. Rusu, M. Bernardino, and P. Pilar (2011). "An operational wave forecasting system for the Portuguese continental coastal area". In: *Journal of Operational Oceanography* 4 (2), pp. 1–11.

Hallermeier, R.J. (1980). "A profile zonation for seasonal sand beaches from wave climate". In: *Coastal Engineering* 4, pp. 253–277.

Hashimoto, N. and K. Kawaguchi (2001). "Extension and Modification of Discrete Interaction Approximation (DIA) for Computing Nonlinear Energy Transfer of Gravity Wave Spectra". In: *Ocean Wave Measurement and Analysis*, pp. 530–539.

Hasselmann, K. (1962). "On the non-linear energy transfer in a gravity-wave spectrum Part 1. General theory". In: *Journal of Fluid Mechanics* 12 (4), pp. 481–500.

— (1963a). "On the non-linear energy transfer in a gravity wave spectrum Part 2. Conservation theorems; wave-particle analogy; irrevesibility". In: *Journal of Fluid Mechanics* 15 (2), pp. 273–281.

— (1963b). "On the non-linear energy transfer in a gravity-wave spectrum. Part 3. Evaluation of the energy flux and swell-sea interaction for a Neumann spectrum". In: *Journal of Fluid Mechanics* 15 (3), pp. 385–398.

— (1974). "On the spectral dissipation of ocean waves due to white capping". In: *Boundary-Layer Meteorology* 6 (1-2), pp. 107–127.

Hasselmann, K., T.P. Barnett, E. Bouws, H. Carlson, D.E. Cartwright, K. Enke, J.A. Ewing, H. Gienapp, D.E. Hasselmann, P. Kruseman, A. Meerburg, P. Müller, D.J. Olbers, K. Richter, W. Sell, and H. Walden (1973). "Measurement of Wind-Wave Growth and Swell Decay during the Joint North Sea Wave Project (JONSWAP)". In: *Deutsch. Hydrog. Inst.* A8 (12).

Hasselmann, K. and J.I. Collins (1968). "Spectral dissipation of finite depth gravity waves due to turbulent bottom friction". In: *Journal of Marine Research* 26, pp. 1–12.

Hasselmann, S., K. Hasselmann, J.H. Allender, and T.P. Barnett (1985). "Computation and Parameterization of the Nonlinear Energy Transfer in a Gravity-Wave Spectrum. Part II: Parameterization of the Nonlinear Energy Transfer for application in Wave Models". In: *Journal of Physical Oceanography* 15 (11), pp. 1378–1391.

Hersbach, H. and P.A.E.M. Janssen (1999). "Improvement of the short-fetch behavior in the Wave Ocean Model (WAM)". In: *Journal of Atmospheric and Oceanic Technology* 16 (7), pp. 884–892.

Holthuijsen, L.H. (2007). *Waves in Oceanic and Coastal Waters.* Cambridge University Press.

Holthuijsen, L.H., N. Booij, and T.H.C. Herbers (1989). "A prediction model for stationary, short-crested waves in shallow water with ambient currents". In: *Coastal Engineering* 13 (1), pp. 23–54.

Il Tirreno (2011). *News section of Massa, 16 December.*

Janssen, P.A.E.M. (1991). "Quasi-linear Theory of Wind-Wave Generation Applied to Wave Forecasting". In: *Journal of Physical Oceanography* 21 (11), pp. 1631–1642.

Janssen, T.T. and J.A. Battjes (2007). "A note on wave energy dissipation over steep beaches". In: *Coastal Engineering* 54 (9), pp. 711–716.

Kirby, J.T. (2003). "Boussinesq Models and Applications to Nearshore Propagation, Surf Zone Processes and Wave-Induced Currents". In: *Advances in Coastal Modeling.* Ed. by C. Lakhan, pp. 1–41.

Kirby, J.T. and R.A. Dalrymple (1983). "A parabolic equation for the combined refraction-diffraction of Stokes waves by mildy varying topography". In: *J. Fluid Mech.* 136, pp. 453–466.

— (1994). *REF/DIF 1 - Version 2.5. Documentation and User's Manual. CACR Report No. 94-22.* Tech. rep.

Knabb, R.D., J.R. Rhome, and D.P. Brown (2005). *Tropical Cyclone Report: Hurricane Katrina.* Tech. rep. National Hurricane Center (NHC), pp. 1–43.

Kolen, B., R. Slomp, W. van Balen, T. Terpstra, M. Bottema, and S. Nieuwenhuis (2010). *Learning from French experiences with storm Xynthia. Dameges after a flood.*

Komen, G. J., K. Hasselmann, and K. Hasselmann (1984). "On the Existence of a Fully Developed Wind-Sea Spectrum". In: *Journal of Physical Oceanography* 14 (8), pp. 1271–1285.

Komen, G.L., L. Cavaleri, M. Donelan, K. Hasselmann, S. Hasselmann, and P.A.E.M. Janssen (1994). *Dynamics and modelling of ocean waves.* Cambridge university press, p. 532.

Kraus, N.C., M. Larson, and A.W. Wise (1998). "Depyh of Closure in Baech-fill Design". In: *Coastal Engineering Technical Note, U.S. Army Engineer Waterways Experiment Station, Vicksburg, MS.* CETN II-40.

Leonard, B. P. (1991). "The ULTIMATE conservative difference scheme applied to unsteady one-dimensional advection". In: *Computer Methods in Applied Mechanics and Engineering* 88 (1), pp. 17–74.

Leonard, B.P. (1979). "A Stable and Accurate Convective Modelling Procedure Based on Quadratic Upstream Interpolation". In: *Computational Methods in Applied Mechanical Engineering* 19, pp. 59–98.

Li, Jian-Guo (2008). "Upstream Nonoscillatory Advection Schemes". In: *Monthly Weather Review* 136 (12), pp. 4709–4729.

Longuet-Higgins, M.S. and R.W. Stewart (1964). "Radiation stresses in water waves; a physical discussion, with applications". In: *Deep-Sea Research* 11, pp. 529–562.

Lynett, P.J., P.L.-F. Liu, K.I. Sitanggang, and D.-H. Kim (2008). *Modeling Wave Generation , Evolution , and Interaction with Depth-Integrated , Dispersive Wave Equations - COULWAVE Code Manual - Cornell University Long and Intermediate Wave Modeling Package v. 2.0.*

Madsen, O.S., Y.-K. Poon, and H.C. Graber (1988). "Spectral wave attenuation by bottom friction: theory". In: *Proceedings of the 21st International Conference on Coastal Engineering.* Malaga, pp. 492–504.

Massey, T.C., M.E. Anderson, J. McKee Smith, J. Gomez, and R. Jones (2011). *STWAVE: Steady-State Spectral Wave Model User's Manual for STWAVE, Version 6.0.*

Mccall, R .T., J.S.M. Van Thiel De Vries, N.G. Plant, A.R. Van Dongeren, J.A. Roelvink, D.M. Thompson, and A.J.H.M. Reniers (2010). "Two-dimensional time dependent hurricane overwash and erosion modeling at Santa Rosa Island". In: *Coastal Engineering* 57 (7), pp. 668–683.

McCall, Robert T. (2008). "The Longshore Dimension In Dune Overwash Modelling". PhD thesis. Delft University of Technology, p. 147.

Mendonça, A., M.G. Neves, and C.J. Fortes (2009). "Numerical study of hydrodynamics around an artificial surf reef for São. Pedro do Estoril, Portugal". In: *Journal of Coastal Research* (56), pp. 1010–1014.

Mentaschi, L., G. Besio, F. Cassola, and A. Mazzino (2013). "Developing and validating a forecast / hindcast system for the Mediterranean Sea". In: *Journal of Coastal Research, Special Issue* (65), pp. 1551–1556.

— (2015). "Performance evaluation of Wavewatch III in the Mediterranean Sea". In: *Ocean Modelling* 90, pp. 82–94.

Miles, J. W. (1957). "On the generation of surface waves by shear flows". In: *Journal of Fluid Mechanics* 3 (02), pp. 185–204.

Mirfenderesk, H. and I.R. Young (2003). "Direct measurements of the bottom friction factor beneath surface gravity waves". In: *Applied Ocean Research* 25 (5), pp. 269–287.

Nederhoff, C.M. (Kees) (2014). "Modelling the effects of hard structures on dune erosion and overwash. Hindcasting the impact of Hurricane Sandy on New Jersey with XBeach". PhD thesis. TU Delft, p. 188.

Neumann, B., A.T. Vafeidis, J. Zimmermann, and R.J. Nicholls (2015). "Future coastal population growth and exposure to sea-level rise and coastal flooding - A global assessment". In: *Plose One* 10 (3), pp. 1–34.

Ng, Chiu O. (2000). "Water waves over a muddy bed: A two-layer Stokes' boundary layer model". In: *Coastal Engineering* 40 (3), pp. 221–242.

Nwogu, O. (1994). "Nonlinear evolution of directional wave spectra in shallow water". In: *Proceeding of the 24th International Confonference on Coastal Enginneering*, pp. 467–481.

Onken, Reiner, Allan R. Robinson, Lakshmi Kantha, Carlos J. Lozano, Patrick J. Haley, and Sandro Carniel (2005). "A rapid response nowcast/forecast system using multiply nested ocean models and distributed data systems". In: *Journal of Marine Systems* 56 (1-2), pp. 45–66.

Padilla-Hernandez, R. and J. Monbaliu (2001). "Energy balance o f wind w aves as a function o f the bottom friction formulation". In: *Coastal Engineering* 43, pp. 131–148.

Paramygin, V., Y.P. Sheng, and J.R. Davis (2017). "Towards the Development of an Operational Forecast System for the Florida Coast". In: *Journal of Marine Science and Engineering* 5 (1), p. 8.

Pelli, D. (2011). "Criteri metodologici per la previsione rapida del moto ondoso sulla base di dati ECMWF a scala 0.5°: Applicazione del modello spettrale SWAN al litorale liguretoscano". PhD thesis. Università di Pisa.

— (2016). *WWIII report*. Tech. rep. University of Florence, TU Braunschweig.

Pelli, D., L. Cappietti, and H. Oumeraci (2015a). *Nested modelling of wave processes from deep to shallow water: State of the Art*. Tech. rep. University of Florence, TU Braunschweig.

— (2015b). "Wave modelling in the Western Mediterranean Sea with WWIII". In: *Proceeding of the Twefith International Conference on Mediterranean Coastal Environment*. Varna, pp. 757–758.

— (2016). "Assessing the wave energy potential in the Mediterranean Sea using WAVEWATCH III". In: *Progress in Renewable Energies Offshore*. Taylor & Francis Group, 6000 Broken Sound Parkway NW, Suite 300, Boca Raton, FL 33487-2742: CRC Press, pp. 21–26.

Perrie, W. and D.T. Resio (2009). "A Two-Scale Approximation for Efficient Representation of Nonlinear Energy Transfers in a Wind Wave Spectrum. Part II: Application to Observed Wave Spectra". In: *Journal of Physical Oceanography* 39 (10), pp. 2451–2476.

Phillips, O M (1977). *The dynamics of the upper ocean Cambridge University Press*. Ed. by Cambrige University Press, p. 366.

Phillips, O.M. (1985). "Spectral and statistical properties of the equilibrium range in wind-generated gravity waves". In: *Journal of Fluid Mechanics* 156, pp. 505–531.

Polnikov, V. G. (1993). "On a description of a wind-wave energy dissipation function". In: *The Air-sea Interface. Radio and Acoustic Sensing, Turbulence and Wave Dynamics*. Ed. by M.A. Donelan, W.H. Hui, and W.J. Plant. Rosenstiel School of Marine and Atmospheric Science, University of Miami, Miami, FL, pp. 277–282.

Reniers, A.J.H.M., J.A. Roelvink, and E.B. Thornton (2004). "Morphodynamic modeling of an embayed beach under wave group forcing". In: *Journal of Geophysical Research* 109 (C1), p. C01030.

Resio, D. and W. Perrie (1991). "A numerical study of nonlinear energy fluxes due to wave-wave interactions Part 1: Methodology and basic results". In: *Journal of Fluid Mechanics* 223, pp. 603–629.

Resio, D.T. and W. Perrie (2008). "A Two-Scale Approximation for Efficient Representation of Nonlinear Energy Transfers in a Wind Wave Spectrum. Part I: Theoretical Development". In: *Journal of Physical Oceanography* 38 (12), pp. 2801–2816.

Roelvink, D., A. Reniers, A. van Dongeren, J. van Thiel de Vries, R. McCall, and J. Lescinski (2009). "Modelling storm impacts on beaches, dunes and barrier islands". In: *Coastal Engineering* 56 (11-12), pp. 1133–1152.

Roelvink, D., A. van Dongeren, R. McCall, B. Hoonhout, A. van Rooijen, P. van Geer, L. de Vet, K. Nederhoff, and E. Quataert (2015). *XBeach Technical Reference : Kingsday Release*. Ed. by Deltares.

Roelvink, J.A. (1993). "Dissipation in random wave groups incident on a beach". In: *Journal of Chemical Information and Modeling* 19, pp. 127–150.

Rogers, E.W., A.V. Babanin, and D.W. Wang (2012). "Observation-consistent input and whitecapping dissipation in a model for wind-generated surface waves: Description and simple calculations". In: *Journal of Atmospheric and Oceanic Technology* 29 (9), pp. 1329–1346.

Rogers, W. E., J. M. Kaihatu, H. A H Petit, N. Booij, and L. H. Holthuijsen (2002). "Diffusion reduction in an arbitrary scale third generation wind wave model". In: *Ocean Engineering* 29 (11), pp. 1357–1390.

Ruessink, B. G., J. R. Miles, F. Feddersen, R. T. Guza, and Steve Elgar (2001). "Modeling the alongshore current on barred beaches". In: *Journal of Geophysical Research: Oceans* 106 (C10), pp. 22451–22463.

Ruessink, B. G., G. Ramaekers, and L. C. Van Rijn (2012). "On the parameterization of the free-stream non-linear wave orbital motion in nearshore morphodynamic models". In: *Coastal Engineering* 65, pp. 56–63.

Ruessink, B.G., Y. Kuriyama, A.J.H.M. Reniers, J.A. Roelvink, and D.J.R Walstra (2007). "Modeling cross-shore sandbar behavior on the timescale of weeks". In: *Journal of Geophysical Research* 112, pp. 1–15.

Rugbjerg, M., O. R. Sørensen, and V. Jacobsen (2006). "Wave forecasting for offshore wind farms". In: *Proceeding of the 9th International Workshop on Wave Hindcasting and Forecasting*. Victoria, British Columbia, Canada.

Rusu, E. and C. Guedes Soares (2009). "Numerical modelling to estimate the spatial distribution of the wave energy in the Portuguese nearshore". In: *Renewable Energy* 34 (6), pp. 1501–1516.

— (2013). "Modeling Waves in Open Coastal Areas and Harbors with Phase-Resolving and Phase-Averaged Models". In: *Journal of Coastal Research* 29 (6), pp. 1309–1325.

Saha, S., S. Moorthi, X. Wu, Jiande Wang, Sudhir Nadiga, Patrick Tripp, David Behringer, Yu-Tai Hou, Hui-ya Chuang, Mark Iredell, Michael Ek, Jesse Meng, Rongqian Yang, Malaquías Peña Mendez, Huug van den Dool, Qin Zhang, Wanqiu Wang, Mingyue Chen, Emily Becker, Suranjana Saha, Shrinivas Moorthi, Xingren Wu, Jiande Wang, Sudhir Nadiga, Patrick Tripp, David Behringer, Yu-Tai Hou, Hui-ya Chuang, Mark Iredell, Michael Ek, Jesse Meng, Rongqian Yang, Malaquías Peña Mendez, Huug van den Dool, Qin Zhang, Wanqiu Wang, Mingyue Chen, and Emily Becker (2014). "The NCEP Climate Forecast System Version 2". In: *Journal of Climate* 27 (6), pp. 2185–2208.

Saha, Suranjana, Shrinivas Moorthi, Hua Lu Pan, Xingren Wu, Jiande Wang, Sudhir Nadiga, Patrick Tripp, Robert Kistler, John Woollen, David Behringer, Haixia Liu, Diane Stokes, Robert Grumbine, George Gayno, Jun Wang, Yu Tai Hou, Hui Ya Chuang, Hann Ming H Juang, Joe Sela, Mark Iredell, Russ Treadon, Daryl Kleist, Paul Van Delst, Dennis Keyser, John Derber, Michael Ek, Jesse Meng, Helin Wei, Rongqian Yang, Stephen Lord, Huug Van Den Dool, Arun Kumar, Wanqiu Wang, Craig Long, Muthuvel Chelliah, Yan Xue, Boyin Huang, Jae Kyung Schemm, Wesley Ebisuzaki, Roger Lin, Pingping Xie, Mingyue Chen, Shuntai Zhou, Wayne Higgins, Cheng Zhi Zou, Quanhua Liu, Yong Chen, Yong Han, Lidia Cucurull, Richard W. Reynolds, Glenn Rutledge, and Mitch Goldberg

(2010). "The NCEP climate forecast system reanalysis". In: *Bulletin of the American Meteorological Society* 91 (8), pp. 1015–1057.

Shi, F., B. Tehranirad, J.T. Kirby, C.H. Harris, and S. Grilli (2013). *FUNWAVE-TVD. Fully Nonlinear Boussinesq Wave Model with TVD Solver. Documentation and User 's Manual (Version 2.1)*.

Smith, G.A., A.V. Babanin, P. Riedel, I.R. Young, S. Oliver, and G. Hubbert (2011). "Introduction of a new friction routine into the SWAN model that evaluates roughness due to bedform and sediment size changes". In: *Coastal Engineering* 58 (4), pp. 317–326.

Snyder, R.L., F.W. Dobson, J.A. Elliott, and R.B. Long (1981). "Array measurements of atmospheric pressure fluctuations above surface gravity waves". In: *Journal of Fluid Mechanics* 102, pp. 1–59.

Soulsby, R. (1997). *Dynamics of marine sands*. Thomas Telford.

Soulsby, R.L. and J.S. Damgaard (2005). "Bedload sediment transport in coastal waters". In: *Coastal Engineering* 52 (8), pp. 673–689.

Spall, M.A. and A.R. Robinson (1989). "A new open ocean, hybrid coordinate primitive equation model". In: *Mathematics and Computers in Simulation* 31 (3), pp. 241–269.

Stelling, G. and J. Leendertse (1992). "Approximation of convective processes by cyclic AOI methods". In: *Estuarine and Coastal Modeling*. ASCE, pp. 771–782.

Sverdrup, H. U. and W. H. Munk (1946). "Theoretical and empirical relations in forecasting breakers and surf". In: *Transactions, American Geophysical Union* 27, pp. 828–836.

— (1947). *Wind, sea, and swell: theory of relations for forecasting*. Tech. rep. 601. U. S. Hydrographic Office.

SWAMP Group (1985). *Ocean wave modelling*. New York: Plenum Press.

SWASH Team (2014). *SWASH - User manual, version 2.00A*.

The SWAN Team (2016a). *SWAN Cycle III v. 41.10: Scientific and Technical Doucumentation*.

— (2016b). *SWAN Cycle III version 41.10. Implementation Manual*.

— (2016c). *USER MANUAL SWAN - Cycle III version 41.10*.

Tolman, H.L. (2008). "A mosaic approach to wind wave modeling". In: *Ocean Modelling* 25 (1-2), pp. 35–47.

— (2013). "A Generalized Multiple Discrete Interaction Approximation for resonant four-wave interactions in wind wave models". In: *Ocean Modelling* 70, pp. 11–24.

— (2014). *User manual and system documentation of WAVEWATCH III version 4.18*.

— (2015). *User manual and system documentation of WAVEWATCH III version 5.08*. Ed. by NOAA.

Tolman, H.L., B. Balasubramaniyan, L.D. Burroughs, D.V. Chalikov, Y.Y. Chao, H.S. Chen, and V.M. Gerald (2002). "Development and implementation of wind-generated ocean surface wave models at NCEP". In: *Weather and Forecasting* 17 (2), pp. 311–333.

Tolman, H.L., M.L. Banner, and J.M. Kaihatu (2013). "The NOPP operational wave model improvement project". In: *Ocean Modelling* 70, pp. 2–10.

Tolman, H.L. and D. Chalikov (1996). "Source Terms in a Third-Generation Wind Wave Model". In: *Journal of Physical Oceanography* 26, pp. 2497–2518.

Tolman, H.L. and R.W. Grumbine (2013). "Holistic genetic optimization of a Generalized Multiple Discrete Interaction Approximation for wind waves". In: *Ocean Modelling* 70, pp. 25–37.

Tracy, B.A. and D.T. Resio (1982). *Theory and calculation of the nonlinear energy transfer between sea waves in deep water*. Tech. rep. WIS Technical Report 11, US Army Engineer Waterways Experiment Station, Vicksburg, MS, USA.

Uchiyama, Y., J.C. McWilliams, and A.F. Shchepetkin (2010). "Wave–current interaction in an oceanic circulation model with a vortex-force formalism: Application to the surf zone". In: *Ocean Modelling* 34 (1-2), pp. 16–35.

Van der Westhuysen, A.J. (2007). "Advances in the spectral modelling of wind waves in the nearshore". Ph.D. Delft University of Technology, The Nederlands.

Van Dongeren, A., R. Lowe, A. Pomeroy, D.M. Trang, D. Roelvink, G. Symonds, and R. Ranasinghe (2013). "Numerical modeling of low-frequency wave dynamics over a fringing coral reef". In: *Coastal Engineering* 73, pp. 178–190.

Van Koningsveld, M., M. Davidson, D. Huntley, R. Medina, S. Aarninkhof, J.A. Jiménez, J. Ridgewell, and A. de Kruif (2007). "A critical review of the CoastView project: Recent and future developments in coastal management video systems". In: *Coastal Engineering* 54 (6-7), pp. 567–576.

van Thiel de Vries, J.S.M. (2009). "Dune erosion during storm surges". PhD thesis.

Van Rijn, L. C., D. J R Wasltra, B. Grasmeijer, J. Sutherland, S. Pan, and J. P. Sierra (2003). "The predictability of cross-shore bed evolution of sandy beaches at the time scale of storms and seasons using process-based profile models". In: *Coastal Engineering* 47 (3), pp. 295–327.

Van Rijn, L.C. (1984). "Sediment Transport, Part III: Bed forms and Alluvial Roughness". In: *Journal of Hydraulic Engineering* 110 (12), pp. 1733–1754.

— (2007a). "Unified View of Sediment Transport by Currents and Waves. I: Initian of Motion, Bed Roughness, and Bad-Load Transport". In: *Journal of Hydraulic Engineering* 133 (7), pp. 776–793.

— (2007b). "Unified View of Sediment Transport by Currents and Waves. II: Suspended Transport". In: *Journal of Hydraulic Engineering* 133 (6), pp. 668–689.

Van Rijn, L.C., P.K. Tonnon, and D.J.R. Walstra (2011). "Numerical modelling of erosion and accretion of plane sloping beaches at different scales". In: *Coastal Engineering* 58 (7), pp. 637–655.

Van Rijn, L.C., D.-J.R. Walstra, and M. van Ormondt (2007). "Unified View of Sediment Transport by Currents and Waves. IV: Application of Morphodynamic Model". In: *Journal of Hydraulic Engineering* 133 (7), pp. 776–793.

Van Vledder, G.Ph. (2006). "The WRT method for the computation of non-linear four-wave interactions in discrete spectral wave models". In: *Coastal Engineering* 53 (2-3), pp. 223–242.

Veeramony, J., M.D. Orzech, K.L. Edwards, M. Gilligan, J. Choi, E. Terrill, and T. De Paolo (2014). "Navy nearshore ocean prediction systems". In: *Oceanography* 27 (3), pp. 80–91.

Vousdoukas, M.I., Ó. Ferreira, L.P. Almeida, and A. Pacheco (2012). "Toward reliable storm-hazard forecasts: XBeach calibration and its potential application in an operational early-warning system". In: *Ocean Dynamics* 62 (7), pp. 1001–1015.

Walstra, D.J.R., J.A. Roelvink, and J. Groeneweg (2000). "Calculation of Wave-Driven Currents in a 3D Mean Flow Model". In: *Proceedings of the 27th International Conference on Coastal Engineering*, pp. 1050–1063.

WAMDI Group (1988). "The WAM model - A third generation ocean wave prediction model". In: *Journal of Physical Oceanography* 18 (12), pp. 1775–1810.

Warner, J.C., N. Perlin, and E.D. Skyllingstad (2008a). "Using the Model Coupling Toolkit to couple earth system models". In: *Environmental Modeling & Software* 23, pp. 1240–1249.

Warner, J.C., C.R. Sherwood, R.P. Signell, C.K. Harris, and H.G. Arango (2008b). "Development of a three-dimensional, regional, coupled wave, current, and sediment-transport model". In: *Computers & Geosciences* 34 (10), pp. 1284–1306.

Webb, D.J. (1978). "Non-linear transfers between sea waves". In: *Deep-Sea Research* 25 (3), pp. 279–298.

Yan, L. (1987). *An improved wind input source term for third generation ocean wave modelling*. Tech. rep. WR-87-8. KNMI.

Young, I.R. and A.V. Babanin (2006). "Spectral Distribution of Energy Dissipation of Wind-Generated Waves due to Dominant Wave Breaking". In: *Journal of Physical Oceanography* 36 (3), pp. 376–394.

Young, I.R. and L.A. Verhagen (1996). "The growth of fetch limited waves in water of finite depth. Part 1. Total energy and peak frequency". In: *Coastal Engineering* 29 (1-2), pp. 47–78.

Yuan, Y., C.C. Tung, and N.E. Huang (1986). "Statistical characteristics of breaking waves". In: *Wave Dynamics and Radio Probing of the Ocean Surface*. Ed. by O.M. Phillips and K. Hasselmann. Springer US, pp. 265–272.

Zijlema, M., G. Stelling, and P. Smit (2011). "SWASH: An operational public domain code for simulating wave fields and rapidly varied flows in coastal waters". In: *Coastal Engineering* 58 (10), pp. 992–1012.

List of Notations and Symbols

Roman Symbols

m	Coordinate perpendicular to s [-]
s	Coordinate in the direction θ [-]
A_s	Wave asymmetry [-]
C	Deep-averaged sediment concentration [-]
c	Phase speed [$\mathrm{m\,s^{-1}}$]
C_{eq}	Deep-averaged sediment eqilibium concentration [-]
C_f	Dissipation coefficient [$\mathrm{m\,s^{-1}}$]
c_g	Group velocity [$\mathrm{m\,s^{-1}}$]
c_σ	Propagation σ-component velocities in the spectral sapce (σ, θ) [$\mathrm{m\,s^{-1}}$]
c_θ	Propagation θ-component velocities in the spectral sapce (σ, θ) [$\mathrm{m\,s^{-1}}$]
D	Sediment diffusion coefficient [-]
d	local bed level [m]
$\bar{D}_{\mathrm{br}}$	Mean breaking dissipation rate [$\mathrm{J\,m^{-2}\,s^{-1}}$]
E	Wave energy [$\mathrm{m^2\,s}$]
F	Wave induced stress [N]
f	Wave frequency [Hz]
f_0	Zero-crossing frequency of breaking wave [Hz]
f_c	Coefficient of Coriolis [-]
f_{mor}	Morphological acceleration factor [-]
f_p	Wave frequency peak [Hz
g	Gravitational acceleration [$\mathrm{m\,s^{-2}}$]
H	Wave height [m]
H_I	Incident wave height [m]
H_{max}	Maximum wave height [m]

H_R Reflected wave height [m]

H_{rms} Root-mean square wave height [m]

k Wave number [m^{-1}]

K_R Reflection coefficient [-]

N Action density [$\mathrm{m}^2\,\mathrm{Hz}^{-1}$]

p Porosity [-]

Q_b Probability that a wave height is associated with breaking [-]

$q_{(x,y)}$ Sediment transport rates in x- and y-direction [m/per/second]

R Radius of the Earth [m]

S Generic source or sink term [m^2]

S_{bfr} Bottom friction sink term [m^2]

S_{br} Depth-induced breaking sink term [m^2]

S_{ds} Dissipation due to whitecapping sink term [m^2]

S_{in} Wind input source term [m^2]

S_k Wave skewness [-]

S_{ln} Linear input source term [m^2]

S_{v} Vegetation sink term [m^2]

S_{nl3} Triad wave-wave interactions source term [m^2]

S_{nl4} Nonlinear qaudruplet wave-wave interaction source term [m^2]

S_{xx} Normal radiation stress in the x-direction [$\mathrm{N\,m}^{-1}$]

S_{xy} Shear component of the radiation stress [$\mathrm{N\,m}^{-1}$]

S_{yy} Normal radiation stress in the y-direction [$\mathrm{N\,m}^{-1}$]

T_{m01} Wave mean period [s]

T_p Wave peak period [s]

T_s Adaption time [s]

$\vec{U}$ Current velocity [$\mathrm{m\,s}^{-1}$]

u_a Asymmetry and skewness velocity effect [m]

u_{bk} Orbital velocity at bottom for wave number k [$\mathrm{m\,s}^{-1}$]

u_E Eulerian velocity in x-direction [$\mathrm{m\,s}^{-1}$]

u_S Stokes drift in x-direction [$\mathrm{m\,s}^{-1}$]

v_E Eulerian velocity in y-direction [$\mathrm{m\,s}^{-1}$]

v_S Stokes drift in y-direction [$\mathrm{m\,s}^{-1}$]

u_L Lagrangian velocity in x-direction [$\mathrm{m\,s^{-1}}$]

U_λ Longitude current velocity component [$\mathrm{m\,s^{-1}}$]

U_ϕ Latitude current velocity component [$\mathrm{m\,s^{-1}}$]

u_{rms} Root-mean square velocity [m]

U_w Wind speed

v_h Horizzontal viscosity [Pa s]

v_L Lagrangian velocity in y-direction [$\mathrm{m\,s^{-1}}$]

w_s Sediment fall velocity [$\mathrm{m\,s^{-1}}$]

z Bottom level [m]

z_b Bed level [m]

Greek Symbols

α_{BJ} Breaker index [-]

α Wave phase [rad]

$\beta_{1.2}$ Magnitude of energy transfer of the biphase [°]

β Miles parameter [-]

β_{max} Non-dimensional growth parameter of wind input source term [-]

δ_d Standard deviation of difference [-]

Δt_d Dynamic time step [s]

Δt_g Global time step [s]

Δt_k Intra-spectra propagation time step [s]

Δt_p Spatial propagation time step [s]

Δt_s Source term time step [s]

η Water surface elevation [m]

$\bar{\eta}$ Water set-up or set-down [m]

λ Longitude [°]

ω Absolute radian frequency [Hz]

ϕ Latitude [°]

ρ Water density [$\mathrm{kg^3\,m^{-1}}$]

σ Relative or intrinsic radian frequency [$\mathrm{rad\,s^{-1}}$]

τ_b Bed shear-stress [Pa]

τ_s Wind shear stress [Pa]

θ Angle of waves propagation [°]

θ_w Angle of wind propagation [°]

Acronyms

AB Action Balance equation

ABP Active Boundary Point

AR* Ardhuin et al. (2010) wind input + whitecapping source term with modified $\beta_{\max}$ parameter

AR Ardhuin et al. (2010) wind input + whitecapping source term

BJA Bidlot, Janssen and Abdallah whitecapping sink term (Bidlot et al., 2005)

BSS Brier Skill Score

BT Boussinesq-type equations

BYDZR Babanin, Young, Donelan, Rogers and Zieger wind input + whitecapping source term (Rogers et al., 2012).

CEWS Coastal Early Warning System

CFL Courant-Fredrichs-Levy criterion

CFSR Climate Forecast System Reanalysis

CPU Central Processing Unit

CR Coarse resolution

DC Data Collection

DIA Discrete Interaction Approximation

DW Deep water

ECMWF European Centre for Medium-Range Weather Forecast

ECWAM Bidlot et al. (2005) wind input + whitecapping source term

EMODnet European Marine Observation and Data Network

ESM Earth System Modelling

FR1 First frequency in WWIII

GCM Global Circulation Model

GEBCO General Bathymetry Chart of the Oceans

GLM Generalised Lagrangian Mean

GMD Generalized Multiple DIA

GP Grid Pre-processing

HH Symmetrically Normalised Root Mean Square Error

HISWA HIndcast Shallow WAter

HR High resoultion

IBC Initial and Boundary Conditions

ISW Intermediate/shallow water

JONSWAP Joint Notrh Sea Wave Project

KNMI Royal Netherlands Meteorological Institute

LAM Limited Area Model

LES Limited-Eddy Simulation models

LTA Lumped-triad Approximation

MMAB Marine modeling and Analysis Branch (USA)

MSE Mean Square Error

MS Mild slope equation

MS Model Setup

NBI Normalised Bias

NCEP National Centers for Environmental Predictions (USA)

NK Number of frequency in WWIII

NLSW Nonlinear Shallow Water equations

NOAA National Oceanic and Atmospheric Administration (USA)

NRMSE Normalised Root Mean Square Error

NS Nearshore

NTH Number of wave directions in WWIII

OWMS Operational Wave Model System

RANS Reynolds Averaged Navier-Stokes equations

MR Running Model

RMSE Root Mean Square Error

ROMS Regional Ocean Modeling System

RON Rete Ondametrica Nazionale - Italian Wavemeter Network

SII Specific Impact Indicators

SI Scatter Index

S&L Stelling and Leendertse (1992) second order propagation scheme

SPH Smoothed Particle Hydrodynamics

SWAMP Sea Wave Modeling Project

SWAN Simulating WAves Nearshore

SWASH Simulating WAves till SHore

SWL Still Water Level

TC Tolman and Chalikov (1996) wind input + whitecapping source term

TSA Two Scale Approximation

USA United States of America

WAMDI The WAve Model Development and Implementation Group

WBC Wave Boundary Conditions

WEP Wave Energy Park

WP Work Package

WRT Webb-Resio-Tracy

WR Semiempirical wind-wave relationships

WWIII WAVEWATCH III model

XFR Frequency increment factor in WWIII

YV Young and Verhagen (1996) formula

List of Figures

List of Tables